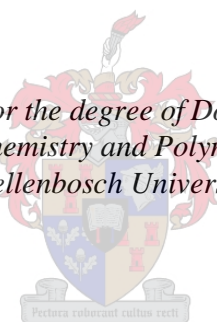# Immobilized Ru(II) Catalysts for Transfer Hydrogenation and Oxidative Alkene Cleavage Reactions

by
Hendrik de Vries Kotzé

Dissertation presented for the degree of Doctor of Philosophy in the Faculty of Chemistry and Polymer Science at Stellenbosch University

Supervisor: Prof. Selwyn Frank Mapolie

March 2015

Declaration

By submitting this thesis electronically, I declare that the entirety of the work contained therein is my own, original work, that I am the authorship owner thereof (unless to the extent explicitly otherwise stated) and that I have not previously in its entirety or in part submitted it for obtaining any qualification.

January 2015

II

Abstract

The synthesis of a range of siloxane functionalized Ru(arene)Cl(N,N) complexes allowing for the synthesis of novel MCM-41 and SBA-15 immobilized ruthenium(II) catalysts, is described in this thesis. Two distinctly different approaches were envisaged to achieve successful heterogenization of these siloxane functionalized complexes. Condensation of the siloxane functionalized complexes, **C2.4**-**C2.6** (siloxane tether attached to imine nitrogen) and **C3.5**-**C3.7** (siloxane tether via the arene ring), with the surface silanols of the synthesized silica support materials MCM-41 and SBA-15, afforded immobilized catalysts **IC4.1**-**IC4.6** (siloxane tether attached to imine nitrogen) and **IC4.7**-**IC4.12** (siloxane tether via the arene ring).

Model and siloxane functionalized complexes **C2.1**-**C2.6** were prepared by the reaction of diimine Schiff base ligands **L2.1**-**L2.6** with the [Ru(p-cymene)$_2$Cl$_2$]$_2$ dimer. A second, novel, approach involved the introduction of the siloxane tether on the arene ligand of the complex. Cationic arene functionalized Ru(arene)Cl(N,N) complexes, **C3.1**-**C3.4**, were prepared with varying N,N ligands including bipyridine and a range of diimine ligands, with either propyl or diisopropyl(phenyl) substituents at the imine nitrogen (greater steric bulk around the metal center). The reaction of these propanol functionalized complexes with 3-(triethoxysilyl)propyl isocyanate, afforded urethane linked siloxane functionalized complexes **C3.5**-**C3.8**, where the siloxane tether is attached to the arene ring of the complex.

The complexes were fully characterized by FT-IR spectroscopy, NMR (^{1}H and ^{13}C) spectroscopy, ESI-MS analysis and microanalysis. Suitable crystals for the alcohol functionalized complex **C3.1** were obtained and the resultant orange crystals were analyzed by single crystal XRD. The heterogenized catalysts, **IC4.1**-**IC4.12**, were characterized by small-angle powder X-ray diffraction, scanning and transmission electron microscopy (SEM and TEM), thermal gravimetric analysis (TGA), inductively coupled plasma optical emission spectroscopy (ICP-OES) and nitrogen adsorption/desorption (BET) surface analysis to name but a few. ICP-OES allowed for direct comparison of the model and immobilized systems during catalysis ensuring that the ruthenium loadings were kept constant.

The application of the model complexes **C2.1**-**C2.3** and **C3.1**-**C3.3**, as well as their immobilized counterparts, **IC4.1**-**IC4.12**, as catalyst precursors in the oxidative cleavage of alkenes (1-octene

and styrene), were investigated. The proposed active species for the cleavage reactions was confirmed to be RuO_4 (UV-Vis spectroscopy). In general it was observed that at lower conversions, aldehyde was formed as the major product. Increased reaction times resulted in the conversion of the formed aldehyde to the corresponding carboxylic acid. For the oxidative cleavage of 1-octene using the systems with the siloxane tether attached to the imine nitrogen, the immobilized systems outperformed the model systems in all regards. Higher conversions and selectivities of 1-octene towards heptaldehyde were obtained when using immobilized catalysts **IC4.1**-**IC4.6**, as compared to their non-immobilized model counterparts (**C2.1**-**C2.3**) at similar times. It was found that the immobilized catalysts could be used at ruthenium loadings as low as 0.05 mol %, compared to the model systems where 0.5 mol % ruthenium was required to give favorable results. Complete conversion of 1-octene could be achieved at almost half the time needed when using the model systems as catalyst precursors. The activity of the model systems seems to increase with the increase in steric bulk around the metal center. These model and immobilized systems were also found to cleave styrene affording benzaldehyde in almost quantitative yield in some case (shorter reaction times).

The systems, with the siloxane tether via the arene ring, were found to be less active for the cleavage of 1-octene when compared to the above mentioned systems (siloxane tether attached to the imine nitrogen). The immobilized systems **IC4.7**-**IC4.12** performed well compared to their model counterparts, but could not achieve the same conversions at the shorter reaction times as were the case for **IC4.1**-**IC4.6**. This lower activity was ascribed to the decreased stability of these systems in solution compared to the above mentioned systems with the tether attached to the imine nitrogen. This was confirmed by monitoring the conversion of the complex (catalyst precursor) to the active species in the absence of substrate (monitored by UV-Vis spectroscopy). It was observed that model complex **C3.1** could not be detected in solution after 1 hour, compared to complex **C2.2** which was detected in solution even after 24 hours.

Experiments were carried out where MCM-41 was added to a solution of model complex **C2.2** under typical cleavage reaction conditions. A dramatic increase in the conversion was achieved when compared to a reaction in the absence of MCM-41. An investigation into the effect of the support material on the formation of the expected active species was carried out using UV-Vis spectroscopy. The presence of the active species, RuO_4, could be observed at shorter reaction times in the presence of MCM-41. This suggested that the silica support facilitates the formation

of the active species from the complex during the reaction, therefore resulting in an increased activity.   It was also observed that RuO_4 is present in solution in reactions where the immobilized catalyst systems are used after very short reaction times, compared to the prolonged times required for this to occur as is the case for the model systems.

Model and immobilized catalysts, **C2.1**-**C2.3** and **IC4.1**-**IC4.6**, were also applied as catalysts for the transfer hydrogenation of various ketones. The immobilized systems could be recovered and reused for three consecutive runs before the catalysts became inactive (transfer hydrogenation of acetophenone). Moderate to good conversion were obtained using the immobilized systems, but were found to be less active their model counterparts **C2.1**-**C2.3**.

Opsomming

Die sintese van `n reeks siloksaan gefunksioneerde Ru(areen)Cl(N,N) komplekse, wat die sintese van nuwe MCM-41 en SBA-15 geimmobiliseerede rutenium(II) katalisatore toelaat, word in hierdie tesis beskryf. Twee ooglopend verskillende metodes is voorgestel om die suksesvolle immobilisering van die siloksaan gefunksioneerde komplekse te bereik. Die kondensasie van die siloksaan gefunksioneerde komplekse, **C2.4**-**C2.6** (siloksaan ketting geheg aan die imien stikstof) en **C3.5**-**C3.7** (siloksaan ketting geheg aan die areen ligand), met die oppervlak silanol groepe van die silika materiale MCM-41 en SBA-15, laat die sintese van geimmobiliseerde katalisatore **IC4.1**-**IC4.6** (siloksaan ketting geheg aan die imien stikstof) en **IC4.7**-**IC4.12** (siloksaan ketting geheg aan die areen ligand) toe.

Model en siloksaan gefunksioneerde komplekse **C2.6**-**C2.6** is berei deur die reaksie tussen Schiff basis ligande, **L2.1**-**L2.6**, en die [Ru(p-simeen)$_2$Cl$_2$]$_2$ dimeer. `n Tweede, nuwe benadering wat die sintese van komplekse met die siloksaan ketting geheg aan die areen ligand behels, is ook gevolg.  Kationiese areen gefunksioneerde Ru(areen)Cl(N,N) komplekse, **C3.1**-**C3.4**, is berei deur die N,N ligande rondom die metaal sentrum te wissel vanaf bipiridien tot `n reeks diimien ligande met propiel of diisopropielfeniel substituente by die imien stikstof. Hierdie propanol gefunksioneerde komplekse is met 3-(triëtoksiesiliel)propiel-isosianaat gereageer om sodoende die uretaan gekoppelde siloksaan gefunksioneerde komplekse **C3.5**-**C3.8** op te lewer.

Al die komplekse is ten volle gekaraktariseer deur van FT-IR spektroskopie, KMR (^{1}H and ^{13}C) spektroskopie, ESI-MS analise en mikroanalise gebruik te maak. In die geval van model kompleks **C3.1**, is `n kristalstruktuurbepaling ook uitgevoer. Die heterogene katalisatore, **IC4.1**-**IC4.12**, is gekaraktariseer deur poeier X-straaldiffraksie, skandeer- en transmissie-elektronmikroskopie, termogravimetriese analise (TGA), induktief gekoppelde plasma optiese emissie spektroskopie (IKP-OES) en BET oppervlak analises, om net `n paar te noem.  IKP-OES het ons toegelaat om `n direkte vergelyking te tref tussen die model en geimmobiliseerde sisteme tydens die katalise reaksies.

Model komplekse **C2.1**-**C2.3** en **C3.1**-**C3.3**, sowel as hul geimmobiliseerde eweknieë **IC4.1**-**IC4.12**, is vir die oksidatiewe splyting van alkene (1-okteen en stireen) getoets. Die voorgestelde aktiewe spesie wat tydens hierdie reaksie gevorm word, RuO$_4$, is bevestig deur van

UV-Vis spektroskopie gebruik te maak. Oor die algemeen is dit gevind dat aldehied oorheersend gevorm word by laer omsetting. Wanneer die reaksietyd verleng is, is daar gevind dat die aldehied na die ooreenstemmende karboksielsuur omgeskakel is. Wanneer die geimmobiliseerde katalisatore gebruik is tydens die oksidatiewe splitsing van 1-okteen, het die sisteme, met die ketting geheg aan die imien stikstof, deurgangs beter as die model sisteme gevaar. Hoër omskakelings van 1-okteen en hoë selektiwiteite vir heptaldehied is behaal wanneer die geimobiliseerded katalisatore **IC4.1**-**IC4.6** met die nie-geimmobiliseerde model sisteme (**C2.1**-**C2.3**) vergelyk is by dieselfde reaksietye. Die geimmobiliseerde sisteme kon by rutenium beladings van so laag as 0.05 mol % gebruik word. Dit is in teenstelling met die model sisteme waar 0.5 mol % rutenium nodig was om die reaksie suksesvol te laat plaasvind. Die totale omskakeling van 1-okteen is bereik in die helfte van die tyd wat nodig was wanneer die model sisteme gebruik is. Dit is gevind dat die aktiwiteit van die model sisteme toeneem met `n toename in die steriese grootte van die ligand rondom die metaal. Beide die model en geimmobilseerde sisteme kon ook gebruik word vir die oksidatiewe splyting van stireen. Bensaldehied kon in kwantitiewe opbrengs gevorm word in sommige gevalle.

`n Laer aktiwiteit vir die oksidatiewe splyting van 1-okteen is vir die sisteme waar die siloksaan ketting aan die areen ligand geheg is, waargeneem. Hoewel die geimmobiliseerde sisteme **IC4.7**-**IC4.12** beter as hul model eweknieë gevaar het, kon die aktiwiteite wat met **IC4.1**-**IC4.6** bereik is nie geewenaar word nie. Hierdie laer aktiwiteit is toegeskryf aan die verlaagde stabiliteit van dié sisteme in oplossing in vergelyking met **IC4.1**-**IC4.6** (ketting geheg aan die imine stikstof). Die stabiliteit van beide sisteme is getoets deur die omskakeling van die model komplekse (**C2.2** en **C3.1**; katalise voorgangers) na die aktiewe spesie te monitor (UV-Vis spektroskopie). Na 1 uur kon die model kompleks **C3.1** nie meer in die oplossing waargeneem word nie. In teenstelling kon model kompleks **C2.2** nog selfs na 24 uur in die oplossing bespeur word.

Om die rol van die silika materiale tydens die reaksie te ondersoek, is `n eksperiment uitgevoer waar MCM-41 by `n oplossing van kompleks **C2.2** gevoeg is. `n Toename in die omskakeling van 1-okteen is waargeneem in vergelyking met `n reaksie waar geen silika teenwoordig was nie. UV-Vis spektroskopie is gebruik om die invloed van die silika op die vorming van die aktiewe spesie te ondersoek. In eksperimente waar MCM-41 teenwoordig was, kon die aktiewe spesie, RuO_4, by baie korter reaksietye waargeneem word. Dit wil blyk of die silika materiaal die

VII

vorming van die aktiewe spesie vanaf die kompleks aanhelp en sodoende `n toename in die spoed van die reaksie bewerkstellig. RuO_4 kon ook by baie korter reaksietye waargeneem word wanneer die geimmobiliseerde sisteme gebruik is.

Beide model en geimmobiliseerde sisteme, **C2.1**-**C2.3** en **IC4.1**-**IC4.6**, is getoets vir die oordrag hidrogenering van verskilende ketone. Dit was moontlik om die geimmobiliseerde sisteme drie keer te herwin en vir daaropvolgende reaksies te gebruik. Vir die geimmobiliseerde sisteme kon egter slegs gemiddelde omskakelings verkryg word en het swakker gevaar as hul model ekwivalente sisteme, **C2.1**-**C2.3**.

Acknowledgements

Firstly, I would like to thank my supervisor, Prof. Selwyn Mapolie, for his patience, guidance and support throughout the pursuit of my degree.

I would also like to thank my colleagues of the Organometallic Research Group at Stellenbosch University (past and present); Drs. Andrew Swarts and Rehana Malgas-Enus, Derik Wilbers, Corli Joubert, Angelique Blanckenberg, Jacquin October, Cassiem Joseph, Ené Slazus, Manana Moletsane, Dr. Ripul Mehrotra and Annick van Niekerk, for their friendship, extensive support and invaluable discussions.

A big thank you for the assistance of Sylette, Malcolm Taylor and Malcolm Maclean, Johnny, Chalon and Moebarik during the time I spent in the Inorganic Chemistry building.

I would like to thank the staff in the Department of Chemistry and Polymer Science of University of Stellenbosch, especially the CAF group, for assisting with various analytical techniques.

Financial support from the SASOL is greatly appreciated.

A special thanks to my family and friends for their support throughout.

Lastly, I cannot be more grateful to my wife, Karen, for her unwavering support and encouragement throughout the last few years. You supported me and always reminded me to never give up, even though times seemed tough. Love you lots!

Conference Contributions

Hennie Kotzé and Prof S.F. Mapolie

Oral presentation titled: ***Transfer hydrogenation of acetophenone and benzophenone utilizing immobilized RuCl(p-cymene) catalysts***

Catalysis Society of South Africa (CATSA), Langebaan (Club Mykonos), South Africa, 2012.

Hennie Kotzé and Prof S.F. Mapolie

Poster presentation titled: ***Routes towards silica-immobilized ruthenium catalysts for organic transformations***

Catalysis Society of South Africa (CATSA), Kwazulu-Natal (Wild Coast Sun), South Africa, 2013.

Table of Content

Chapter one: *An introduction to heterogenized transition metal catalysts*

Chapter two: *Synthesis and characterization of model and siloxane functionalized RuCl(p-cymene)(N,N) complexes containing a siloxane tether at the imine nitrogen*

Chapter three: *Synthesis and characterization of model and siloxane functionalized RuCl(arene)(N,N) complexes with siloxane tether via the arene ring*

Chapter four: *Immobilization of RuCl(arene)(N,N) complexes on MCM-41 and SBA-15*

Chapter five: *Oxidative cleavage of selected alkenes*

Chapter six: *Transfer hydrogenation of selected ketones*

Chapter seven: *Concluding remarks and future prospects*

List of Figures

Chapter one

Chapter two

Chapter three

Chapter four

Chapter five

Chapter six

List of Schemes

Chapter three

Chapter four

Chapter five

Chapter six

List of Tables

Chapter four

Chapter five

Chapter six

Abbreviations

°	degrees
ºC	degrees Celsius
δ	chemical shift
ATR	attenuated total reflectance
BET	Brunauer Emmett Teller
bipy	bipyridine
BJH	Barret-Joyner-Halenda
bs	broad singlet
c:s:b	catalyst:substrate:base
CTAB	cetyltrimethylammonium bromide
d	doublet
DCM	dichloromethane
DMSO	dimethyl sulfoxide
ee	enantiomeric excess
ESI-MS	electrospray ionization mass spectrometry
Et	ethyl
FT-IR	Fourier Transform infrared spectroscopy
GC	gas chromatography
HPLC	high performance liquid chromatography
Hz	Hertz

HMDS	hexamethyl disilazane
ICP-OES	inductively coupled plasma optical emission spectroscopy
K	Kelvin
LCT	liquid templating
m	multiplet
m/z	mass-to-charge ratio
MAS	magic-angle spinning
MCM	Mobil crystalline material
MeCN	acetonitrile
MHz	Megahertz
MLCT	metal-to-ligand charge transfer
mol	mole
mmol	millimole
MOFs	metal–organic frameworks
MP	methyl-pyridine
MSU	Michigan State University
NMO	*N*-methylmorpholine-*N*-oxide
MP-A	methyl-pyridine-diisopropylaniline
NMR	nuclear magnetic resonance
$^-$OAc	acetate
OMM	ordered mesoporous material
P	pyridine

P/Po	relative pressure
P-A	pyridine-diisopropylaniline
PEG	polyethylene glycol
ph	phenyl
P-P	pyridine-propyl
PMOs	periodic mesoporous materials
POPs	porous organic polymers
PPG	polypropylene glycol
pta	phosphaadamantane
q	quartet
Q	quinoline
HPLC	high performance liquid chromatography
s	singlet
SBA	Santa Barbara amorphous
SEM	scanning electron microscopy
t	triplet
^{t}BuOOH	tert-butyl hydroperoxide
TEA	triethylamine
TEM	transmission electron microscopy
TEOS	tetraethylorthosilicate
TGA	thermal gravimetric analysis
THF	tetrahydrofuran

TOF   turn-over frequency

UV-Vis   ultraviolet-visible

XRD   X-ray diffraction

Chapter 1: An Introduction to Heterogenized Transition Metal Catalysts

1.1 Precious metals in catalysis

The pursuit of greener more environmentally friendly processes for both the pharmaceutical and chemical industries is very high on the agenda of current scientific research. The minimization of waste and the cost of chemical transformations can be greatly improved by making use of recyclable catalysts. Homogeneous catalysts are potentially very attractive for use in industry due to the numerous advantages they possess over their heterogeneous counterparts. The higher selectivity and activity when compared to heterogeneous catalyst systems are as a result of more complex catalytic sites (increased selectivity) and ease of access to the reagents (increased activity) brought upon by the catalyst being in solution. This coupled with the usually milder reaction conditions and better heat transfer in solution are the main reasons why homogeneous catalysts are such an attractive option. The major drawback however is that it is not possible to effectively recover homogeneous catalysts from the reaction mixture after the reaction is completed. This is where heterogeneous catalysts, although usually not able to compete with the activity and selectivity of homogeneous catalysts, have one major advantage over homogeneous catalysts systems. The ease by which a heterogeneous catalyst can be separated from the reaction media and recycled for further runs is probably one of the main reasons why industry mostly employ heterogeneous catalysts for large scale transformations [1-3].

Precious metals find application as catalysts in numerous chemical transformations in industry. In the oil refining industry for instance they are responsible for catalytic reforming, isomerization and hydrocracking. These precious metals are also used as catalysts for hydrogenations, the synthesis of bulk chemicals and in catalytic converters in the exhaust systems of motor vehicles. Platinum and palladium are usually involved in these processes but other platinum group metals (PGM's) can also be used either in conjunction with platinum and palladium or on their own. Ruthenium, together with gold, silver, platinum, palladium, rhodium and iridium are classified as high-grade precious metals and their recovery from catalytic cycles are crucial in today's economy [4]. A lot of money, time and effort are spent on the recovery of these precious metals

Chapter 1: An Introduction to Heterogenized Transition Metal Catalysts

after the lifetime of a certain catalyst has expired and it is due to the metals being supported on various carriers like alumina, silica and zeolites that this recovery process is possible [5].

Supported metal complexes have to a lesser extent been applied as catalysts for the synthesis of specialty and fine chemicals. This is mainly due to the higher selectivity instilled in molecular catalysts resulting from the presence of well-defined homogeneous active sites. The development of reusable solid catalysts with high selectivity for organic transformations has however recently been a very actively studied area of research [3,6]. A very rewarding approach for catalysis would be to combine the properties of homogeneous and heterogeneous catalysts to afford a catalyst which would not only have high activity and selectivity but also the major advantage of being readily separable from the reaction mixture. This process is known as heterogenization of homogeneous catalysts. Scheme 1.1 serves as a summary for the evolution of a successful homogeneous catalyst into a covalently anchored heterogenized catalyst.

Homogeneous catalysis	Reusable homogeneous catalytic systems	Heterogeneous catalysts	Covalent anchoring
Successful process	-Supercritical fluids -Perfluorinated solvents -Ionic liquids	-Physisorption -Dipolar interaction -Coordinative bond	-Stability of the complex -Highest productivity
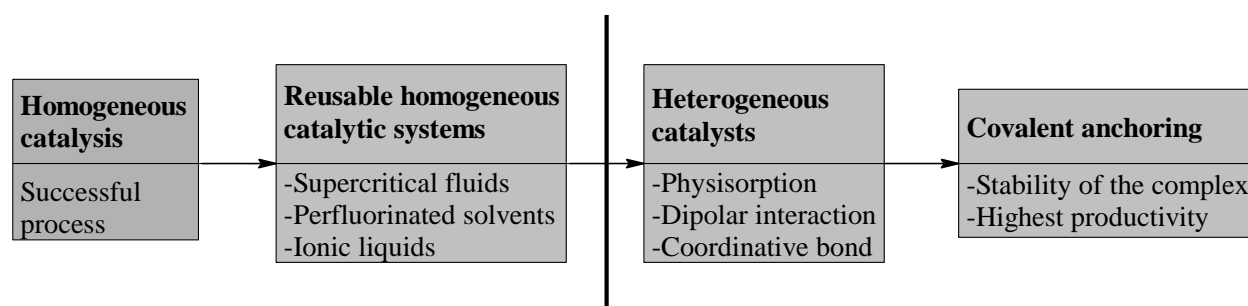
Scheme 1.1   The evolution of a homogeneous catalyst to a covalently anchored heterogeneous catalyst [3].

To merge the fields of homogeneous and heterogeneous catalysis successfully would require the merging of the properties that characterize each of these systems. Achieving this would involve the integration of a discrete molecular homogeneous catalyst and a suitable support material which would instill the heterogeneous properties in the obtained catalyst. A discussion on different support materials and methods to achieve successful heterogenization will follow and covers possible advantages and disadvantages of each system.

Chapter 1: An Introduction to Heterogenized Transition Metal Catalysts

1.2 Heterogenization of molecular catalysts

A well-studied and widely reported approach to enable successful catalyst/product separation is the attachment of a molecular homogeneous catalyst to either insoluble organic, inorganic or polymeric supports [7-14]. A summary of the advantages and disadvantages of both homogeneous and heterogeneous catalyst systems is shown in Table 1.1. Although the activity and selectivity of heterogeneous systems in general is lower than its homogeneous counterparts, the advantage of separation and recovery of the catalyst outweigh these drawbacks. It is however important to ensure that the activity and selectivity of the homogeneous catalyst to be immobilized is not dramatically altered by the heterogenization process.

Table 1.1   A comparison of the properties of homogeneous and heterogeneous catalyst systems.

Homogeneous	Heterogeneous
Requires a multistep synthetic process	Synthesis usually easy
Monophasic	Multiphasic
High activity	Low activity
High selectivity	Low selectivity
Separation of catalyst difficult	Easy separation through filtration
Not recyclable	Recyclable

Attempts at the successful heterogenization of discrete homogeneous catalyst systems have attracted widespread research interest with the main objective being to retain the properties that makes homogeneous systems so attractive (high activity and selectivity) and combine it with the

recovery and recyclability of heterogeneous catalysts. This makes the selection of the appropriate support material very important. Examples of different organic and inorganic supports are discussed in more detail in the sections which follow.

1.2.1   Dendrimers

Dendrimers are large, highly branched, mono-dispersed macromolecules with well-defined architecture [15]. The first reports of the synthesis of dendrimers date back to 1985 when the groups of Tomalia and Newkome independently reported their newly synthesized branched molecules respectively termed *dendrimers* and *arborols* [16,17]. Dendrimers can be synthesized using two distinctly different approaches, namely the divergent and convergent routes. The divergent approach involves the addition of repeat units from the core outwards through consecutive reactions on the periphery (most outward part of molecule) of the growing molecule. New generations are formed by each repetitive unit that is added and an example of this is shown is Scheme 1.2.
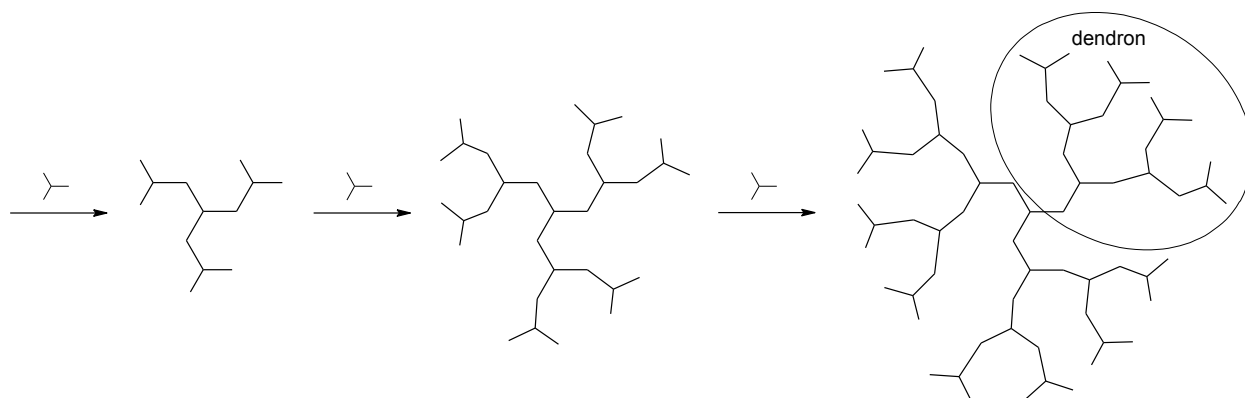
Scheme 1.2 Divergent synthesis of a third generation dendrimer [15].

The convergent method was first reported by Hawker and Fréchet in 1990 and is loosely based on an approach whereby dendron wedges are first synthesized separately and then subsequently attached to a suitable core in the last step [18]. The incorporation of metal centers into the

architecture of a dendrimer results in the formation of what is known as metallodendrimers. Metallodendrimers can be categorized into distinct groups and these groups are summarized in Figure 1.1 below. Metals are mainly found in the architecture of metallodendrimers as cores, connectors between branching centers or as terminal groups on the periphery [7].
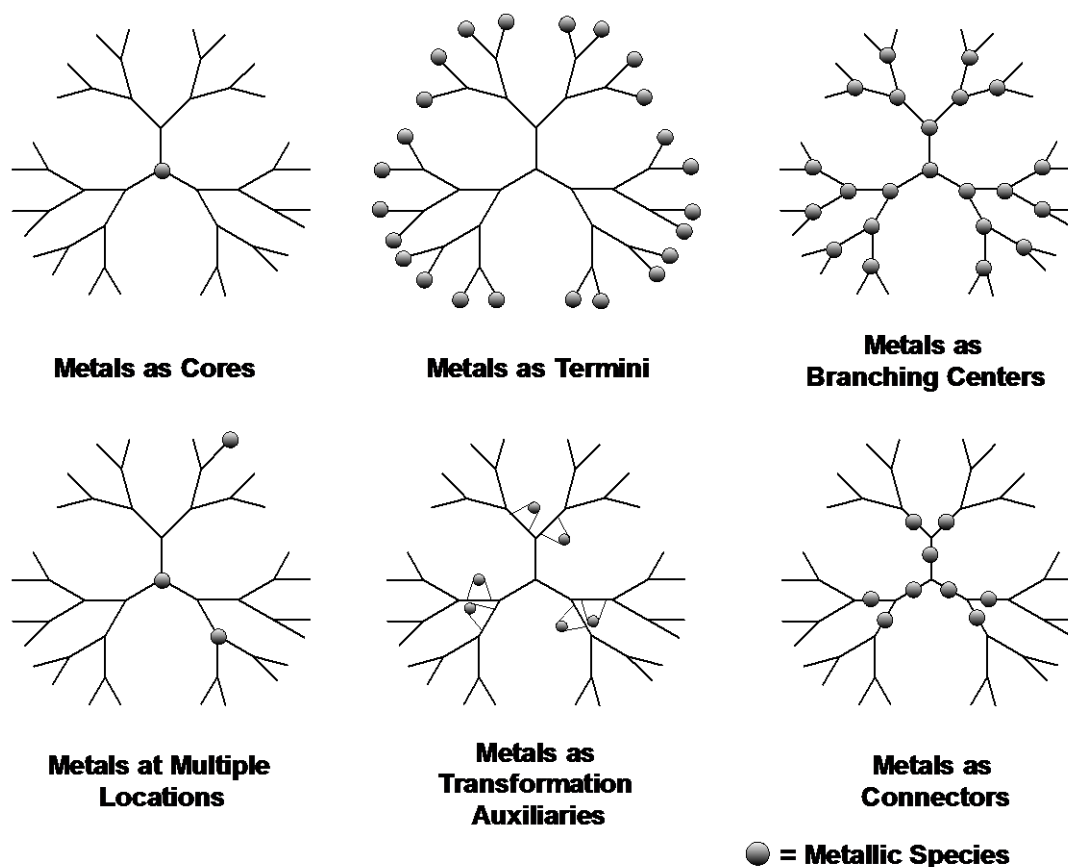
Figure 1.1 The different roles metals can play in metallodendrimers [7].

Hoveyda and his group reported the synthesis and application of two efficient and recyclable Ru-based metathesis catalysts based on a four-directional Si-centered dendrimer scaffold and is shown in Figure 1.2 [19]. Ring-closing metathesis of $TsN(CH_2CH=CH_2)_2$ using a 5 mol % of Ru-based dendritic catalyst **1** was reported to proceed at 99 % conversion. After recovery of the catalyst however a 13 % Ru loss was observed. Continuous use yielded 91 % conversion of $TsN(CH_2CH=CH_2)_2$ with the high activity being attributed to the release of a highly active

Chapter 1: An Introduction to Heterogenized Transition Metal Catalysts

monophosphine Ru complex into solution. This monophosphine complex is thought to be stabilized by the styrenyl ether ligand arm of the dendrimer.
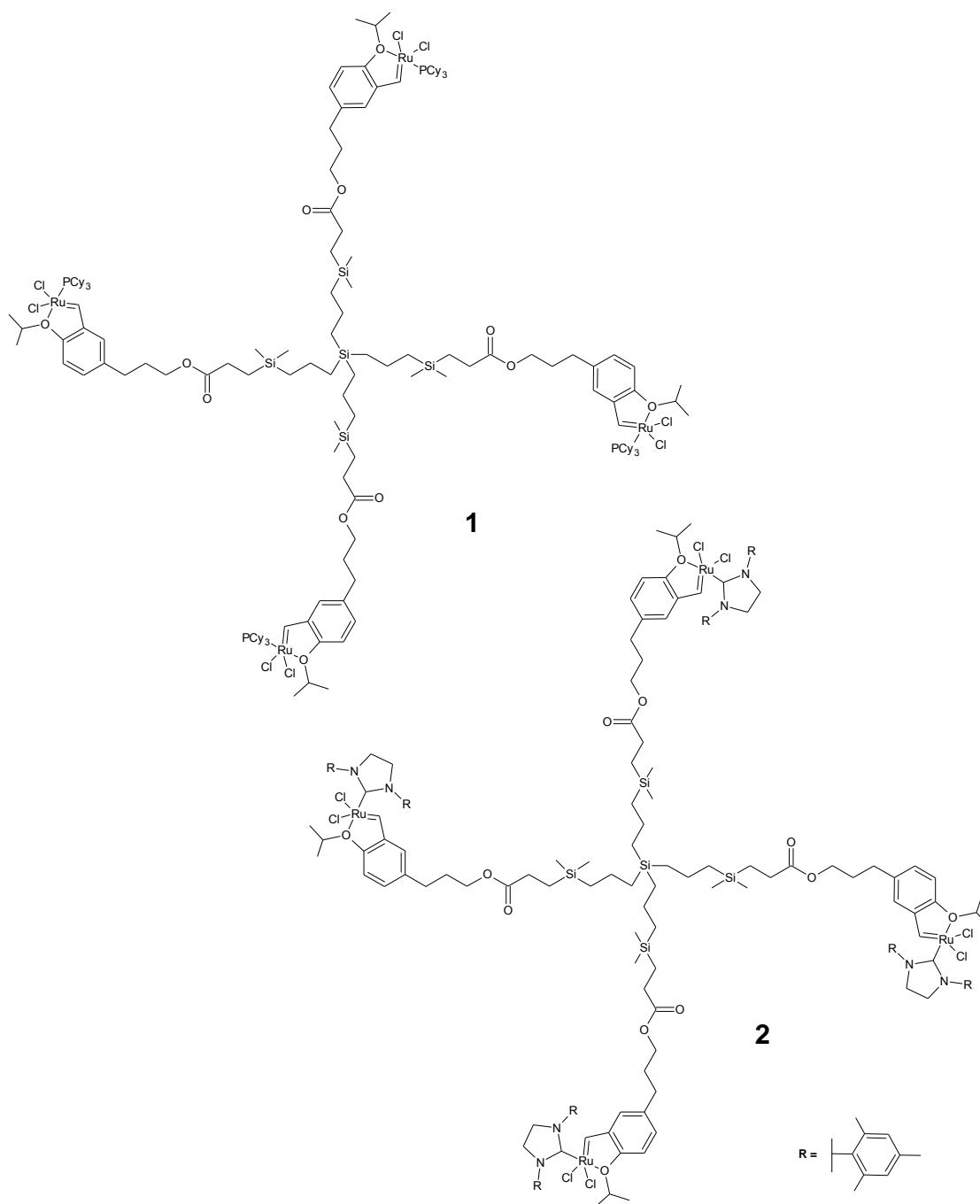
Figure 1.2 Ru-based dendritic metathesis catalysts designed by Hoveyda *et al.* [19].

Chapter 1: An Introduction to Heterogenized Transition Metal Catalysts

An analogous metallodendrimer **2** was also prepared where the phosphine ligand was replaced with an N-heterocyclic carbene ligand similar to that used in Grubbs generation 2 catalysts. This catalyst showed increased activity when compared to the former and was also found to be able to catalyze tandem ring-opening and-closing metathesis and could be more readily separated from reaction mixtures due to its high polarity and molecular weight.

The high loading capacity and uniformity are two of the advantages that make dendrimers attractive materials for catalyst supports. The former allows dendrimers to carry and store a wide range of metals, organic and inorganic molecules by either encapsulation or adsorption. The synthetic process to produce dendrimers in itself results in supports with uniform sizes, ability to incorporate well defined surface functionalities and to limit the formation of impurities. The relatively large size of dendrimers allows separation from a reaction mixture after a catalytic run by micro filtration techniques. Although this allows for the separation of the dendrimeric catalysts from the reaction mixture it still is not as easy as filtering a solid from a slurry. The correct molecular weight cutoff membrane filters are required for different supported catalysts to allow for efficient separation. This potentially is one of the drawbacks associated with the use of dendrimers as catalyst supports when compared to a discrete heterogeneous catalyst which can be filtered and separated from the reaction mixture by conventional filtration techniques.

1.2.2 Polymeric supports

Probably the best known example of the utilization of a polymer as a support for synthesis is the Merrifield resin reported by Merrifield and his group in the 1960's (Figure 1.3). This chloromethylated polystyrene polymer was employed as a heterogeneous support for solid-phase peptide synthesis and since then the field has expanded exponentially. Not only has polymers been found to be effective as supports for solid-phase synthesis but has also found application in the fields of reagent and catalyst immobilization. Polymers are attractive for use as catalyst support materials mainly because of the relative ease of synthesis and incorporation of functional groups needed for catalyst incorporation [20].

The integration of a molecular catalyst and polymeric material can be achieved by either coupling appropriately functionalized metal containing complexes with the support material

Chapter 1: An Introduction to Heterogenized Transition Metal Catalysts

making use of synthetically introduced functional groups on the surface of the polymer or by complexing metals salts with chelating groups built into the polymer backbone. A third method involves physically trapping catalytic species in the polymer by encapsulation.

3
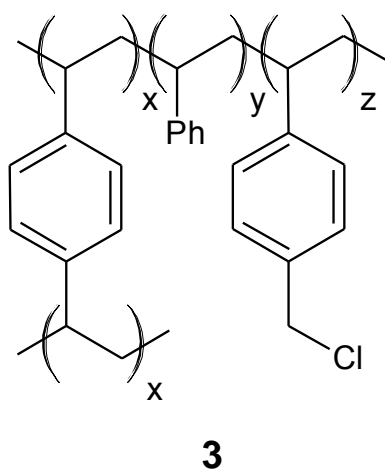
Figure 1.3 A simplified representation of a Merrifield resin [20].

1.2.2.1   Functionalized organic polymers

Various organic polymers have been employed as support materials for catalysis. Polyalkenes, polyisobutylene, poly(styrene-*co*-maleic anhydride), polyacrylates and polyacrylamides are just a few examples found in literature [20]. The possibilities of functionalizing polymers are essentially endless with the basic polymer backbone staying intact with the modification of incorporated functional groups providing coordination sites for metal centers.

An example of this is a supported Pd(dibenzylideneacetone)(triarylphosphine) catalyst **4** shown in Figure 1.4. This "heterogeneous" homogeneous catalyst was prepared by the reaction of a commercially available Tentagel-supported phosphine with Pd$_2$(dibenzylideneacetone)$_3 \cdot$CHCl$_3$ in toluene as solvent. This system was applied as a catalyst for the cyclo-isomerization of 1,6-enynes in water. The reaction occurred in the polystyrene portion of the resin caused by the diffusion of the hydrophobic substrates into the polymer backbone of the resin. Products remained entrapped throughout the reaction and were only recovered after the reaction was

complete. Recovery of the products involved washing of the filtered polymer with supercritical carbon dioxide affording the products as well as the catalyst which could be reused without a drop in activity [21].
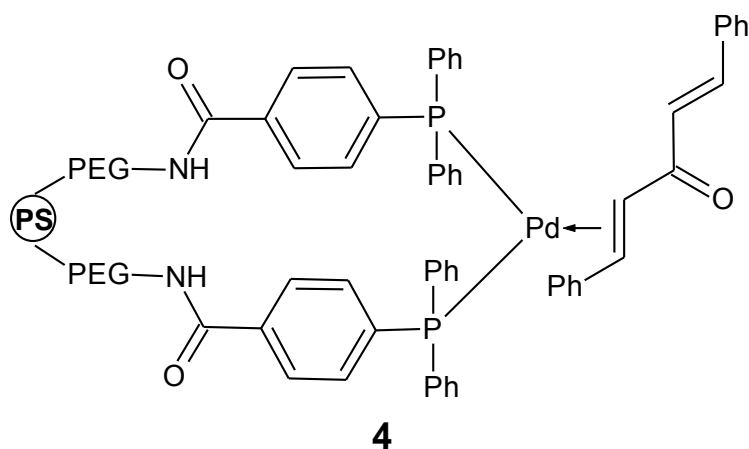
Figure 1.4 Tentagel supported Pd(dba)(triarylphosphine) catalyst [21].

1.2.2.2   Porous organic polymers

Porous organic polymers (POPs) are amorphous, microporous organic polymers synthesized from catalytically active molecular building blocks. Although these materials are easily synthesized they are however ill-defined and have non-uniform pores which make their catalytic behavior more difficult to control and understand. What makes POPs so attractive though is that the catalytically active species can be introduced with relative ease during or after the synthesis of the material. Homogeneous catalysts can be introduced as a polymer building block during the synthesis while other materials allow the post-synthetic modification to create the heterogenized catalyst. Metal nanoclusters or nanoparticles can also be stabilized and encapsulated in the pores of POPs [22].

McKeown *et al.* developed a contorted tetrahedral co-monomer strategy for the synthesis of microporous porphyrin network polymers from 5,5`6,6`-tetrahydroxy-3,3,3`3`-tetramethyl-1,1`-spirobisindane and a preformed fluoro functionalized porphyrin (Scheme 1.3). This iron-

Chapter 1: An Introduction to Heterogenized Transition Metal Catalysts

containing polymer **5** is formed by linking the metalloporphyrin and the spiro co-monomer through a C-C-bonded dibenzodioxane unit [23]. The surface area of the formed compound **5** was found to be between 900 and 1000 cm^2g^{-1} and successfully catalyzed the oxidation of hydroquinone at a rate of 64 mol.cat^{-1} which was better than a similar homogeneous catalyst (43 mol.cat^{-1}).

(i) K_2CO_3, NMP, 170 °C, 5 h
(ii) $FeCl_3$, NMP, 120 °C, 24 h

5
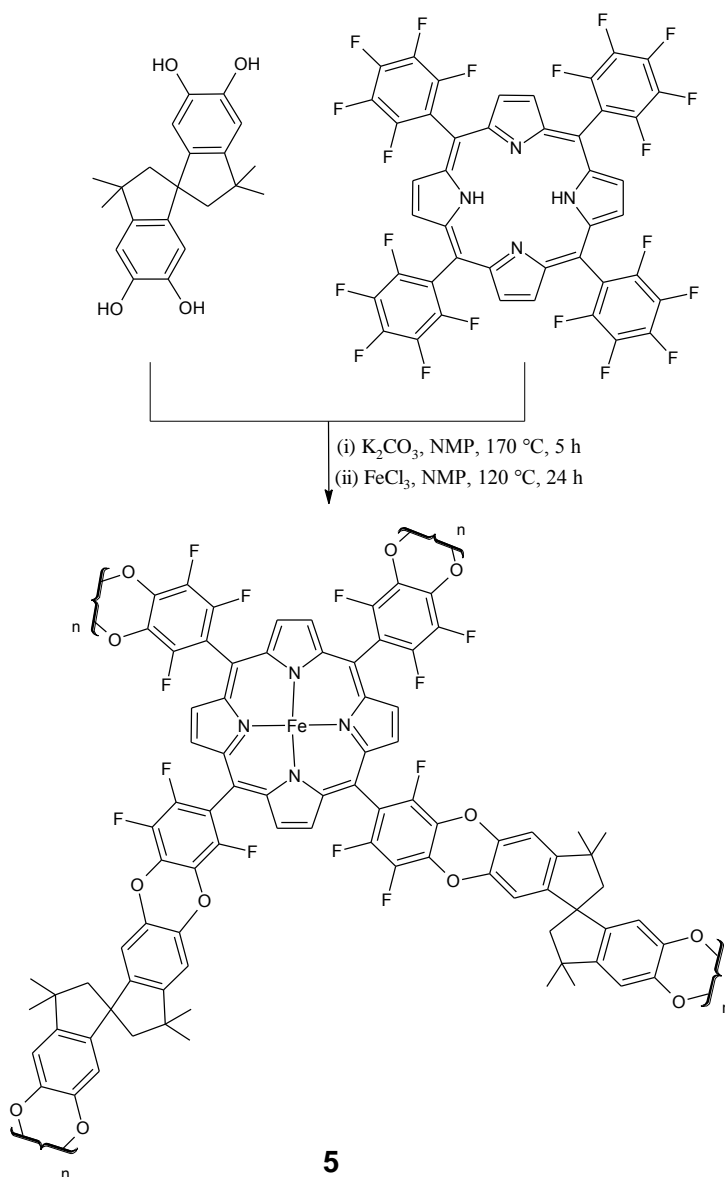
Scheme 1.3 Synthesis of an iron porphyrin-based network from a spiro-bis-indane and a preformed fluorinated porphyrin to form compound 5 [23].

Chapter 1: An Introduction to Heterogenized Transition Metal Catalysts

1.2.2.3   Polymer encapsulated catalysts

Metal centers can also be incorporated into the polymer itself, instead of being tethered to the polymer through a functional group. Catalysts can be physically enveloped by the polymer backbone and stabilized by the interaction between π electrons of the benzene rings of the polystyrenes in the backbone and the vacant orbitals of the catalysts. Kobayashi *et al.* reported the encapsulation of Sc, Os, Pd and Ru catalysts that were successfully applied as heterogeneous catalysts for various reactions with good activity and recyclability without any loss of activity [14].

Nagashima and his group reported the encapsulation and application of a ruthenium cluster, $(\mu_3,\eta^2,\eta^3,\eta^5$-acenaphthylene)-$Ru_3(CO)_7$, for the reduction of carboxamides with polymethyl-hydrosiloxane. This polymer encapsulated ruthenium cluster allowed the successful separation of the catalyst as well as the silicone byproducts from the reaction mixture after a catalytic run. The procedure for the synthesis of such a system is shown in Scheme 1.4 below and involves the reduction of the amides in the presence of a polymer-reducing agent containing Si-H groups (polymethylhydrosiloxane) and the catalytically active ruthenium-cluster which affords the desired amines.   During the reaction the ruthenium catalyzes the cross-linking of the polymethylhydrosiloxane resulting in the formation of a polymer gel.
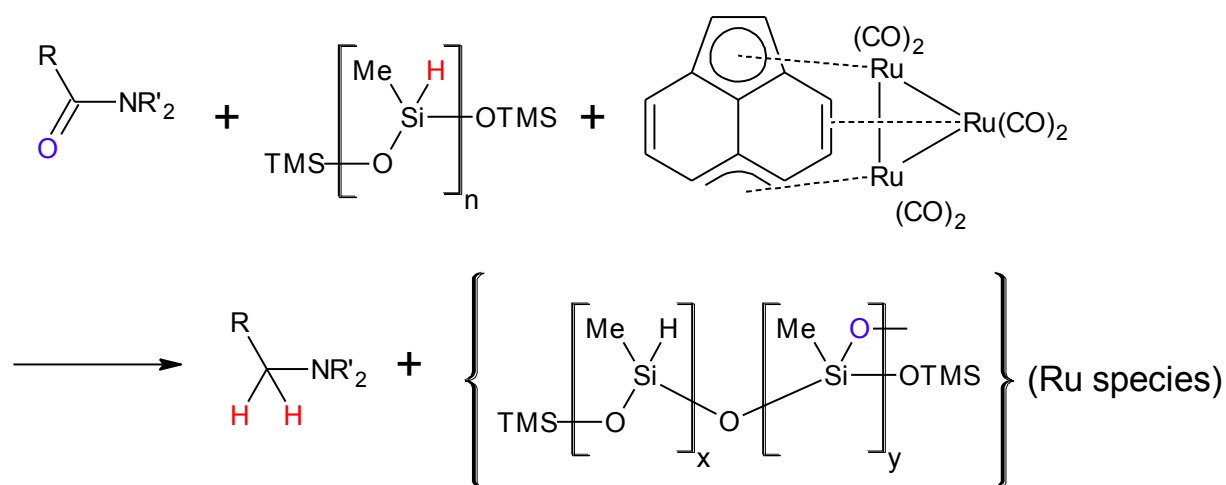
Scheme 1.4   The catalytic reduction of amides affording amines and a polymer encapsulated ruthenium catalyst [24].

Chapter 1: An Introduction to Heterogenized Transition Metal Catalysts

This ruthenium encapsulated polymer gel can then be readily separated from the reaction mixture affording the amines and encapsulated catalyst. Further catalytic runs using the encapsulated catalyst could then be carried out with relatively low leaching of ruthenium into the reaction mixture [24].

1.2.3   Inorganic supports

Inorganic supports are usually preferred over organic supports due to their higher thermal stability. Porous materials are classified into several types based on their physical composition and pore sizes. High surface areas and large pore sizes are of great importance when selecting a material to act as carrier or support for a catalyst. In Table 1.2 the different classes of porous materials based on their pore sizes, together with some examples of each class, are listed. By definition microporous materials have pore sizes <2 nm, mesoporous materials have pore sizes in the range of 2-50 nm and macroporous materials have pore sizes in excess of 50 nm.

Table 1.2 Pore sizes of typical porous inorganic materials [25,26-29].

Classification	Definition	Examples	Actual pore size
Microporous	<2 nm	Zeolites	<1.4 nm
		Metal-Organic Frameworks (MOFs)	<1.7 nm
Mesoporous	2-50 nm	MCM-41	1.5-10 nm
		SBA-15	3.6-12 nm
		Aerogels	>10 nm
Macroporous	>50 nm	Glasses	>50 nm

1.2.3.1   Metal–organic frameworks (MOFs)

Metal-organic frameworks, also known as coordination polymers, are a relatively new class of material that finds widespread application in gas storage and heterogeneous catalysis. Some of the earliest reports of compounds that today would be considered as MOFs were however reported by Tomic and his group as early as 1965 [30]. MOFs consist of metal ions or clusters that are coordinated to organic molecules to form highly crystalline and porous materials with very high surface areas (Figure 1.5).
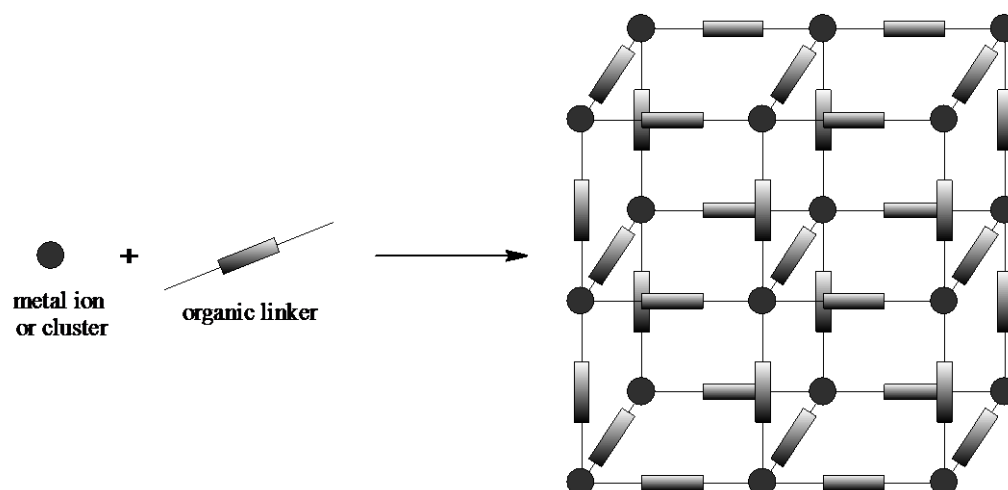
Figure 1.5 Schematic representation of the synthesis of a MOF.

MOFs are easily synthesized by making use of highly soluble metal salts (metal nitrates, sulfates or acetates) and organic moieties which are mostly mono-, di-, tri- and tetracarboxylic acids. These metal and organic components, which act as building blocks for MOF-synthesis, are reacted with each other in polar organic solvents (amines or amides) followed by the self-assembly at different temperatures [31,32].

MOFs have found widespread application in the fields of gas storage, gas separation and gas purification. Properties that make them suitable for this type of application is their high porosity and lack of hidden volumes (dead volume) which makes them perfect candidates for volume specific applications in gas related fields [31]. The absence of so called 'dead volume' and high

Chapter 1: An Introduction to Heterogenized Transition Metal Catalysts

concentration of catalytic active sites in MOFs makes them attractive alternatives for heterogeneous catalysis. Catalytic sites can be introduced into the structure of a MOF at the organic linkers connecting the metal nodes or by encapsulation of the catalytically active species into the pores. Another method to incorporate a catalytic species into the MOF framework is via the modification of the linker moiety post-synthetically by the reaction with an appropriate metal salt [32]. A 3D representation of different MOFs, as summarized by Broom *et al.*, is shown in Figure 1.6 [33].

Numerous examples of MOFs and their application as catalysts are available in the literature and the review by Ulrich Müller *et al.* probably serves as the best summary for most types of MOFs being applied as catalysts [31].
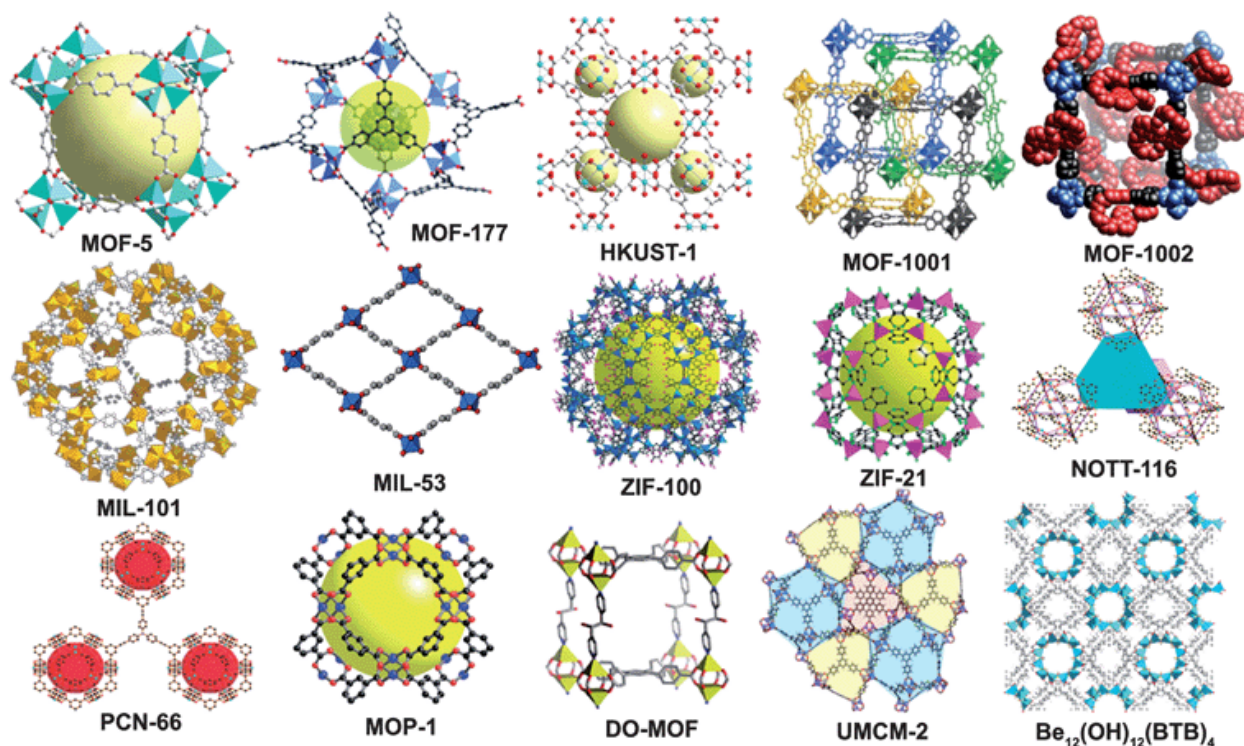
Figure 1.6 The 3D structures of representative MOFs as summarized by Broom *et al.* [33].

Chapter 1: An Introduction to Heterogenized Transition Metal Catalysts

1.2.3.2   Ordered mesoporous materials

Ever since the synthesis of a new family of mesoporous silicate/aluminosilicate molecular sieves designated as M41S by Beck and his group at the Mobil Research and Development Corporation in 1992, the field of mesoporous silicate synthesis has grown significantly. MCM-41 (Mobil Crystalline Material), probably one of the most well-known and widely studied silicate materials of this family, exhibited a hexagonal array of uniform mesopores in which pore sizes ranged in diameter from 15 Å to more than 100 Å [25]. SBA-15 (Santa Barbara University) and MSU-X (Michigan State University) materials soon followed with both expanding the field dramatically [34,35].

These materials have received considerable attention mainly because of their high surface areas, large pore volumes and the well-ordered arrangement of their uniformly sized mesopores which make them suitable candidates for use as inorganic catalyst supports [26]. The general procedure for the synthesis of these newly discovered mesoporous M41S materials were achieved by the combination of appropriate amounts of a templating agent (surfactant), a silica source, a base and water.   Examples of these materials are tetraethylortosilicate (TEOS) as silica source, cetyltrimethylammonium bromide (CTAB) as surfactant and sodium hydroxide as base. For the synthesis of SBA-type materials acidic conditions were employed instead of the basic conditions needed for MCM-type materials together with the use of a different templating agent (triblock co-polymer). By adjusting the ratios of reactants and pH of the reaction mixture the physical properties of these mesoporous materials can be fine-tuned to afford materials with varying pore sizes and surface areas.

Various mechanisms for the formation of these mesoporous materials employing the above mentioned synthetic procedure are proposed. The liquid templating (LCT) mechanism was proposed by the Mobil researchers who were responsible for the synthesis of M41S class of mesoporous materials. The general mechanism for the formation of MCM-41, which falls in this class, is shown in Scheme 1.5.

Firstly the templating agent arranges to form micelles, with the hydrophobic part of the surfactant arranging towards the inside of the micelle and the hydrophilic part towards the outside. These micelles then arrange to form micellar rods followed by the arrangement of these micellar rods to form a hexagonal array.

Chapter 1: An Introduction to Heterogenized Transition Metal Catalysts
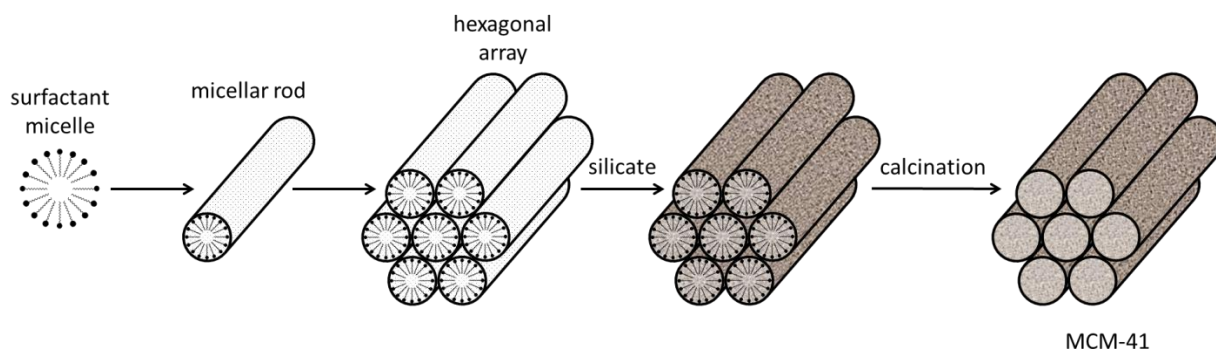
Scheme 1.5 Mechanism for the formation of MCM-41 [26,36].

At this stage the silica source, like TEOS, is introduced which now forms a layer around this hexagonal array.   After removal of the templating agent through calcination the open mesoporous MCM-41 framework remains [26,36].

1.2.3.2.1   Periodic mesoporous materials

Periodic mesoporous materials (PMOs) are crystalline porous materials with a homogeneous distribution of functional organic groups within the structured mesoporous material and therefore consist of both inorganic and organic fragments. In Scheme 1.6 a representation for the general synthesis of PMOs by employing an appropriate organic-inorganic precursor $(R`O)_3SiRSi(OR`)_3$ in the presence of surfactants that act as templates to form structured mesoporous hybrid materials is shown [37,38]. This method is in contrast with the grafting of homogeneous catalysts on the surface of the inorganic support material through a suitable linker which is the better known and more widely studied method of inclusion of homogeneous catalysts into mesoporous support materials.
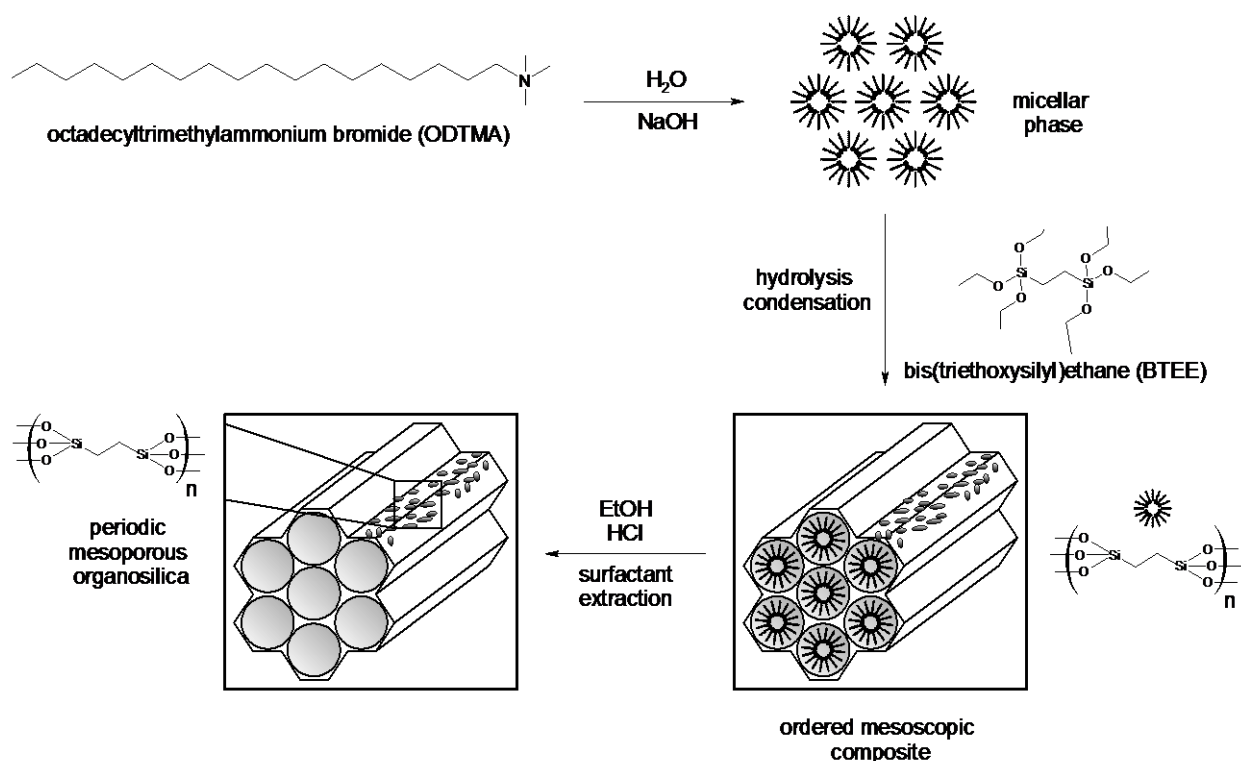
Scheme 1.6   The self-assembling procedure to obtain PMOs in the presence of surfactants [37].

1.2.3.2.2   Grafting of molecular catalysts onto mesoporous materials (heterogenization)

Several reports on the immobilization of molecular catalysts onto a solid support like MCM-41 or SBA-15 are available in literature and all of them have one thing in common, the utilization of an appropriate functionality on the molecule/catalyst used for immobilization. For a catalyst to be immobilized to a silica support it should be compatible with the free silanol groups present on the surface of the support. Ramírez *et al*. showed that the types of silanols present on the silica surface depended on the way in which the surfactants were removed from the mesoporous silica after its synthesis, e.g. calcination. This calcination process could result in the formation of either single, hydrogen bonded or geminal silanol groups on the surface of the support as shown in Figure 1.7 [39]. Molecular catalysts functionalized with either ethoxy or methoxy siloxane functional groups can be reacted and tethered onto the surface of the support through the condensation of these surface silanols and the ethoxy/methoxy moieties.
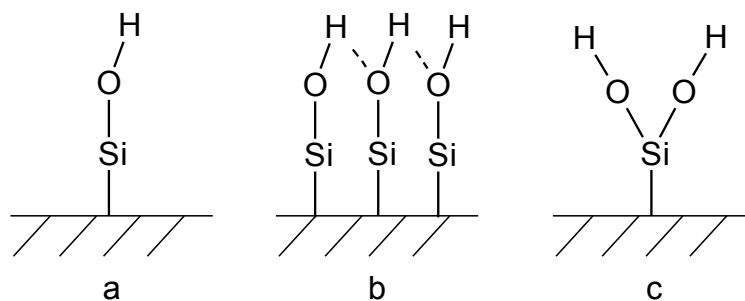
Figure 1.7   Different silanol groups on the surface of a silica support: (a) single, (b) hydrogen bonded and (c) geminal silanol groups [39].

The heterogenization of molecular homogeneous catalysts onto inorganic silica supports can be achieved through two distinctly different methods very similar to the divergent and convergent synthesis techniques employed for the assembly of dendrimers. The one method involves the complete synthesis and full characterization of the required complex with the functional group necessary for immobilization incorporated into the ligand of the complex. Immobilization of this complex onto the support is known as convergent immobilization. The second method entails the sequential building of the complex molecule onto the support starting first with the immobilization of the ligand followed by reaction with the required metal salt.

1.2.3.2.2.1   Sequential immobilization

Sequential immobilization, as stated earlier, involves the synthesis of the immobilized ligand through solid-state synthesis before it is reacted with the appropriate metal salt to form the immobilized catalyst. In Scheme 1.7 the synthesis of heterogenized Pd and Ni catalysts is shown.   Supported ligands were obtained by refluxing an appropriate precursor, 3-(triethoxysilyl)propyl isocyanate, and the respective support in toluene for 16 hours.

Chapter 1: An Introduction to Heterogenized Transition Metal Catalysts
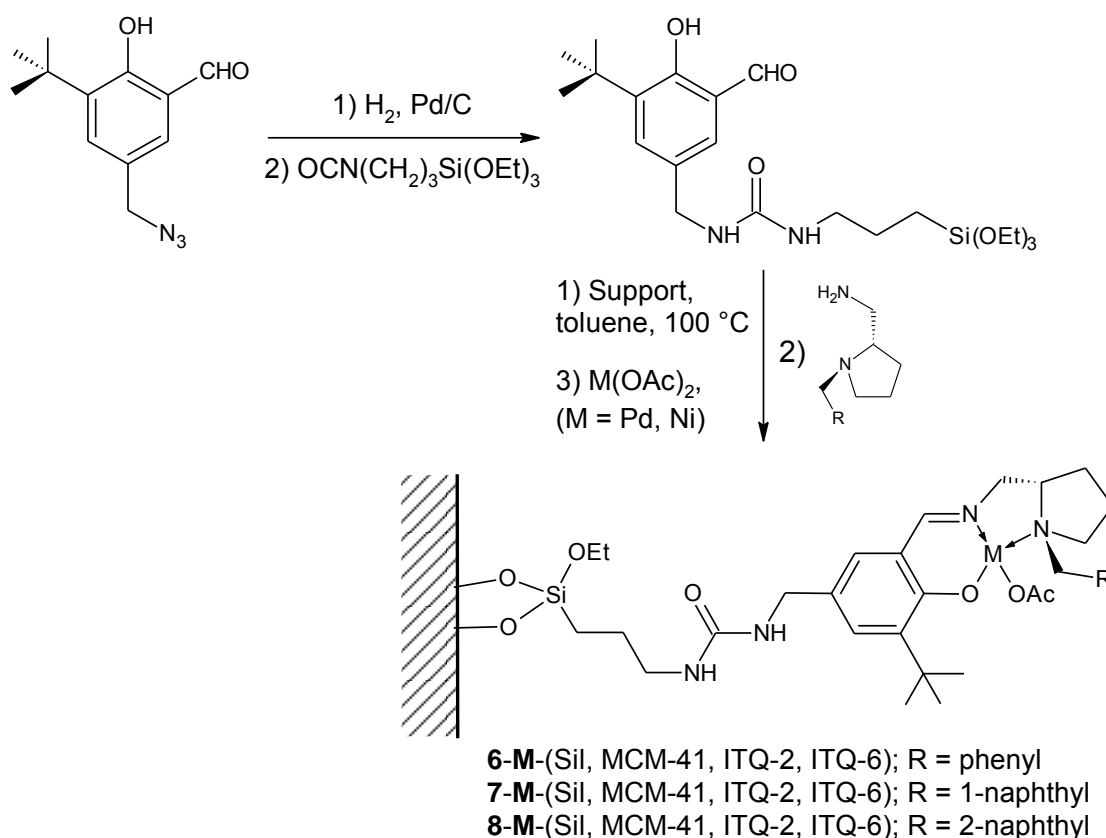
Scheme 1.7 Sequential synthesis of heterogenized ligands and Pd and Ni complexes 6-8-Pd and 6-8-Ni [40].

These anchored aldehyde-functionalized ligands were subsequently reacted with an equimolar amount of (S)-(N-benzyl-2-pyrrolidinyl) methylamine, (S)-[1-(1-naphthylmethyl)-2-pyrrolidinyl] methylamine or (S)-[1-(2-naphthylmethyl)-2-pyrrolidinyl] methylamine to afford the supported chiral Schiff base ligands. These supported ligands were then complexed with either Pd(II) or Ni(II) acetate salts to afford corresponding immobilized catalysts **6-8-**Pd and **6-8-**Ni [40].

Although this method of heterogenization seems fairly straight forward it does however pose a problem that it is not possible to know if all of the metal salt reacts and is coordinated to the nitrogen-chelating ligand or if it is just simply physically adsorbed directly on the surface of the support or in the pores. This makes it difficult to fully characterize the catalyst and prove whether the catalysis is facilitated by the discretely immobilized metal complex or the free metal salt adsorbed onto the surface of the support. For this reason the sequential immobilization

approach was not considered for this project. The convergent approach was chosen for our study because it involves the synthesis and full characterization of the so called functionalized complex before immobilization onto the support.

1.2.3.2.2.2   Convergent immobilization

Convergent immobilization entails the synthesis and full characterization of the metal complex followed by the immobilization onto the support through an appropriate functional group incorporated into the ligand of the complex as is shown in Scheme 1.8. This example was reported in a review by Hutchings and his group [41].

After the successful synthesis and characterization of the complex, immobilization can be accomplished by the condensation of the incorporated ethoxy/methoxy functionality with the free surface silanol groups on the silica support. All of the active metal species is now associated with the discrete metal complex and one can assume with a high level of certainty that no uncoordinated metal is present on the surface of the support material.
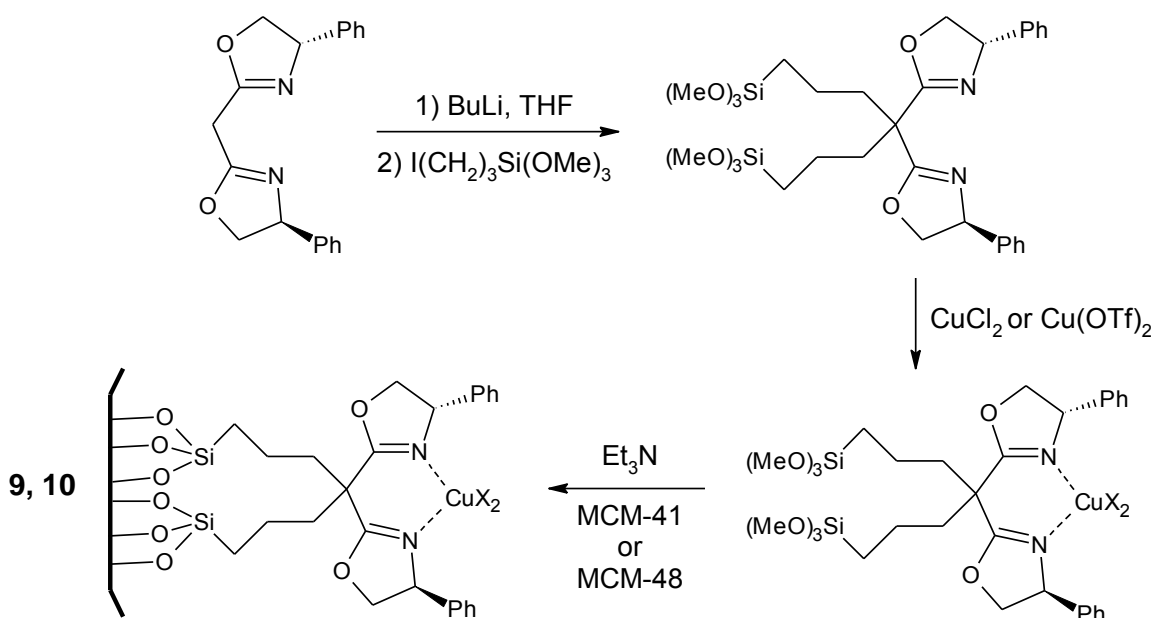
Scheme 1.8   Convergent immobilization of chiral copper(II) bisoxazoline onto MCM-41 and MCM-41 for the enantioselective cyclopropanation of styrene [41].

Chapter 1: An Introduction to Heterogenized Transition Metal Catalysts

1.2.3.2.3   Application of different mesoporous supported catalysts in catalysis

Qi and his group recently reported the synthesis of mesoporous silica-supported copper catalysts and their application for the homocoupling reaction of terminal alkynes at room-temperature [42]. Their system (divergent synthesis) involved the functionalization of the surface of SBA-15 with (3-chloropropyl)trimethoxysilane followed by reaction of the functional group with either triethylenediamine or 1,4-diaza-bicyclo-[2.2.2]octan-2-ylmethanol. Upon the reaction of these silica supported ligands with CuCl in acetone they were able to isolate SBA-15@OAmine-Cu (**11**) and SBA-15@Amine-Cu (**12**) respectively (Scheme 1.9). These systems were found to be very active catalysts for the homocoupling of terminal alkynes and in some cases were found to be more active than the homogeneous analogues reported in literature. The recyclability of both catalysts was evaluated by recovery of the catalysts from the initial coupling reactions of phenyl acetylene.

Further runs, under the exact same reaction conditions, were carried out to evaluate the activity of the catalysts after each recovery attempt. Even after 4 runs a yield of 81 % and 76 % respectively was obtained for the catalysts after a 4 h period (Table 1.3).

Table 1.3 Recycling study of SBA-15@Amine-Cu (12) catalyst [42].
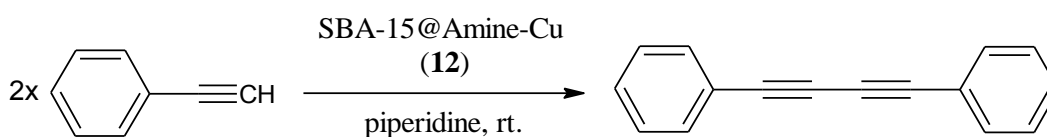
Run	1	2	3	4	5	6
Yield^b (%)	100	97	90	81 (85^d)	68 (73^e)	63 (68^f)
Yield^{b,c} (%)	100	91	55	76 (82^d)	61 (65^e)	-

[a] Reaction conditions: substrate (0.5 mmol), SBA-15@amine-Cu (5 mol %) and piperidine (2.5 mL) at room temperature under air; [b] Determined by GC using biphenyl as internal standard; [c] SBA-15@Oamine-Cu (5 mol %) as the catalyst; [d] 6 h; [e] 8 h; [f] 12 h.

Chapter 1: An Introduction to Heterogenized Transition Metal Catalysts
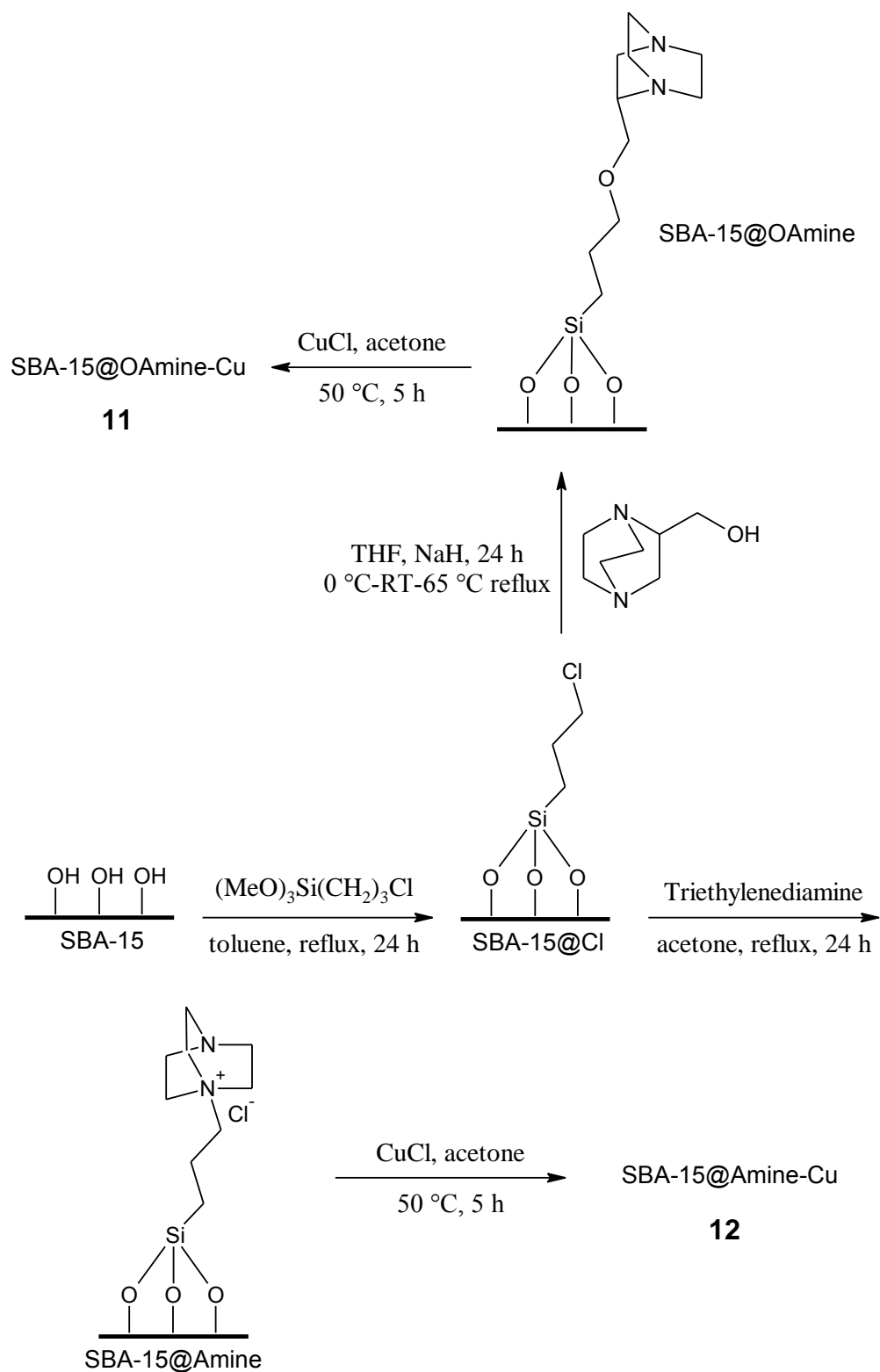
Scheme 1.9   Procedure for the preparation of SBA-15@OAmine-Cu (11) and SBA-15@Amine-Cu (12) [42].

Chapter 1: An Introduction to Heterogenized Transition Metal Catalysts

The heterogenization of functionalized Cu(II) and VO(IV) Schiff base complexes of the type [M(N$_2$O$_2$), M=Cu or VO] by direct immobilization onto amino-modified SBA-15 [(3-aminopropyl)trimethoxysilane] and their application as styrene oxidation catalysts have been reported by Kan *et al* [43]. Two discretely different tethering techniques were employed for the heterogenization of the Cu(II) and VO(IV) (**13** and **14**) systems respectively (Scheme 1.10). Although these systems showed a decrease in activities for the oxidation of styrene after the first recycling run, VO–Salen–SBA catalyst showed high activity with 78.6 % conversion of styrene being observed after 8 h (TOF 63.0 h^{-1}), while the fresh Cu–Salen–SBA catalyst showed lower activity with 26.9 % conversion after 8 h (TOF 37.4 h^{-1}), an increased activity was observed when comparing the immobilized systems to their homogeneous counterparts under the exact reaction conditions. The VO–Salen–SBA catalyst could however be recycled for up to 4 runs with no real leaching of the vanadium into the reaction medium being observed.
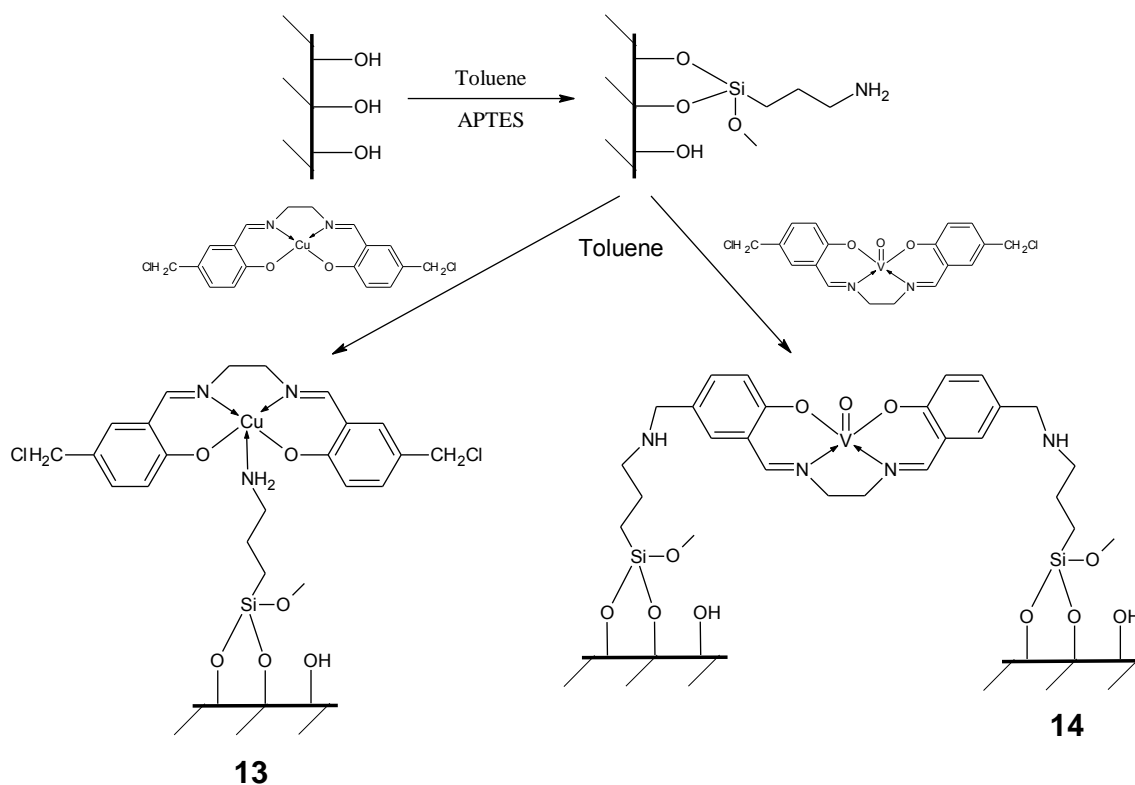
Scheme 1.10 Schematic outlines of syntheses of anchored metal complexes of copper(II) and oxovanadium(IV) 13 and 14 [43].

Chapter 1: An Introduction to Heterogenized Transition Metal Catalysts

Both examples discussed above made use of the divergent synthetic procedure whereby the support is modified with either amine or chloro functionalities by reaction of the native support with an appropriately functionalized ethoxy/methoxy linker molecule. The following example involves the synthesis of an ethoxy/methoxy functionalized complex followed by coupling to the support material.

Sánchez *et al.* reported unsymmetrical pincer-type complexes of rhodium and gold which showed high activity towards the hydrogenation of alkenes such as (E)-diethyl 2-benzylidene succinate and diethyl itaconate (Scheme 1.11) [44]. TOFs in excess of 3000 h^{-1} for the hydrogenation of [(E)-diethyl 2-benzylidene succinate could be achieved under 4 atmospheres of pressure. Even higher TOFs were obtained for the hydrogenation of diethyl itaconate (>25000 h^{-1}). Compared to their homogeneous counterparts (500 h^{-1} and 3500 h^{-1} respectively) the immobilized systems were far superior with increased selectivity and activity relative to the homogeneous unsupported counterparts being observed throughout. Successful recovery of catalyst **16** was achieved with almost no drop in the activity or *ee* being observed after 4 recycling runs.
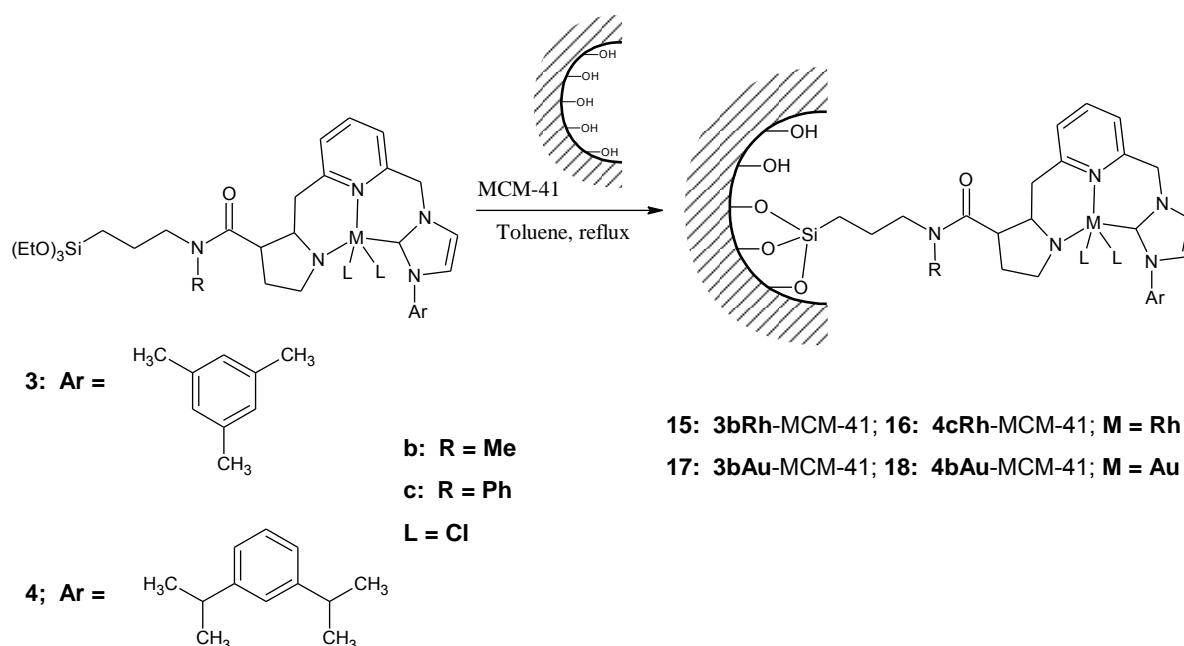
Scheme 1.11 Immobilization of rhodium and gold pincer-type complexes on MCM-41 [44].

Chapter 1: An Introduction to Heterogenized Transition Metal Catalysts

1.2.3.2.4   Other applications of mesoporous materials

Mesoporous materials have found application in other fields of chemistry and are not only limited to use as catalyst supports. Their high surface areas, thermal stability, organized porous structure and ease of surface modification make them suitable materials for use as stationary phases for HPLC columns [36,39]. Bioactive molecules can be supported on silica materials making use of similar methods employed for the immobilization of catalysts. These have been applied in protein sequestration and release, enzyme immobilization and drug delivery. Silicates find widespread application as materials for controlled drug delivery because they are biocompatible and inert in the human body [45-47].

1.3   Concluding remarks

Although dendrimers have numerous advantages as scaffold for the stabilization of metal centers used as catalysts the major drawback is still the need for ultrafiltration techniques using membranes with certain molecular cutoffs. The advantage of a true heterogeneous catalyst is the presence of discrete phases which allows for the separation of the catalyst from the reaction mixture by normal filtration techniques.

Although polymer supports provide multiple sites and possibilities to incorporate molecular catalysts into the structure the thermal stability still remain lower than that of inorganic support materials like mesoporous silicas for instance.

The high surface areas of metal organic frameworks' (MOFs) coupled with the high concentration of catalytic active sites makes these materials viable as heterogeneous catalysts but these materials have yet to really find industrial application.

Mesoporous supports have a major advantage compared to other systems namely its high surface areas which are available for functionalization thus allowing incorporation of possible catalysts. High thermal stability coupled with the ease of synthesis and ease whereby complexes can be tethered to the surface makes mesoporous supports very attractive materials for catalysis.

The most important feature of the complex to be immobilized is the presence of the appropriate functional group, be it an ethoxy or methoxy moiety. It is very important that the incorporation of this functionality can be done easily and in high yields to afford the appropriate functionalized ligand for complex synthesis.

Schiff base ligands have for a number of years now been popular among coordination chemists due to their ease of synthesis and modification to incorporate steric or electronic substituents. The imine, formed during Schiff base condensation, is a relatively soft donor and stabilizes lower oxidation states of transition metals effectively. These factors are the reasons why Schiff bases have such a rich coordination chemistry which involves a wide range of metals in the periodic table. Complexes of Schiff bases have found application in organic synthesis, as anticancer agents and molecular switches to name a few [48].

1.4 Project objectives

The selection of an appropriate ligand system and support is essential for the successful synthesis of an immobilized catalyst. For our study MCM-41 and SBA-15 were selected as solid supports for the targeted immobilization of cationic Ru(arene) compounds. The use of Schiff base ligands allow us to modify and incorporate the required functionalities needed for immobilization as well as instilling steric bulk and/or electronic properties in the ligand close to the metal center. The absence in literature of tethered Ru(arene)-type compounds have sparked our interest to synthesize a range of new RuCl(arene)(N,N) complexes and to successfully immobilize these onto silica supports and evaluate these as catalyst precursors for organic transformations. Recovery of the catalyst was also an important focus. Immobilization through a conventional siloxane tether via the imine as well as a novel siloxane tether via the arene ring are investigated. Comparison of the effect of these methods of immobilization on the activity and stability of the resultant catalysts would provide insight into the effect the tethering has on the supported catalyst. Two different catalytic processes were investigated viz. the transfer hydrogenation of ketones and the oxidative cleavage of alkenes. Immobilized systems were recycled to determine to what extent the catalyst could be reused for further runs. The effect of the support material on the activity of the catalyst precursors were also investigated.

Chapter 1: An Introduction to Heterogenized Transition Metal Catalysts

Chapter two describes the synthesis and characterization of siloxane functionalized RuCl(*p*-cymene)(N,N) complexes with the tether via the imine functionality. The incorporation of the siloxane moiety into the obtained complexes is achieved through Schiff base condensation of an appropriate aldehyde and a siloxane functionalized amine. Ligands and complexes were characterized utilizing several analytical techniques such as infrared (IR) spectroscopy, nuclear magnetic resonance (NMR) spectroscopy, mass spectrometry (MS) and elemental analysis.

The synthesis of novel siloxane functionalized urethane linked RuCl(arene)(N,N) complexes where the siloxane tether is incorporated via the arene ring is discussed in **Chapter three**. This system differs from the one discussed in **Chapter two** in that the position of the siloxane functionality is not incorporated into the Schiff base ligand but rather into the arene ring. Instead of functionalizing the pyridine ligand with a siloxane moiety to incorporate the needed siloxane group into the complex, the siloxane was tethered to the arene ligand coordinated to the ruthenium metal center instead.

The synthesis and characterization of the MCM-41 and SBA-15 immobilized catalysts are described in **Chapter four**. The immobilization of these systems was achieved by the reaction between the siloxane functionalities of the complexes and the free surface silanol groups of the support materials. The immobilized catalysts were characterized by a wide range of solid state techniques which included powder XRD, inductively coupled plasma atomic emission spectroscopy (ICP-AES), nitrogen adsorption/desorption analysis and thermal gravimetrical analysis (TGA) to name but a few.

In **Chapters five** and **six** we discuss the application of these systems, both model and immobilized, in the oxidative cleavage of alkenes to form aldehydes and/or carboxylic acids as well as the catalytic transformation of ketones to alcohols (transfer hydrogenation). Comparison between the model and heterogenized systems in terms of activity and selectivity as well as possible recovery of the immobilized catalysts are discussed in detail. The influence of the support material on the activity of the catalyst is also covered.

1.5   References

1.   S. Schneider, W. Bannwarth, *Angew. Chem. Int. Ed.*, **2000**, 39, 4142.

2.   C.C. Tzschucke, C. Markert, W. Bannwarth, S. Roller, A.Hebel, R.Haag, *Angew. Chem. Int. Ed.*, **2002**, 41, 3694.

3.   A. Corma, H. Garcia, *Adv. Synth. Catal.*, **2006**, 348, 1391.

4.   Y-H. Su, *Noble Metals, Intech*, **2012**, 301.

5.   C. Hagelúken, M. Verhelst; *Recycling of precious metal catalysts; ptqcatalysts*, **200**4, 21.

6.   J.A. Gladysz, *Chem. Rev.*, **2002**, 102, 3215.

7.   S-H. Hwang, C.D. Shreiner, C.N. Moorefield, G.R. Newkome, *New J. Chem.*, **2007**, 31, 1192.

8.   R. van Heerbeek, P.C.J. Kamer, P.W.N.M. van Leeuwen, J.N.H. Reek, *Chem. Rev.*, **2002**, 102, 3717.

9.   P.A. Chase, R.J.M. Klein Gebbink, G. van Koten, *J. Organomet. Chem.*, **2004**, 689, 4016.

10.   C. González-Arellano, A. Corma M. Iglesias, F. Sánchez, *Adv. Synth. Catal.*, **2004**, 346, 1316.

11.   J.M. Notestein, A. Katz, *Chem. Eur. J.*, **2006**, 12, 3954.

12.   J. Lu, P.H. Toy, *Chem. Rev.*, **2009**, 109, 815.

13.   D.E. Bergbreiter, *Catal. Today*, 1998, 42 ,389.

14.   S. Kobayashi, R. Akiyama, *Chem. Commun.*, **2003**, 449.

15.   A.S.H. King, L.J. Twyman, *J. Chem. Soc., Perkin Trans.*, **2002**, 1, 2209.

16.   D.A. Tomalia, H. Baker, J. Dewald, M. Hall, G. Kallos, S. Martin, J. Roeck, J. Ryder, P. Smith, *Polym. J.*, **1995**, 17, 117.

17.   G.R. Newkome, Z.Q. Yao, G.R. Baker, V.K. Gupta, *J. Org. Chem.*, **1985**, 50, 2003.

Chapter 1: An Introduction to Heterogenized Transition Metal Catalysts

18.   C. Hawker, J.M.J. Fréchet, *J. Am. Chem. Soc.*, **1990**, 112, 7638.

19.   S.B. Garber, J.S. Kingsbury, B.L. Gray, A.H. Hoveyda, *J. Am. Chem. Soc.*, **2000**, 122, 8168.

20.   R.B. Merrifield, *J. Am. Chem. Soc.*, **1963**, 85, 2149.

21.   Y. Nakai, Y. Uozumi, *Org. Lett.*, **2005**, 7, 291.

22.   P. Kaur, J.T. Hupp, S.T. Nguyen, *ACS Catal.*, **2011**, 1, 819.

23.   N.B. McKeown, S. Hanif, K. Msayib, C.E. Tattershall, P.M. Budd, *Chem. Commun.*, **2002**, 23, 2782.

24.   Y. Motoyama, K. Mitsui, T. Ishida, H. Nagashima, *J. Am. Chem. Soc.*, **2005**, 127, 13150.

25.   J.S. Beck, J.C. Vartuli, W.J. Roth, M. Leonowicz, E. Kresge, C.T. Schmitt, K.D.C. Chu, T-W.D. Olson, H.E. Sheppard, W. McCullen, S.B. Higgins, J.B. Schlenkert, *J. Am. Chem. Soc.*, **1992**, 114, 10834.

26.   J.Y. Ying, C.P. Mehnert, M.S. Wong, *Angew. Chem. Int. Ed.*, **1999**, 38, 56.

27.   A.R. Millward, O.M. Yaghi, *J. Am. Chem. Soc.*, **2005**, 127, 17998.

28.   M. Kruk, M. Jaroniec, *Langmuir*, **1997**, 13, 23.

29.   Y. Wang, M. Noguchi, Y. Takahashi, Y. Ohtsuka, *Catal. Today*, **2001**, 68, 3.

30.   E.A. Tomic, *J. Appl. Polym. Sci.*, **1965**, 9, 3745.

31.   A.U. Czaja, N. Trukhanb, U. Müller, *Chem. Soc. Rev.*, **2009**, 38, 1284.

32.   P. Valvekens, F. Vermoortele, D.de Vos, *Catal. Sci. Technol.*, **2013**, 3, 1435.

33.   Z. Xiang, D. Cao, J. Lan, W. Wanga, D.P. Broom, *Energy Environ. Sci.*, **2010**, 3, 1469.

34.   D. Zhao, Q. Huo, J. Feng, B.F. Chmelka, G.D. Stucky, *J. Am. Chem. Soc.*, **1998**, 120, 6024.

35.   S.A. Bagshaw, E. Prouzet, T.J. Pinnavaia, *Science*, **1995**, 269, 1242.

36.   C.T. Kresge, M.E. Leonowicz, W.J. Roth, J.C. Vartuli, J.S. Beck, *Nature*, **1992**, 359, 710.

37.   F. Hoffmann, M. Cornelius, J. Morell, M. Fröba, *Angew. Chem. Int. Ed.*, **2006**, 45, 3216.

38.   U. Díaz, M. Boronat, A. Corma, *Proc. R. Soc. A*, **2012**, 1.

39.   A. Ramírez, B.L. Lopez, L. Sierra, *J. Phys. Chem. B*, **2003**, 107, 9275.

40.   C. González-Arellano, A. Corma, M. Iglesias, F. Sánchez, *Adv. Synth. Catal.*, **2004**, 346, 1316.

41.   P. McMorn, G.J. Hutchings, *Chem. Soc. Rev.*, **2004**, 33, 108.

42.   H. Li, M. Yang, X. Zhang, L. Yan, J. Li, Y. Qi, *New J. Chem.*, **2013**, 37, 1343.

43.   Y. Yang, Y. Zhang, S. Hao, J. Guaa, H. Ding, F. Shang, P. Qiu, Q. Kan, *Appl. Catal., A*, **2010**, 381, 274.

44.   C. del Pozo, A. Corma, M. Iglesias, F. Sánchez, *Organometallics*, **2010**, 29, 4491.

45.   Y-J. Han, G.D. Stucky, A. Butler, *J. Am. Chem. Soc.*, **1999**, 121, 9897.

46.   J.F. Díaz, K.J. Balkus, *J. Mol. Catal. B: Enzym.*, **1996**, 2, 115.

47.   F. Balas, M. Manzano, P. Horcajada, M. Vallet-Regi, *J. Am. Chem. Soc.*, **2006**, 128.

48.   V. Dragutan, F. Verpoort, *Coord. Chem. Rev.*, **2005**, 249, 3055.

Chapter 2: Synthesis and Characterization of Model and Siloxane Functionalized RuCl(p-cymene)(N,N) Complexes Containing a Siloxane Tether at the Imine Nitrogen

2.1 Ruthenium and its applications

Ruthenium can exist in oxidation states varying from -2 to +8, making it the element with the widest range of oxidation states in the periodic table (Figure 2.1). As a result of this wide range of oxidation states ruthenium is able to adopt numerous coordination geometries which include trigonal bipyramidal, octahedral and tetrahedral. Corresponding examples of these are $Ru(0)(CO)_5$, $Ru(II)Cl_2(bipy)_2$ and $Ru(VIII)O_4$ respectively. This can be attributed to its high electron transfer ability, high Lewis acidity, low redox potentials and the formation of stable metallic species such as metallacycles and carbenes [1]. The unique chemistry of ruthenium has resulted in its complexes being extensively applied as catalyst precursors for various organic transformations. Progress in this regard can mainly be attributed to recently introduced ligands such as N-heterocyclic carbenes, Schiff bases, N, N,S, N,N, N,O and other multidentate donor ligands [2-6].
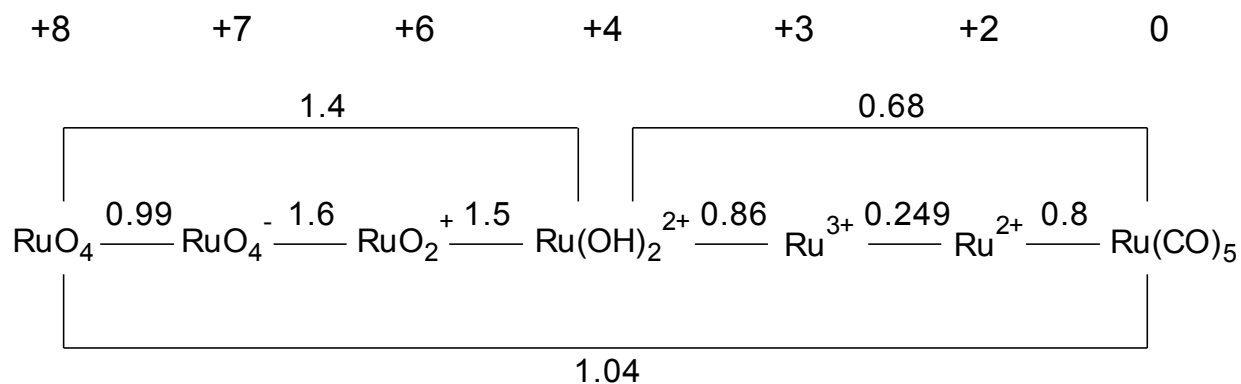
Figure 2.1 Various oxidation states and redox potentials of ruthenium.

Chapter 2:   Synthesis and Characterization of Model and Siloxane Functionalized RuCl(p-cymene)(N,N) Complexes Containing a Siloxane Tether at the Imine Nitrogen

2.1.1   Ru(arene) compounds

Ruthenium(II) compounds of the form $[(\eta^6\text{-arene})Ru^{II}(\textbf{N-N})Cl]^+$ (where **N-N** = ethylenediamine or other bis chelating ligands; arene = benzene, *p*-cymene, tetrahydroanthracene, dihydroanthracene and biphenyl) adopt a pseudo-octahedral "piano-stool" conformation with the neutral arene occupying the top three coordination positions (seat) of the formed complex. The chelating **N-N** ligand and the chloride occupy the other three coordination sites and form the so-called "legs" of the "piano-stool" conformation of which an example is shown in Figure 2.2 where **N**-**N** is any bis chelating ligand. The labile part of this type of complex is thought to be the Ru-Cl bond. The Ru(II) oxidation state is stabilized by the arene and prevents oxidation of the compound to Ru(III) [7].
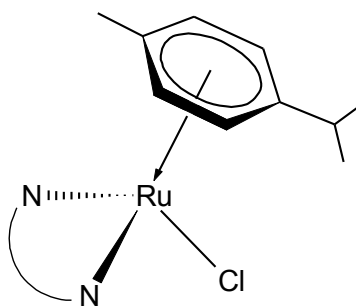
Figure 2.2 "Piano-stool" conformation of a RuCl(N,N)(*p*-cymene) complex.

2.1.1.1   Application of Ru compounds in catalysis

Ruthenium arene type complexes have found widespread application as catalyst precursors in numerous catalytic processes. Transfer hydrogenation of ketones and the oxidation of alcohols is two of the better known transformations that is catalyzed by Ru(arene) complexes. Diels-Alder reactions, allylic substitutions and ring opening/closing metathesis reactions have been shown to be catalyzed by these types of catalysts with very good results [8]. The versatility of Ru(arene) compounds has fueled widespread interest in the development of new systems to improve catalyst recovery and/or increase the activity of these types of systems.

Chapter 2: Synthesis and Characterization of Model and Siloxane Functionalized RuCl(p-cymene)(N,N) Complexes Containing a Siloxane Tether at the Imine Nitrogen

For interest and relevance to the project not all of the above mentioned catalytic transformations will be discussed in further detail. The transfer hydrogenation of ketones and the oxidation of alcohols and/or alkenes will be discussed in more detail in the sections to follow.

2.1.1.1.1 Transfer hydrogenation

The reduction of aldehydes and ketones to afford corresponding primary and secondary alcohols through transfer hydrogenation has been extensively studied over the past decade [9-14]. Compared to normal reduction reactions which necessitate the use of high hydrogen pressure or dangerous reducing agents, transfer hydrogenation reactions require milder conditions and offer a more environmentally friendly and selective alternative [15]. Ruthenium has shown favorable reactivity and selectivity towards the reduction of polar bonds and has even been found to exceed the performance of traditional hydrogenation catalyst derivatives of rhodium and iridium [16-20].

In Scheme 2.1 a typical transfer hydrogenation reaction is shown. The hydrogen source, usually hydrogen gas, is replaced with *i*-PrOH which acts as the hydrogen source during the reaction. For most reactions a base like KOH is required but it has been shown that some catalysts catalyze the reaction without the addition of base [11].
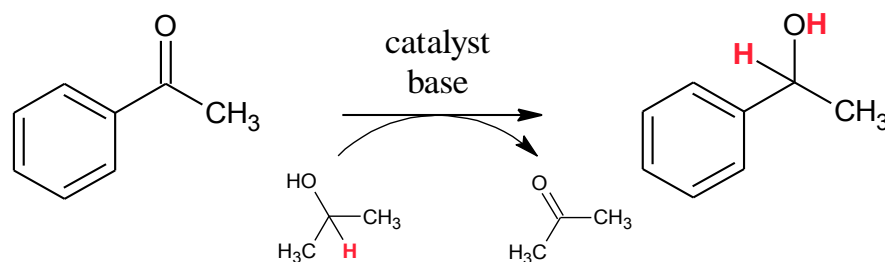
Scheme 2.1 A representation of a typical transfer hydrogenation reaction: conversion of acetophenone to 1-phenylethanol.

Chapter 2: Synthesis and Characterization of Model and Siloxane Functionalized RuCl(p-cymene)(N,N) Complexes Containing a Siloxane Tether at the Imine Nitrogen

2.1.1.1.2 Oxidation

The oxidation of alcohols (both primary and secondary) to their corresponding carbonyl compounds without over oxidation to carboxylic acids is a very important reaction in synthetic chemistry. Sigh *et al.* have reported a wide range of Ru(arene) complexes that have been found to oxidize primary and secondary alcohols to their corresponding carbonyl compounds in fairly high yields.   Various co-oxidants were employed which included: tertbutylhydroperoxide (*t*BuOOH), *N*-methylmorpholine-*N*-oxide (NMO), sodium oxychloride (NaOCl) and sodium periodate (NaIO$_4$) [21].

Oxidative cleavage of alkenes is a very important reaction for organic chemistry to obtain carbonyl compounds. By varying the reaction conditions it is possible to form aldehydes or ketones as well as carboxylic acids, which is usually not wanted. This process is usually performed using stoichiometric amounts of ozone, which is not only an expensive oxidant but can be very dangerous too [22]. From as early as 1953 it has been known that ruthenium compounds can also be utilized as an inorganic oxidant in the form of ruthenium tetroxide [23]. Since then numerous reports have shown that ruthenium compounds can successfully cleave or oxidize alkenes to form either diols, aldehydes or carboxylic acids [22,24,25].

2.1.2 Ligand systems

The tunability of the steric and electronic properties of nitrogen containing ligands have made them attractive building blocks for the synthesis of transition metal complexes [18,26-29]. Recently, although not that regularly seen, nitrogen containing Ru(II) (N,N; N,N,N) complexes have started to become more frequently applied as catalysts for transfer hydrogenation [30,31]. Diimine Schiff base type systems (N,N and N,O) however received very little attention and only a hand full of reports can be found [6,30,32,33]. In our lab we have previously synthesized and reported numerous Schiff base ligands and complexes which were successfully applied as catalysts in a wide range of catalytic reactions [34-37]. Ru(II)(*p*-cymene) complexes have shown enhanced activity towards transfer hydrogenation reactions [30,32,38,39]. Most of these systems are however homogeneous systems and recovery of the catalyst after the reaction is not

Chapter 2: Synthesis and Characterization of Model and Siloxane Functionalized RuCl(p-cymene)(N,N) Complexes Containing a Siloxane Tether at the Imine Nitrogen

possible. As discussed earlier in Chapter 1, two modes for immobilization (sequential and convergent) exist and the convergent (**2**) approach was favored above the sequential (**1**) approach due to the difficulty in controlling the last step; metal addition. Scheme 2.2 serves as a summary of these two approaches.
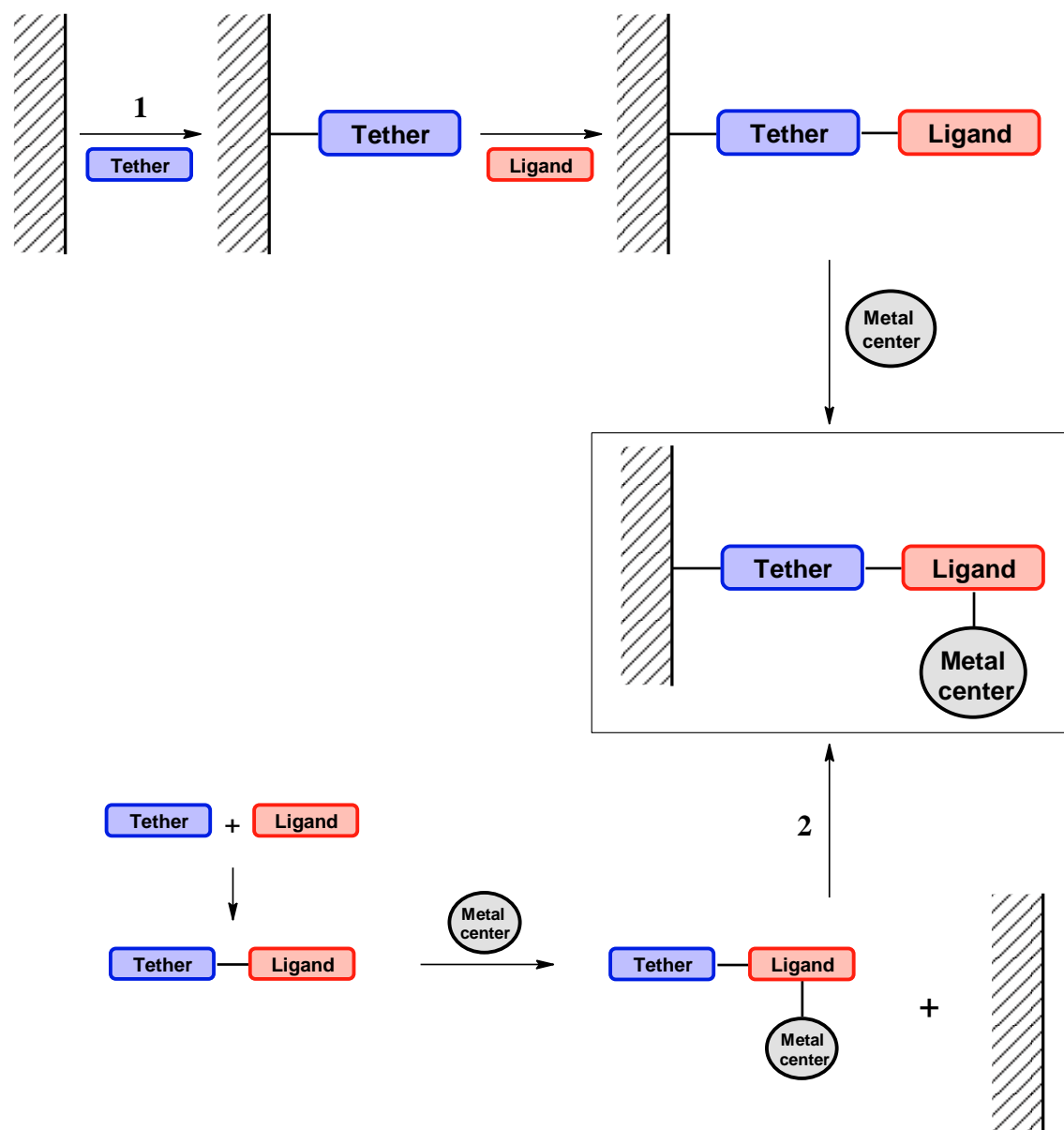
Scheme 2.2 A representation of the sequential (1) and convergent (2) approaches for the synthesis of immobilized catalysts.

Chapter 2: Synthesis and Characterization of Model and Siloxane Functionalized RuCl(p-cymene)(N,N) Complexes Containing a Siloxane Tether at the Imine Nitrogen

The selection of an appropriate ligand system is of paramount importance for the successful introduction of a functional group to achieve effective immobilization. Both approaches rely on the presence of a functional group in the ligand which can react and act as a tether to the surface of the support material. Ethoxy or methoxy siloxane groups have been shown to be very reactive and form stable bonds when condensed with the surface silanol (-OH) groups on the surface of the silica support material. The ease whereby these functional ethoxy groups can be introduced into the required ligand system is the most important aspect in the design of these ligands.

With all of this in mind, the synthesis of different Schiff base diimine ligand systems were attempted to obtain siloxane functionalized ligands which could be potential precursors to obtain the required Ru(arene) target molecules. These included the synthesis of mono- and binuclear iminopyridyl diimine ligand systems as well as their reduced amino derivatives.

2.2 Results and discussion

2.2.1 Synthesis and characterization of model and siloxane functionalized iminopyridyl diimine ligands L2.1-L2.6

Model ligands were prepared using a procedure similar to that described by Chen *et al*. and Cloete *et al* [36,37]. Ligands **L2.1**-**L2.3** were synthesized through Schiff base condensation of pyridine-2-carboxaldehyde, quinoline-2-carboxaldehyde and 6-methyl-2-pyridinecarboxaldehyde with *n*-propylamine in a 1:1 mole ratio in diethylether as solvent (MgSO$_4$ added to remove formed water). Siloxane functionalized ligands **L2.4**-**L2.6** were obtained by the substitution of *n*-propylamine with 3-aminopropyltriethoxysilane. Attempts to synthesize the chloro derivatives were unsuccessful as the product decomposed during workup. The introduced siloxane functionality will be used as the connection point to achieve the immobilization of the complexes to the silica supports. Both model and functionalized ligands were obtained as either yellow, colorless or brown oils. Ligands were found to be stable in both air and in solution. It was however decided that functionalized ligands would be stored in a glove box as a precaution until further use. A summary of the synthetic procedure for all ligands is shown in Scheme 2.3. The

Chapter 2: Synthesis and Characterization of Model and Siloxane Functionalized RuCl(p-cymene)(N,N) Complexes Containing a Siloxane Tether at the Imine Nitrogen

Schiff base condensation reaction to form ligands **L2.1**-**L2.6** was followed by FT-IR and ^{1}H NMR spectroscopy.

L2.1; R$_1$ = R$_2$ = H

L2.2; R$_1$ = CH$_3$, R$_2$ = H

L2.4; R$_1$ = H, R$_2$ = Si(OEt)$_3$

L2.5; R$_1$ = CH$_3$, R$_2$ = Si(OEt)$_3$

L2.3; R$_2$ = H

L2.6; R$_2$ = Si(OEt)$_3$
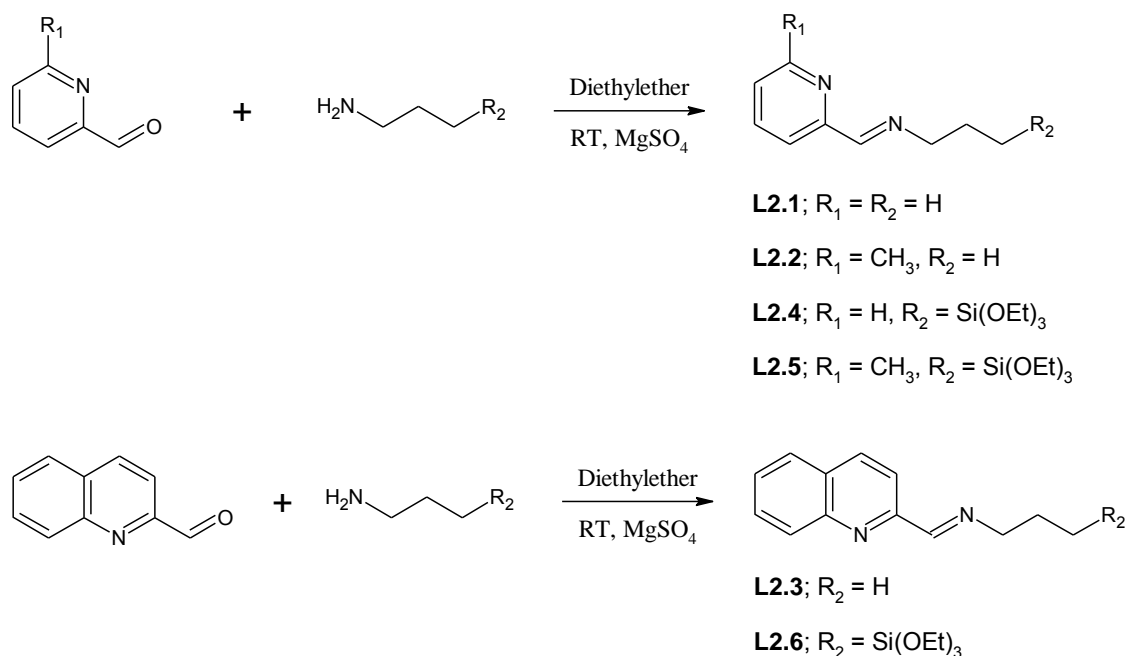
Scheme 2.3 Synthesis of model and siloxane functionalized iminopyridyl diimine ligands L2.1-L2.6.

2.2.1.1   Characterization of model and functionalized iminopyridyl diimine ligands using FT-IR spectroscopy

The formation of the expected imine and disappearance of the aldehyde stretch during Schiff base condensation was monitored by means of FT-IR. The carbonyl stretch of the free aldehyde is normally observed in the region of 1700-1720 cm^{-1}, whereas the newly formed imine is found at lower wave numbers in the region of 1643-1649 cm^{-1}. This was observed for both the model and functionalized ligand systems. Other important vibrational bands are observed in the regions of 1586-1596 cm^{-1} and 1560-1573 cm^{-1}, corresponding respectively to the $v_{C=N}$ and $v_{C=C}$ vibrations of the pyridine ring functionality respectively. Very intense absorption bands are

Chapter 2:   Synthesis and Characterization of Model and Siloxane Functionalized RuCl(p-cymene)(N,N) Complexes Containing a Siloxane Tether at the Imine Nitrogen

observed for the siloxane functionalized ligands **L2.4-L2.6** which correspond to the stretching vibrations of the Si-O bonds of the siloxane functionality (1072-1100 cm^{-1} and 748-791 cm^{-1}). The presence of these bands is very important and an absence from the IR would suggest the loss of the siloxane functionality during the reaction. Care was taken throughout to make sure that these characteristic IR vibrations were present after each step of the synthetic process. Selected IR vibrations are summarized in Table 2.1 below.

Table 2.1 Selected IR vibrations of model and functionalized iminopyridyl diimine ligands L2.1-L2.6.[a]

Ligand	Imine:	Pyridine ring:		Siloxane [-Si(OEt)$_3$]:	
	$v_{C=N}$ cm^{-1}	$v_{C=N}$ cm^{-1}	$v_{C=C}$ cm^{-1}	v_{Si-O} cm^{-1}	v_{Si-O} cm^{-1}
L2.1	1649	1586	1567	-	-
L2.2	1649	1591	1573	-	-
L2.3	1645	1596	1561	-	-
L2.4	1648	1587	1567	1071	769
L2.5	1650	1590	1573	1072-1100	766-791
L2.6	1643	1596	1560	1073-1100	748

[a] Oils recorded as neat samples using an ATR accessory

A typical IR spectrum for the siloxane functionalized ligand (**L2.4**) is shown in Figure 2.3 with the vibrations resulting from the presence of the siloxane functionality being clearly visible with very intense bands being observed at 1071, 951 and 769 cm^{-1}. This distinct pattern observed for

Chapter 2:   Synthesis and Characterization of Model and Siloxane Functionalized RuCl(p-cymene)(N,N) Complexes Containing a Siloxane Tether at the Imine Nitrogen

the siloxane functionality is used as a guide to confirm that the siloxane functionality is in no way altered during further reactions. The imine band is also clearly visible at 1648 cm^{-1}.
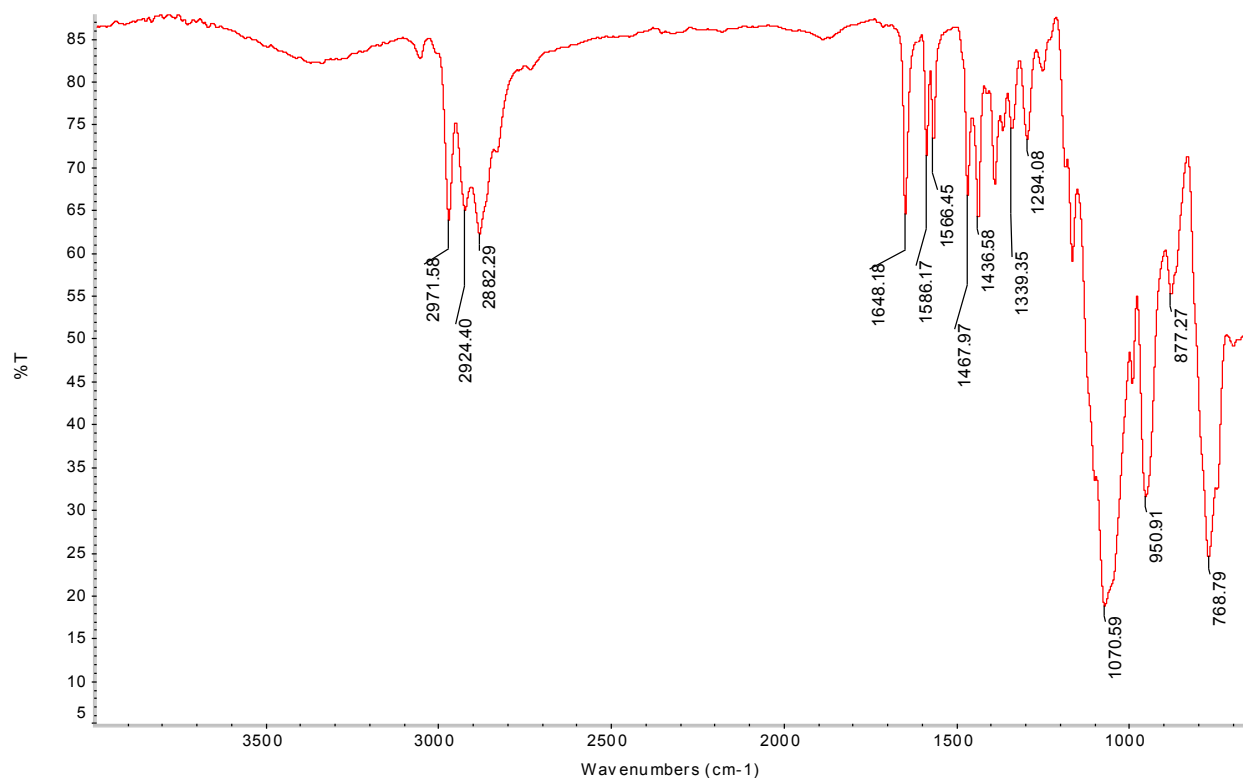
Figure 2.3 IR spectrum of functionalized pyridine ligand L2.4.

2.2.1.2   Characterization of model and functionalized iminopyridyl diimine ligands using ^{1}H NMR spectroscopy

^{1}H NMR spectroscopy proved to be an invaluable tool to confirm successful synthesis of the ligands by the presence of a resonance corresponding to the proton of the newly formed imine functionality in the aromatic region and the disappearance of the aldehyde proton resonance. Selected ^{1}H NMR resonances for ligands **L2.1**-**L2.6** are summarized in Table 2.2. The imine proton resonances for all ligands appear in the range of 8.26-8.56 ppm.

Table 2.2 Selected ^{1}H NMR data for model and siloxane functionalized iminopyridyl diimine ligands L2.1-L2.6.[a]

Ligand	Siloxane Functionality:		ArH	Imine:
	$Si(OCH_2CH_3)_3$	$Si(OCH_2CH_3)_3$		$N=CH$
L2.1	-	-	8.54 (d), 7.88 (d), 7.62 (t), 7.19 (t)	8.27 (s)
L2.2	-	-	7.77 (d), 7.59 (t), 7.14 (d)	8.33 (s)
L2.3	-	-	8.20 (d), 8.16 (d), 8.14 (d), 7.85 (d), 7.75 (t), 7.58 (t)	8.56 (s)
L2.4	1.17 (t, 9H)	3.78 (q, 6H)	8.59 (d), 7.92 (d), 7.68 (t), 7.26 (t)	8.32 (s)
L2.5	1.14 (t, 9H)	3.74 (q, 6H)	7.71 (d), 7.54 (t), 7.09 (d)	8.26 (s)
L2.6	1.23 (t, 9H)	3.84 (q, 6H)	8.19 (d), 8.15 (d), 8.13 (d), 7.85 (d), 7.74 (t), 7.58 (t)	8.55 (s)

[a] Recorded in Chloroform-*d*

Chapter 2:   Synthesis and Characterization of Model and Siloxane Functionalized RuCl(p-cymene)(N,N) Complexes Containing a Siloxane Tether at the Imine Nitrogen

Two distinct resonances, a triplet and a quartet, corresponding to the methyl and methylene protons of the siloxane functionality of ligands **L2.4**-**L2.6** are observed in the aliphatic region at around 1.14-1.23 ppm and 3.74-3.84 ppm respectively.

2.2.2 Attempted synthesis and characterization of siloxane functionalized bis(pyridylimino-3-propyl)-amine and bis(pyridylamino-3-propyl)-amine ligands

The route towards an alternative ligand system that was envisaged is shown in Scheme 2.4 below.   It was envisaged that the reaction of 2-pyridinecarboxaldehyde and bis(3,3'-aminopropyl)amine could afford ligand **L2.7**.

Scheme 2.4   Possible synthetic route towards siloxane functionalized bis(pyridylimino-3-propyl)-amine and bis(pyridylamino-3-propyl)-amine ligands L2.8 and L2.9.

Chapter 2: **Synthesis and Characterization of Model and Siloxane Functionalized RuCl(p-cymene)(N,N) Complexes Containing a Siloxane Tether at the Imine Nitrogen**

The isolation and subsequent reduction of ligand **L2.8** to ligand **L2.9** could allow us to potentially synthesize siloxane functionalized dinuclear Ru(*p*-cymene)(N,N) complexes (incorporating bis(imine) or bis(amine) ligands). Previous attempts at reducing siloxane functionalized ligands with NaBH$_4$ were found to be successful but unfortunately also resulted in some transformation of the siloxane functionality which was confirmed by IR and ^{1}H NMR spectroscopy. It was however decided to continue and attempt the synthesis of the siloxane functionalized bis-imine derivative **L2.8** even though reduction to form compound **L2.9** could possibly result in the loss of the siloxane functionality. The condensation reaction between the aldehyde and the amine was monitored by FT-IR spectroscopy. The disappearance of the amine and aldehyde stretches around 3100 and 1700 cm^{-1} respectively and the presence of a newly formed imine functionality at 1647 cm^{-1} confirmed successful condensation. Characterization by means of ^{1}H NMR spectroscopy was however not as straight forward and problems were observed from the outset. Ligand **L2.7** is a symmetrical compound and one would expect a rather simple spectrum with three aliphatic and five aromatic resonances corresponding to the propyl backbone and iminopyridyl regions respectively. Instead a very complex spectrum is obtained with eight aromatic resonances present between 7-9 ppm (Figure 2.4).

In the aliphatic region an even larger cluster of resonances were observed. The singlet at 8.16 ppm was assigned to the imine signal and the rest of the resonances were integrated relative to it. For ligand **L2.7** a relative integration of 1:4 would be expected if it was formed as shown above but instead a relative integration of 1:8 is observed. This meant that only one imine functionality was present in the molecule or that a mixture of different products possibly formed although TLC suggested only one product was obtained.

To get more insight into the nature of the obtained compound a small sample was submitted for ESI$^+$ mass spectrometry analysis. The base peak was observed at 310.2 m/z and corresponded to the [M+H]$^+$ of the target molecule (monoisotopic mass of target ligand **L2.7** is 309.195 Da). At 221.2 m/z a fragment corresponding to the loss of a pyridinecarboxaldehyde unit can be accounted for. This only confirmed that a molecule with the same molecular weight was obtained as a product and brought us no closer to elucidating the structure of the compound.

Chapter 2: Synthesis and Characterization of Model and Siloxane Functionalized RuCl(p-cymene)(N,N) Complexes Containing a Siloxane Tether at the Imine Nitrogen
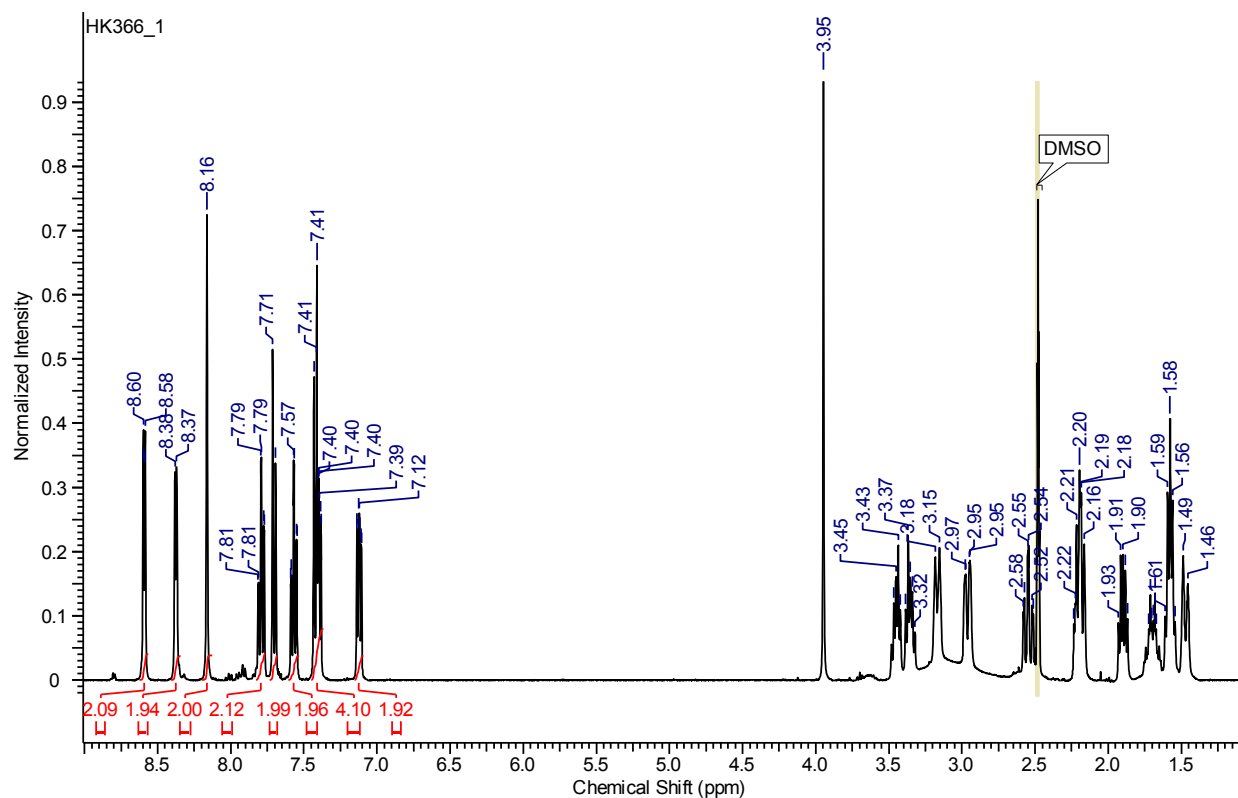
Figure 2.4 ¹H NMR spectrum of bis(pyridylimino-3-propyl)-amine ligand L2.7.

After an intense literature search a paper published by Boča *et al*. was found in which it was described that two different products could potentially be formed when reacting 2-pyridinecarboxaldehyde-*N*-Oxide with polyamines. They found that FT-IR spectroscopy was not sufficient to confirm the condensation product because it could not distinguish between cyclic secondary amines or aliphatic secondary amines, since the N–H vibrations are similar. This lead them to carry out a complete NMR study on the products formed during different condensation reactions between 2-pyridinecarboxaldehyde-*N*-Oxide and polyamines. The resulting product was expected to be a symmetrical (eight peaks expected) compound (**19**) but instead they observed, as in our case, 16 different resonances. This meant an unsymmetrical compound (**20**) was formed irrespective of the ratios of reagents or reaction conditions (Scheme 2.5) [40].

Chapter 2: Synthesis and Characterization of Model and Siloxane Functionalized RuCl(p-cymene)(N,N) Complexes Containing a Siloxane Tether at the Imine Nitrogen
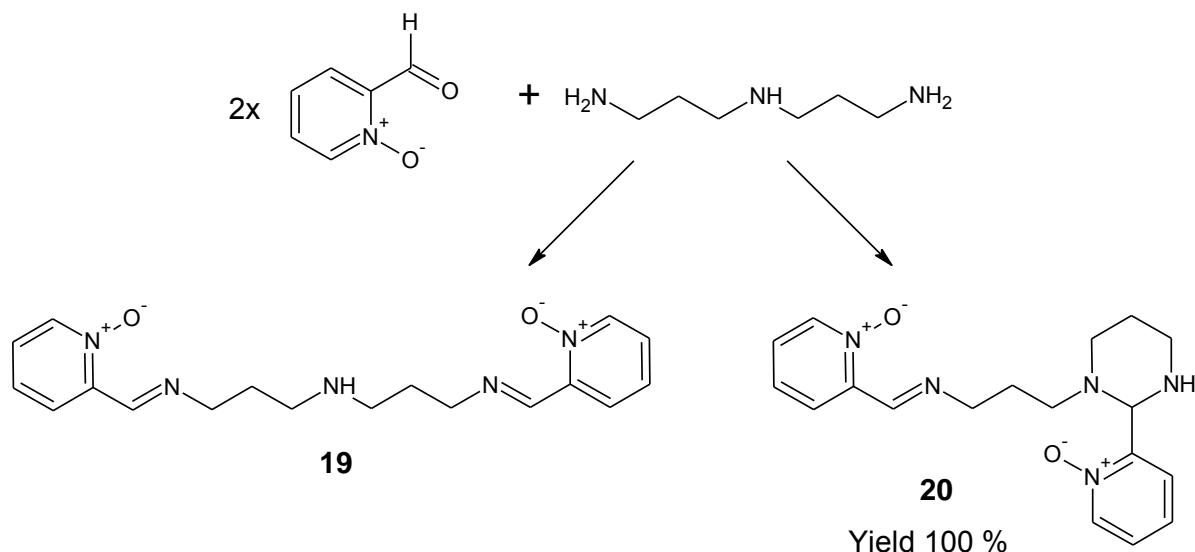

Scheme 2.5 Possible products for the reaction of 2-pyridinecarboxaldehyde-*N*-Oxide and bis(3,3'-aminopropyl)amine [40].

Boča *et al.* suggested that the stabilization of the obtained cyclic condensation products originated from the intramolecular hydrogen bonds between the formed imidazolidine NH groups and the oxygen atoms situated in the *N*-oxide of the pyridine rings.

Bréfuel *et al.* however disagreed with this proposal and proposed an alternative mechanism because they observed that, as in our case, there was no need for this *N*-oxide to be present for this type of unsymmetrical product formation to occur [41]. The proposed mechanism involves the nucleophilic attack of the nitrogen leading to the formation of the hemiaminal (**21a**) as an initial step (adapted mechanism is shown in Scheme 2.6). After consecutive addition of a proton, compound **21b** is formed after which two subsequent pathways are possible. The first being the addition of water followed by ring closure that leads to the formation of the carbocation **21c** which is stabilized by conjugation, whereas the second route involves the direct elimination of water yielding compound **21d**. The iminium form **21e** gives rise to the imidazolidine intermediate **21f** which after Schiff base condensation of the free amino group will afford the unsymmetrical cyclic condensation product.
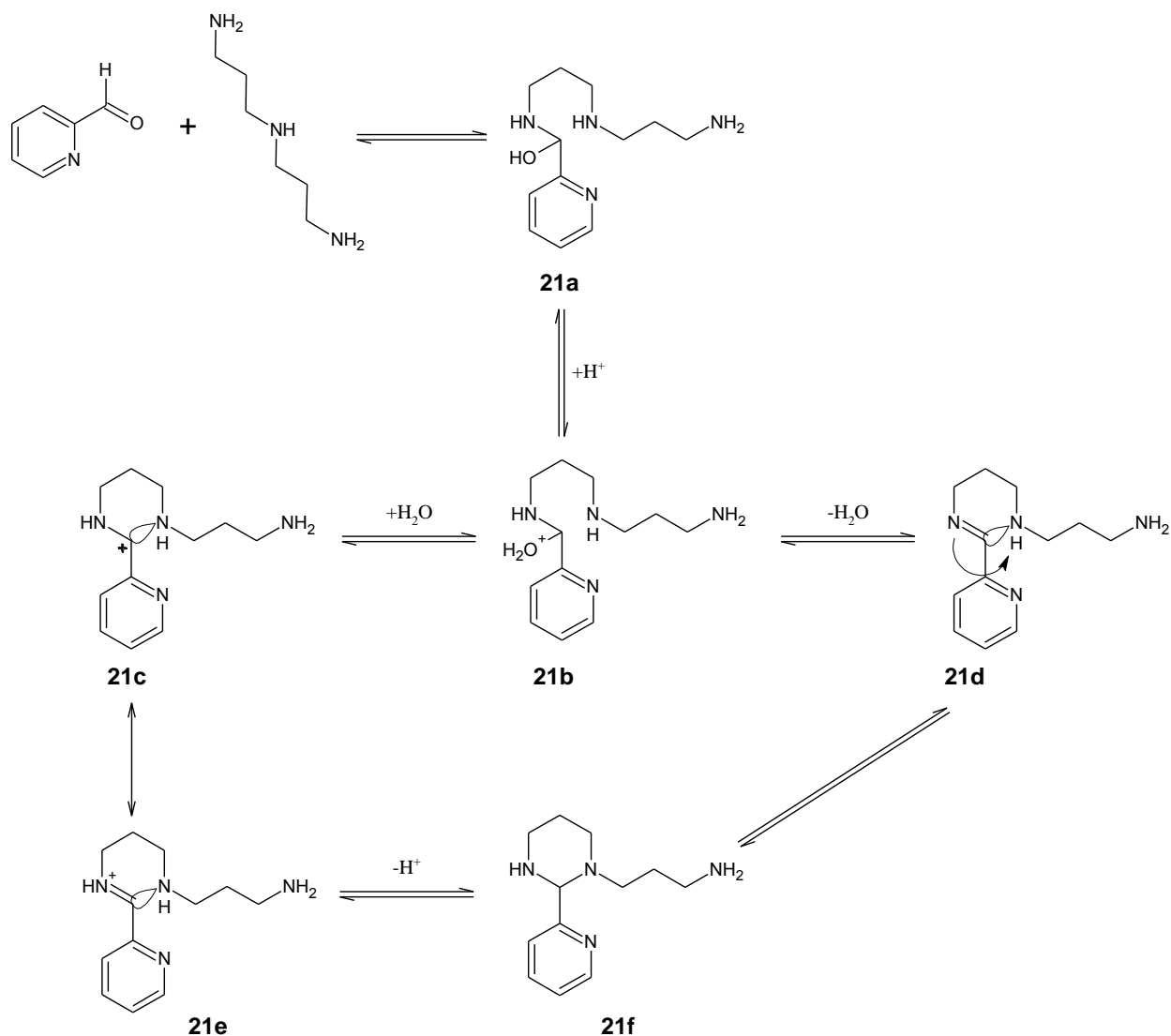
Scheme 2.6 Possible mechanism yielding the imidazolidine derivative (21f) resulting from a 1:1 condensation of 2-pyridinecarboxaldehyde and bis(3,3'-aminopropyl)amine [41].

With this in mind the actual identity of the compound isolated from our reaction is shown in Figure 2.5 as compound **L2.7B**. The characterization data now all point to the formation of ligand **L2.7B**. The ^{1}H NMR spectrum shown earlier compare fairly well to a computationally simulated ^{1}H NMR spectrum and all integrations relative to the imine present now makes complete sense. Eight distinctly different aromatic resonances would be expected for ligand

Chapter 2: Synthesis and Characterization of Model and Siloxane Functionalized RuCl(p-cymene)(N,N) Complexes Containing a Siloxane Tether at the Imine Nitrogen

L2.7B with only one imine expected as a singlet. The distinctly different aliphatic protons in the aliphatic region are as a result of both an aliphatic chain as well as an aliphatic ring being present in the obtained compound **L2.7B**. The monoisotopic mass of both ligands **L2.7A** and **L2.7B** are also found to be exactly the same (309.195 Da) making it impossible to distinguish between these two compounds using ESI-MS.

monoisotopic mass: 309.195 Da

L2.7A

monoisotopic mass: 309.195 Da

L2.7B
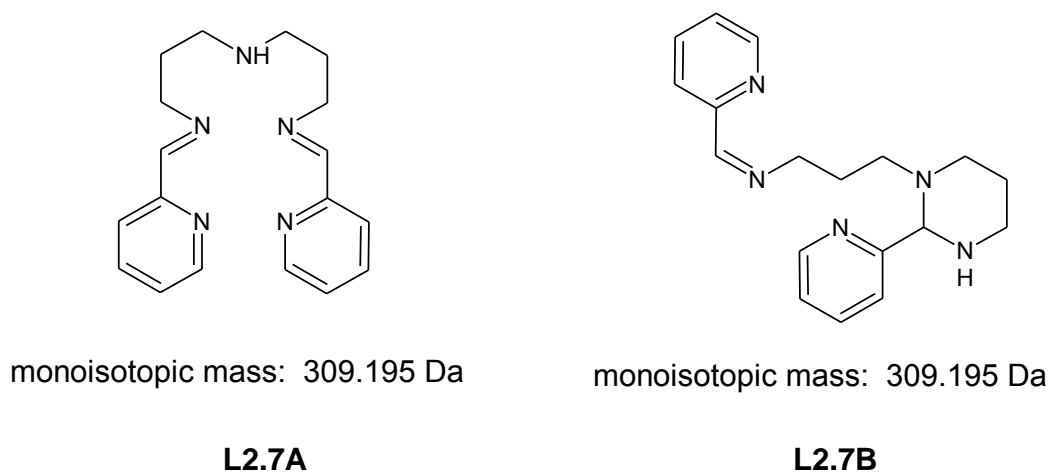
Figure 2.5   Possible products of the reaction between 2-pyridinecarboxaldehyde and bis(3,3'-aminopropyl)amine.

2.2.3 Synthesis and characterization of model and functionalized iminopyridyl diimine RuCl(*p*-cymene) complexes C2.1I-C2.3I and C2.1-C2.6

Complexes were synthesized by adapting a procedure reported in the literature [42]. The [Ru(*p*-cymene)Cl$_2$]$_2$ dimer (precursor) was synthesized using a literature procedure which involved refluxing RuCl$_3$·xH$_2$O and excess amounts of α-terpinine in ethanol [30]. For the synthesis of model complex **C2.1** for instance, ligand **L2.1** was reacted with the [Ru(*p*-cymene)Cl$_2$]$_2$ dimer in a 2:1 mole ratio in dry ethanol/DCM followed by the addition of the sodium salt of the appropriate counter-ion, NaPF$_6$ or NaB(Ph)$_4$ (Scheme 2.7). Complexes

Chapter 2: Synthesis and Characterization of Model and Siloxane Functionalized RuCl(p-cymene)(N,N) Complexes Containing a Siloxane Tether at the Imine Nitrogen

were isolated as either their hexafluorophosphate (initial model complexes **C2.1I**-**C2.3I**) or tetraphenylborate salts (model and functionalized complexes **C2.1**-**C2.6**).

L2.1; R$_1$ = R$_2$ = H

L2.2; R$_1$ = CH$_3$, R$_2$ = H

L2.3; R$_2$ = H (Quinoline)

L2.4; R$_1$ = H, R$_2$ = Si(OEt)$_3$

L2.5; R$_1$ = CH$_3$, R$_2$ = Si(OEt)$_3$

L2.6; R$_2$ = Si(OEt)$_3$ (Quinoline)

C2.1I; R$_1$ = R$_2$ = H, X = PF$_6$ **C2.1**; R$_1$ = R$_2$ = H, X = B(Ph)$_4$

C2.2I; R$_1$ = CH$_3$, R$_2$ = H, X = PF$_6$ **C2.2**; R$_1$ = CH$_3$, R$_2$ = H, X = B(Ph)$_4$

C2.3I; R$_2$ = H (Quinoline), X = PF$_6$ **C2.3**; R$_2$ = H (Quinoline), X = B(Ph)$_4$

C2.4; R$_1$ = H, R$_2$ = Si(OEt)$_3$, X = B(Ph)$_4$

C2.5; R$_1$ = CH$_3$, R$_2$ = Si(OEt)$_3$, X = B(Ph)$_4$

C2.6; R$_2$ = Si(OEt)$_3$ (Quinoline), X = B(Ph)$_4$
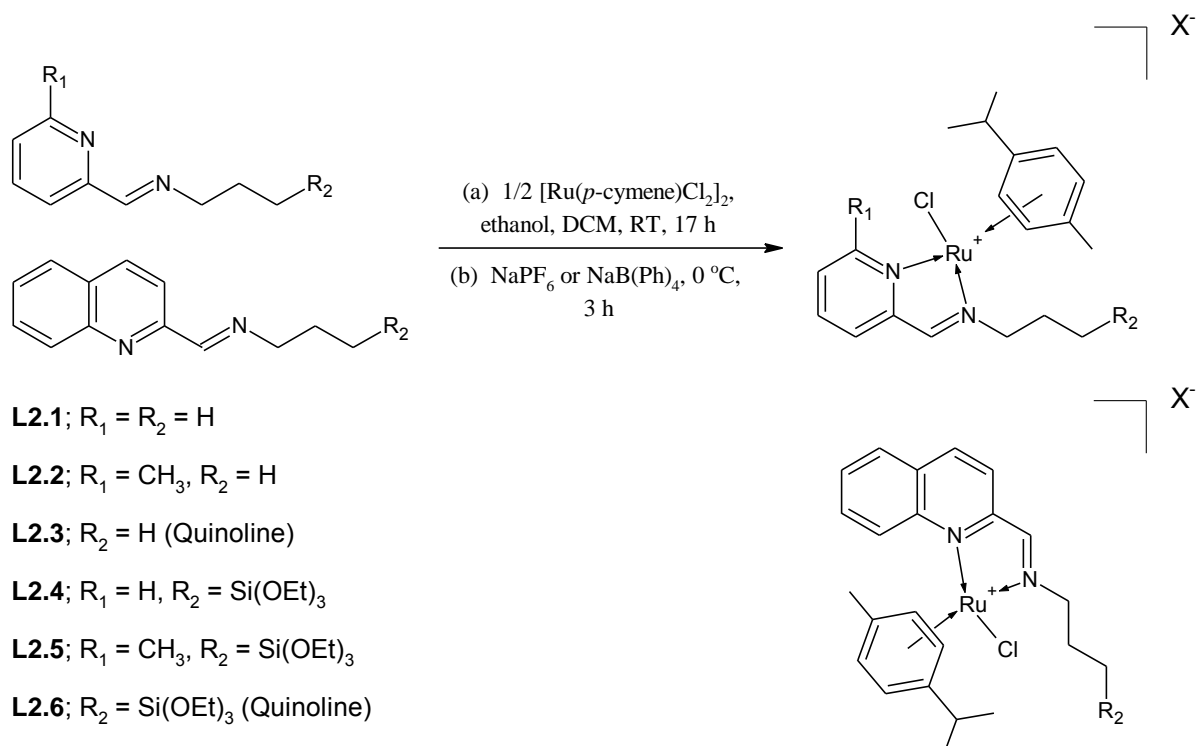
Scheme 2.7   Synthesis of model cationic complexes C2.1I-C2.3I (hexafluorophosphate counter-ion) and model and functionalized cationic complexes C2.1-C2.6 (tetraphenylborate counter-ion).

Chapter 2: Synthesis and Characterization of Model and Siloxane Functionalized RuCl(p-cymene)(N,N) Complexes Containing a Siloxane Tether at the Imine Nitrogen

2.2.3.1 Synthesis of model iminopyridyl diimine RuCl(p-cymene) complexes C2.1I-C2.3I (hexafluorophosphate derivatives)

The model pyridine, methyl-pyridine and quinoline derivatives **C2.1I**, **C2.2I** and **C2.3I** were isolated as their hexafluorophosphate salts as orange to brown solids in yields of 72-82 %. Complexes **C2.1I** and **C2.2I** were recrystallized from DCM/pentane and were recovered as needle-like crystalline materials [42]. The functionalized complexes **C2.4**-**C2.6** could not be isolated as their hexafluorophosphate salts. The formed products were found to be very unstable and decomposed during workup and attempts to isolate the solids under nitrogen only resulted in the formation of a gunky residue. This necessitated the use of a larger counter-ion, such as $B(Ph)_4^-$.

2.2.3.2 Synthesis of model and functionalized iminopyridyl diimine RuCl(p-cymene) complexes C2.1-C2.6 (tetraphenylborate derivatives)

Upon the substitution of PF_6^- with the much larger $B(Ph)_4^-$ counter-ion we were able to isolate a stable solid for the siloxane functionalized complexes. Model complexes **C2.1**-**C2.3** could also be isolated as their tetraphenylborate salts in very high yields. All three functionalized complexes were isolated in the form of their tetraphenylborate salts as very stable powders (orange to brown). Attempts to isolate single crystals of these solids were however unsuccessful. The obtained yields for functionalized complexes **C2.4**-**C2.6** were very low and this required that a different approach be taken in an attempt to improve the yields. Ethanol was substituted with dichloromethane as the reaction solvent due to enhanced solubility of the ligand in the latter solvent and immediately an increase in the yield from around 20-30 % to more than 60 % was observed.

Complexes were all isolated as orange to brown solids (some model complexes could be purified by recrystallization from DCM/pentane or acetone/pentane) and were fully characterized by FT-IR, ^{1}H and ^{13}C NMR spectroscopy, ESI mass spectrometry, melting point determination and microanalyses.

Chapter 2: **Synthesis and Characterization of Model and Siloxane Functionalized RuCl(p-cymene)(N,N) Complexes Containing a Siloxane Tether at the Imine Nitrogen**

2.2.3.3 Characterization of model and functionalized complexes C2.1I-C2.3I and C2.1-C2.6 using FT-IR spectroscopy

Selected IR vibrations for all model and functionalized complexes, **C2.1I**-**C2.3I** and **C2.1**-**C2.6**, are summarized in Table 2.3 below. FT-IR spectroscopy proved to be a very useful tool to monitor coordination of the Schiff base diimine ligands to the ruthenium metal center.

Table 2.3 Selected IR vibrations of model and functionalized complexes C2.1I-C2.3I and C2.1-C2.6.[a]

Complex	$v_{C=N}$ cm^{-1} (imine)		Siloxane tail [-Si(OEt)$_3$]		PF_6^-, $B(Ph)_4^-$ (counter-ion)
	Ligand (L1-L6)	Complex	v_{Si-O} cm^{-1}	v_{Si-O} cm^{-1}	
C2.1I	1649	1599	-	-	832[c]
C2.2I	1649	1598	-	-	832[c]
C2.3I	1645	1593	-	-	833[c]
C2.1	1649	1597	-	-	704, 734[d]
C2.2	1649	1598	-	-	707, 735[d]
C2.3	1645	1592	-	-	706, 732[d]
C2.4	1649	1596	1031-1115	768	705, 733[d]
C2.5	1650	1597	1031-1072	750	705, 733[d]
C2.6[b]	1643	1594	1031-1068	-	702, 732[d]

[a] Solids recorded as neat samples using an ATR accessory; [b] Overlap with counter-ion peaks; [c] hexafluorophosphate derivatives; [d] tetraphenylborate derivatives

Chapter 2: Synthesis and Characterization of Model and Siloxane Functionalized RuCl(p-cymene)(N,N) Complexes Containing a Siloxane Tether at the Imine Nitrogen

A typical shift from around 1650 cm^{-1} to just below 1600 cm^{-1} was observed for all complexes confirming successful complexation. The tetraphenylborate absorption bands are observed as very intense bands at around 735 and 702 cm^{-1} for complexes **C2.1**-**C2.6**. For the hexafluorophosphate derivatives **C2.1I**-**C2.3I** a strong absorption band at 832 cm^{-1}, corresponding to peaks of the counter-ion (PF$_6^-$), was observed.

2.2.3.4   Characterization of model and functionalized complexes C2.1I-C2.3I and C2.1-C2.6 using NMR spectroscopy

The ^{1}H NMR spectrum of the complexes showed a general downfield shift of all the aromatic signals relative to the free ligand resulting from the cationic nature of the obtained complexes. The imine proton resonance, observed as a singlet, shows a downfield shift from its original position in the free ligand as a result of the change in the double bond character of the imine functionality caused by the successful coordination to the metal center. As an example the ^{1}H NMR spectrum of complex **C2.1** is shown in Figure 2.6 below. Resonances corresponding to the arene ring protons of the *p*-cymene ligand are observed as a triplet and two doublets resonating at 5.91, 6.17 and 6.24 ppm respectively. The methyl proton resonances of *p*-cymene are observed as a singlet at 2.16 ppm while the methyl protons of the *iso*-propyl resonate as two doublets at 0.92 and 1.01 ppm respectively. This confirms that the two methyl groups are in two different chemical environments. The expected multiplet for the methylene proton of the *iso*-propyl group of the *p*-cymene is obscured by the DMSO-*d*6 solvent peak at 2.5 ppm. Three intense resonances corresponding to the protons of the tetraphenylborate counter-ion are observed at 6.79, 6.92 and 7.17 ppm respectively integrating to a total of 20 protons. An important downfield shift for the imine proton resonance from 8.27 ppm for the free ligand to 8.73 ppm for the complex is observed confirming successful complexation. The imine proton resonances for complexes **C2.1I**-**C2.3I** and **C2.1**-**C2.6** are summarized in Table 2.4 showing a general downfield shift from around 8.26-8.56 ppm to 8.67-9.00 ppm. The signals assigned to the protons of the propyl chain are observed at 0.94 (triplet), 1.85-1.95 (multiplet) and 4.28-4.48 ppm (multiplet) respectively.
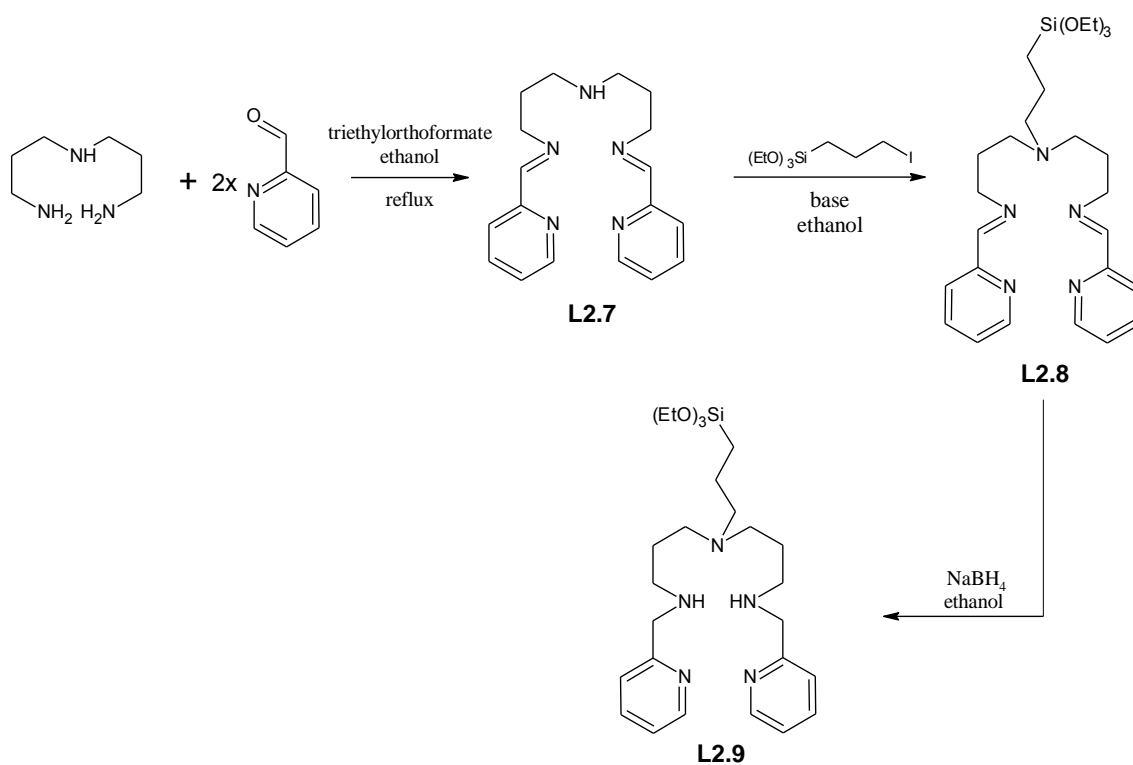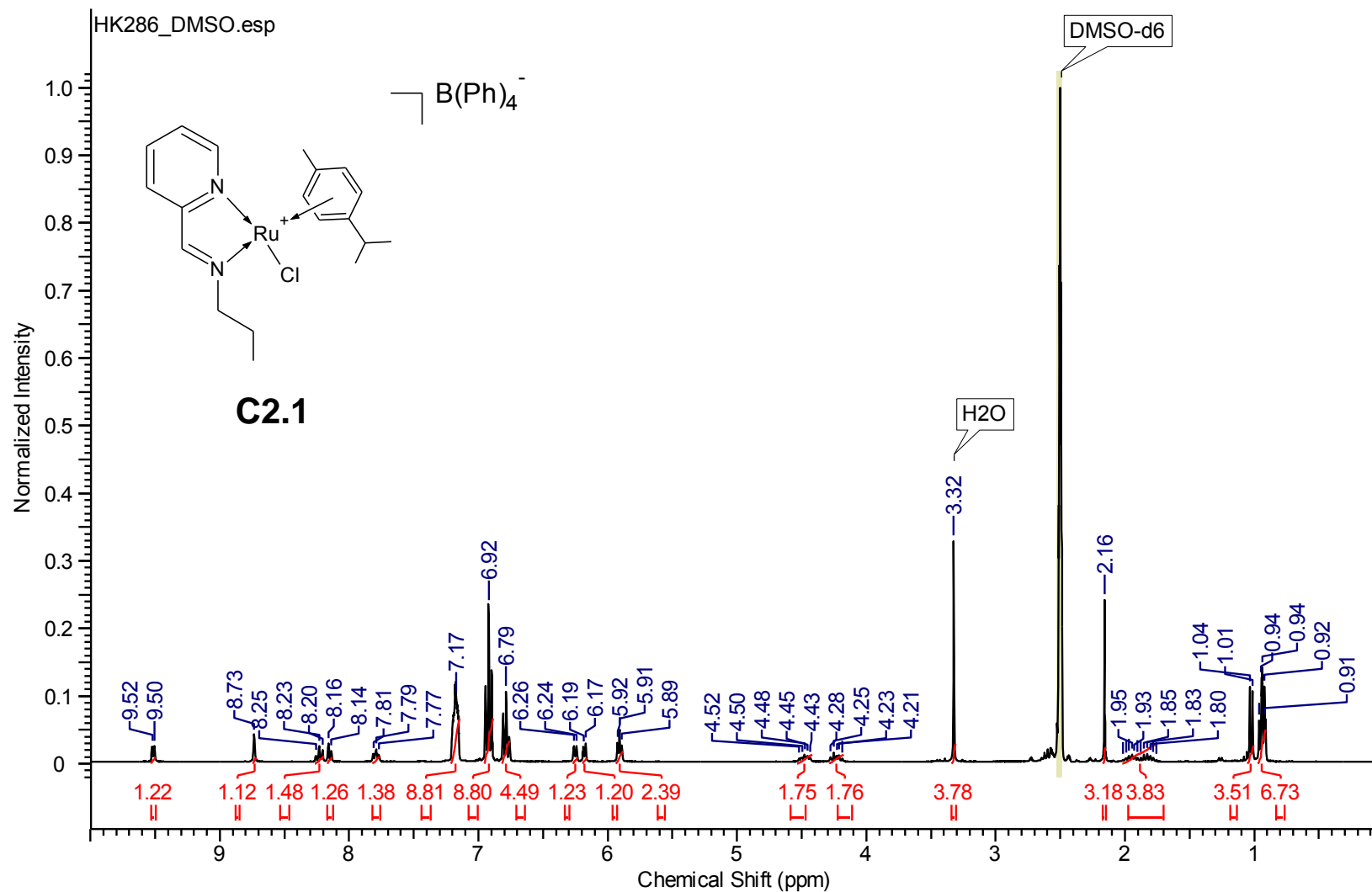
Figure 2.6 ^{1}H NMR spectrum of model complex C2.1.

Chapter 2: Synthesis and Characterization of Model and Siloxane Functionalized RuCl(p-cymene)(N,N) Complexes Containing a Siloxane Tether at the Imine Nitrogen

Table 2.4 Summary of ^{1}H and ^{13}C NMR data of complexes C2.1I-C2.3I[a] and C2.1-C2.6.[b]

Complex	^{1}H NMR Imine Proton (ppm)		Arene Ring: *p*-cymene		^{13}C NMR Imine Carbon (ppm)
	Ligand (L1-L6)	Complex	Aromatic	Aliphatic	
C2.1I	8.27	8.81	6.29 (d), 6.22 (d), 5.96 (t)	2.31 (s), 1.17 (d), 1.09 (d)	-
C2.2I	8.33	8.75	6.39 (d), 6.30 (d), 5.95 (t)	2.32 (s), 1.14 (d), 1.07 (d)	-
C2.3I	8.56	9.06	6.35 (d), 6.24 (s), 6.04 (d)	2.28 (s), 1.01 (d), 0.90 (d)	-
C2.1	8.27	8.73	6.24 (d), 6.17 (d), 5.91 (t)	2.16 (s), 1.01 (d), 0.93 (d)	167.1
C2.2	8.33	8.67	6.33 (d), 6.24 (d) 5.88 (d)	2.17 (s), 0.89 (d), 0.97 (d)	167.6
C2.3	8.56	9.00	6.34 (d), 6.23 (d), 6.11 (d)	2.15 (s), 0.84 (d), 0.73 (d)	167.9
C2.4	8.32	8.70	6.25 (d), 6.11 (d), 5.87 (t)	2.16 (s), 1.02 (d), 0.90 (d)	167.3
C2.5	8.26	8.68	6.33 (s), 6.20 (d) 5.90 (d)	2.17 (s), 0.97 (d), 0.91 (d)	167.7
C2.6	8.55	8.99	6.30 (d), 6.23 (d), 6.13 (d), 5.94 (d)	2.15 (s), 0.84 (d), 0.73 (d)	167.9

[a] Recorded in Acetone-*d*6; [b] Recorded in DMSO-*d*6

Chapter 2:   Synthesis and Characterization of Model and Siloxane Functionalized RuCl(p-cymene)(N,N) Complexes Containing a Siloxane Tether at the Imine Nitrogen

2.2.3.5   Characterization of model and functionalized complexes C2.1I-C2.3I and C2.1-C2.6 using ESI mass spectrometry, melting point determination and microanalyses

ESI-MS data, melting points and microanalyses of all the model and functionalized complexes are summarized in Table 2.5. The model complexes **C2.1I**-**C2.3I** and **C2.1**-**C2.6** were found to have melting points in the range of 190-225 ˚C and 176-219 ˚C respectively. The functionalized complexes **C2.4**-**C2.6** decomposed without melting at 140, 160 and 176 ˚C respectively.

Table 2.5   ESI-MS, microanalyses and melting points of model and functionalized complexes C2.1I-C2.3I and C2.1-C2.6.

Complex	ESI-MS [M]+ (m/z) Calculated (Found)	Microanalysis: Calculated (Found)			Melting Point (˚C)
		C	H	N	
C2.1I	419.1 (419.1)	40.47 (40.74)	4.65 (4.79)	4.97 (4.63)	190-192
C2.2I	433.1 (433.1)	41.56 (41.62)	4.88 (4.93)	4.85 (4.58)	210-212
C2.3I	469.1 (469.1)	44.99 (44.98)	4.60 (4.66)	4.56 (4.37)	223-225
C2.1	419.1 (419.1)	69.96 (69.63)	6.28 (6.28)	3.79 (3.49)	176-178
C2.2	433.1 (433.1)	70.26 (69.93)	6.43 (6.15)	3.72 (3.38)	206-209
C2.3[a]	469.1 (469.1)	64.69 (64.96)	5.88 (5.75)	3.14 (2.93)	216-219
C2.4	581.2 (581.2)	65.36 (64.97)	6.72 (6.12)	3.11 (2.97)	140-145[b]
C2.5	595.2 (595.2)	65.67 (64.96)	6.83 (6.34)	3.06 (2.72)	160-165[b]
C2.6	631.2 (631.2)	66.97 (66.14)	6.57 (6.42)	2.95 (2.66)	173-176[b]

[a] M·1.0H$_2$O+1.0DCM; [b] decomposed without melting

Chapter 2:   Synthesis and Characterization of Model and Siloxane Functionalized RuCl(p-cymene)(N,N) Complexes Containing a Siloxane Tether at the Imine Nitrogen

Microanalysis confirmed that the obtained complexes were isolated in high purity with the only exception being model complex **C2.3** which was found to be hygroscopic and was isolated as the trihydrate. ESI-MS proved to be an important tool to confirm the successful synthesis of the model and functionalized Ru(*p*-cymene) complexes. Ruthenium compounds, because of the many naturally occurring isotopes, give rise to very distinct isotopic splitting patterns in the mass spectra of the compounds. By theoretical simulation of the expected isotopic cluster and comparing it to the experimentally obtained clusters it is possible to conclusively elucidate the structure of a certain fragment in the mass spectrum. The calculated and obtained monoisotopic masses of the complexes compare very well and are summarized in Table 2.5. In Figure 2.7 a proposed structure representing a possible binuclear species (**C2.4**-**C2.4**) corresponding to the base peak with a m/z of 544.1 (doubly charged species) is shown. The calculated isotopic distribution of both compounds are shown in Figure 2.8 and correspond very well to the experimentally obtained spectrum of functionalized complex **C2.4**.

C2.4

Molecular Formula   = $C_{25}H_{40}ClN_2O_3RuSi$
Monoisotopic Mass = 581.153511 Da

C2.4-C2.4

Molecular Formula   = $C_{46}H_{70}Cl_2N_4O_5Ru_2Si_2$
Monoisotopic Mass = 1088.233858 Da
m/2   = 544.1
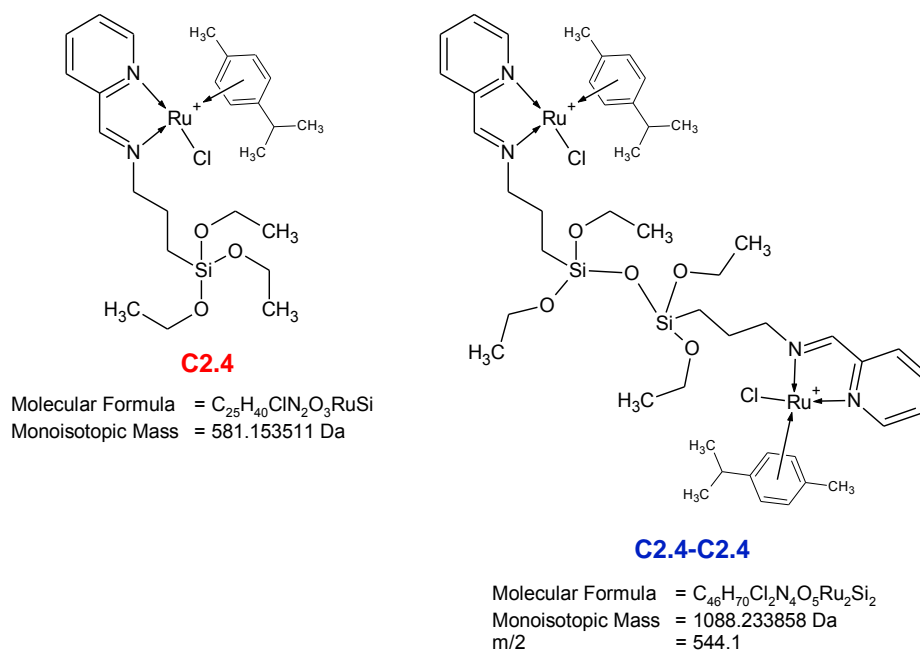
Figure 2.7   Functionalized complex C2.4 and a proposed structure for the binuclear complex formed under ESI-MS (positive mode) conditions.

Figure 2.8 ESI-MS (positive mode) spectrum of functionalized complex C2.4.

Chapter 2: Synthesis and Characterization of Model and Siloxane Functionalized RuCl(p-cymene)(N,N) Complexes Containing a Siloxane Tether at the Imine Nitrogen

The mass spectrum of the functionalized complex **C2.4** was also recorded in the negative mode to confirm the presence of the counter-ion. The base peak (only peak observed) corresponds to the counter-ion ([M]$^-$ = 319.16) fragment and confirms the presence of the counter-ion in the complex.

Figure 2.9 ESI-MS (negative mode) of functionalized complex C2.4.

The obtained ESI-MS spectra for the model complexes were far less cluttered when compared to the functionalized complexes. The absence of the siloxane functionality inhibits the formation of a binuclear species resulting in the presence of only one isotopic cluster at m/z = 469 which compares very well with the simulated isotopic pattern (Figure 2.10). Other significant peaks

Chapter 2: Synthesis and Characterization of Model and Siloxane Functionalized RuCl(p-cymene)(N,N) Complexes Containing a Siloxane Tether at the Imine Nitrogen

that are observed in the mass spectra of all of these compounds are found at m/z 355.2, 321.2 and 260.2. These peaks were found to be ammonia adducts of the tetraphenylborate counter-ion, which could be confirmed using high resolution mass spectrometry.
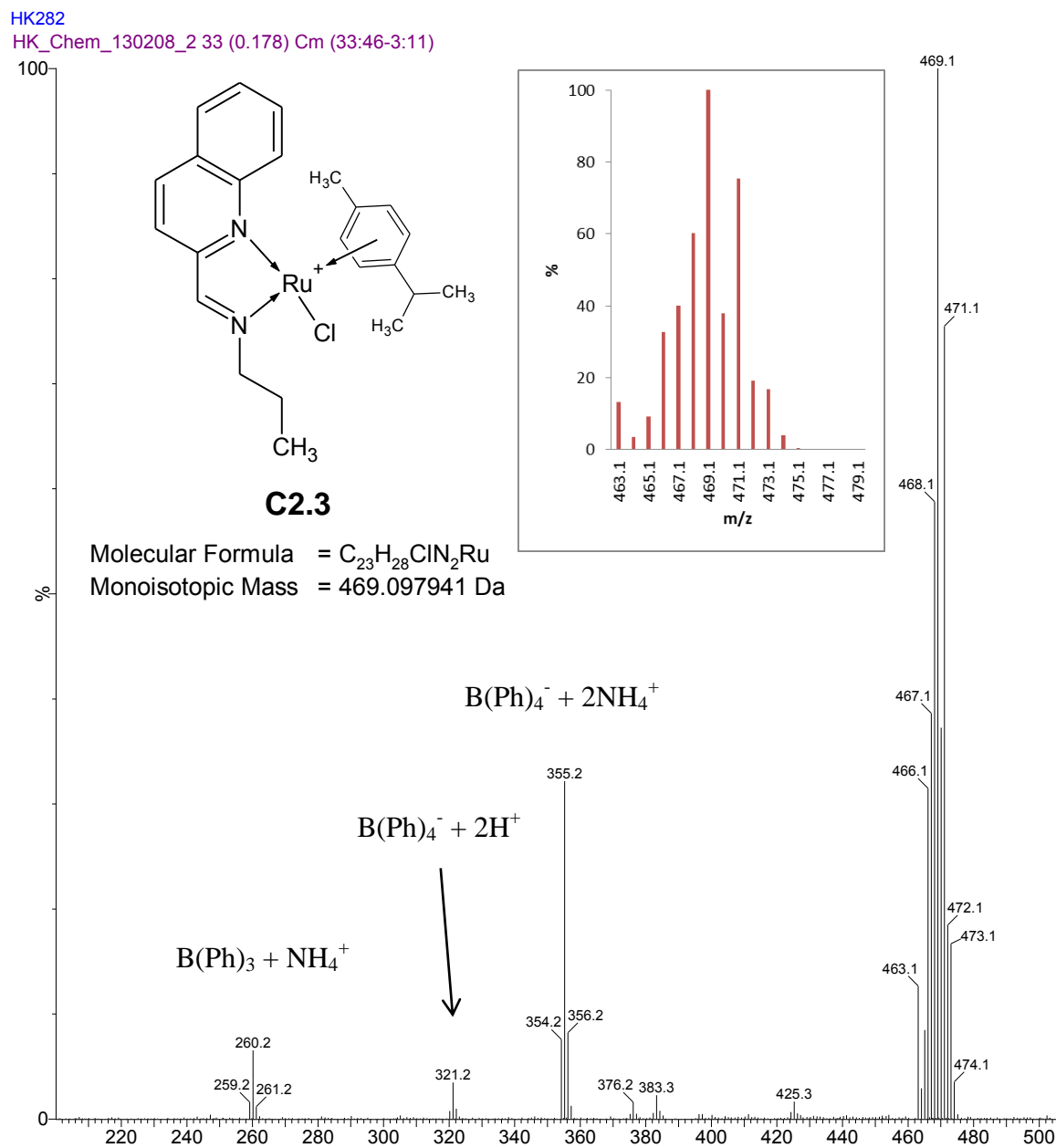
Figure 2.10 ESI-MS (positive mode) spectrum of model complex C2.3.

Chapter 2: **Synthesis and Characterization of Model and Siloxane Functionalized RuCl(p-cymene)(N,N) Complexes Containing a Siloxane Tether at the Imine Nitrogen**

2.3 Concluding remarks

Model and functionalized ligands **L2.1**-**L2.6** were successfully synthesized and reacted with RuCl$_2$(*p*-cymene)]$_2$ to afford the model and functionalized complexes **C2.1I**-**C2.3I** and **C2.1**-**C2.6** as their respective hexafluorophosphate and tetraphenylborate salts in moderate to high yields. The hexafluorophosphate counter-ion was not large enough to efficiently stabilize the formed functionalized complexes and therefore it was opted to use the tetraphenylborate counter-ion instead. This allowed for the isolation of the functionalized complexes as stable orange to brown solids and in moderate yields and by changing the solvent from ethanol to DCM allowed an even further increase in the yield. This increase in the yield was of paramount importance because fairly large quantities of functionalized complex were needed to produce a sufficient amount of immobilized catalyst. This will however be discussed in more detail in the chapters to follow.

The presence of the siloxane functionalities of the functionalized complexes **C2.4**-**C2.6** were monitored throughout to ensure it did not undergo reduction or get hydrolyzed during any step of the synthetic procedure which could potentially lead to problems in subsequent reactions.

In general both the model and functionalized complexes showed decent thermal stability with the functionalized complexes decomposing without melting around 200 ˚C compared to a varied melting point range for the model complexes (176-223 ˚C).

Attempts to reduce the imine functionality of ligands **L2.4**-**L2.6** to try and afford amine ligands were successful but unfortunately also resulted in the reduction of the siloxane functionality. An attempt to avoid this problem by synthesizing a binuclear type ligand system was also unsuccessful and resulted in the formation of an unsymmetrical cyclic bis(pyridylimino-3-propyl)-amine ligand.

Chapter 2: Synthesis and Characterization of Model and Siloxane Functionalized RuCl(p-cymene)(N,N) Complexes Containing a Siloxane Tether at the Imine Nitrogen

2.4 Experimental section

2.4.1 General remarks and instrumentation

All reactions were carried out under a nitrogen atmosphere making use of standard Schlenk techniques. Highly air-sensitive materials were stored in a nitrogen purged glovebox and all manipulations with these materials were carried out in the glovebox to prevent decomposition or oxidation. [RuCl$_2$(p-cymene)]$_2$ was prepared according to literature procedures [30].

Fourier transform infrared (FT-IR) spectra were recorded using an ATR accessory on a Nicolet Avatar 330 FT-IR spectrometer. ^{1}H and ^{13}C NMR spectra were recorded on a Varian Unity Inova instrument at 300, 400 and 600 MHz for ^{1}H and 75, 100 and 150 MHz for ^{13}C. ESI mass spectra were recorded by direct injection into a stream of acetonitrile and 0.1 % formic acid employing a cone voltage of 15V using a Waters API Quattro Micro spectrometer. A Thermo Elemental Analyzer CHNS-O was used for the accurate determination of the elemental composition of samples.

2.4.2 Materials

Reagents were purchased from Sigma-Aldrich and used as received; these include 2-pyridinecarboxaldehyde, 2-quinolinecarboxaldehyde, 6-methyl-2-pyridinecarboxaldehyde, *n*-propylamine, 3-aminopropyltriethoxysilane and *α*-terpinine. Ruthenium(III) chloride hydrate (RuCl$_3$·xH$_2$O) was obtained from SA Precious Metals [Pty] Limited. Solvents were purchased from Sigma-Aldrich and Kimix Chemicals and were dried by refluxing over the appropriate drying agents. Dichloromethane (DCM) and acetonitrile were dried over phosphorous pentoxide, hexane and pentane over sodium wire and diethyl ether, tetrahydrofuran (THF) and toluene over sodium wire and benzophenone. Ethanol and methanol were dried over dry magnesium turnings and iodine. Dimethyl sulfoxide was dried over 0.4 nm molecular sieves.

Chapter 2: Synthesis and Characterization of Model and Siloxane Functionalized RuCl(p-cymene)(N,N) Complexes Containing a Siloxane Tether at the Imine Nitrogen

2.4.3 Synthesis of model and functionalized ligands L2.1-L2.6

2.4.3.1 Synthesis of model ligands L2.1-L2.3

For model ligand **L2.1**: 2-pyridinecarboxaldehyde (0.403 g, 3.73 mmol) was dissolved in dry diethyl ether (10 mL) in a 50 mL round bottomed flask. To this stirring solution, *n*-propylamine (0.223 g, 3.73 mmol) was added followed by the addition of a small amount of $MgSO_4$. This solution was allowed to stir at room temperature for a further 3 hours and was filtered to remove the $MgSO_4$. The solvent was removed on a rotary evaporator and a yellow oily product was obtained. This oil was dissolved in minimum amount of DCM and washed with distilled water (2x20 mL) to remove any unreacted aldehyde. The organic layer was separated from the water layer and dried over $MgSO_4$ and filtered. After removal of the solvent under vacuum a pure yellow oil was obtained as product in high yield.

Model ligand **L2.1**: Yellow oil, yield 78 %. IR: FT-IR, v/cm^{-1}: 1649 (s, imine, C=N). ^{1}H NMR (300 MHz, (CDCl$_3$): δ (ppm) = 0.93 (t, $^3J_{H-H}$ = 7.3 Hz, 3H, NCH$_2$CH$_2$C**H**$_3$), 1.73 (m, 2H, NCH$_2$C**H**$_2$CH$_3$), 3.62 (td, J_{H-H} = 7.0, 1.5 Hz, 2H, NC**H**$_2$CH$_2$CH$_3$), 7.27 (dd, $^3J_{H-H}$ = 7.6, 5.0 Hz, 1H, Pyr), 7.70 (td, J_{H-H} = 8.1, 1.6 Hz, 1H, Pyr), 7.97 (d, $^3J_{H-H}$ = 7.7 Hz, 1H, Pyr), 8.54 (d, $^3J_{H-H}$ = 4.8 Hz, 1H, Pyr), 8.35 (s, 1H, C**H**-*imine*).

Model ligand **L2.2**: Colorless oil, yield 82 %. IR: FT-IR, v/cm^{-1}: 1649 (s, imine, C=N). ^{1}H NMR (300 MHz, (CDCl$_3$): δ (ppm) = 0.93 (t, $^3J_{H-H}$ = 7.3 Hz, 3H, NCH$_2$CH$_2$C**H**$_3$), 1.73 (m, 2H, NCH$_2$C**H**$_2$CH$_3$), 2.56 (s, 3H, Pyr-C**H**$_3$), 3.60 (td, 2H, J_{H-H} = 6.9, 1.3 Hz, NC**H**$_2$CH$_2$CH$_3$), 7.15 (d, $^3J_{H-H}$ = 7.6 Hz, 1H, Pyr), 7.59 (t, $^3J_{H-H}$ = 7.8 Hz, 1H, Pyr), 7.78 (d, $^3J_{H-H}$ = 7.8 Hz, 1H, Pyr), 8.33 (s, 1H, C**H**-*imine*).

Model ligand **L2.3**: Sticky Yellow oil, yield 79 %. IR: FT-IR, v/cm^{-1}: 1645 (s, imine, C=N). ^{1}H NMR (400 MHz, (CDCl$_3$): δ (ppm) = 1.00 (t, $^3J_{H-H}$ = 7.4 Hz, 3H, NCH$_2$CH$_2$C**H**$_3$), 1.81 (m, 2H, NCH$_2$C**H**$_2$CH$_3$), 3.73 (td, J_{H-H} = 6.8, 1.4 Hz, 2H, NC**H**$_2$CH$_2$CH$_3$), 7.58 (t, $^3J_{H-H}$ = 8.2 Hz, 1H,

Chapter 2: **Synthesis and Characterization of Model and Siloxane Functionalized RuCl(p-cymene)(N,N) Complexes Containing a Siloxane Tether at the Imine Nitrogen**

Pyr), 7.75 (t, $^3J_{H-H}$ = 8.4 Hz, 1H, Pyr), 7.86 (d, $^3J_{H-H}$ = 7.6 Hz, 1H, Pyr), 8.15 (d, $^3J_{H-H}$ = 8.8 Hz, 1H, Pyr), 8.17 (d, $^3J_{H-H}$ = 8.6 Hz, 1H, Pyr), 8.20 (d, $^3J_{H-H}$ = 8.6 Hz, 1H, Pyr), 8.56 (s, 1H, C**H-***imine*).

2.4.3.2 Synthesis of functionalized ligands L2.4-L2.6

For functionalized ligand **L2.6**: 2-quinolinecarboxaldehyde (0.418 g, 2.66 mmol) was dissolved in dry diethyl ether (10 mL) and added to a 50 mL round bottomed flask. To this stirring solution 3-aminopropyltriethoxysilane (0.589 g, 2.66 mmol) was added followed by the addition of a small amount of MgSO$_4$. This solution was allowed to stir at room temperature for a further 17 hours and was filtered to remove the MgSO$_4$. The solvent was removed on a rotary evaporator and a brown oil was isolated in high yield.

Functionalized ligand **L2.4**: Yellow oil, yield 75 %. IR: FT-IR, v/cm^{-1}: 1649 (s, imine, C=N). ^{1}H NMR (300 MHz, (CDCl$_3$): δ (ppm) = 0.67 (t, $^3J_{H-H}$ = 8.5 Hz, 2H, NCH$_2$CH$_2$C**H**$_2$Si), 1.17 (t, 9H, $^3J_{H-H}$ = 6.9 Hz, CH$_2$CH$_2$Si(OCH$_2$C**H**$_3$)$_3$), 1.84 (m, 2H, NCH$_2$C**H**$_2$CH$_2$Si), 3.66 (t, 2H, $^3J_{H-H}$ = 7.0 Hz, NC**H**$_2$CH$_2$CH$_2$Si), 3.78 (q, $^3J_{H-H}$ = 6.9 Hz, 6H, CH$_2$CH$_2$Si(OC**H**$_2$CH$_3$)$_3$), 7.28 (dd, J_{H-H} = 7.5, 4.8 Hz, 1H, Pyr), 7.71 (td, J_{H-H} = 7.5, 1.8 Hz, 1H, Pyr), 7.98 (dt, J_{H-H} = 7.9, 1.0 Hz, 1H, Pyr), 8.62 (d, $^3J_{H-H}$ = 4.8 Hz, 1H, Pyr), 8.35 (s, 1H, C**H-***imine*).

Functionalized ligand **L2.5**: Yellow oil, yield 83 %. IR: FT-IR, v/cm^{-1}: 1649 (s, imine, C=N). ^{1}H NMR (300 MHz, (CDCl$_3$): δ (ppm) = 0.55 (t, $^3J_{H-H}$ = 8.4 Hz, 2H, NCH$_2$CH$_2$C**H**$_2$Si), 1.14 (t, $^3J_{H-H}$ = 6.9 Hz, 9H, CH$_2$CH$_2$Si(OCH$_2$C**H**$_3$)$_3$), 1.47 (m, 2H, NCH$_2$C**H**$_2$CH$_2$Si), 2.51 (s, 3H, Pyr-C**H**$_3$), 3.58 (t, 2H, $^3J_{H-H}$ = 7.0 Hz, NC**H**$_2$CH$_2$CH$_2$Si), 3.75 (q, $^3J_{H-H}$ = 6.9 Hz, 6H, CH$_2$CH$_2$Si(OC**H**$_2$CH$_3$)$_3$), 7.10 (d, $^3J_{H-H}$ = 7.3 Hz, 1H, Pyr), 7.54 (t, $^3J_{H-H}$ = 7.6 Hz, 1H, Pyr), 7.72 (d, $^3J_{H-H}$ = 7.6 Hz, 1H, Pyr), 8.26 (s, 1H, C**H-***imine*).

Functionalized ligand **L2.6**: Brown/orange oil, yield 85 %. IR: FT-IR, v/cm^{-1}: 1645 (s, imine, C=N). ^{1}H NMR (400 MHz, (CDCl$_3$): δ (ppm) = 0.73 (t, $^3J_{H-H}$ = 8.6 Hz, 3H, NCH$_2$CH$_2$C**H**$_2$Si),
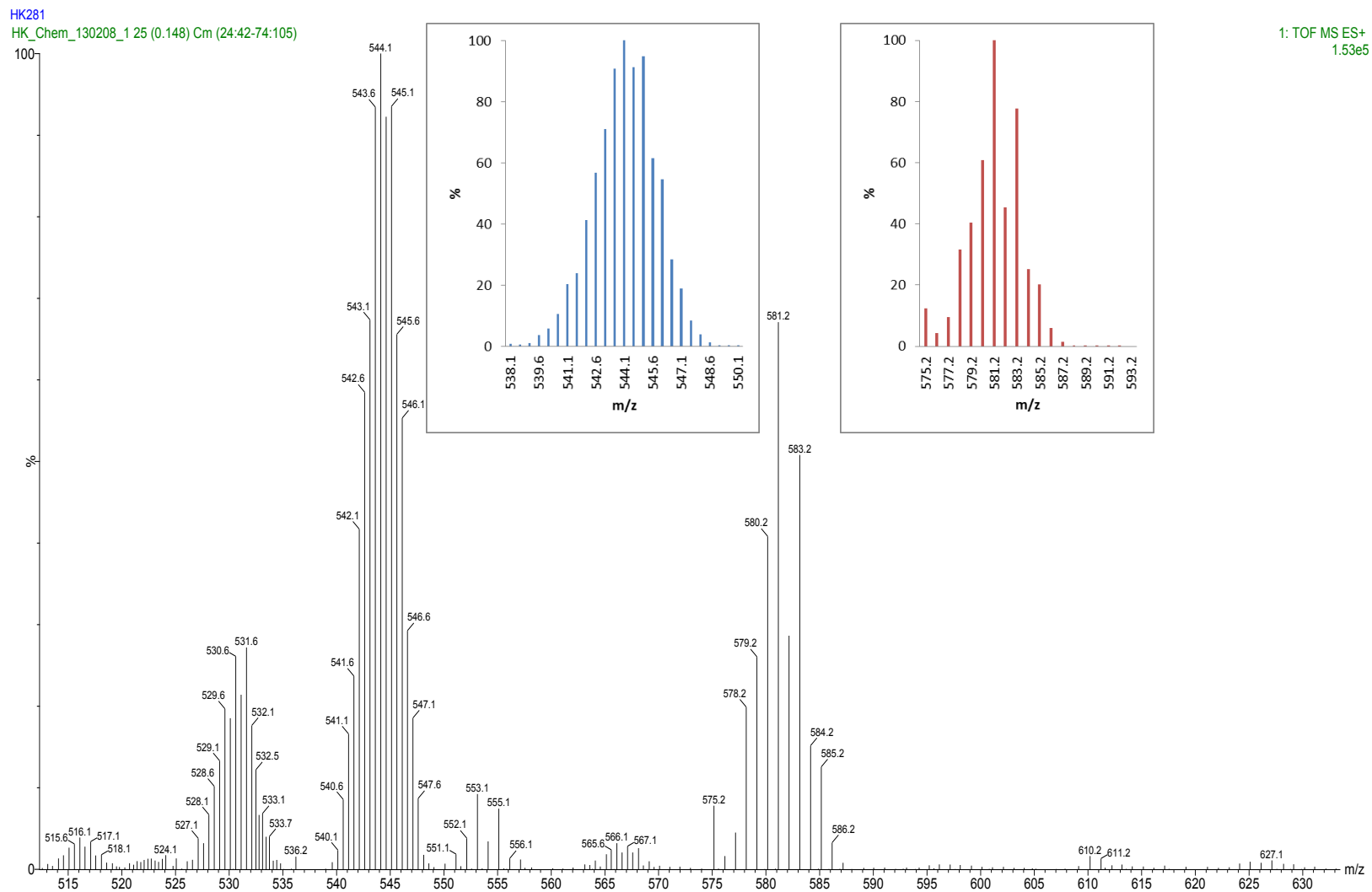
Chapter 2:   Synthesis and Characterization of Model and Siloxane Functionalized RuCl(p-cymene)(N,N) Complexes Containing a Siloxane Tether at the Imine Nitrogen

1.23 (t, $^3J_{\text{H-H}}$ = 6.8 Hz, 9H, CH$_2$CH$_2$Si(OCH$_2$C**H**$_3$)$_3$), 1.90 (m, 2H, NCH$_2$C**H**$_2$CH$_2$Si), 3.75 (t, 2H, $^3J_{\text{H-H}}$ = 6.8 Hz, NC**H**$_2$CH$_2$CH$_2$Si), 3.85 (q, $^3J_{\text{H-H}}$ = 7.0 Hz, 6H, CH$_2$CH$_2$Si(OC**H**$_2$CH$_3$)$_3$), 7.58 (t, $^3J_{\text{H-H}}$ = 8.2 Hz, 1H, Pyr), 7.74 (t, $^3J_{\text{H-H}}$ = 8.4 Hz, 1H, Pyr), 7.85 (d, $^3J_{\text{H-H}}$ = 8.2 Hz, 1H, Pyr), 8.14 (d, $^3J_{\text{H-H}}$ = 8.4 Hz, 1H, Pyr), 8.16 (d, $^3J_{\text{H-H}}$ = 8.6 Hz, 1H, Pyr), 8.20 (d, $^3J_{\text{H-H}}$ = 8.6 Hz, 1H, Pyr), 8.55 (s, 1H, C**H**-*imine*).

2.4.4 Synthesis of model complexes C2.1I-C2.3I and model and functionalized complexes C2.1-C2.6

2.4.4.1   Synthesis of model complexes C2.1I-C2.3I (hexafluorophosphate as counter-ion)

Model complex **C2.1I**:   Model ligand **L2.1** (0.063 g, 0.425 mmol) was dissolved in ethanol (5.0 mL) and the solution added drop-wise to a stirred solution of [Ru(*p*-cymene)Cl$_2$]$_2$ (0.121 g, 0.198 mmol) in ethanol (25 mL). The orange/brown solution was allowed to stir for 18 hours at room temperature under a nitrogen atmosphere. After the allotted time the reaction volume was reduced by half and NaPF$_6$ (0.034 g, 0.202 mmol) added. This mixture was stirred at 0 ˚C for 3 hours after which it was placed in the fridge overnight (precipitate already started to form during this time). The mixture was filtered and a yellow solid was recovered as product. The solid was washed with cold ethanol and dried under vacuum.

Model complex **C2.1I**: Yellow solid, yield 82 %. IR: FT-IR, v/cm^{-1}: 1599 (s, imine, C=N), 832 (s, P-F). ^{1}H NMR (300 MHz, (CD$_3$)$_2$CO): δ (ppm) = 0.99 (t, $^3J_{\text{H-H}}$ = 7.3 Hz, 3H, NCH$_2$CH$_2$C**H**$_3$), 1.09 (d, $^3J_{\text{H-H}}$ = 6.9 Hz, 3H, CH(C**H**$_3$)$_{2\ CYE}$), 1.17 (d, $^3J_{\text{H-H}}$ = 6.9 Hz, 3H, CH(C**H**$_3$)$_{2\ CYE}$), 2.00 (m, 2H, NCH$_2$C**H**$_2$CH$_3$, *masked by (CD$_3$)$_2$CO signal*), 2.81 (s, 3H, C**H**$_{3\ CYE}$), 2.00 (sep, 1H, C**H**(CH$_3$)$_{2\ CYE,}$ *masked by (CD$_3$)$_2$CO signal*), 4.65 & 4.40 (m, 2H, NC**H**$_2$CH$_2$CH$_3$), 5.96 (t, 2H, $^3J_{\text{H-H}}$ = 7.3 Hz, Ar$_{CYE}$), 6.24 (d, $^3J_{\text{H-H}}$ = 6.5 Hz, 1H, Ar$_{CYE}$), 6.29 (d, $^3J_{\text{H-H}}$ = 6.9 Hz, 1H, Ar$_{CYE}$), 7.84 (t, $^3J_{\text{H-H}}$ = 5.6 Hz, 1H, Pyr), 8.26 (d, $^3J_{\text{H-H}}$ = 7.8 Hz, 1H, Pyr), 8.31 (t, $^3J_{\text{H-H}}$ = 7.8 Hz, 1H, Pyr), 9.60 (d, $^3J_{\text{H-H}}$ = 5.5 Hz, 1H, Pyr), 8.81 (s, 1H, C**H**-*imine*). Elemental Analysis (%): Calc.
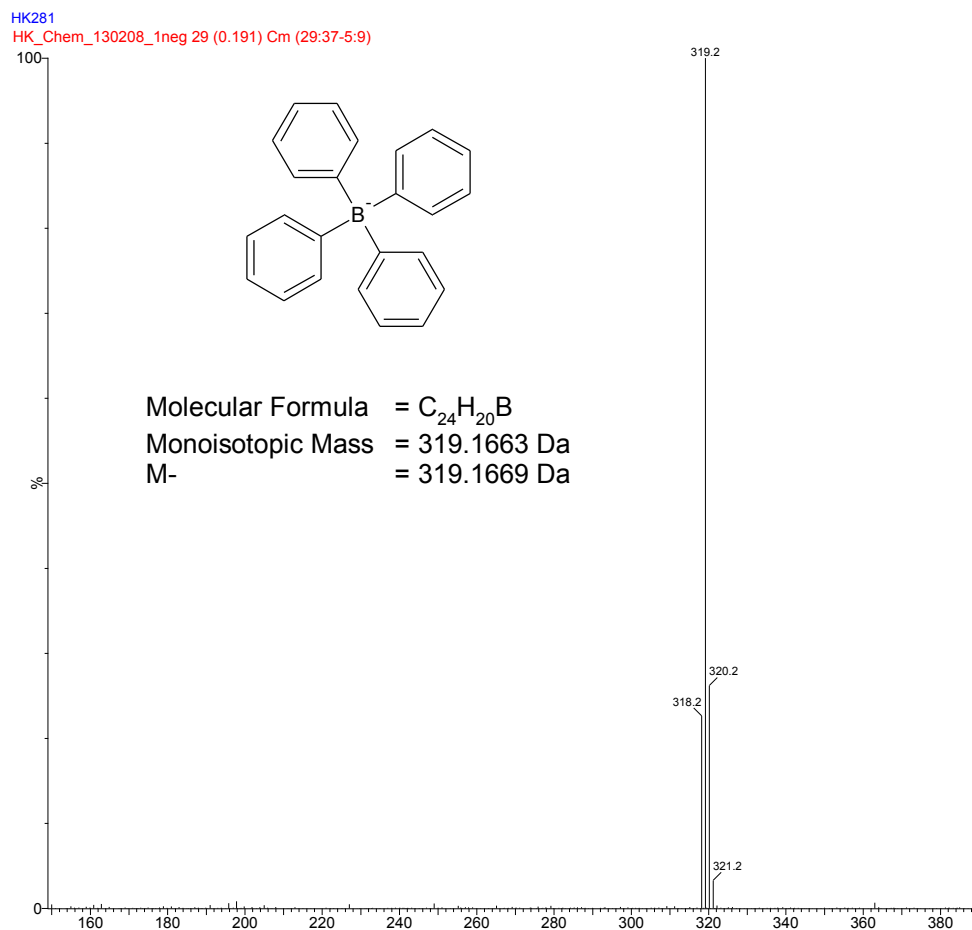
Chapter 2: Synthesis and Characterization of Model and Siloxane Functionalized RuCl(p-cymene)(N,N) Complexes Containing a Siloxane Tether at the Imine Nitrogen

For $C_{43}H_{46}BClN_2Ru$ (738.2): C, 40.47; H, 4.65; N, 4.97; Found: C, 40.74; H, 4.79; N, 4.63. MS (ESI, m/z): 419.1 $[M]^+$. Melting Point: 190-192 ˚C

Model complex **C2.2I**: Orange solid, yield 89 %. IR: FT-IR, v/cm^{-1}: 1598 (s, imine, C=N), 832 (s, P-F). ^{1}H NMR (300 MHz, (CD$_3$)$_2$CO): δ (ppm) = 0.95 (t, $^3J_{H-H}$ = 7.3 Hz, 3H, NCH$_2$CH$_2$**CH$_3$**), 1.07 (d, $^3J_{H-H}$ = 6.9 Hz, 3H, CH(**CH$_3$**)$_2$ *CYE*), 1.14 (d, $^3J_{H-H}$ = 6.9 Hz, 3H, CH(**CH$_3$**)$_2$ *CYE*), 2.00 (m, 2H, NCH$_2$**CH$_2$**CH$_3$, *masked by (CD$_3$)$_2$CO signal*), 2.32 (s, 3H, **CH$_3$** *CYE*), 2.74 (sep, 1H, **CH**(CH$_3$)$_2$ *CYE*), 3.23 (s, 3H, **CH$_3$** *Pyr*), 4.39 & 4.65 (m, 2H, N**CH$_2$**CH$_2$CH$_3$), 5.96 (d, 2H, $^3J_{H-H}$ = 7.3 Hz, Ar$_{CYE}$), 6.30 (d, $^3J_{H-H}$ = 6.3 Hz, 1H, Ar$_{CYE}$), 6.36 (d, $^3J_{H-H}$ = 6.8 Hz, 1H, Ar$_{CYE}$), 7.83 (d, $^3J_{H-H}$ = 7.8 Hz, 1H, Pyr), 8.07 (d, $^3J_{H-H}$ = 7.6 Hz, 1H, Pyr), 8.15 (t, $^3J_{H-H}$ = 7.6 Hz, 1H, Pyr), 8.75 (s, 1H, **CH**-*imine*). Elemental Analysis (%): Calc. For $C_{44}H_{48}BClN_2Ru$ (752.2): C, 41.56; H, 4.88; N, 4.85; Found: C, 41.62; H, 4.93; N, 4.58. MS (ESI, m/z): 433.1 $[M]^+$. Melting Point: 210-212 ˚C

Model complex **C2.3I**: Dark orange solid, yield 80 %. IR: FT-IR, v/cm^{-1}: 1593 (s, imine, C=N), 833 (s, P-F). ^{1}H NMR (300 MHz, (CD$_3$)$_2$CO): δ (ppm) = 0.99 (t, 3H, NCH$_2$CH$_2$**CH$_3$**, *overlapping with* CH(**CH$_3$**)$_2$ *CYE*), 0.90 (d, $^3J_{H-H}$ = 6.9 Hz, 3H, CH(**CH$_3$**)$_2$ *CYE*), 1.01 (d, 3H, CH(**CH$_3$**)$_2$ *CYE, overlapping with* NCH$_2$CH$_2$**CH$_3$**), 2.15 (m, 2H, NCH$_2$**CH$_2$**CH$_3$, *masked by (CD$_3$)$_2$CO signal*), 2.28 (s, 3H, **CH$_3$** *CYE*), 2.50 (sep, 1H, **CH**(CH$_3$)$_2$ *CYE*), 4.59 & 4.81 (m, 2H, N**CH$_2$**CH$_2$CH$_3$), 6.04 (d, 1H, $^3J_{H-H}$ = 6.0 Hz, Ar$_{CYE}$), 6.24 (s, 1H, Ar$_{CYE}$), 6.37 (d, $^3J_{H-H}$ = 6.2 Hz, 1H, Ar$_{CYE}$), 8.00 (t, $^3J_{H-H}$ = 8.0 Hz, 1H, Pyr), 8.15 (t, $^3J_{H-H}$ = 8.5 Hz, 1H, Pyr), 8.29 (d, $^3J_{H-H}$ = 8.0 Hz, 1H, Pyr), 8.34 (d, $^3J_{H-H}$ = 8.2 Hz, 1H, Pyr), 8.86 (d, $^3J_{H-H}$ = 5.4 Hz, 1H, Pyr), 8.89 (d, $^3J_{H-H}$ = 5.0 Hz, 1H, Ar), 9.06 (s, 1H, **CH**-*imine*). Elemental Analysis (%): Calc. For $C_{47}H_{48}BClN_2Ru$ (788.2): C, 44.99; H, 4.60; N, 4.56; Found: C, 44.98; H, 4.66; N, 4.37. MS (ESI, m/z): 469.1 $[M]^+$. Melting Point: 223-225 ˚C

Chapter 2: Synthesis and Characterization of Model and Siloxane Functionalized RuCl(p-cymene)(N,N) Complexes Containing a Siloxane Tether at the Imine Nitrogen

2.4.4.2   Synthesis of model complexes C2.1-C2.3 (tetraphenylborate as counter-ion)

Model complex **C2.1**:   Model ligand **L2.1** (0.048 g, 0.33 mmol) was dissolved in ethanol (5.0 mL) and added drop-wise to a stirred solution of [Ru(*p*-cymene)Cl$_2$]$_2$ (0.100 g, 0.163 mmol) in ethanol (10 mL). The solution was allowed to stir overnight at room temperature under a nitrogen atmosphere. The volume of the resulting solution was reduced to about half after the allotted time. NaB(Ph)$_4$ (0.112 g, 0.326 mmol) was added and the reaction mixture was stirred at 0 ˚C for a further 3 h. The flask was left in the freezer overnight to precipitate the product, which was filtered, washed with ethanol and diethyl ether and dried under vacuum. The product was isolated as a yellow powder in moderate to high yield.

Model complex **C2.1**: Orange solid, yield 73 %. IR: FT-IR, v/cm^{-1}: 1597 (s, imine, C=N), 734, 704 (s, B-C). ^{1}H NMR (300 MHz, (CD$_3$)$_2$SO): δ (ppm) = 0.94 (t, $^3J_{H-H}$ = 7.3 Hz, 3H, NCH$_2$CH$_2$C**H**$_3$), 0.92 (d, $^3J_{H-H}$ = 6.9 Hz, 3H, CH(C**H**$_3$)$_2$ *CYE*), 1.01 (d, $^3J_{H-H}$ = 6.8 Hz, 3H, CH(C**H**$_3$)$_2$ *CYE*), 1.83 & 1.95 (m, 2H, NCH$_2$C**H**$_2$CH$_3$), 2.16 (s, 3H, C**H**$_3$ *CYE*), 2.50 (sep, 1H, C**H**(CH$_3$)$_2$ *CYE, masked by DMSO signal*), 4.23 & 4.48 (m, 2H, NC**H**$_2$CH$_2$CH$_3$), 5.91 (t, $^3J_{H-H}$ = 5.2 Hz, 2H, Ar$_{CYE}$), 6.17 (d, $^3J_{H-H}$ = 5.9 Hz, 1H, Ar$_{CYE}$), 6.24 (d, $^3J_{H-H}$ = 6.3 Hz, 1H, Ar$_{CYE}$), 6.79, 6.92, 7.19 (t, t, m, 20H, B(Ph)$_4$), 7.79 (t, $^3J_{H-H}$ = 6.0 Hz, 1H, Pyr), 8.14 (d, $^3J_{H-H}$ = 6.6 Hz, 1H, Pyr), 8.23 (t, $^3J_{H-H}$ = 7.6 Hz, 1H, Pyr), 9.60 (d, $^3J_{H-H}$ = 5.4 Hz, 1H, Pyr), 8.73 (s, 1H, C**H**-*imine*). ^{13}C {^{1}H} NMR (75 MHz, (CD$_3$)$_2$SO): δ (ppm) = 11.3 (**C**H$_3$); 21.3, 22.1, 22.4 (**C**H$_3$ *CYE*); 18.3, 67.7 (**C**H$_2$); 30.4, 84.2, 84.8, 84.9, 87.2 (**C**H$_{CYE}$); 103.0, 104.4 (**C**$_{CYE}$), 128.2, 128.6, 139.7, 154.4, (**C**H*pyr*); 155.8 (**C***pyr*); 167.1 (**C**H-*imine*). Elemental Analysis (%): Calc. For C$_{43}$H$_{46}$BClN$_2$Ru (738.2): C, 69.96; H, 6.28; N, 3.79; Found: C, 69.63; H, 6.28; N, 3.49. MS (ESI, *m/z*): 419.1 [M]$^+$. Melting Point: 176-178 ˚C

Model complex **C2.2**: Light brown solid, yield 70 %. IR: FT-IR, v/cm^{-1}: 1598 (s, imine, C=N), 735, 707 (s, B-C). ^{1}H NMR (300 MHz, (CD$_3$)$_2$SO): δ (ppm) = 0.89 (t, $^3J_{H-H}$ = 7.3 Hz, 3H, NCH$_2$CH$_2$C**H**$_3$), 0.89 (d, $^3J_{H-H}$ = 7.3 Hz, 3H, CH(C**H**$_3$)$_2$ *CYE*), 0.97 (d, $^3J_{H-H}$ = 7 Hz, 3H, CH(C**H**$_3$)$_2$ *CYE*), 1.82 & 1.92 (m, 2H, NCH$_2$C**H**$_2$CH$_3$), 2.17 (s, 3H, C**H**$_3$ *CYE*), 2.50 (sep, 1H,

CH(CH$_3$)$_2$ $_{CYE,}$ *masked by DMSO signal*), 3.10 (s, 3H, **CH$_3$** *Pyr*), 4.22 & 4.45 (m, 2H, NC**H$_2$**CH$_2$CH$_3$), 5.84 (d, $^3J_{H-H}$ = 6.2 Hz, 1H, Ar$_{CYE}$), 5.88 (d, $^3J_{H-H}$ = 6.2 Hz, 1H, Ar$_{CYE}$), 6.24 (d, $^3J_{H-H}$ = 5.9 Hz, 1H, Ar$_{CYE}$), 6.33 (d, $^3J_{H-H}$ = 5.9 Hz, 1H, Ar$_{CYE}$), 6.79, 6.92, 7.17 (t, t, m, 20H, B(Ph)$_4$), 7.75 (d, $^3J_{H-H}$ = 6.5 Hz, 1H, Pyr), 7.95 (d, $^3J_{H-H}$ = 7.3 Hz, 1H, Pyr), 8.09 (t, $^3J_{H-H}$ = 8.1 Hz, 1H, Pyr), 8.67 (s, 1H, **C**H-*imine*). ^{13}C {^{1}H} NMR (75 MHz, (CD$_3$)$_2$SO): δ (ppm) = 11.3 (**CH$_3$**); 21.5, 22.1, 22.2 (**CH$_3$** $_{CYE}$); 18.5, 67.7 (**CH$_2$**); 28.0 (Pyr$_{CH3}$) 30.5, 81.4, 83.7, 86.9, 89.8 (**CH**$_{CYE}$); 126.6, 128.6, 139.1, 154.8 (**CH**pyr); 155.2 (**C**pyr); 167.6 (**CH**-*imine*). Elemental Analysis (%): Calc. For C$_{44}$H$_{48}$BClN$_2$Ru (752.2): C, 70.26; H, 6.43; N, 3.72; Found: C, 69.93; H, 6.15; N, 3.38. MS (ESI, *m/z*): 433.1 [M]$^+$. Melting Point: 206-209 ˚C

Model complex **C2.3**: Brown solid, yield 78 %. IR: FT-IR, v/cm^{-1}: 1592 (s, imine, C=N), 732, 706 (s, B-C). ^{1}H NMR (300 MHz, (CD$_3$)$_2$SO): δ (ppm) = 0.94 (t, $^3J_{H-H}$ = 7.3 Hz, 3H, NCH$_2$CH$_2$C**H$_3$**), 0.73 (d, $^3J_{H-H}$ = 6.7 Hz, 3H, CH(C**H$_3$**)$_2$ *CYE*), 0.84 (d, $^3J_{H-H}$ = 7 Hz, 3H, CH(C**H$_3$**)$_2$ $_{CYE}$), 1.91 & 2.00 (m, 2H, NCH$_2$C**H$_2$**CH$_3$), 2.15 (s, 3H, **CH$_3$** $_{CYE}$), 2.50 (sep, 1H, **CH**(CH$_3$)$_2$ $_{CYE,}$ *masked by DMSO signal*), 4.41 & 4.62 (m, 2H, NC**H$_2$**CH$_2$CH$_3$), 5.93 (d, $^3J_{H-H}$ = 6.2 Hz, 1H, Ar$_{CYE}$), 6.11 (d, $^3J_{H-H}$ = 6.2 Hz, 1H,Ar$_{CYE}$), 6.23 (d, $^3J_{H-H}$ = 6.5 Hz, 1H, Ar$_{CYE}$), 6.34 (d, $^3J_{H-H}$ = 6.2 Hz, 1H, Ar$_{CYE}$), 6.78, 6.92, 7.18 (t, t, m, 20H, B(Ph)$_4$), 7.98 (t, $^3J_{H-H}$ = 8 Hz, 1H, Pyr), 8.13 (t, $^3J_{H-H}$ = 8.1 Hz, 1H, Pyr), 8.23 (d, $^3J_{H-H}$ = 8.2 Hz, 1H, Pyr), 8.27 (d, $^3J_{H-H}$ = 8.3 Hz, 1H, Pyr), 8.65 (d, $^3J_{H-H}$ = 8.5 Hz, 1H, Pyr), 8.85 (d, $^3J_{H-H}$ = 8.2 Hz, 1H, Ar), 9.00 (s, 1H, **CH-***imine*). ^{13}C {^{1}H} NMR (75 MHz, (CD$_3$)$_2$SO): δ (ppm) = 11.3 (**CH$_3$**); 21.1, 21.9, 22.4 (**CH$_3$** $_{CYE}$); 18.4, 68.2 (**CH$_2$**); 30.5, 83.7, 84.6, 86.3, 87.0 (**CH**$_{CYE}$); 104.7, 104.5 (**C**$_{CYE}$), 123.5, 128.8, 130.0, 133.0, 140.7, 148.4, 155.6 (**CH**pyr); 155.2 (**C**pyr); 167.9 (**CH**-*imine*). Elemental Analysis (%): Calc. For C$_{47}$H$_{48}$BClN$_2$Ru·H$_2$O,CH$_2$Cl$_2$ (890.23): C, 64.69; H, 5.88; N, 3.14; Found: C, 64.96; H, 5.75; N, 2.93. MS (ESI, *m/z*): 469.1 [M]$^+$. Melting Point: 216-219 ˚C

Chapter 2: Synthesis and Characterization of Model and Siloxane Functionalized RuCl(p-cymene)(N,N) Complexes Containing a Siloxane Tether at the Imine Nitrogen

2.4.4.3   Synthesis of functionalized complexes C2.4-C2.6 (tetraphenylborate)

Functionalized complex **C2.4**: Functionalized ligand **L2.4** (0.101 g, 0.326 mmol) was dissolved in DCM (5.0 mL) and added drop-wise to a stirred solution of [Ru(*p*-cymene)Cl$_2$]$_2$ (0.100 g, 0.163 mmol) in DCM (10 mL). The solution was allowed to stir overnight at room temperature under nitrogen atmosphere. The volume of the resulting solution was reduced to about half after the allotted time. NaB(Ph)$_4$ (0.110 g, 0.326 mmol) was added and the reaction was stirred at 0 ˚C for a further 3 h. The flask was left in the freezer overnight to precipitate the product, which was filtered, washed with ethanol and diethyl ether and dried under vacuum. The product was isolated as a yellow powder in moderate to high yield.

Functionalized complex **C2.4**: Orange solid, yield 65 %. IR: FT-IR, v/cm^{-1}: 1596 (s, imine, C=N), 733, 705 (s, B-C). ^{1}H NMR (400 MHz, (CD$_3$)$_2$SO): δ (ppm) = 0.69 (t, $^3J_{\text{H-H}}$ = 7.3 Hz, 3H, NCH$_2$CH$_2$**CH**$_2$Si), 0.92 (d, $^3J_{\text{H-H}}$ = 6.9 Hz, 3H, CH(C**H**$_3$)$_2$ *CYE*), 1.01 (d, $^3J_{\text{H-H}}$ = 6.8 Hz, 3H, CH(C**H**$_3$)$_2$ *CYE*), 1.19 (t, $^3J_{\text{H-H}}$ = 8.0 Hz, 9H, CH$_2$CH$_2$Si(OCH$_2$C**H**$_3$)$_3$), 1.83 & 1.95 (m, 2H, NCH$_2$**CH**$_2$CH$_2$Si), 2.16 (s, 3H, **CH**$_3$ *CYE*), 2.50 (sep, 1H, **CH**(CH$_3$)$_2$ *CYE, masked by DMSO signal*), 3.84 (q, $^3J_{\text{H-H}}$ = 6.9 Hz, 6H, CH$_2$CH$_2$Si(O**CH**$_2$CH$_3$)$_3$), 4.23 & 4.48 (m, 2H, N**CH**$_2$CH$_2$CH$_2$Si), 5.91 (t, $^3J_{\text{H-H}}$ = 5.2 Hz, 2H, Ar*CYE*), 6.17 (d, $^3J_{\text{H-H}}$ = 5.9 Hz, 1H, Ar*CYE*), 6.24 (d, $^3J_{\text{H-H}}$ = 6.3 Hz, 1H, Ar*CYE*), 6.79, 6.92, 7.19 (t, t, m, 20H, B(Ph)$_4$), 7.79 (t, $^3J_{\text{H-H}}$ = 6.0 Hz, 1H, Pyr), 8.14 (d, $^3J_{\text{H-H}}$ = 6.6 Hz, 1H, Pyr), 8.23 (t, $^3J_{\text{H-H}}$ = 7.6 Hz, 1H, Pyr), 9.60 (d, $^3J_{\text{H-H}}$ = 5.4 Hz, 1H, Pyr), 8.73 (s, 1H, C**H**-*imine*). ^{13}C {^{1}H} NMR (150 MHz, (CD$_3$)$_2$SO): δ (ppm) = 11.3 (**CH**$_3$); 18.2, 57.8 (Si(O**CH**$_2$**CH**$_3$)$_3$); 21.3, 22.1, 22.4 (**CH**$_3$ *CYE*); 18.3, 67.7 (**CH**$_2$); 30.4, 84.2, 84.8, 84.9, 87.2 (**CH**$_{CYE}$); 103.0, 104.4 (**C**$_{CYE}$), 128.2, 128.6, 139.7, 154.4, (**CH**pyr); 155.8 (**C**pyr); 167.1 (**CH**-*imine*). Elemental Analysis (%): Calc. For C$_{49}$H$_{60}$BClN$_2$O$_3$RuSi (900.4): C, 65.36; H, 6.72; N, 3.11; Found: C, 64.97; H, 6.12; N, 2.97. MS (ESI, *m/z*): 581.2 [M]$^+$. Melting Point: Decomposed without melting (140-145 ˚C)

Functionalized complex **C2.5**: Light brown solid, yield 68 %. IR: FT-IR, v/cm^{-1}: 1597 (s, imine, C=N), 733, 705 (s, B-C). ^{1}H NMR (400 MHz, (CD$_3$)$_2$SO): δ (ppm) = 0.61 (t, $^3J_{\text{H-H}}$ = 7.3 Hz, 3H,

Chapter 2: Synthesis and Characterization of Model and Siloxane Functionalized RuCl(p-cymene)(N,N) Complexes Containing a Siloxane Tether at the Imine Nitrogen

---

$NCH_2CH_2\textbf{CH}_2Si$), 0.91 (d, $^3J_{H-H}$ = 7.3 Hz, 3H, $CH(\textbf{CH}_3)_2$ *CYE*), 0.97 (d, $^3J_{H-H}$ = 7 Hz, 3H, $CH(\textbf{CH}_3)_{2\ CYE}$), 1.16 (t, $^3J_{H-H}$ = 8.0 Hz, 9H, $CH_2CH_2Si(OCH_2\textbf{CH}_3)_3$), 1.82 & 1.92 (m, 2H, $NCH_2\textbf{CH}_2CH_2Si$), 2.17 (s, 3H, $\textbf{CH}_3$ *CYE*), 2.50 (sep, 1H, $\textbf{CH}(CH_3)_{2\ CYE}$, *masked by DMSO signal*), 3.10 (s, 3H, $\textbf{CH}_3$ *Pyr*), 3.84 (q, $^3J_{H-H}$ = 8.0 Hz, 6H, $CH_2CH_2Si(O\textbf{CH}_2CH_3)_3$), 4.22 & 4.45 (m, 2H, $N\textbf{CH}_2CH_2CH_2Si$), 5.84 (d, $^3J_{H-H}$ = 6.2 Hz, 1H, Ar_{CYE}), 5.88 (d, $^3J_{H-H}$ = 6.2 Hz, 1H, Ar_{CYE}), 6.24 (d, $^3J_{H-H}$ = 5.9 Hz, 1H, Ar_{CYE}), 6.33 (d, $^3J_{H-H}$ = 5.9 Hz, 1H, Ar_{CYE}), 6.79, 6.92, 7.17 (t, t, m, 20H, $B(Ph)_4$), 7.75 (d, $^3J_{H-H}$ = 6.5 Hz, 1H, Pyr), 7.96 (d, $^3J_{H-H}$ = 7.3 Hz, 1H, Pyr), 8.09 (t, $^3J_{H-H}$ = 8.1 Hz, 1H, Pyr), 8.67 (s, 1H, C**H**imine). ^{13}C {^1H} NMR (150 MHz, $(CD_3)_2SO$): δ (ppm) = 11.3 ($\textbf{CH}_3$); 18.1, 57.7 ($Si(O\textbf{CH}_2\textbf{CH}_3)_3$); 21.4, 22.1, 22.7 ($\textbf{CH}_{3\ CYE}$); 18.4, 67.7 ($\textbf{CH}_2$); 27.9 ($Pyr_{CH3}$) 30.5, 82.7, 83.7, 86.5, 89.8 ($\textbf{CH}_{CYE}$); 126.6, 128.6, 139.1, 154.8 ($\textbf{CH}pyr$); 155.2 (C*pyr*); 167.6 (**CH**-*imine*). ^{13}C {1H} NMR (75 MHz, $(CD_3)_2SO$): δ (ppm) = 11.3 ($\textbf{CH}_3$); 21.1, 21.9, 22.4 ($\textbf{CH}_{3\ CYE}$); 18.4, 68.2 ($\textbf{CH}_2$); 30.5, 83.7, 84.6, 86.3, 87.0 ($\textbf{CH}_{CYE}$); 121.4, 126.6, 128.5, 135.5, 139.0, 148.4, 154.7 (**CH***pyr*); 154.7 (C*pyr*); 167.7 (**CH**-*imine*). Elemental Analysis (%): Calc. For $C_{50}H_{62}BClN_2O_3RuSi$ (914.5): C, 65.67; H, 6.83; N, 3.06; Found: C, 64.96; H, 6.34; N, 2.72. MS (ESI, *m/z*): 595.2 $[M]^+$. Melting Point: Decomposed without melting (160-165 °C)

Functionalized complex **C2.6**: Brown solid, yield 73 %. IR: FT-IR, v/cm^{-1}: 1594 (s, imine, C=N), 732, 702 (s, B-C). ^1H NMR (400 MHz, $(CD_3)_2SO$): δ (ppm) = 0.94 (t, $^3J_{H-H}$ = 7.3 Hz, 3H, $NCH_2CH_2\textbf{CH}_2Si$), 0.73 (d, $^3J_{H-H}$ = 6.7 Hz, 3H, $CH(\textbf{CH}_3)_2$ *CYE*), 0.84 (d, $^3J_{H-H}$ = 7 Hz, 3H, $CH(\textbf{CH}_3)_{2\ CYE}$), 1.16 (t, $^3J_{H-H}$ = 8.0 Hz, 9H, $CH_2CH_2Si(OCH_2\textbf{CH}_3)_3$), 1.91 & 2.00 (m, 2H, $NCH_2\textbf{CH}_2CH_2Si$), 2.15 (s, 3H, $\textbf{CH}_{3\ CYE}$), 2.50 (sep, 1H, $\textbf{CH}(CH_3)_{2\ CYE}$, *masked by DMSO signal*), 3.78 (q, $^3J_{H-H}$ = 8.0 Hz, 6H, $CH_2CH_2Si(O\textbf{CH}_2CH_3)_3$), 4.41 & 4.62 (m, 2H, $N\textbf{CH}_2CH_2CH_2Si$), 5.93 (d, $^3J_{H-H}$ = 6.2 Hz, 1H, Ar_{CYE}), 6.11 (d, $^3J_{H-H}$ = 6.2 Hz, 1H, Ar_{CYE}), 6.23 (d, $^3J_{H-H}$ = 6.5 Hz, 1H, Ar_{CYE}), 6.34 (d, $^3J_{H-H}$ = 6.2 Hz, 1H, Ar_{CYE}), 6.78, 6.92, 7.18 (t, t, m, 20H, $B(Ph)_4$), 7.98 (t, $^3J_{H-H}$ = 8 Hz, 1H, Pyr), 8.13 (t, $^3J_{H-H}$ = 8.1 Hz, 1H, Pyr), 8.23 (d, $^3J_{H-H}$ = 8.2 Hz, 1H, Pyr), 8.27 (d, $^3J_{H-H}$ = 8.3 Hz, 1H, Pyr), 8.65 (d, $^3J_{H-H}$ = 8.5 Hz, 1H, Pyr), 8.85 (d, $^3J_{H-H}$ = 8.2 Hz, 1H, Ar), 9.00 (s, 1H, C**H**-*imine*). ^{13}C {^1H} NMR (75 MHz, $(CD_3)_2SO$): δ (ppm) = 11.3 ($\textbf{CH}_3$); 21.1, 21.9, 22.4 ($\textbf{CH}_{3\ CYE}$); 18.4, 68.2 ($\textbf{CH}_2$); 30.5, 83.7, 84.6, 86.3, 87.0 ($\textbf{CH}_{CYE}$); 104.7, 104.5 ($\textbf{C}_{CYE}$), 123.5, 128.8, 130.0, 133.0, 140.7, 148.4, 155.6 (**CH***pyr*); 155.2 (C*pyr*); 167.9 (**CH**-

Stellenbosch University http://scholar.sun.ac.za

Chapter 2: Synthesis and Characterization of Model and Siloxane Functionalized RuCl(p-cymene)(N,N) Complexes Containing a Siloxane Tether at the Imine Nitrogen

imine). Elemental Analysis (%): Calc. For $C_{53}H_{62}BClN_2O_3RuSi$ (950.5): C, 66.97; H, 6.57; N, 2.95; Found: C, 66.14; H, 6.42; N, 2.66. MS (ESI, *m/z*): 631.2 $[M]^+$. Melting Point: Decomposed without melting (173-176 ˚C)

Chapter 2:   Synthesis and Characterization of Model and Siloxane Functionalized RuCl(p-cymene)(N,N) Complexes Containing a Siloxane Tether at the Imine Nitrogen

2.5 References

1.   T. Naota, H. Takaya, S-I. Murahashi, *Chem. Rev.*, **1998,** 98*,* 2599.

2.   V. Dragutan, I. Dragutan, *J. Org. Chem.*, **2006**, 691, 5129.

3.   M.P. Doyle, D.C. Forbes, *Chem. Rev.*, **1998**, 98, 911.

4.   B.M. Trost, F.D. Toste, A.B. Pinkerton, *Chem. Rev.*, **2001**, 101, 2067.

5.   G. Maas, *Chem. Soc. Rev.*, **2004**, 23, 183.

6.   F. Ding, Y. Sun, S. Monsaert, R. Drozdzak, I. Dragutan, V. Dragutan, F. Verpoort, *Curr. Org. Synth.*, **2008**, 5, 291.

8.   P. Kumar, R.K. G.D.S. Pandey, *Chem. Soc. Rev.,* **2014**, 43, 707.

9.   A.M. Hayes, D.J. Morris, G.J. Clarkson, M. Wills, *J. Am. Chem. Soc.*, **2005**, 127, 7318.

10.   O. Dayan, B. Çetinkaya, *J. Mol. Catal. A: Chem.*, **2007**, 271, 134.

11.   M.C. Carrión, F. Sepúlveda, F.A. Jalón, B.R. Manzano, *Organometallics*, **2009**, 28, 3822.

12.   A.N. Ajjou, J-L. Pinet, *J. Mol. Catal. A: Chem.*, **2004**, 214, 203.

13.   C. Pelizzi, U. Rizzotti, D. Rogolino, *Organometallics*, **2005**, 24, 5836.

14.   S. Gladiali, E. Alberico, *Chem. Soc. Rev.*, **2006**, 35, 226.

15.   P. Crochet, M.A. Fernaández-Zumel, C. Beauquis, J. Gimeno, *Inorg. Chim. Acta*, **2003**, 356, 114.

16.   R. Noyori, H. Takaya, *Acc. Chem. Res.*, **1990**, 23, 345.

17.   B.R. James, *Catal. Today*, **1997**, 37, 209.

18.   F. Fache, E. Schulz, M.L. Tommasino, M. Lemaire, *Chem. Rev.*, **2000**, 100, 2159.

19.   R. Noyori, *Angew. Chem. Int. Ed. Engl.*, **2002**, 41, 2008.

20.   H-U. Blaser, C. Malan, B. Pugin, F. Spindler, H. Steiner, M. Studer, *Adv. Synth. Catal.*, **2003**, 345, 103.

21.   P. Singh, A. K. Singh, *Organometallics*, **2010**, 29, 6433.

22.   A. Behr, N. Tenhumberg, A. Wintzer, *RSC Adv.*, **2013**, 3, 172.

23.   C. Djerassi, R.R. Engle, *J. Am. Chem. Soc.*, **1963**, 75, 3838.

24.   E.C. Ashby, A.B. Goel, *J. Org. Chem.*, **1981**, 46, 3937.

25.   K. Kaneda, S. Haruna, T. Imanaka, K. Kawamoto, *J. Chem. Soc., Chem. Commun.*, **1990**, 1467.

26.   W. Baratta, P. Rigo, *Eur. J. Inorg. Chem.*, **2008**, 4041.

27.   Z.K. Yu, F.L. Zeng, X.J. Sun, H.X. Deng, J.H. Dong, J.Z. Chen, H.M. Wang, C.X.J. Pei, *Organomet. Chem.*, **2007**, 692, 2306.

28.   O. Dayan, B.J. Cetinkaya, *J. Mol. Catal. A: Chem.*, **2007**, 271, 134.

29.   G. van Koten, K. Vrieze, *Adv. Organomet. Chem.*, **1982**, 21, 151.

30.   M.A. Bennet, T.-N. Huang, T.W. Matheson, A.K. Smith, *Inorg. Synth.*, **1982**, 21, 74.

31.   M. Zhao, Z. Yu, S. Yan, Y. Li, *Tetrahedron Lett.*, **2009**, 50, 4624.

32.   P. Govindaswamy, M. Nethaji, A.R. Chakravarty, *J. Organomet. Chem.*, **2007**, 692, 3664.

33.   R.K. Rath, *J. Organomet. Chem.*, **2001**, 633, 79.

34.   R. Malgas-Enus, S.F. Mapolie, G.S. Smith, *J. Organomet. Chem.*, **2008**, 693, 2279.

35.   G.S. Smith and S.F. Mapolie, *J. Mol. Catal. A: Chem.*, **2004**, 213, 187.

36.   J. Cloete, S.F. Mapolie, *J. Mol. Catal., A: Chem.*, **2006**, 243, 221.

37.   R. Chen, J. Bacsa, S.F. Mapolie, *Polyhedron*, **2003**, 22, 2855.

Stellenbosch University http://scholar.sun.ac.za

Chapter 2: **Synthesis and Characterization of Model and Siloxane Functionalized RuCl(p-cymene)(N,N) Complexes Containing a Siloxane Tether at the Imine Nitrogen**

38. C. Romain, S. Gaillard, M. K. Elmkaddem, L. Toupet, C. Fischmeister, C.M. Thomas, J-L. Renaud, *Organometallics*, **2010**, 29, 1992.

39. M.U. Raja, N. Raja, R. Ramesh, *The Open Catalysis Journal*, **2010**, 3, 30.

40. M. Boča, D. Valigura, W. Linert, *Tetrahedron*, **2000**, 56, 441.

41. N. Bréfuel, C. Lepetit, S. Shova, F. Dahan, J-P. Tuchagues, *Inorg. Chem.*, **2005**, 44, 8916

42. P. Govender, A.K. Renfrew, C.M. Clavel, P.J. Dyson, B. Therrien, G.S. Smith, *Dalton Trans.*, **2011**, 40, 1158.

Chapter 3: Synthesis and Characterization of Model and Siloxane Functionalized RuCl(arene)(N,N) Complexes with Siloxane Tether via the Arene Ring

3.1 Introduction

The synthesis of novel siloxane functionalized urethane linked RuCl(arene)(N,N) complexes, where the siloxane tether is incorporated onto the arene ring, was envisaged that it could afford a system that differs from the one discussed in Chapter 2 where the mode of tethering was via the imine nitrogen as opposed to being via the arene ring. Instead of functionalizing the diimine ligand with a siloxane moiety to incorporate the required siloxane group into the complex, the siloxane tether was to be introduced onto the arene ligand coordinated to the ruthenium metal center instead.   Miyaki *et al*. reported the synthesis of alcohol-containing η^6 ruthenium complexes $[Ru(\eta^6\text{-}C_6H_5(CH_2)_3OH)(PR_3)Cl_2]$ and $[Ru(\eta^6\text{-}C_6H_5(CH_2)_3OH)L_2Cl]BF_4$ (R = Ph, Et; L_2 = 2,2`-bipyridine, 1,10-phenanthroline, 2,2-bis[4(R)-phenyl-1,3-oxazolon-2-yl]propane) from an alcohol functionalized $[Ru(\eta^6\text{-}C_6H_5(CH_2)_3OH)Cl_2]_2$ dimer. Reaction of these complexes with $AgBF_4$ resulted in the formation of alkoxy chelated ruthenium complexes. A summary of these complexes is given in Scheme 3.1 [1].
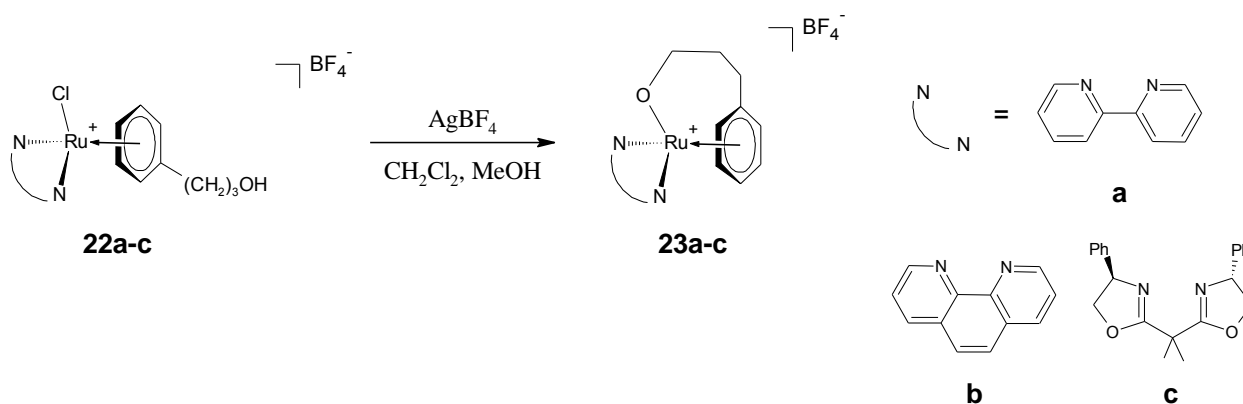
Scheme 3.1 Synthesis of alcohol chelated ruthenium complexes [1].

Chapter 3: Synthesis and Characterization of Model and Siloxane Functionalized RuCl(arene)(N,N) Complexes with Siloxane Tether via the Arene Ring

Similar work was reported by Matsinha *et al*. where they synthesized alcohol-containing mono and binuclear iminopyridyl and salicylaldimine Ru(arene) complexes. The only difference was the use of a 2-hydroxyethoxy moiety instead of the propanol moiety reported by the group of Miyaki *et al.* [2]. Further examples of the use of a 2-hydroxyethoxy moiety have been reported by Soleimannejad and White *et al.* [3,4]. By utilizing this introduced alcohol functionality for further functionalization, it could potentially allow one to attach an appropriate siloxane moiety which could be used to immobilize the complex onto a silica support. This functionalization however can be accomplished by following the two different approaches. A summary of these two envisaged approaches is shown in Scheme 3.2 below.
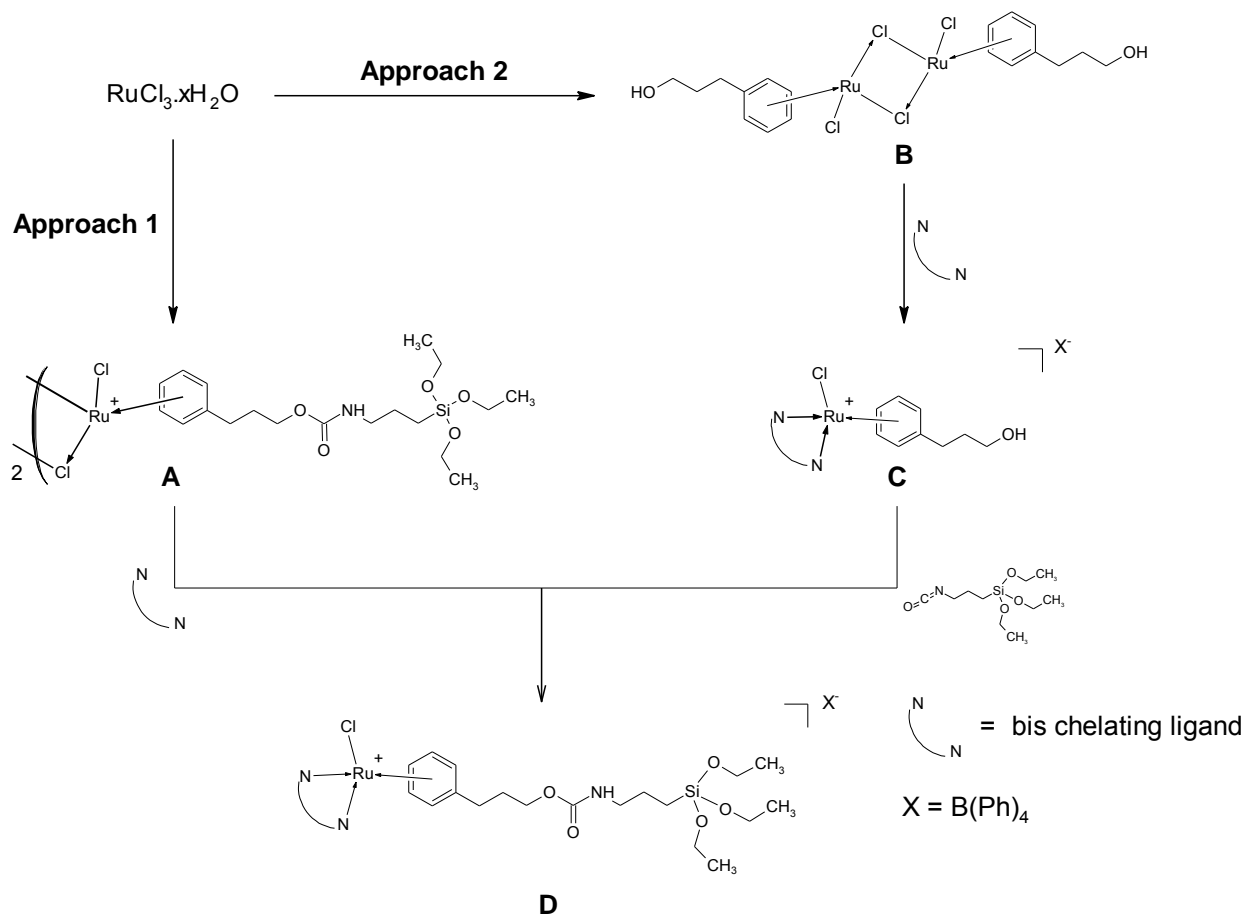
Scheme 3.2 The two different approaches envisaged for the synthesis of the required urethane linked siloxane functionalized target molecules D.

Chapter 3: Synthesis and Characterization of Model and Siloxane Functionalized RuCl(arene)(N,N) Complexes with Siloxane Tether via the Arene Ring

Approach 1 involves the functionalization of an appropriate diene molecule with the siloxane functionality followed by the formation and cleavage of the formed Ru-dimer **A** with a diimine ligand to afford the target molecule **D**. **Approach 2** however would firstly involve the synthesis of the appropriately functionalized Ru-dimer **B** followed by the formation of the propanol functionalized Ru(arene)(N,N) complex **C** similar to previously discussed complexes synthesized by Matsinha and Miyaka. The reaction of the alcohol functionalized complex **C** with the siloxane linker affords the urethane linked siloxane functionalized target molecule **D**.

3.2   Results and discussion

3.2.1   Approach 1: Attempted synthesis of urethane linked siloxane functionalized Ru(arene)(N,N) complexes through the cleavage of a siloxane functionalized Ru-dimer

It was decided to firstly attempt to synthesize the required target molecule by making use of **approach 1** seeing that it would involve one less synthetic step and seemingly looked like the easier of the two approaches. **Approach 1** initially involves the synthesis of a novel siloxane functionalized Ru-dimer **D3.1** (Scheme 3.3) followed by the cleavage of said dimer with appropriate diimine ligands to afford the siloxane functionalized Ru(arene)(N,N) complexes (with the siloxane tether via the arene ring).

3.2.1.1 Synthesis and characterization of urethane linked siloxane functionalized Ru-dimer D3.1

The synthesis of the Ru-dimer **D3.1** was inspired by work carried out by Furrer *et al*. where they reacted 1,4-cyclohexadiene-1-propanol or 1,4-cyclohexadiene-1-propanamine with 1-pyrene-butyric acid to yield their dienyl ligands as either an ester or an amide. This enabled them to synthesize Ru-dimers of the form $[RuCl_2(\eta^6\text{-arene-pyrenyl})]_2$ which forms pyrenylarene ruthenium complexes $[Ru(\eta^6\text{-arene-pyrenyl})Cl_2(pta)]$ when cleaved with 1,3,5-triaza-7-

Chapter 3: Synthesis and Characterization of Model and Siloxane Functionalized RuCl(arene)(N,N) Complexes with Siloxane Tether via the Arene Ring

phosphaadamantane (pta) in a 1:2 ratio [5]. Ang *et al.* were able to successfully synthesize a Ru-dimer functionalized with a 1-methylamide-4-formylphenoxyacetyl moiety [6]. This prompted us to investigate the feasibility of the synthesis of a similar dimer, **D3.1**, as shown in Scheme 3.3. The synthesis of the urethane linked siloxane functionalized diene ligand **DL3.2** was achieved by the reaction between the propanol functionalized diene, 1,4-cyclohexadiene-1-propanol (diene ligand **DL3.1**), synthesized from 3-phenyl-1-propanol by the *Birch reduction* [7], and 3-(triethoxysilyl)propyl isocyanate.
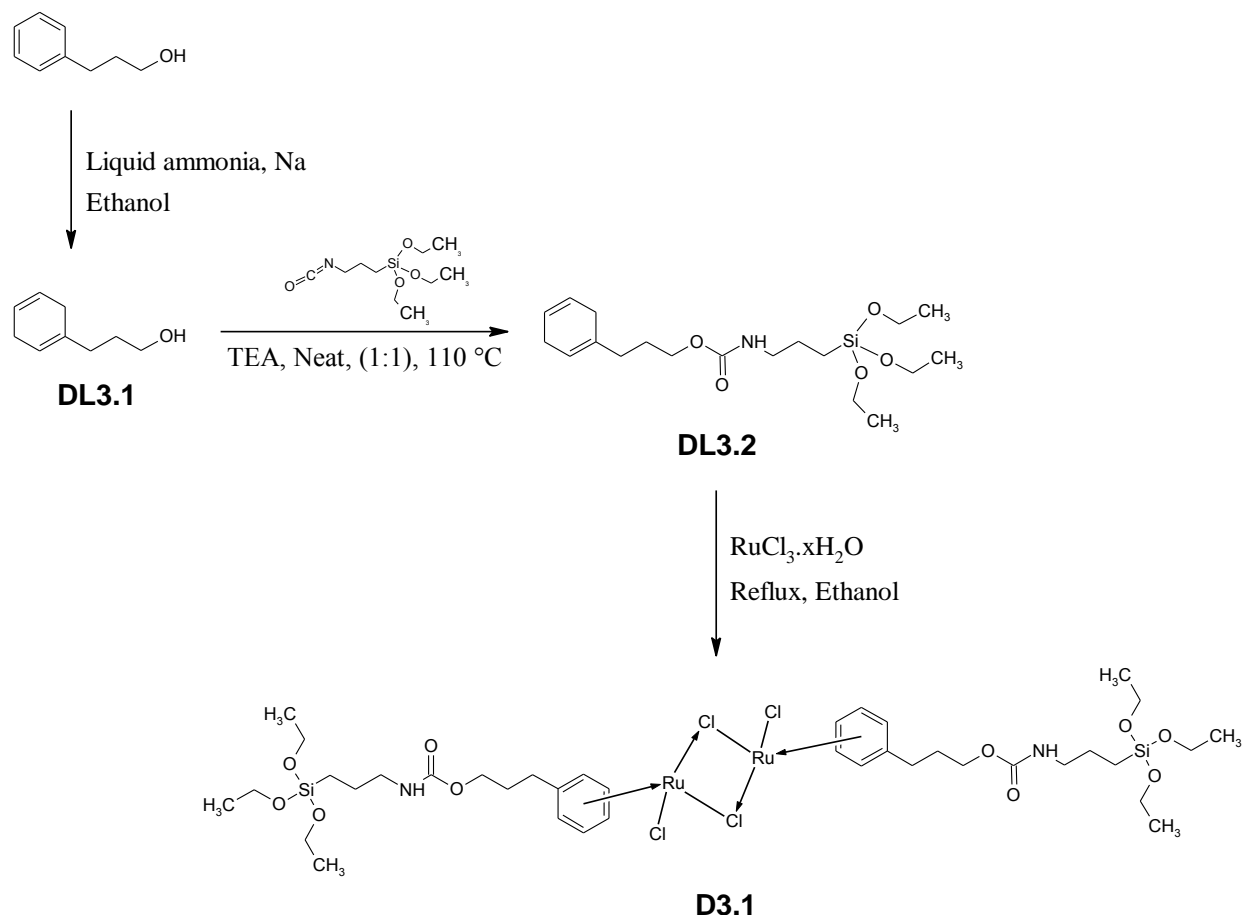
Scheme 3.3 Approach 1: Proposed synthesis of the urethane linked siloxane functionalized Ru(arene)-dimer D3.1.

Chapter 3: Synthesis and Characterization of Model and Siloxane Functionalized RuCl(arene)(N,N) Complexes with Siloxane Tether via the Arene Ring

The diene ligand **DL3.2** was obtained by the reaction of the alcohol and the isocyanate in a 1:1 mole ratio under solventless conditions at 110 °C for 17 hours. Attempts to do the reaction at lower temperatures and ratios resulted in the need for additional workup, which could be avoided with this method. The addition of the triethylamine (TEA) was important as without it the reaction did not go to completion. The reaction was monitored using IR spectroscopy. The carbonyl absorption band of the newly formed urethane was observed at 1698 cm^{-1} with the unreacted isocyanate moiety having a very characteristic absorption band at 2269 cm^{-1} (Figure 3.1).
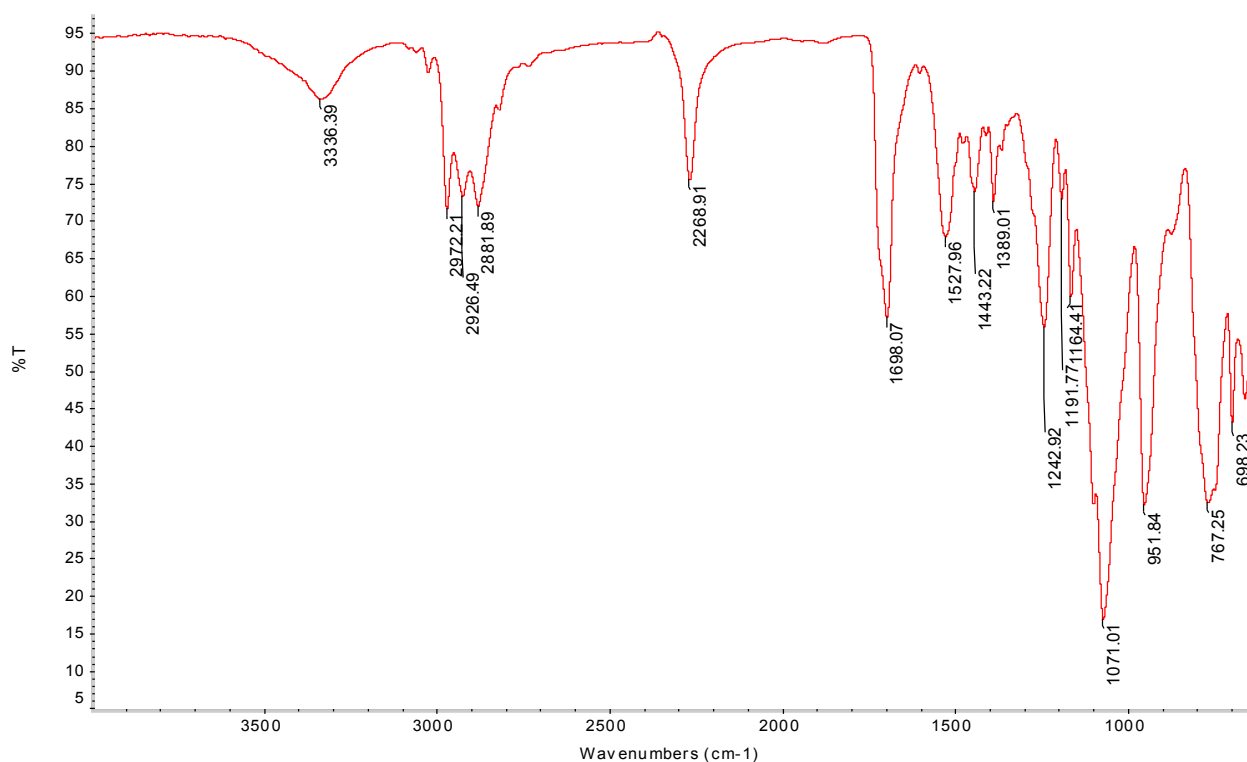
Figure 3.1   IR spectrum of an incomplete urethane linkage reaction for the synthesis of diene ligand DL3.2.

Chapter 3: Synthesis and Characterization of Model and Siloxane Functionalized RuCl(arene)(N,N) Complexes with Siloxane Tether via the Arene Ring

This urethane linked siloxane functionalized diene ligand (**DL3.2**) was also characterized using ^{1}H NMR spectroscopy to confirm the successful synthesis, but will not be discussed here. In the second step to synthesize the siloxane functionalized Ru-dimer **D3.1**, RuCl$_3$·xH$_2$O was refluxed together with the newly synthesized diene ligand **DL3.2** (excess; 1.5:1 mole ratio) in ethanol for 24 hours. Almost immediately after the addition of the diene to the ruthenium salt in ethanol, a black precipitate started forming. The solution turned orange/red from an initial dark brown color (ruthenium precursor in ethanol). The black precipitate was isolated by hot filtration of the mixture followed by the recovery of an orange solid which precipitated from the filtrate after cooling at -5°C overnight. IR analysis of these two solids revealed it to be the same compound with both being only sparingly soluble in DMSO (Figure 3.2).
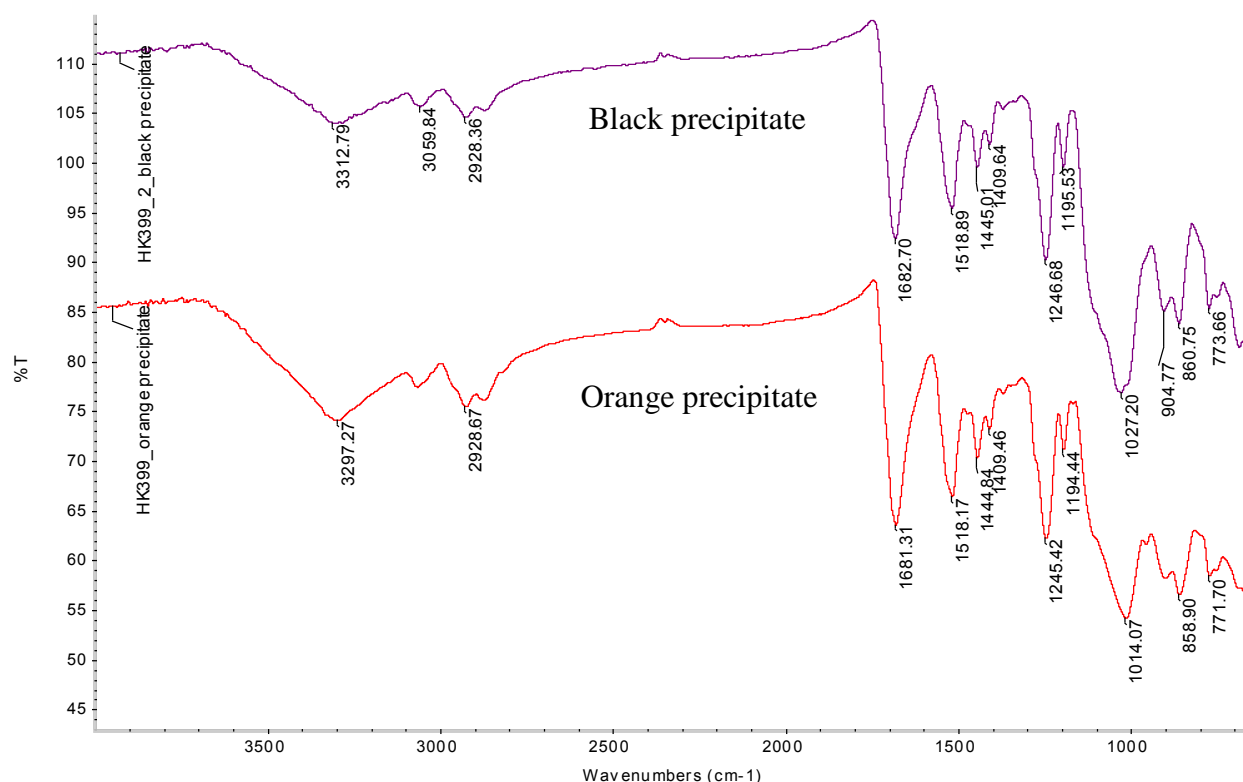
Figure 3.2 IR spectra of products recovered during the attempted synthesis of the target Ru-dimer D3.1.

Chapter 3: Synthesis and Characterization of Model and Siloxane Functionalized RuCl(arene)(N,N) Complexes with Siloxane Tether via the Arene Ring

At first glance, according to the IR spectra, it seems that the formation of the siloxane functionalized dimer was a success. The presence of the urethane moiety can be observed at 1681 cm^{-1} although it is slightly shifted when compared to the diene ligand. The absorption bands at 1027 and 771 cm^{-1} corresponding to the siloxane functionality are also present in the IR spectrum, although being of lower intensity when compared to the diene **DL3.2**. However examination of the ^{1}H NMR spectrum revealed unexpected results (Figure 3.3). In the obtained ^{1}H NMR spectrum wide unresolved peaks are observed at more or less the same chemical shifts as the diene **DL3.2**. However no resonances are observed corresponding to the ethyl group of the siloxane functionality which one would expect as a very intense quartet and triplet resonating around 3.7 and 1.1 ppm respectively.
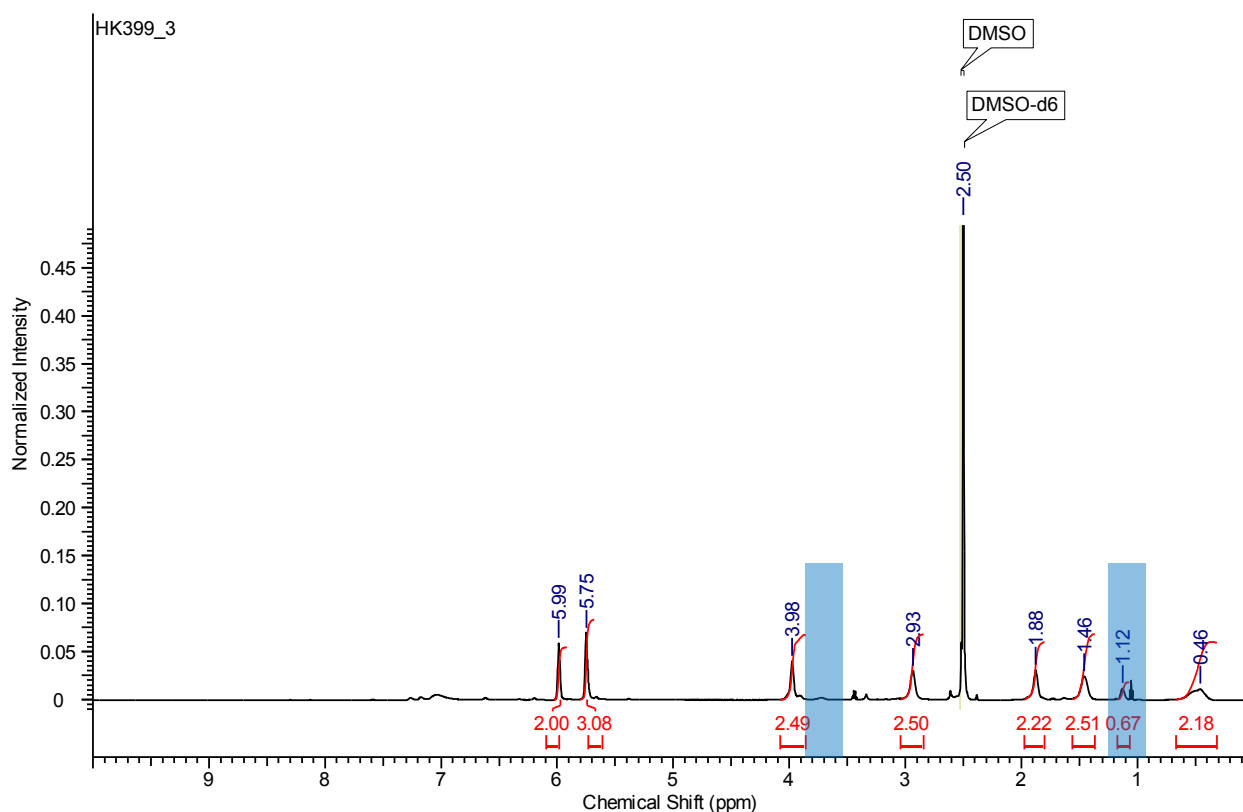
Figure 3.3 ^{1}H NMR spectrum of products recovered during the synthesis of the siloxane functionalized Ru-dimer D3.1.

Chapter 3: Synthesis and Characterization of Model and Siloxane Functionalized RuCl(arene)(N,N) Complexes with Siloxane Tether via the Arene Ring

---

The fact that one can still see an absorption band at 1020 cm^{-1} in the IR spectrum of the obtained product gives an indication that the product still contains some Si-O bonds. This coupled with the decreased solubility and loss of the siloxane functionality in ^{1}H NMR spectrum points to possible polymer formation. This compound was submitted for ESI-MS analysis but no spectrum could be obtained due to its very poor solubility in organic solvents. This reaction was also carried out at shorter reaction times (30 mins to 1 h) and at a lower temperature (60 °C) with no change in the obtained product. Given that the Ru-dimer **D3.1** could not be successfully synthesized; it was decided to abandon **approach 1** and continue with **approach 2**.

3.2.2 Approach 2: Synthesis and characterization of urethane linked siloxane functionalized Ru(arene)(N,N) complexes through the functionalization of propanol functionalized complexes

The second approach involves the synthesis of similar complexes to that previously reported by Matsinha and Miyaki *et al.* and is shown in Scheme 3.4 as complex **C** [1,2]. These alcohol functionalized Ru(arene)(N,N) complexes (**C**) can then be treated with 3-(triethoxysilyl)propyl isocyanate under the appropriate reaction conditions to potentially afford the urethane linked siloxane functionalized complexes **D**.

The first step of this reaction procedure involves the synthesis of the alcohol functionalized Ru-dimer **D3.2** formed by the treatment of RuCl$_3$·xH$_2$O with excess 1,4-cyclohexadiene-1-propanol (**DL3.1**) in refluxing ethanol for 6 hours. The dimer **D3.2**, [Ru(C$_6$H$_5$)(CH$_2$)$_3$OH)Cl$_2$]$_2$, was recovered as orange/red crystals after allowing it to cool to room temperature. Successful synthesis of this alcohol functionalized Ru-dimer was confirmed by IR and ^{1}H NMR spectroscopy with the obtained spectra correlating well to those reported in the literature [1].

Chapter 3: Synthesis and Characterization of Model and Siloxane Functionalized RuCl(arene)(N,N) Complexes with Siloxane Tether via the Arene Ring

Scheme 3.4 Approach 2: Proposed synthesis of the urethane linked siloxane functionalized Ru(arene)(N,N) complex D.

3.2.2.1 Synthesis and characterization of alcohol functionalized Ru(arene)(N,N) complexes C3.1-C3.4.

Initially, it was decided to use the same reaction conditions that were employed for the synthesis of the Ru(*p*-cymene)(N,N) complexes, **C2.1**-**C2.6** reported in Chapter 2. This involved stirring the dimer and ligand in ethanol overnight followed by the addition of the counter-ion.

Relatively low yields were obtained which were partially due to the low solubility of the Ru-dimer in ethanol as well as the workup method employed. Substitution of the solvent with

Chapter 3: Synthesis and Characterization of Model and Siloxane Functionalized RuCl(arene)(N,N) Complexes with Siloxane Tether via the Arene Ring

acetonitrile, as was reported by Miyaki *et al.*, allowed for the successful synthesis of the required Ru(arene)(N,N) complexes **C3.1**-**C3.4**. A more detailed reaction scheme for this synthesis is shown in Scheme 3.5. The alcohol functionalized Ru(arene)(N,N) complexes **C3.1**-**C3.4** were fully characterized using FT-IR, ^{1}H and ^{13}C NMR spectroscopy, ESI mass spectrometry, melting point determination, microanalysis and single crystal XRD for complex **C3.1**. Ligands **L3.1** and **L3.2** were synthesized through Schiff base condensation under similar reaction conditions employed for the synthesis of ligands **L2.1**-**L2.6** reported in Chapter 2 (Scheme 3.6). These ligands were also characterized by IR and ^{1}H NMR spectroscopy to confirm their successful synthesis.

C3.1; Pyridine-propyl (P-P)

C3.2; Pyridine-diisopropylaniline (P-A)

C3.3; Methyl-pyridine-diisopropylaniline (MP-A)

C3.4; Bipyridine (Bipy)
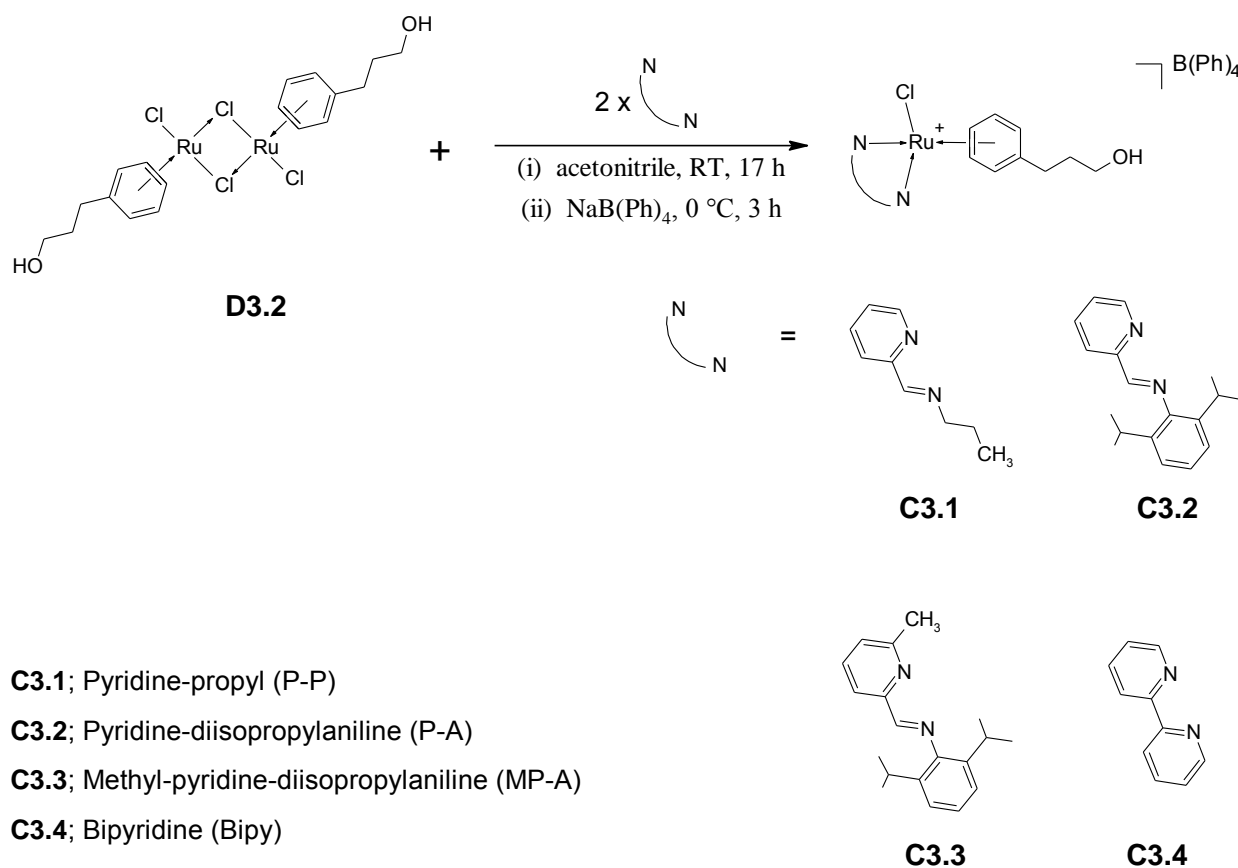
Scheme 3.5 Synthesis of alcohol functionalized Ru(arene)(N,N) complexes C3.1-C3.4.

Chapter 3: Synthesis and Characterization of Model and Siloxane Functionalized RuCl(arene)(N,N) Complexes with Siloxane Tether via the Arene Ring
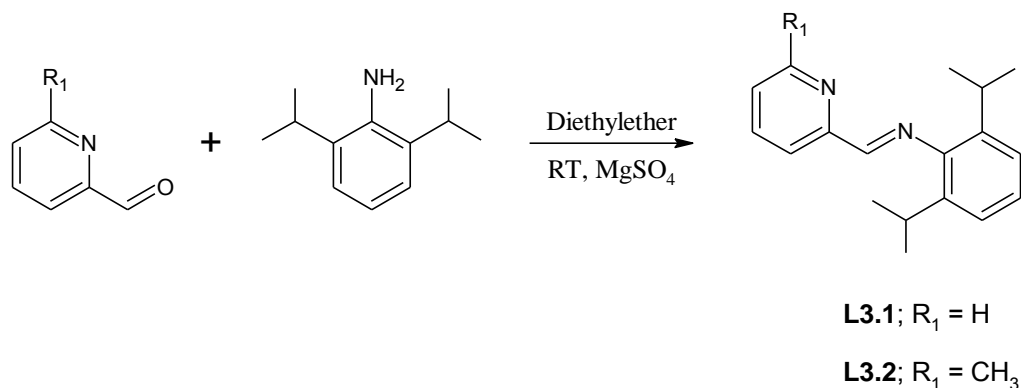
Scheme 3.6 Synthesis of ligands L3.1 and L3.2 through Schiff base condensation.

3.2.2.1.1 Characterization of alcohol functionalized Ru(arene)(N,N) complexes C3.1-C3.4 using FT-IR spectroscopy

The Schiff base ligands (**L2.1**, **L3.1** and **L3.2**) were synthesized through condensation of the appropriate aldehyde and amine and were characterized by FT-IR and ^{1}H NMR spectroscopy. The successful complexation of these complexes was observed by monitoring the shift in the imine absorption band of the free ligand relative to that of the complex using IR spectroscopy. Selected IR vibrations are summarized in Table 3.1.

A noticeable shift in the imine absorption band to lower wave numbers of around 50 cm^{-1} is observed which is indicative of successful complexation of the ligand. For the bipyridine (bipy) derivative **C3.4** a shift to higher wavenumbers from 1577 cm^{-1} to 1603 cm^{-1} is observed for the $v_{C=N}$ of the pyridine ring. The presence of the alcohol functionality is observed as a weak broad band at around 3500 cm^{-1} for complexes **C3.1**-**C3.3** and a sharp narrow band at 3515 cm^{-1} for complex **C3.4**. Two distinct bands are observed around 701-706 cm^{-1} and 732 cm^{-1} and were assigned to the tetraphenylborate counter-ion. FT-IR spectroscopy was found to be a useful technique to monitor the formation of the alcohol functionalized complexes and provided proof that the incorporated alcohol moiety was still present on the arene ring after complexation.

Chapter 3: Synthesis and Characterization of Model and Siloxane Functionalized RuCl(arene)(N,N) Complexes with Siloxane Tether via the Arene Ring

Table 3.1 Selected IR vibrations of alcohol functionalized complexes C3.1-C3.4.[a]

Complex	Imine: $\upsilon_{C=N}$ (cm^{-1})		Pyridine Ring (cm^{-1})				-(CH$_2$)$_3$OH (cm^{-1})	B(Ph)$_4^-$ (cm^{-1})
			Ligand		Complex			
	Ligand	Complex	$\upsilon_{C=N}$	$\upsilon_{C=C}$	$\upsilon_{C=N}$	$\upsilon_{C=C}$		
C3.1	1649	1600	1587	1567	1579	1557	3528	708, 737
C3.2	1639	1613	1584	1566	1579	1557	3339	702, 732
C3.3	1640	1619	1588	1573	1589	1579	3414	701, 732
C3.4	-	-	1577	1556	1603	1578	3518	706, 732

[a] Solids recorded as neat samples using an ATR accessory

3.2.2.1.2 Characterization of alcohol functionalized Ru(arene)(N,N) complexes C3.1-C3.4 using ^{1}H and ^{13}C NMR spectroscopy

^{1}H NMR spectroscopy confirmed successful complex formation with a shift in the resonance of the imine proton being observed for complexes **C3.1**-**C3.3**. A general downfield shift of between 0.5-0.7 ppm was observed for these complexes caused by the change in double bond character as a result of the complexation of the ligand to the precursor. Important resonances corresponding to the protons of the arene ligand are observed in the region of 5.08-6.57 ppm.

The ^{1}H NMR spectrum of complex **C3.1** is shown in Figure 3.4. The intense resonances observed at 5.82, 6.00 and 6.21 ppm integrating for a total of 20 protons correspond to the aromatic protons of the tetraphenylborate counter-ion. An important downfield shift for the imine proton resonance from 8.27 ppm for the free ligand to 8.72 ppm for the complex is observed confirming successful complexation. The imine proton resonances for complexes **C3.1-C3.4** are summarized in Table 3.2 showing a general downfield shift from around 8.20 ppm to 8.72-9.01 ppm. The proton situated next to the nitrogen in the pyridine ring is observed

Chapter 3:   Synthesis and Characterization of Model and Siloxane Functionalized RuCl(arene)(N,N) Complexes with Siloxane Tether via the Arene Ring

as a doublet at 9.53 ppm as a result of being deshielded by the nitrogen atom. The arene protons are observed as a quartet and two triplets at 6.21 (q), 6.00 (t) and 5.82 (t) ppm respectively.

Six distinctly different aliphatic protons are expected for complex **C3.1** seeing that it has two aliphatic chains; one coupled to the arene ligand and the other to the imine nitrogen. The resonances corresponding to the methyl and methylene protons of the propyl chain attached to the imine nitrogen are observed at 0.93 (triplet), 1.86/1.95 (multiplet) and 4.20/4.50 ppm (multiplet) respectively. The protons of the propanol chain of the arene ring is observed as a multiplet resonating at 1.72 ppm and a multiplet at 3.44 ppm corresponding respectively to the central ($-CH_2$-C**$\underline{H_2}$**-CH_2-OH) methylene protons and the methylene protons adjacent to the –OH moiety. The expected triplet corresponding to the methylene protons next to the arene ring are unfortunately obscured by the DMSO solvent resonance.

A well resolved triplet at 4.60 ppm was however also observed and integrated for one proton. This resonance could be assigned to the –OH functionality of the propanol functionalized arene ligand confirming the presence of the alcohol functionality on the arene ring. This well resolved triplet was observed throughout for complexes **C3.1**-**3.4** with $J_{H-H} = 5$ Hz. Similar results were observed by Fulmer *et al*. when they analyzed the ^{1}H NMR chemical of trace impurities of common laboratory solvents in deuterated solvents and corresponded well to values observed for the –OH moiety of ethanol in DMSO-*d*6. They found that for ethanol in certain solvents the coupling interaction between the CH_2 and the –OH protons may be observed [8].
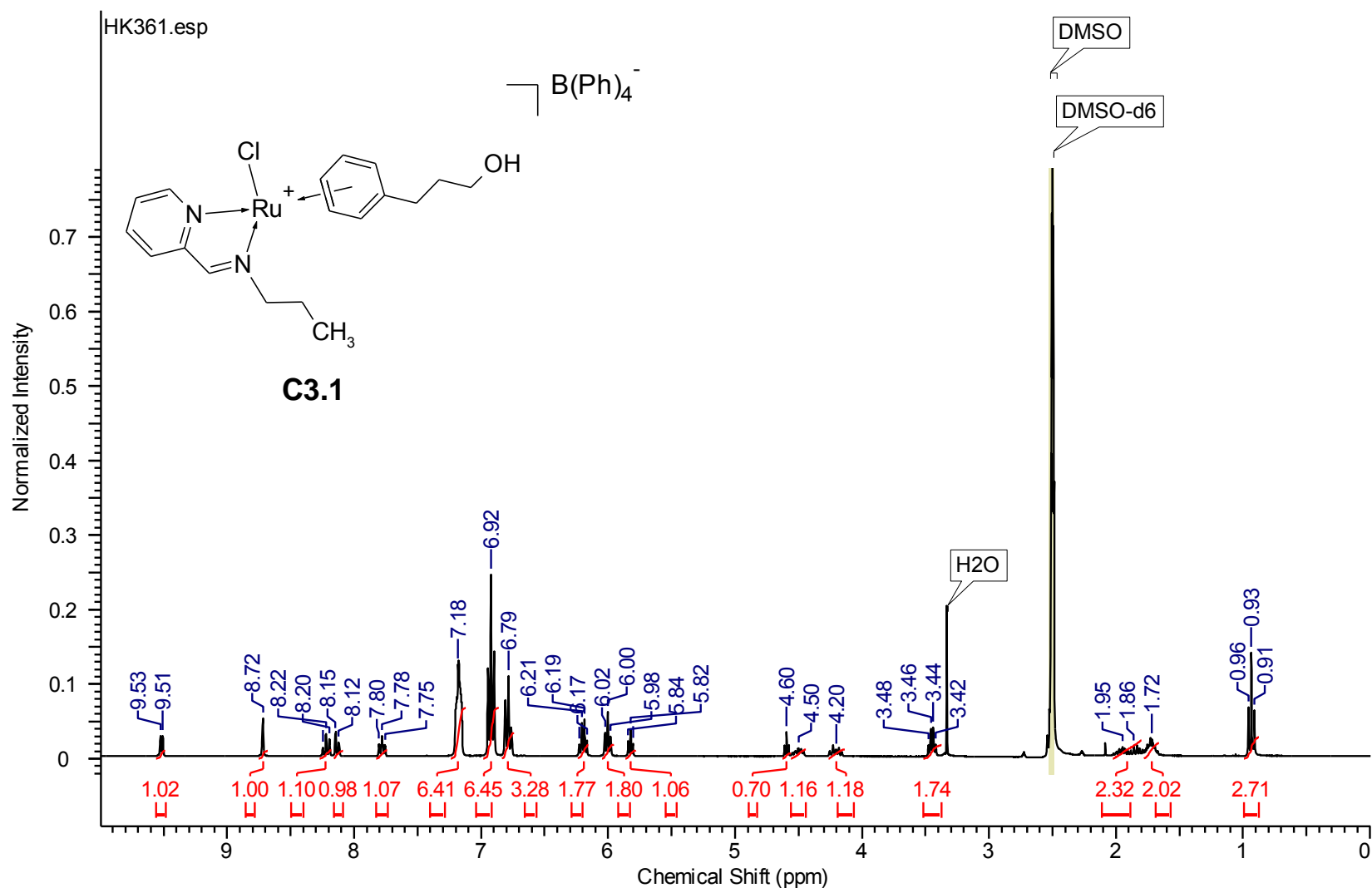
Figure 3.4 ^{1}H NMR spectrum of alcohol functionalized complex C3.1.

Chapter 3: Synthesis and Characterization of Model and Siloxane Functionalized RuCl(arene)(N,N) Complexes with Siloxane Tether via the Arene Ring

Table 3.2 Summary of ^{1}H and ^{13}C NMR data of alcohol functionalized complexes C3.1-C3.4.[a]

| Complex | ^{1}H NMR Imine Proton (ppm) | | Arene Ligand | | ^{13}C NMR Imine Proton (ppm) |
	Ligand	Complex	Arene Ring	Alcohol Functionality	
C3.1	8.27	8.72	6.21 (q), 6.00 (t), 5.82 (t)	4.60 (t)	167.2
C3.2	8.27	9.01	6.22 (t), 5.92 (d), 5.71 (t), 5.38 (d), 5.26 (t)	4.59 (t)	173.6
C3.3	8.20	8.94	6.57 (t), 6.01 (d), 5.80 (t), 5.12 (d), 5.08 (t)	4.60 (t)	174.2
C3.4	-	-	6.27 (t), 6.02 (d), 5.85 (t)	4.59 (t)	-

[a] Recorded in DMSO-*d*6

Chapter 3:   Synthesis and Characterization of Model and Siloxane Functionalized RuCl(arene)(N,N) Complexes with Siloxane Tether via the Arene Ring
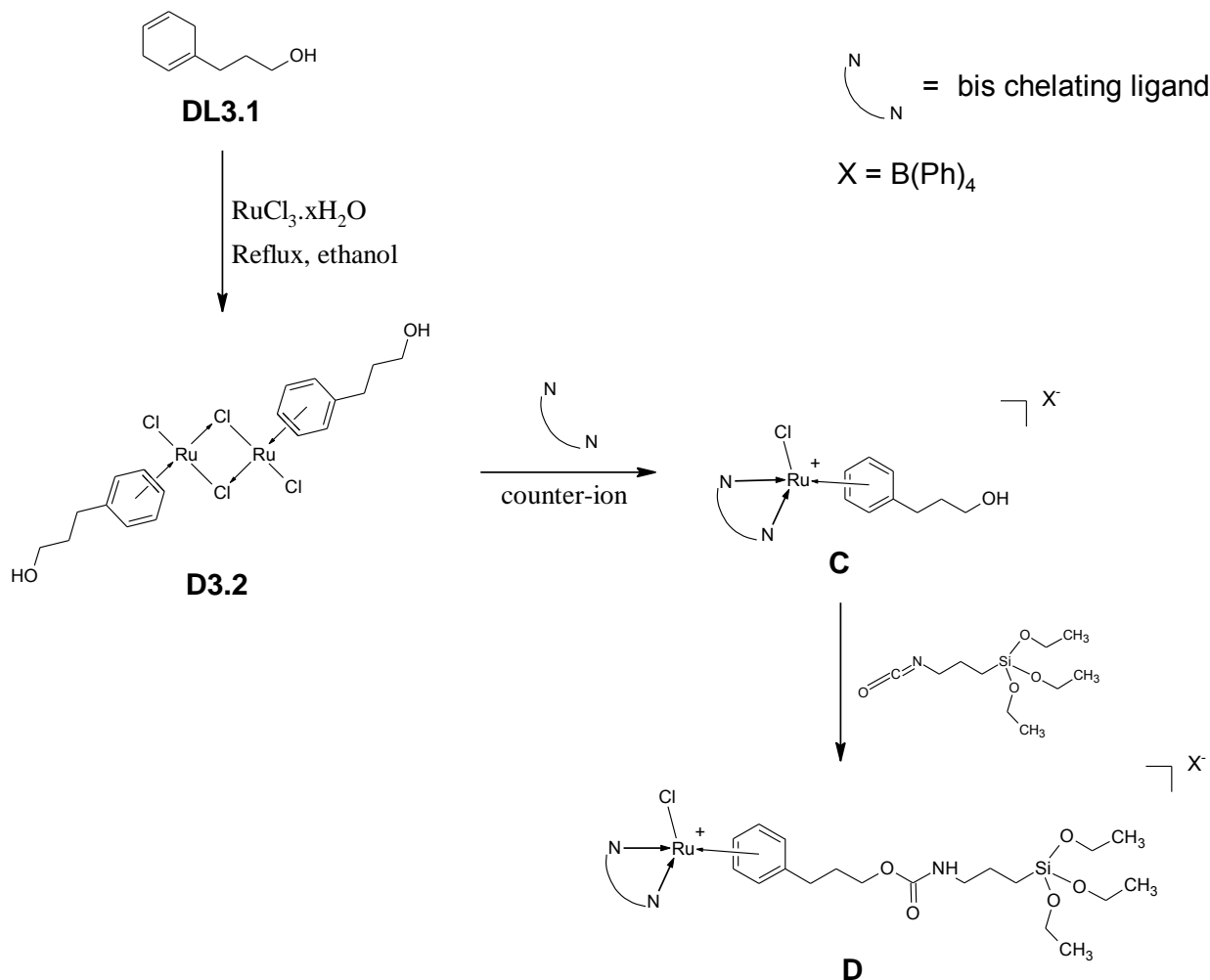
3.2.2.1.3 Characterization of alcohol functionalized complexes C3.1-C3.4 using ESI mass spectrometry, microanalyses and melting point determination

In Table 3.3 ESI-MS, melting points and microanalyses of all the alcohol functionalized complexes are summarized. The alcohol functionalized complexes **C3.1**-**C3.4** were found to have melting points of between 108-115 ˚C for complexes **C3.2** and **C3.3** and 194-213 ˚C for complexes **C3.1** and **C3.4** respectively.

Table 3.3 ESI-MS, microanalyses and melting points of alcohol functionalized complexes C3.1-C3.4.

Complex	ESI-MS [M]$^+$ (m/z) Calculated (Found)	Microanalysis: Calculated (Found)			Melting Point (˚C)
		C	H	N	
C3.1[a]	421.1 (421.1)	67.34 (67.28)	6.05 (6.13)	3.74 (3.47)	194-197
C3.2[a]	539.1 (539.1)	70.62 (70.43)	6.39 (6.60)	3.23 (3.26)	108-112
C3.3[b]	553.2 (553.2)	68.76 (69.10)	6.66 (6.13)	3.08 (3.00)	111-115
C3.4[c]	429.0 (429.0)	67.41 (67.60)	5.53 (5.31)	3.66 (3.51)	210-213

[a] M·0.5H$_2$O; [b] M·2.0H$_2$O; [c] M·1.0H$_2$O

ESI-MS further confirmed the successful synthesis of the alcohol functionalized Ru(arene)(N,N) complexes **C3.1**-**C3.4**. The calculated and obtained monoisotopic masses of the complexes compare very well and are summarized in Table 3.3. The calculated isotopic distribution of complex **C3.1** is shown in Figure 3.5 and corresponds very well to the experimentally obtained spectrum. As discussed earlier in Chapter 2, ruthenium compounds, because of the many naturally occurring isotopes, give rise to very distinct isotopic splitting patterns in the mass spectra of the complexes. The simulation of the expected isotopic cluster followed by

comparison to the experimentally obtained clusters allowed for conclusive confirmation of the chemical structure of the obtained fragment in the mass spectrum hence confirming the presence of the target molecules. The molecular ion [M]$^+$, which is also the base peak, was observed at m/z of 421.1.
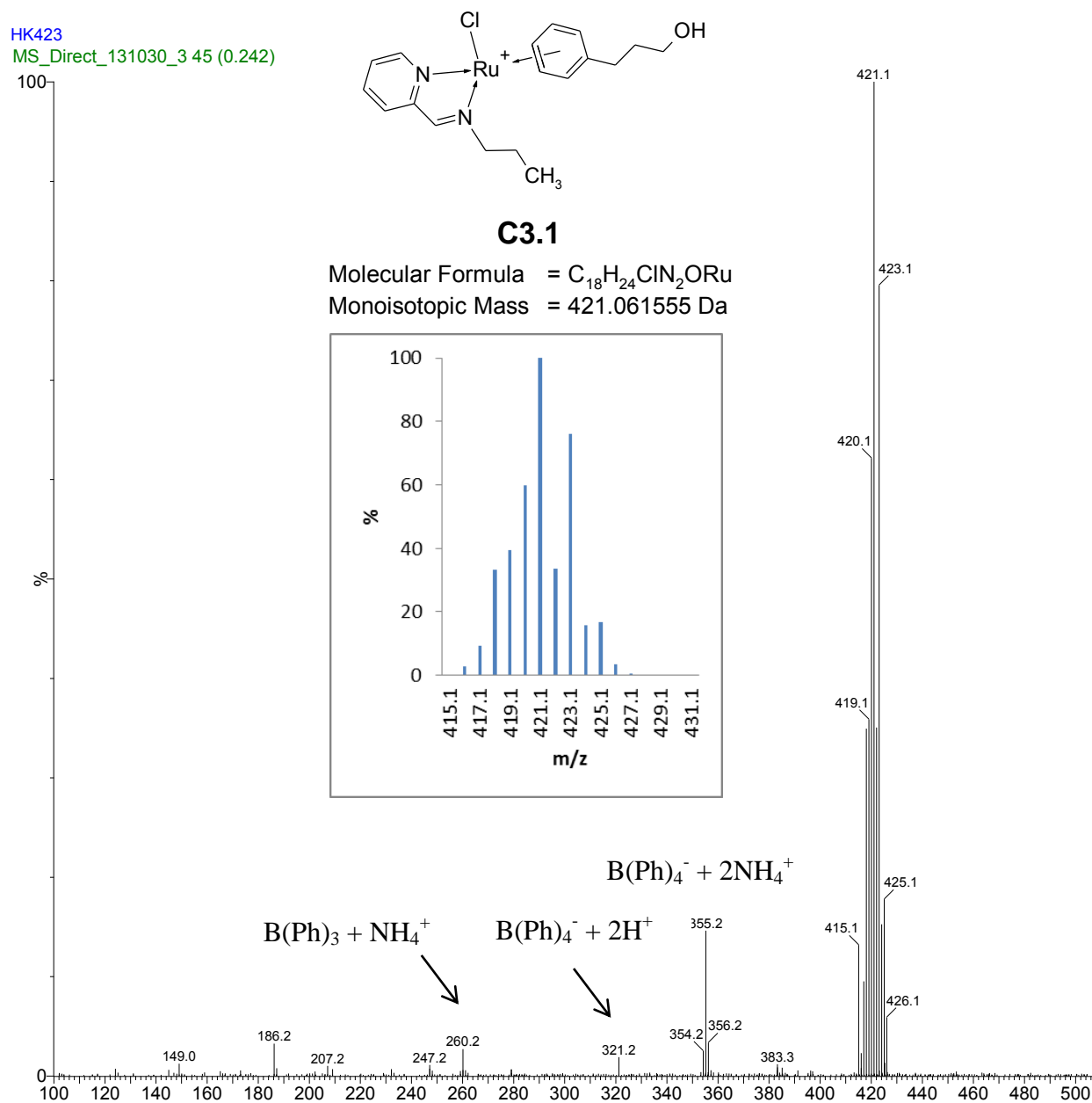
Figure 3.5 ESI-MS (positive mode) spectrum of alcohol functionalized complex C3.1.

Chapter 3: **Synthesis and Characterization of Model and Siloxane Functionalized RuCl(arene)(N,N) Complexes with Siloxane Tether via the Arene Ring**

Adducts of the counter-ion, as discussed in Chapter 2, were also observed for these compounds and were assigned as $B(Ph)_4^- + 2NH_4^+$ (m/z 355.2), $B(Ph)_4^- + 2H^+$ (m/z 321.2) and $B(Ph)_3 + NH_4^+$ respectively.

3.2.2.1.4 Characterization of alcohol functionalized complexes C3.1 using single crystal XRD analysis

Suitable crystals of alcohol functionalized complex **C3.1** were obtained by slow diffusion of hexane into a concentrated solution of the complex in acetone at room temperature. The resultant orange crystals were analyzed by single crystal XRD. The arene ligand is found to be disordered over two positions, A and B, and is shown in Figure 3.6. The asymmetric unit contains one molecule, with some disorder of the propyl and propanol chains being observed, as shown by the ellipsoids in Figure 3.7.

Figure 3.6   Molecular structure of alcohol functionalized complex C3.1 showing the disorder of the arene ligand. The hydrogen atoms have been omitted for clarity.

Chapter 3: **Synthesis and Characterization of Model and Siloxane Functionalized RuCl(arene)(N,N) Complexes with Siloxane Tether via the Arene Ring**
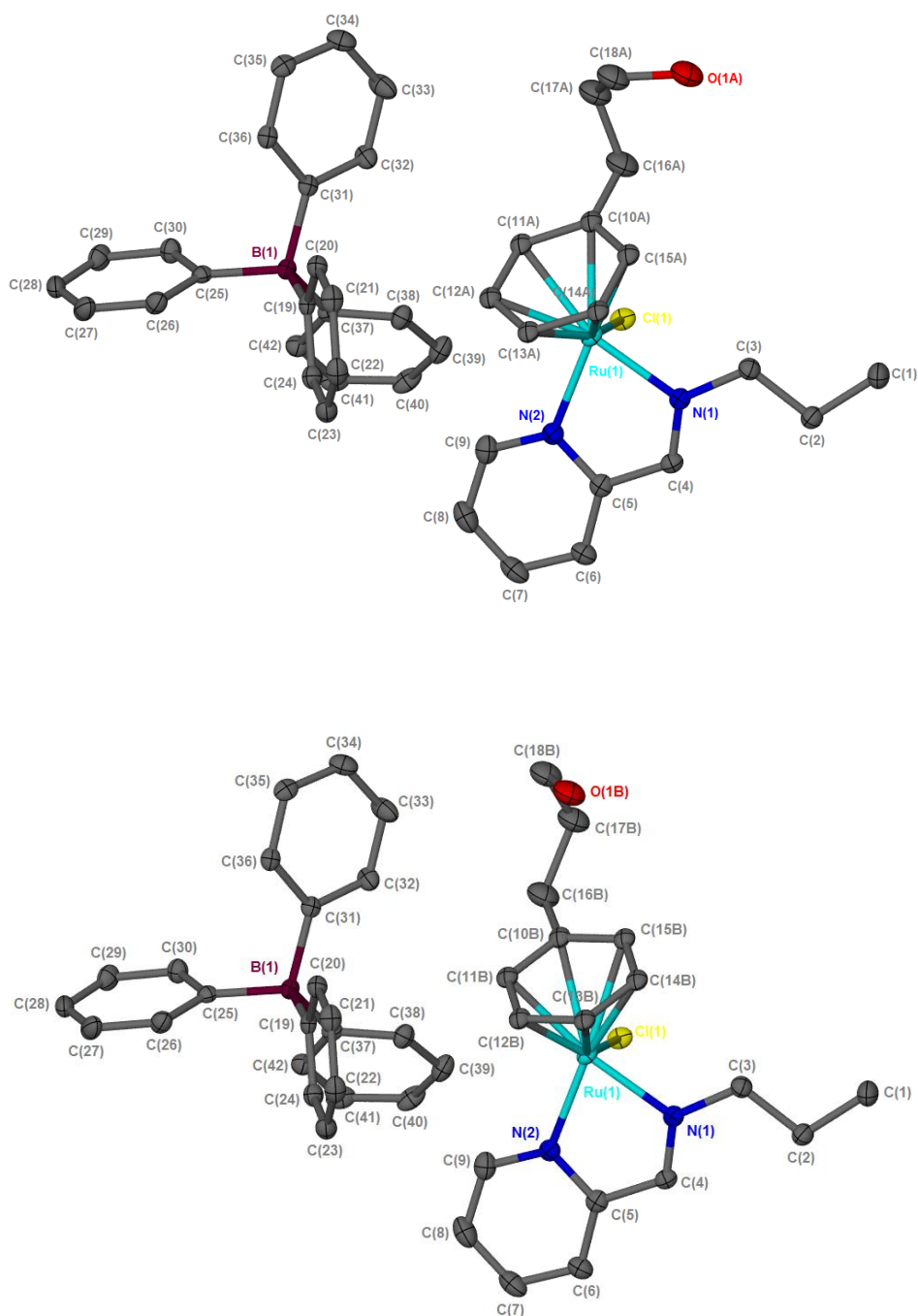
Figure 3.7 Molecular structure of alcohol functionalized complex C3.1 showing the arene ligand in the two positions A and B. The hydrogen atoms have been omitted for clarity.

Chapter 3:   Synthesis and Characterization of Model and Siloxane Functionalized RuCl(arene)(N,N) Complexes with Siloxane Tether via the Arene Ring

The geometry around the ruthenium center is pseudo-tetrahedral with the "piano-stool" conformation clearly visible with the ruthenium coordinated to the bis-chelating nitrogen ligand and a chloride. The chloride and the N,N-chelating ligand occupy the "legs" of the "piano-stool" with the arene resembling the "seat".

The arene ring of the arene ligand is essentially planar and the Ru–C arene distances range from 2.163(3) to 2.219(3) Å for position A and 2.178(18) to 2.428(17) Å for position B. Selected bond lengths and angles are summarized in Table 3.4. This data are consistent with that of similar compounds reported in literature [2].

Table 3.4 Selected bond lengths and angles for the molecular structure of complex C3.1.

Atoms	Interatomic Distances (Å)	Angles (°)
Ru(1)–Cl(1)	2.3869(7)	-
Ru(1)–N(1)	2.075(2)	-
Ru(1)–N(2)	2.088(2)	-
N(1)–Ru(1)–N(2)	-	76.86(9)
N(1)–Ru(1)–Cl(1)	-	83.37(6)
N(2)–Ru(1)–Cl(1)	-	87.39(6)

A summary of the crystal data and parameters is given in Table 3.5.

Chapter 3: Synthesis and Characterization of Model and Siloxane Functionalized RuCl(arene)(N,N) Complexes with Siloxane Tether via the Arene Ring

Table 3.5 Crystal data and structure refinement for complex C3.1.

Parameter	C3.1
Empirical formula	$C_{42}H_{44}BClN_2ORu$
Formula weight (g/mol)	740.12
Temperature (K)	100(2)
Wavelength (Å)	0.71073
Crystal system	triclinic
Space group	P -1
a (Å)	10.7143(8)
b (Å)	11.7230(9)
c (Å)	14.8452(12)
α (°)	104.3700(10)
β (°)	91.2290(10)
γ (°)	102.4830(10)
Volume (Å^3)	1758.0(2)
Z	2
Calculated density (g cm^{-3})	1.398
Absorption coefficient (mm^{-1})	0.558
F_{000}	768
Crystal size (mm^3)	$0.27 \times 0.24 \times 0.15$
θ range for data collection (°)	1.84 to 28.36
Miller index ranges	$-14 \leq h \leq 14, -15 \leq k \leq 15, -19 \leq l \leq 19$
Reflections collected	20547
Independent reflections	7971 [$R_{int} = 0.0262$]
Completeness to θ_{max} (%)	90.7
Max. and min. transmission	0.9224 and 0.8648
Refinement method	Full-matrix least-squares on F^2
Data / restraints / parameters	7971 / 0 / 407
Goodness-of-fit on F^2	1.036
Final R indices [$I > 2\sigma(I)$]	$R1 = 0.0409, wR2 = 0.0895$
R indices (all data)	$R1 = 0.0468, wR2 = 0.0929$
Largest diff. peak and hole (e Å^{-3})	2.351 and -1.857

Chapter 3: Synthesis and Characterization of Model and Siloxane Functionalized RuCl(arene)(N,N) Complexes with Siloxane Tether via the Arene Ring

3.2.2.2 Synthesis and characterization of urethane linked siloxane functionalized Ru(arene)(N,N) complexes, C3.5-C3.8

A general scheme for the synthesis of the urethane linked siloxane functionalized Ru(arene)(N,N) complexes **C3.5**-**C3.8** by the reaction of the alcohol functionalized complexes **C3.1**-**C3.4** with 3-(triethoxysilyl)propyl isocyanate is shown in Scheme 3.7 below. The same reaction conditions that were used to synthesize the urethane linked siloxane functionalized diene **3.2** were initially employed to try and synthesize the required siloxane functionalized complexes **C3.5**-**C3.8**. The lower solubility of complexes **C3.1**-**C3.4** in 3-(triethoxysilyl)propyl isocyanate however required the use of an appropriate solvent for the reaction. Acetonitrile proved to be an appropriate solvent for this reaction and allowed for the synthesis of siloxane functionalized complexes **C3.5**-**C3.8**.
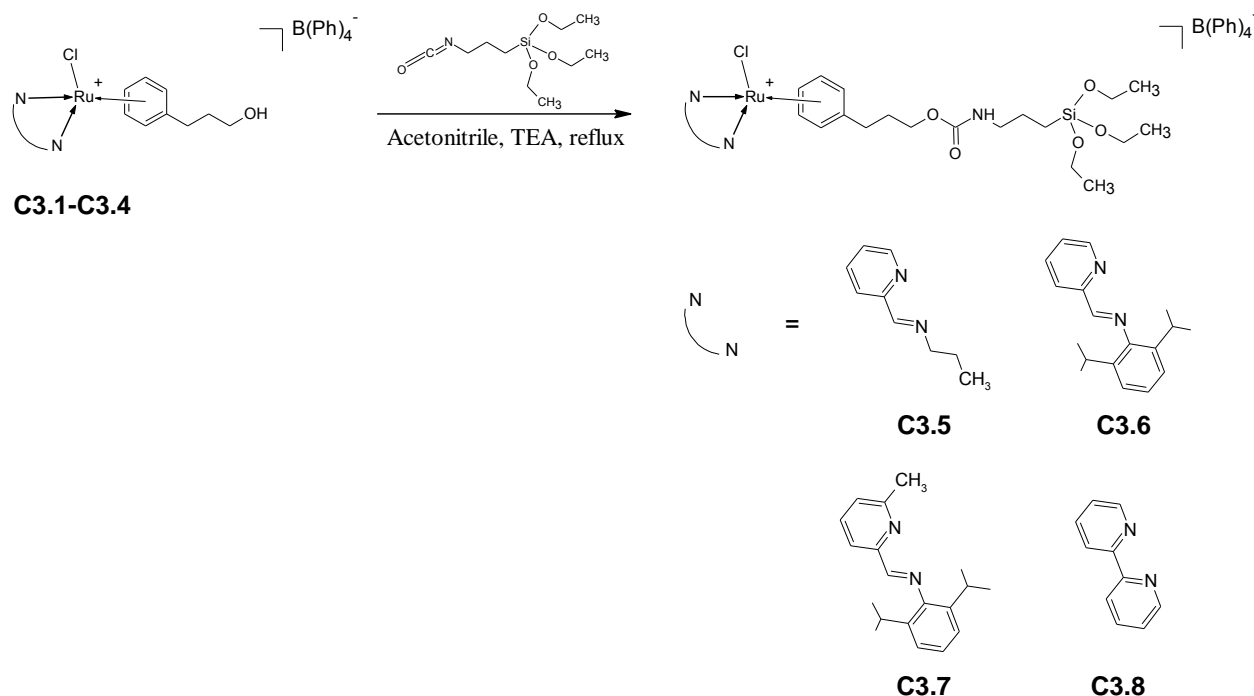
Scheme 3.7 Synthesis of urethane linked siloxane functionalized Ru(arene)(N,N) complexes C3.5-C3.8.

Chapter 3:   Synthesis and Characterization of Model and Siloxane Functionalized RuCl(arene)(N,N) Complexes with Siloxane Tether via the Arene Ring

The urethane linked siloxane functionalized Ru(arene)(N,N) complexes **C3.5**-**C3.8** were fully characterized by FT-IR, ^{1}H and ^{13}C NMR spectroscopy, ESI mass spectrometry, melting point determination and microanalysis.

3.2.2.2.1 Characterization of urethane linked siloxane functionalized Ru(arene)(N,N) complexes C3.5-C3.8 using FT-IR spectroscopy

FT-IR spectroscopy proved to be an invaluable tool to follow the progress of the synthesis of the urethane linked siloxane functionalized Ru(arene)(N,N) complexes. The disappearance of the isocyanate moiety and the formation of the newly formed urethane linkage could be monitored by IR spectroscopy. It was useful to confirm the presence of the siloxane functionality to verify that this functionality was not altered during the reaction. A summary of the most important IR vibrations is shown in Table 3.6. It is however difficult to identify the imine functionality for complexes **C3.5**-**C3.8** and therefore $v_{C=C}$ and $v_{C=N}$ of the pyridine ring are shown in Table 3.5.

Table 3.6 Selected IR vibrations of urethane linked siloxane functionalized complexes C3.5-C3.8.[a]

Complex	Pyridine Ring (cm^{-1})		Urethane Carbonyl (cm^{-1})	Siloxane Functionality (cm^{-1})	B(Ph)$_4$$^-$ (cm^{-1})
	$v_{C=N}$	$v_{C=C}$			
C3.5	1596	1579	1704	1067, 952, 766	703, 732
C3.6	1580	1557	1698	1071, 953, 761	703, 732
C3.7	-	-	1696	1065, 949, 773	703, 732
C3.8	1604	1579	1703	1067, 955, 764	704, 733

[a] Solids recorded as neat samples using an ATR accessory

Chapter 3: Synthesis and Characterization of Model and Siloxane Functionalized RuCl(arene)(N,N) Complexes with Siloxane Tether via the Arene Ring

For complex **C3.7** it is also difficult to assign the pyridine ring $v_{C=C}$ and $v_{C=N}$ bands. The newly formed urethane linkage can be observed by the presence of the characteristic urethane carbonyl band at 1704 cm^{-1} as is shown for complex **C3.5** in Figure 3.8. Other important bands are those associated with the siloxane functionality and these re observed at around 1067, 952 and 766 cm^{-1}. If one now compare these siloxane bands with those obtained for the attempted synthesis of the siloxane functionalized urethane linked Ru(arene)-dimer **D3.1**, it is clear that this important moiety is still intact after the linkage reaction.
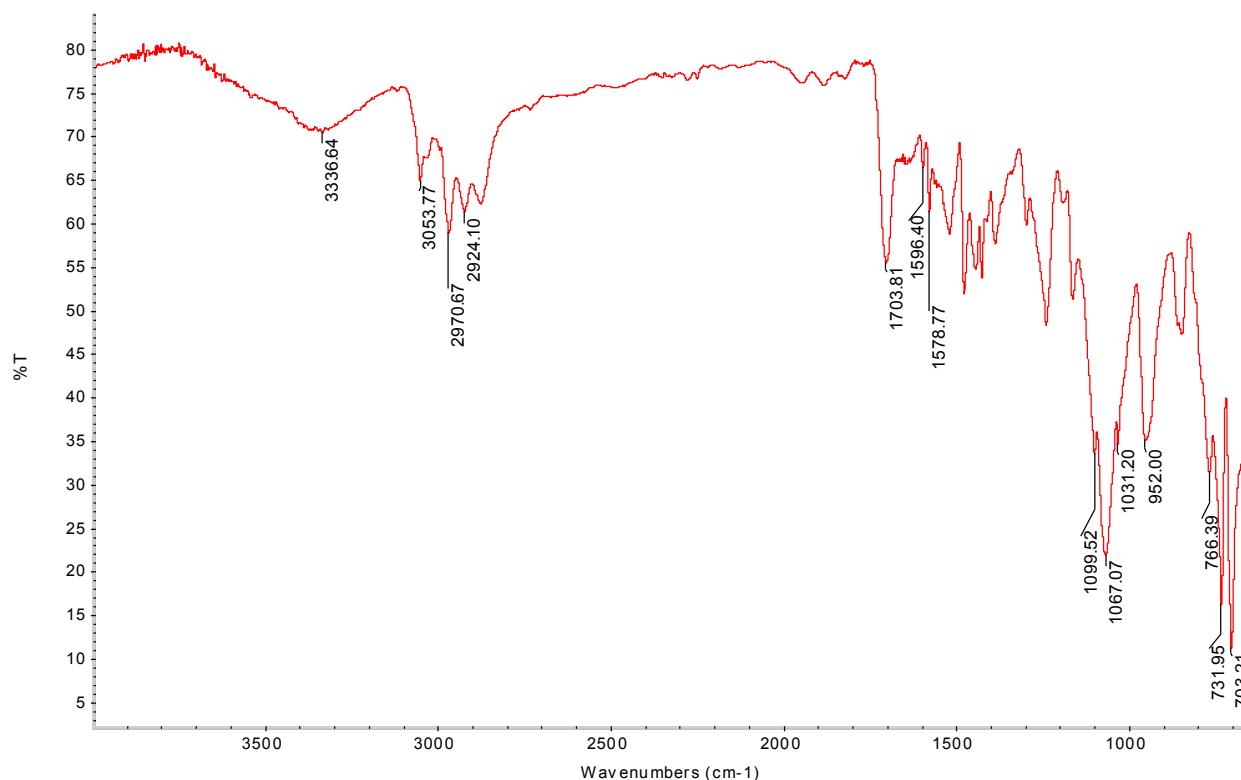
Figure 3.8 IR spectrum of urethane linked siloxane functionalized complex C3.5.

Chapter 3: Synthesis and Characterization of Model and Siloxane Functionalized RuCl(arene)(N,N) Complexes with Siloxane Tether via the Arene Ring

3.2.2.2.2 Characterization of urethane linked siloxane functionalized Ru(arene)(N,N) complexes C3.5-C3.8 using ^{1}H and ^{13}C NMR spectroscopy

^{1}H NMR spectroscopy proved to be an important technique to confirm the successful condensation of the alcohol functionalized complexes **C3.1**-**C3.4** with the isocyanate moiety of the siloxane tether. IR spectroscopy had already confirmed the formation of a new urethane carbonyl around 1700 cm^{-1} as well as the presence of the siloxane functionality. Some of the characterization data are summarized in Table 3.7. The ^{1}H NMR spectrum of the urethane linked siloxane functionalized complex **C3.5** is shown in Figure 3.9. The most important resonances are those corresponding to the newly incorporated siloxane functionality (-Si(OCH$_2$CH$_3$)$_3$) resonating as a triplet and a multiplet at 1.14 and 3.75 ppm respectively.

Table 3.7 Summary of ^{1}H and ^{13}C NMR data of urethane linked siloxane functionalized complexes C3.5-C3.8.[a]

Complex	^{1}H NMR Imine Proton (ppm)	Arene Ring (ppm)	Siloxane Functionality (ppm)	^{13}C NMR Imine Carbon (ppm)
C3.5	8.72	6.21 (q), 6.00 (dd), 5.82 (t)	1.14 (t), 3.75 (m)	167.3
C3.6	9.01	6.23 (t), 5.92 (d), 5.71 (t), 5.39 (d), 5.26 (t)	1.13 (t), 3.75 (m)	173.1
C3.7	8.95	6.59 (d), 6.03 (t), 5.81 (d), 5.10 (s)	1.14 (t), 3.75 (m)	174.2
C3.8[b]	-	6.30 (t), 6.03 (d), 5.89 (t)	1.18 (t), 3.82 (m)	-

[a] Recorded in DMSO-*d*6, unless stated otherwise; [b] Recorded in Acetone-*d*6
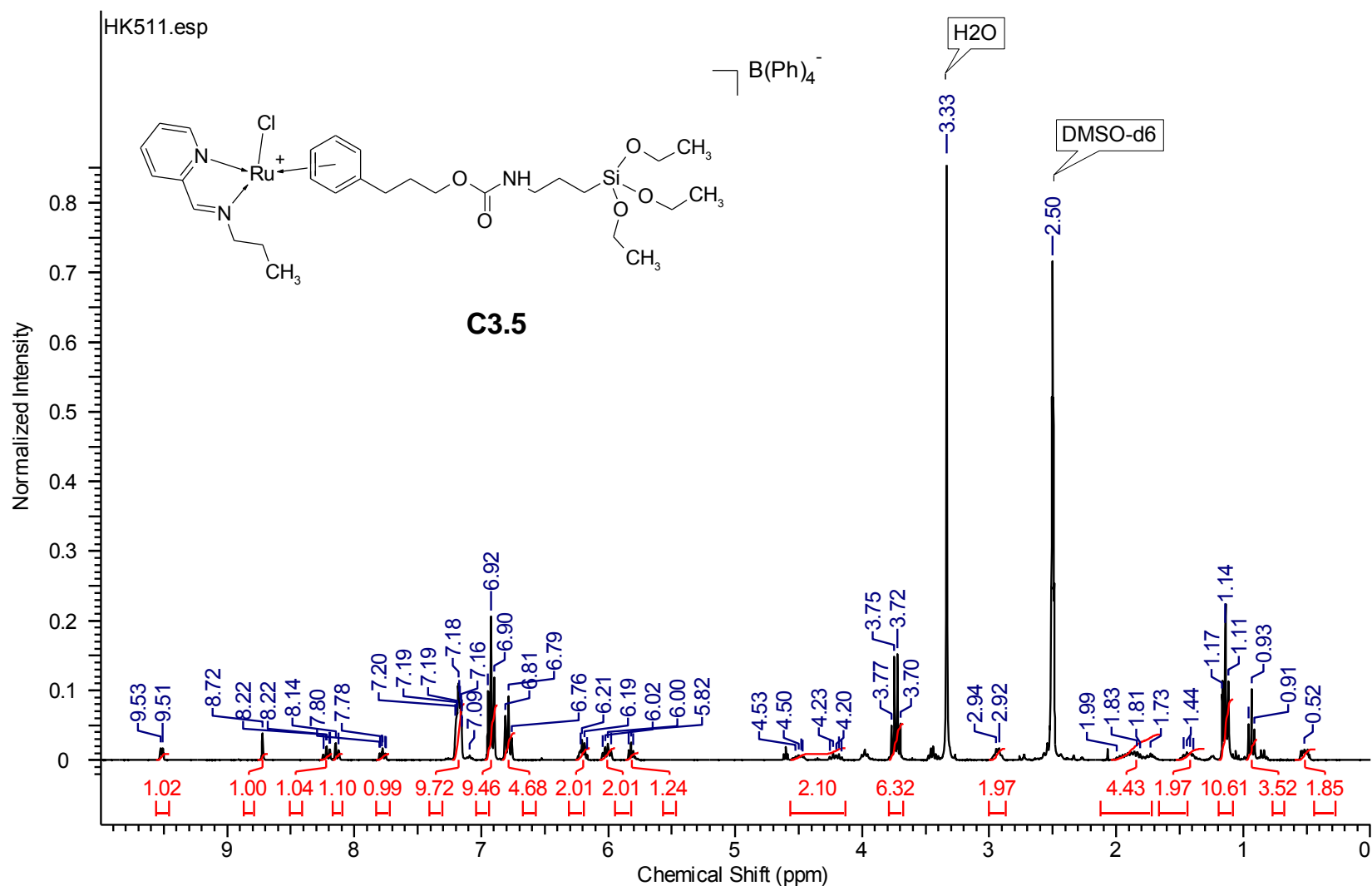
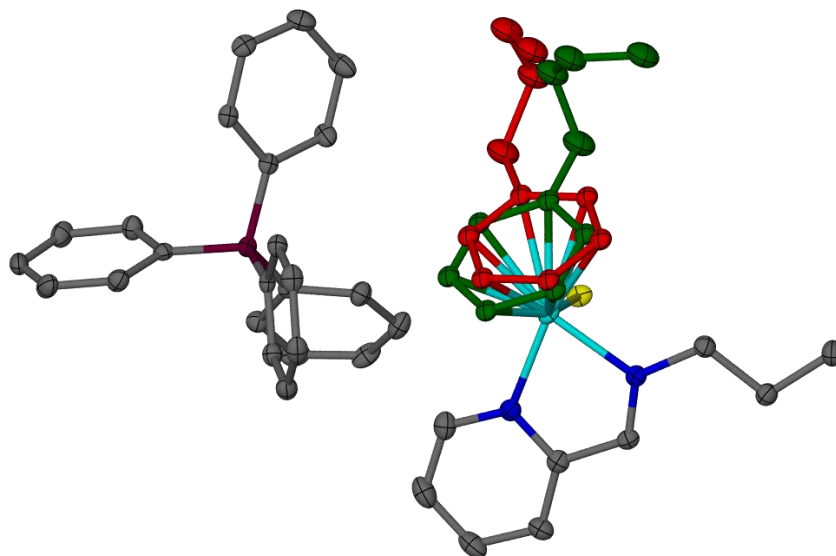**Figure 3.9** ^{1}H NMR spectrum of urethane linked siloxane functionalized complex C3.5.

Chapter 3: Synthesis and Characterization of Model and Siloxane Functionalized RuCl(arene)(N,N) Complexes with Siloxane Tether via the Arene Ring

The methylene protons could all be assigned to their corresponding resonances except for one resonating 2.53 ppm which is masked by the DMSO signal. In the aromatic region the presence of the arene pyridine protons confirms that the organic framework stayed intact during the reaction. The imine proton resonance is observed at the exact same chemical shift as was observed for the alcohol functionalized complex **C3.1** (8.72 ppm).

^{13}C NMR spectroscopy also confirmed the successful linkage with all of the resonances being accounted for. The imine carbon also showed no shift with it resonating at 167.3 ppm.

3.2.2.2.3 Characterization of urethane linked siloxane functionalized Ru(arene)(N,N) complexes C3.5-C3.8 using ESI mass spectrometry, microanalyses and melting point determination

In Table 3.8 ESI-MS, melting points and microanalyses of all the urethane linked siloxane functionalized complexes **C3.5**-**C3.8** are summarized. These complexes were found to have melting points in the range of 110-135 ˚C compared to the much higher melting points obtained for the alcohol functionalized complexes **C3.1**-**C3.4** (108-115 ˚C for complexes **C3.2** and **C3.3** and 194-213 ˚C for complexes **C3.1** and **C3.4**). The complexes with the lower melting points (**C3.2** and **C3.3**) are the two with the diisopropylaniline moiety in the ligand. It seems that the diisopropylaniline moiety decreases the melting point of these complexes when compared to the bipyridine and propyl derivatives **C3.1** and **C3.4**.

As was observed for the alcohol functionalized complexes **C3.1**-**C3.4**, microanalysis confirmed that the urethane linked siloxane functionalized complexes **C3.5**-**C3.8** were also highly hygroscopic and although care was taken during the sample preparation and submission, H_2O was still included (with the exception of complex **C3.6**).

Although IR and NMR spectroscopy have confirmed the successful reaction between complexes **C3.1**-**C3.4** and the isocyanate containing tether to form the urethane linked siloxane functionalized complexes **C3.5**-**C3.8**, we can however only definitively prove successful synthesis by using ESI mass spectrometry.

Chapter 3: Synthesis and Characterization of Model and Siloxane Functionalized RuCl(arene)(N,N) Complexes with Siloxane Tether via the Arene Ring

Table 3.8   ESI-MS, microanalyses and melting points of urethane linked siloxane functionalized complexes C3.5-C3.8.

Complex	ESI-MS [M]+ (m/z) Calculated (Found)	Microanalysis: Calculated (Found)			Melting Point (°C)
		C	H	N	
C3.5[a]	668.2 (668.2)	59.96 (59.99)	6.87 (6.34)	4.03 (4.84)	133-135
C3.6	786.3 (786.3)	66.26 (66.18)	6.84 (6.64)	3.80 (4.14)	110-113
C3.7[a]	800.3 (800.3)	63.44 (63.65)	7.13 (6.55)	3.58 (4.20)	117-120
C3.8[a]	676.2 (676.2)	60.65 (60.17)	6.43 (6.32)	4.00 (4.83)	107-113[b]

[a] M·3H$_2$O; [b] decomposed without melting

The ESI-MS (positive mode) spectrum of the urethane linked siloxane functionalized complex **C3.5** is shown in Figure 3.10. The molecular ion [M]+ is observed at m/z 668.2. The base peak is observed at m/z 421.1 and corresponds to the loss of the isocyanate tether resulting in a fragment corresponding to the alcohol functionalized complex **C3.1**. The calculated isotopic distribution of complex **C3.5** together with its obtained ESI mass spectrum is shown in Figure 3.11 and corresponds very well to the experimentally obtained spectrum.

Chapter 3: Synthesis and Characterization of Model and Siloxane Functionalized RuCl(arene)(N,N) Complexes with Siloxane Tether via the Arene Ring
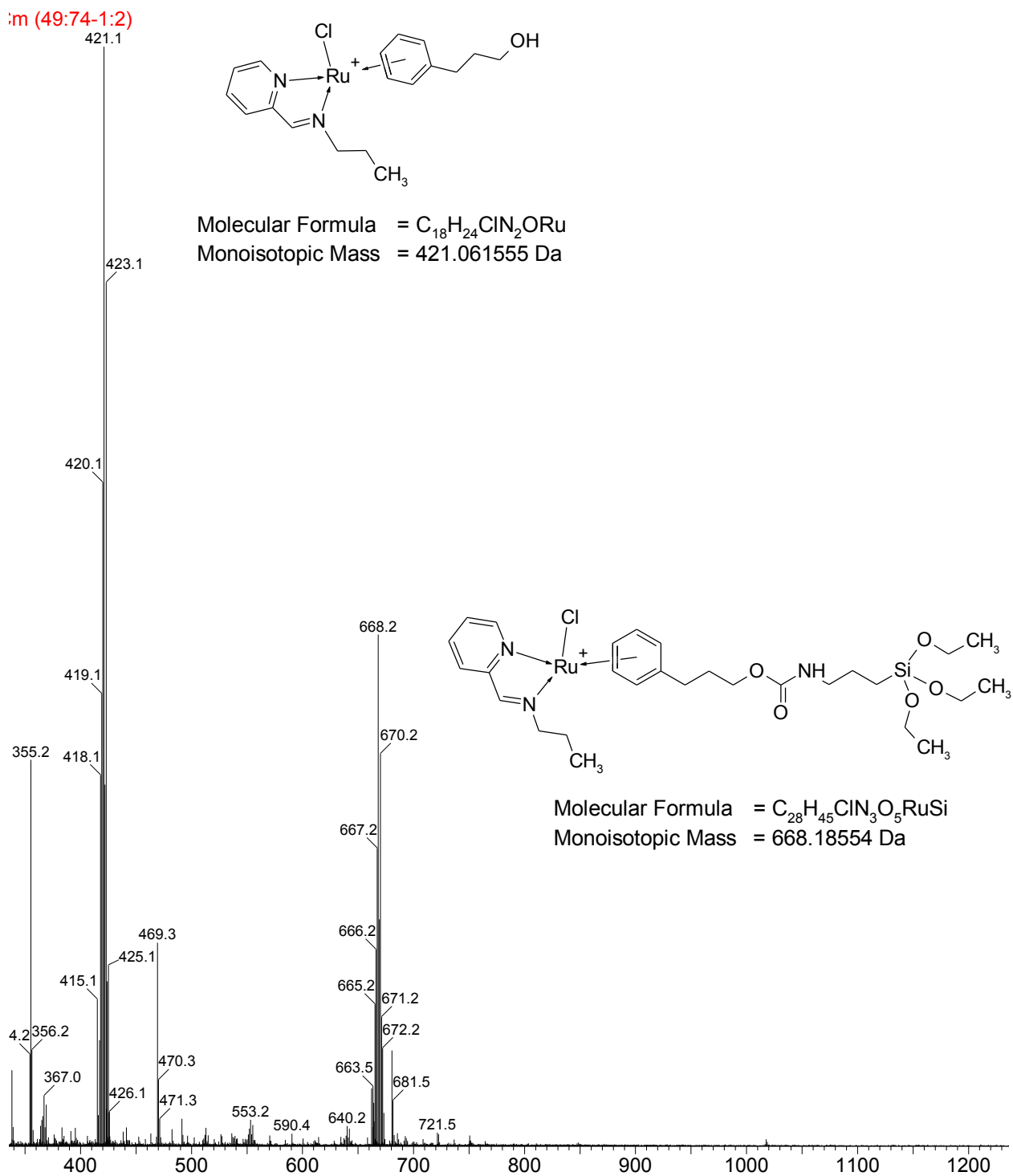
Figure 3.10 ESI-MS (positive mode) spectrum of urethane linked siloxane functionalized complex C3.5.

Chapter 3:   Synthesis and Characterization of Model and Siloxane Functionalized RuCl(arene)(N,N) Complexes with Siloxane Tether via the Arene Ring

Figure 3.11   ESI-MS (positive mode) spectrum together with the simulated spectrum of urethane linked siloxane functionalized complex C3.5.

Chapter 3: Synthesis and Characterization of Model and Siloxane Functionalized RuCl(arene)(N,N) Complexes with Siloxane Tether via the Arene Ring

3.3 Concluding remarks

In this chapter we set out to synthesize novel siloxane tethered complexes with the siloxane tether being via the arene ring instead of connected to the imine nitrogen. Attempts to synthesize a siloxane functionalized Ru-dimer, which could potentially be cleaved with our range of diimine ligands, were unsuccessful and forced us to follow the approach of firstly synthesizing alcohol functionalized complexes and then link these with the siloxane tether. This approach proved to be successful and a range of alcohol functionalized Ru(arene)(N,N) complexes were synthesized and fully characterized. Linkage of these complexes with an appropriate siloxane tether (3-(triethoxysilyl)propyl isocyanate) allowed us to synthesize novel urethane linked siloxane functionalized complexes **C3.5**-**C3.8**. Full characterization of these complexes provided proof of successful linkage without any loss of the structural integrity of the initial complexes.

These complexes, together with their derivatives with the siloxane tether attached to the imine nitrogen, will now be attached to silica support materials MCM-41 and SBA-15 which will be discussed in the next chapter. Comparisons will be drawn with regards to the mode of tethering and how it affects the activity of these catalysts in the oxidative cleavage of alkenes.

3.4 Experimental section

3.4.1 General remarks and instrumentation

All reactions were carried out under a nitrogen atmosphere making use of standard Schlenk techniques. Highly air-sensitive materials were stored in a nitrogen purged glovebox and all manipulations with these materials were carried out in the glovebox to prevent decomposition or oxidation.

Fourier transform infrared (FT-IR) spectra were recorded using an ATR accessory on a Nicolet Avatar 330 FT-IR spectrometer. ^{1}H and ^{13}C NMR spectra were recorded on a Varian Unity Inova instrument at 300, 400 and 600 MHz for ^{1}H and 75, 100 and 150 MHz for ^{13}C. ESI mass spectra were recorded by direct injection into a stream of acetonitrile and 0.1 % formic acid

Chapter 3: Synthesis and Characterization of Model and Siloxane Functionalized RuCl(arene)(N,N) Complexes with Siloxane Tether via the Arene Ring

employing a cone voltage of 15V using a Waters API Quattro Micro spectrometer. A Thermo Elemental Analyzer CHNS-O was used for the accurate determination of elemental composition of samples.

3.4.2 Materials

Reagents were purchased from Sigma-Aldrich and used as received; these include 2-pyridinecarboxaldehyde, *n*-propylamine, diisopropylaniline, bipyridine, 3-phenyl-propan-1-ol and 3-(triethoxysilyl)propyl isocyanate. The diene (**3.1**) was synthesized through *Birch reduction* of 3-phenyl-1-propanol [4]. Ruthenium(III) chloride hydrate (RuCl$_3$·xH$_2$O) was obtained from SA Precious Metals [Pty] Limited. Solvents were purchased from Sigma-Aldrich and Kimix Chemicals and were dried by refluxing over the appropriate drying agents. Dichloromethane (DCM) and acetonitrile were dried over phosphorous pentoxide, hexane and pentane over sodium wire and diethyl ether, tetrahydrofurane (THF) and toluene over sodium wire and benzophenone. Ethanol and methanol were dried over dry magnesium turnings and iodine. Dimethyl sulfoxide was dried over molecular sieves.

3.4.3 Synthesis of alcohol functionalized Ru-dimer D3.2: [Ru(C$_6$H$_5$)(CH$_2$)$_3$OHCl$_2$]$_2$

3.4.3.1 Synthesis of alcohol functionalized diene 1,4-cyclohexadiene-1-propanol (DL3.1)

To stirring liquid ammonia (100 mL) was slowly added a solution of 3-phenyl-propan-1-ol (3.026 g, 22.22 mmol) in ethanol (25 mL). Small pieces of cleaned Na were added to the reaction mixture so that a blue color persisted. Small amounts of ethanol were added throughout the reaction to facilitate with the stirring. The sodium was added over a period of 2 hours. After the allotted time, the reaction mixture was carefully poured over a saturated solution of NH$_4$Cl (100 mL). The formed diene was extracted with DCM (3x25 mL) and dried over MgSO$_4$. After the removal of the solvent a colorless oil was obtained as product.

Chapter 3: Synthesis and Characterization of Model and Siloxane Functionalized RuCl(arene)(N,N) Complexes with Siloxane Tether via the Arene Ring

1,4-cyclohexadiene-1-propanol (**DL3.1**): Colorless oil, yield 97 %. IR: FT-IR, v/cm^{-1}: 3295 (bs, alcohol, -OH). ^{1}H NMR (400 MHz, (CD$_3$CN): δ (ppm) = 1.66 (m, 2H, CH$_2$C**H$_2$**CH$_2$OH), 2.01 (t, $^3J_{H-H}$ = 7.8 Hz, 2H, C**H$_2$**CH$_2$CH$_2$OH), 3.60 (t, $^3J_{H-H}$ = 6.6 Hz, 2H, CH$_2$CH$_2$C**H$_2$**OH), 2.60 (m, 4H, diene C**H$_2$**), 5.43 (bs, 1H, diene C**H**), 5.68 (bt, 2H, diene C**H**).

3.4.3.2 Synthesis of alcohol functionalized Ru-dimer (D3.2): [Ru(C$_6$H$_5$)(CH$_2$)$_3$OHCl$_2$]$_2$

To a stirring solution of hydrated ruthenium trichloride (0.200 g, 0.800 mmol) in ethanol (25 mL) was added 1,4-cyclohexadiene-1-propanol (**DL3.1**) (0.275 g, 2.00 mmol) and the mixture was allowed to reflux for 4-6 hours. An orange/red precipitate was formed and filtered off, washed with diethylether (2x10 mL), and dried under vacuum to afford the alcohol functionalized Ru-dimer.

Ru-dimer (**D3.2**): Orange/red crystalline solid, yield 83 %. IR: FT-IR, v/cm^{-1}: 3412 (s, -OH). ^{1}H NMR (400 MHz, (CD$_3$CN): δ (ppm) = 1.83 (m, 2H, CH$_2$C**H$_2$**CH$_2$OH), 2.60 (t, $^3J_{H-H}$ = 7.8 Hz, 2H, C**H$_2$**CH$_2$CH$_2$OH), 3.59 (m, 2H, CH$_2$CH$_2$C**H$_2$**OH), 5.46 (d, $^3J_{H-H}$ = 5.9 Hz, 2H, Ar$_{ARENE}$), 5.60 (t, $^3J_{H-H}$ = 5.5 Hz, 1H, Ar$_{ARENE}$), 5.69 (t, $^3J_{H-H}$ = 5.9 Hz, 2H, Ar$_{ARENE}$).

3.4.4 Synthesis of alcohol functionalized complexes C3.1-C3.4

Complex **C3.1**: To a stirring solution of **D3.2**, [Ru(C$_6$H$_5$(CH$_2$)$_3$OH)Cl$_2$]$_2$, (0.049 g, 0.080 mmol) in acetonitrile (5 mL) was added a solution of model ligand **L2.1** (0.025 g, 0.17 mmol) in acetonitrile (5 mL). This yellow/brown reaction solution was allowed to stir at room temperature for 18 hours. After the allotted time, NaB(Ph)$_4$ (0.059 g, 0.17 mmol) was added at 0 ˚C and allowed to stir for a further 3 hours. The reaction mixture was filtered and the solvent removed after this time. The obtained yellow solid was stirred in ethanol overnight to remove any unreacted starting material. The yellow powder was filtered and dried under vacuum. This powder was further purified by recrystallization from acetone/pentane to afford orange needle like crystals which were suitable for single crystal XRD analysis.

Chapter 3: Synthesis and Characterization of Model and Siloxane Functionalized RuCl(arene)(N,N) Complexes with Siloxane Tether via the Arene Ring

A similar procedure was followed for complexes **C3.2**-**C3.4** with the only difference being the workup of the final product. Complexes **C3.2** and **C3.3** required a similar workup as was carried out for complex **C3.1**. After removal of the solvent the obtained flaky solids were dissolved in DCM and filtered again to remove any unreacted Ru-dimer (insoluble). Removal of the solvent afforded sticky solids which after triturating with diethylether, afforded orange and brown solids respectively in moderate to high yields. For complex **C3.4** a yellow precipitate was formed almost immediately after the counter-ion was added. This precipitate was filtered off, washed with ethanol and dried under vacuum.

Complex **C3.1**: Orange crystals, yield 78 %. IR: FT-IR, v/cm^{-1}: 3528 (bs, –OH), 1600 (s, imine, C=N), 737, 708 (s, B-C). ^{1}H NMR (400 MHz, (CD$_3$)$_2$SO): δ (ppm) = 0.93 (t, $^3J_{H\text{-}H}$ = 7.4 Hz, 3H, NCH$_2$CH$_2$**CH**$_3$), 1.73 (m, 2H, CH$_2$**CH**$_2$CH$_2$OH), 1.83 & 1.95 (m, 2H, NCH$_2$**CH**$_2$CH$_3$), 2.53 (t, 2H, **CH**$_2$CH$_2$CH$_2$OH, *masked by DMSO signal*), 3.44 (m, 2H, CH$_2$CH$_2$**CH**$_2$OH), 4.19 & 4.50 (m, 2H, N**CH**$_2$CH$_2$CH$_3$), 4.60 (t, $^3J_{H\text{-}H}$ = 5.1 Hz, 1H, CH$_2$CH$_2$CH$_2$O**H**), 5.82 (t, $^3J_{H\text{-}H}$ = 5.5 Hz, 1H, Ar$_{ARENE}$), 6.01 (dd, $^3J_{H\text{-}H}$ = 6.3 Hz, 2H, Ar$_{ARENE}$), 6.21 (dt, $^3J_{H\text{-}H}$ = 5.9 Hz, 2H, Ar$_{ARENE}$), 6.79, 6.92, 7.18 (t, t, m, 20H, B(Ph)$_4$), 7.78 (t, $^3J_{H\text{-}H}$ = 5.9 Hz, 1H, Pyr), 8.14 (d, $^3J_{H\text{-}H}$ = 7.0 Hz, 1H, Pyr), 8.22 (t, $^3J_{H\text{-}H}$ = 7.4 Hz, 1H, Pyr), 9.52 (d, $^3J_{H\text{-}H}$ = 5.5 Hz, 1H, Pyr), 8.72 (s, 1H, **CH**-*imine*). ^{13}C {^{1}H} NMR (100 MHz, (CD$_3$)$_2$SO): δ (ppm) = 11.3 (propyl **CH**$_3$); 22.4, 67.8 (propyl **CH**$_2$); 29.6, 32.4, 60.0 (propanol **CH**$_2$); 82.0, 84.8, 84.9, 88.0, 88.4 (**CH**$_{ARENE}$); 106.8 (**C**$_{ARENE}$), 128.0, 128.5, 139.7, 154.5, (**CH***pyr*); 155.9 (**C***pyr*); 167.2 (**CH**-*imine*). Elemental Analysis (%): Calc. For C$_{42}$H$_{44}$BClN$_2$ORu·0.5H$_2$O (749.2): C, 67.34; H, 6.05; N, 3.74; Found: C, 67.28; H, 6.13; N, 3.47. MS (ESI, *m*/*z*): 421.1 [M]$^+$. Melting Point: 194-197 ˚C

Complex **C3.2**: Flaky brown orange solid, yield 67 %. IR: FT-IR, v/cm^{-1}: 3339 (bs, –OH), 1613 (s, imine, C=N), 732, 702 (s, B-C). ^{1}H NMR (300 MHz, (CD$_3$)$_2$SO): δ (ppm) = 0.92 (d, $^3J_{H\text{-}H}$ = 6.8 Hz, 3H, CH(**CH**$_3$)$_2$ $_{ANILINE}$), 1.13 (d, $^3J_{H\text{-}H}$ = 7.0 Hz, 3H, CH(**CH**$_3$)$_2$ $_{ANILINE}$), 1.26 (d, $^3J_{H\text{-}H}$ = 6.8 Hz, 3H, CH(**CH**$_3$)$_2$ $_{ANILINE}$), 1.40 (d, $^3J_{H\text{-}H}$ = 6.8 Hz, 3H, CH(**CH**$_3$)$_2$ $_{ANILINE}$), 1.70 (m, 2H, CH$_2$**CH**$_2$CH$_2$OH), 2.41 (sep, 1H, **CH**(CH$_3$)$_2$ $_{ANILINE}$), 2.52 (t, 2H, **CH**$_2$CH$_2$CH$_2$OH, *masked by*
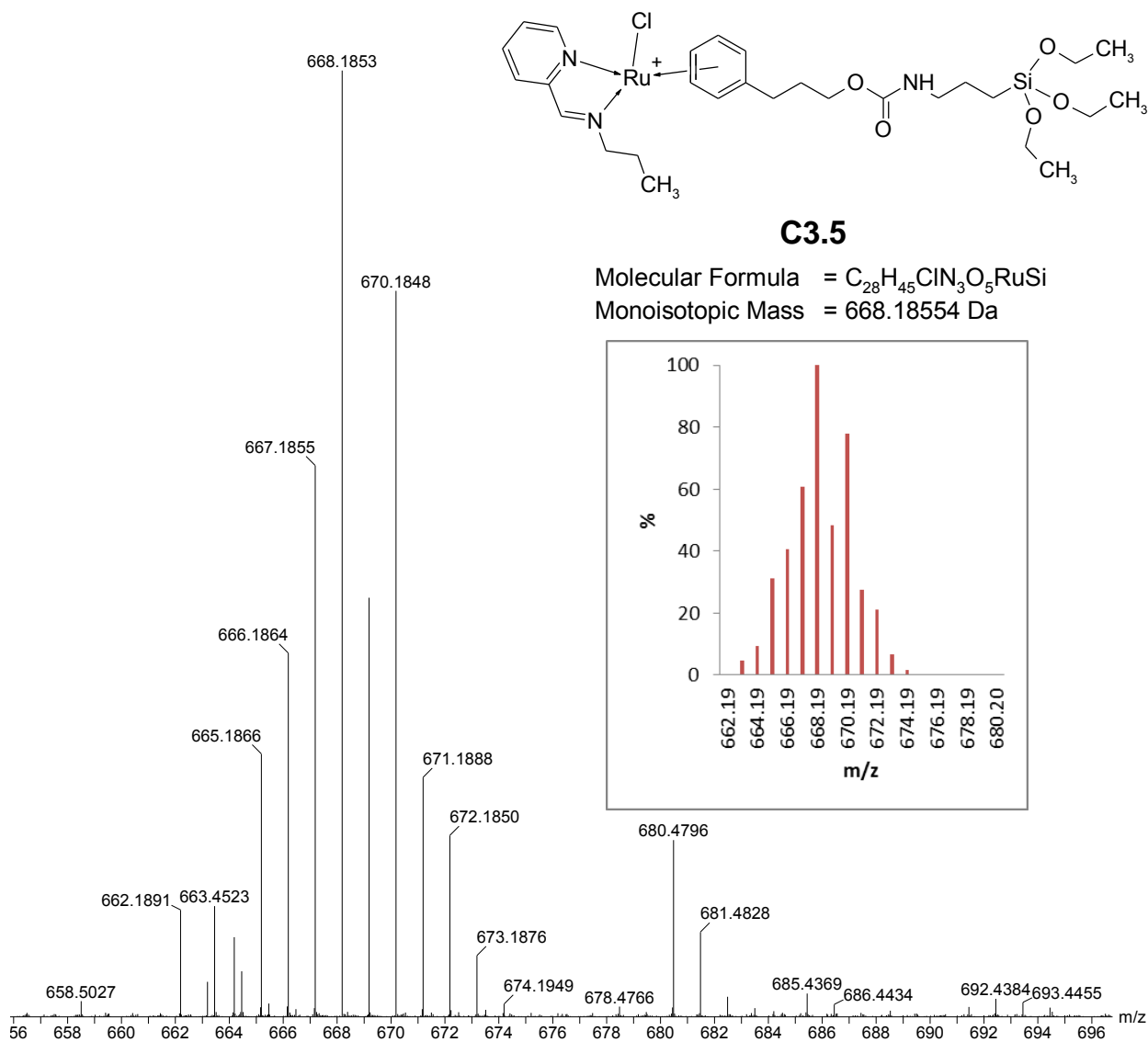
Chapter 3: Synthesis and Characterization of Model and Siloxane Functionalized RuCl(arene)(N,N) Complexes with Siloxane Tether via the Arene Ring

---

DMSO signal), 3.42 & 3.73 (m, 2H, C**H**$_2$CH$_2$C**H**$_2$OH), 4.59 (t, $^3J_{H-H}$ = 5.0 Hz, 1H, CH$_2$CH$_2$CH$_2$O**H**), 5.26 (t, $^3J_{H-H}$ = 5.9 Hz, 1H, Ar$_{ARENE}$), 5.40 (d, $^3J_{H-H}$ = 5.9 Hz, 1H, Ar$_{ARENE}$), 5.71 (t, $^3J_{H-H}$ = 5.6 Hz, 1H, Ar$_{ARENE}$), 5.92 (d, $^3J_{H-H}$ = 6.2 Hz, 1H, Ar$_{ARENE}$), 6.22 (t, $^3J_{H-H}$ = 5.9 Hz, 1H, Ar$_{ARENE}$), 6.78, 6.92, 7.18 (t, t, m, 20H, B(Ph)$_4$), 7.48 (m, 3H, Ar$_{ANILINE}$), 7.93 (t, $^3J_{H-H}$ = 5.6 Hz, 1H, Pyr), 8.29 (m, 2H, Pyr), 9.64 (d, $^3J_{H-H}$ = 5.3 Hz, 1H, Pyr), 9.01 (s, 1H, C**H**-*imine*). ^{13}C {^{1}H} NMR (75 MHz, (CD$_3$)$_2$SO): δ (ppm) = 30.4, 32.7, 60.2 (propanol **C**H$_2$); 27.7 & 28.0 (**C**H(CH$_3$)$_2$ $_{ANILINE}$); 22.6, 23.7, 25.8, 26.9 (CH(**C**H$_3$)$_2$ $_{ANILINE}$); 81.4, 83.2, 83.5, 90.0, 91.0 (**C**H$_{ARENE}$); 110.3 (**C**$_{ARENE}$), 129.6, 129.7, 139.7, 154.4, (**C**H*pyr*); 156.8 (**C***pyr*); 124,8, 125.1, 130.3, 140.8, 141.6, 148.6 (**C**H and **C**$_{ANILINE}$); 173.6 (**C**H-*imine*). Elemental Analysis (%): Calc. For C$_{51}$H$_{54}$BClN$_2$ORu·0.5H$_2$O (867.3): C, 70.62; H, 6.39; N, 3.23; Found: C, 70.43; H, 6.60; N, 3.26. MS (ESI, *m/z*): 539.1 [M]$^+$. Melting Point: 108-112 ˚C

Complex **C3.3**: Brown orange solid, yield 79 %. IR: FT-IR, *v*/cm^{-1}: 3414 (bs, –OH), 1619 (s, imine, C=N), 732, 702 (s, B-C). ^{1}H NMR (300 MHz, (CD$_3$)$_2$SO): δ (ppm) = 0.87 (d, $^3J_{H-H}$ = 6.6 Hz, 3H, CH(C**H**$_3$)$_2$ $_{ANILINE}$), 1.22 (d, $^3J_{H-H}$ = 6.6 Hz, 3H, CH(C**H**$_3$)$_2$ $_{ANILINE}$), 1.30 (d, $^3J_{H-H}$ = 6.6 Hz, 3H, CH(C**H**$_3$)$_2$ $_{ANILINE}$), 1.43 (d, $^3J_{H-H}$ = 6.6 Hz, 3H, CH(C**H**$_3$)$_2$ $_{ANILINE}$), 1.74 (m, 2H, CH$_2$C**H**$_2$CH$_2$OH), 2.43 (sep, 1H, C**H**(CH$_3$)$_2$ $_{ANILINE}$), 2.52 (t, 2H, C**H**$_2$CH$_2$CH$_2$OH, *masked by DMSO signal*), 3.14 (s, 3H, Pyr$_{C**H**3}$), 3.43 & 3.73 (m, 2H, C**H**$_2$CH$_2$C**H**$_2$OH), 4.60 (t, $^3J_{H-H}$ = 5.0 Hz, 1H, CH$_2$CH$_2$CH$_2$O**H**), 5.11 m, 2H, Ar$_{ARENE}$), 5.79 (t, $^3J_{H-H}$ = 5.4 Hz, 1H, Ar$_{ARENE}$), 6.00 (d, $^3J_{H-H}$ = 5.9 Hz, 1H, Ar$_{ARENE}$), 6.57 (t, $^3J_{H-H}$ = 5.7 Hz, 1H, Ar$_{ARENE}$), 6.78, 6.92, 7.18 (t, t, m, 20H, B(Ph)$_4$), 7.44 & 7.51 (m, 3H, Ar$_{ANILINE}$), 7.93 (d, $^3J_{H-H}$ = 7.5 Hz, 1H, Pyr), 8.14 (m, 2H, Pyr), 8.95 (s, 1H, C**H**-*imine*). ^{13}C {^{1}H} NMR (75 MHz, (CD$_3$)$_2$SO): δ (ppm) = 30.4, 31.9, 59.8 (propanol **C**H$_2$); 28.5 (Pyr$_{C**H**3}$); 27.2 & 27.6 (**C**H(CH$_3$)$_2$ $_{ANILINE}$); 21.9, 23.1, 25.4, 26.3 (CH(**C**H$_3$)$_2$ $_{ANILINE}$); 79.3, 79.3, 82.4, 88.7, 93.7 (**C**H$_{ARENE}$); 111.9 (**C**$_{ARENE}$), 129.3, 129.7, 139.7, (**C**H*pyr*); 154.2 (**C***pyr*); 124,8, 125.1, 130.3, 140.8, 141.6, 148.6 (**C**H and **C**$_{ANILINE}$); 162.4 (**C***pyr*(CH$_3$)); 174.2 (**C**H-*imine*). Elemental Analysis (%): Calc. For C$_{52}$H$_{56}$BClN$_2$ORu·2.0H$_2$O (908.3): C, 68.76; H, 6.66; N, 3.08; Found: C, 69.10; H, 6.13; N, 3.00. MS (ESI, *m/z*): 553.2 [M]$^+$. Melting Point: 111-115 ˚C

Chapter 3: Synthesis and Characterization of Model and Siloxane Functionalized RuCl(arene)(N,N) Complexes with Siloxane Tether via the Arene Ring

Complex **C3.4**: Yellow solid, yield 77 %. IR: FT-IR, v/cm^{-1}: 3518 (bs, –OH), 732, 706 (s, B-C). ^{1}H NMR (300 MHz, (CD$_3$)$_2$SO): δ (ppm) = 1.73 (m, 2H, CH$_2$**CH$_2$**CH$_2$OH), 2.53 (t, 2H, *masked by DMSO signal*), 3.45 (m, 2H, CH$_2$CH$_2$**CH$_2$**OH), 4.59 (t, $^3J_{\text{H-H}}$ = 5.0 Hz, 1H, CH$_2$CH$_2$CH$_2$O**H**), 5.85 (t, $^3J_{\text{H-H}}$ = 5.6 Hz, 1H, Ar$_{ARENE}$), 6.02 (d, $^3J_{\text{H-H}}$ = 6.2 Hz, 2H, Ar$_{ARENE}$), 6.27 (t, $^3J_{\text{H-H}}$ = 6.5 Hz, 2H, Ar$_{ARENE}$), 6.79, 6.92, 7.18 (t, t, m, 20H, B(Ph)$_4$), 7.77 (t, $^3J_{\text{H-H}}$ = 5.6 Hz, 2H, Pyr), 8.26 (t, $^3J_{\text{H-H}}$ = 7.6 Hz, 2H, Pyr), 8.63 (d, $^3J_{\text{H-H}}$ = 7.9 Hz, 2H, Pyr), 9.57 (d, $^3J_{\text{H-H}}$ = 5.6 Hz, 2H, Pyr). ^{13}C {^{1}H} NMR (75 MHz, (CD$_3$)$_2$SO): δ (ppm) = 29.6, 32.4, 59.9 (propanol **CH**$_2$); 81.2, 83.3, 89.8 (**CH**$_{ARENE}$); 108.0 (**C**$_{ARENE}$), 123.7, 127.4, 139.8, 154.5, (**CH***pyr*); 155.8 (**C***pyr*). Elemental Analysis (%): Calc. For C$_{43}$H$_{40}$BClN$_2$ORu·1.0H$_2$O (766.2): C, 67.41; H, 5.53; N, 3.66; Found: C, 67.60; H, 5.31; N, 3.51. MS (ESI, *m/z*): 429.0 [M]$^+$. Melting Point: 210-213 ˚C

3.4.5 Synthesis of urethane linked siloxane functionalized complexes C3.5-C3.8

Complex **C3.8**:   To a stirring solution of alcohol functionalized complex **C3.4** (0.110 g, 0.150 mmol) in acetonitrile (5 mL) was added excess 3-(triethoxysilyl)-propyl isocyanate (1.00 g, 4.00 mmol) and triethylamine (1.0 g, 10 mmol) (these ratios were later adjusted to around 1.5 excess of each). This yellow reaction mixture was allowed to reflux under nitrogen for a further 5 hours. After a few hours the yellow mixture turned dark orange in color. Small samples were taken after each hour and analyzed with IR to monitor the disappearance of the – OH functionality. After the allotted time the reaction was allowed to cool to room temperature and all volatiles removed under vacuum. Dry ethanol (10 mL) was added to this mixture followed by the precipitation of a greyish yellow solid. The product was filtered, washed with ethanol and dried under vacuum to afford the product in low to moderate yields.

For complexes **C3.5**, **C3.6** and **C3.8** the reactions were allowed to continue for 5 hours with most of the alcohol functionalized complex having reacted during this time. For complex **C3.7** however much longer reaction times were employed. This reaction was monitored and found to be complete after 24 hours.

Chapter 3:   Synthesis and Characterization of Model and Siloxane Functionalized RuCl(arene)(N,N) Complexes with Siloxane Tether via the Arene Ring

---

Complex **C3.5**: Dark brown solid, yield 35 %. IR: FT-IR, v/cm^{-1}: 1704 (s, urethane carbonyl), 1067, 952, 766 (siloxane), 732, 703 (s, B-C). ^{1}H NMR (300 MHz, (CD$_3$)$_2$SO): δ (ppm) = 0.52 (m, 2H, **CH$_2$**Si(OCH$_2$CH$_3$)$_3$), 0.93 (t, $^3J_{\text{H-H}}$ = 7.2 Hz, 3H, NCH$_2$CH$_2$C**H$_3$**), 1.14 (t, $^3J_{\text{H-H}}$ = 7.0 Hz, 9H, Si(OCH$_2$C**H$_3$**)$_3$), 1,44 (m, 2H, CH$_2$**CH$_2$**CH$_2$Si), 1.73 (m, 2H, CH$_2$**CH$_2$**CH$_2$OCONH), 1.83 & 1.95 (m, 2H, NCH$_2$**CH$_2$**CH$_3$), 2.53 (t, 2H, **CH$_2$**CH$_2$CH$_2$OCONH, *masked by DMSO signal*), 2.94 (m, 2H, NHC**H$_2$**CH$_2$CH$_2$Si), 3.75 (q, $^3J_{\text{H-H}}$ = 6.9 Hz, 6H, Si(OC**H$_2$**CH$_3$)$_3$), 3.98 (t, $^3J_{\text{H-H}}$ = 6.5 Hz, 2H, CH$_2$CH$_2$C**H$_2$**OCONH), 4.20 & 4.50 (m, 2H, NC**H$_2$**CH$_2$CH$_3$), 5.82 (t, $^3J_{\text{H-H}}$ = 5.7 Hz, 1H, Ar$_{ARENE}$), 6.02 (dd, $^3J_{\text{H-H}}$ = 5.2 Hz, 2H, Ar$_{ARENE}$), 6.21 (dt, $^3J_{\text{H-H}}$ = 6.0 Hz, 2H, Ar$_{ARENE}$), 6.79, 6.92, 7.18 (t, t, m, 20H, B(Ph)$_4$), 7.78 (t, $^3J_{\text{H-H}}$ = 5.6 Hz, 1H, Pyr), 8.14 (d, $^3J_{\text{H-H}}$ = 7.6 Hz, 1H, Pyr), 8.22 (t, $^3J_{\text{H-H}}$ = 7.6 Hz, 1H, Pyr), 9.53 (d, $^3J_{\text{H-H}}$ = 5.7 Hz, 1H, Pyr), 8.72 (s, 1H, C**H**-*imine*). ^{13}C {^{1}H} NMR (75 MHz, (CD$_3$)$_2$SO): δ (ppm) = 11.3 (propyl **CH$_3$**); 22.6, 67.8 (propyl **CH$_2$**); 18.2 (ethoxy **CH$_3$**); 7.19, 22.6, 29.6, 32.4, 45.7, 62.7 (tether **CH$_2$**); 57.7 (ethoxy **CH$_2$**); 82.0, 84.8, 84.9, 88.0, 88.5 (**CH**$_{ARENE}$); 106.8 (**C**$_{ARENE}$), 128.0, 128.5, 139.7, 154.5, (**CH***pyr*); 155.9 (**C***pyr*); 167.2 (**CH**-*imine*). Elemental Analysis (%): Calc. For C$_{52}$H$_{65}$BClN$_3$O$_5$RuSi·3.0H$_2$O (1041.4): C, 59.96; H, 6.87; N, 4.33; Found: C, 59.99; H, 6.34; N, 4.84. MS (ESI, m/z): 668.2 [M]$^+$. Melting Point: 133-135 °C

Complex **C3.6**: Dark brown solid, yield 43 %. IR: FT-IR, v/cm^{-1}: 1698 (s, urethane carbonyl), 1071, 953, 761 (siloxane), 732, 703 (s, B-C). ^{1}H NMR (300 MHz, (CD$_3$)$_2$SO): δ (ppm) = 0.51 (m, 2H, **CH$_2$**Si(OCH$_2$CH$_3$)$_3$), 0.86 (d, $^3J_{\text{H-H}}$ = 6.7 Hz, 3H, CH(C**H$_3$**)$_{2\ ANILINE}$), 0.92 (d, $^3J_{\text{H-H}}$ = 6.8 Hz, 3H, CH(C**H$_3$**)$_{2\ ANILINE}$), 1.14 (t, $^3J_{\text{H-H}}$ = 6.9 Hz, 9H, Si(OCH$_2$C**H$_3$**)$_3$), 1.28 (d, $^3J_{\text{H-H}}$ = 6.6 Hz, 3H, CH(C**H$_3$**)$_{2\ ANILINE}$), 1.40 (d, $^3J_{\text{H-H}}$ = 6.8 Hz, 3H, CH(C**H$_3$**)$_{2\ ANILINE}$), 1,44 (m, 2H, CH$_2$**CH$_2$**CH$_2$Si, *masked by CH(CH$_3$)$_2$ groups of aniline*), 1.70 & 1.85 (m, 2H, CH$_2$**CH$_2$**CH$_2$OCONH), 2.53 (t, 2H, **CH$_2$**CH$_2$CH$_2$OCONH, *masked by DMSO signal*), 2.92 (m, 2H, NHC**H$_2$**CH$_2$CH$_2$Si), 3.75 (q, $^3J_{\text{H-H}}$ = 6.9 Hz, Si(OC**H$_2$**CH$_3$)$_3$), 3.98 (t, $^3J_{\text{H-H}}$ = 6.9 Hz, 2H, CH$_2$CH$_2$C**H$_2$**OCONH), 5.26 (t, $^3J_{\text{H-H}}$ = 5.9 Hz, 1H, Ar$_{ARENE}$), 5.41 (d, $^3J_{\text{H-H}}$ = 6.3 Hz, 1H, Ar$_{ARENE}$), 5.71 (t, $^3J_{\text{H-H}}$ = 5.4 Hz, 1H, Ar$_{ARENE}$), 5.92 (d, $^3J_{\text{H-H}}$ = 6.0 Hz, 1H, Ar$_{ARENE}$), 6.23 (t, $^3J_{\text{H-H}}$ = 6.0 Hz, 1H, Ar$_{ARENE}$), 6.78, 6.92, 7.18 (t, t, m, 20H, B(Ph)$_4$), 7.48 (m, 3H, Ar$_{ANILINE}$), 7.93 (t, $^3J_{\text{H-H}}$ = 5.6 Hz, 1H, Pyr), 8.28 (m, 2H, Pyr), 9.65 (d, $^3J_{\text{H-H}}$ = 5.6 Hz, 1H, Pyr), 9.01 (s, 1H, C**H-**

imine). ^{13}C {^{1}H} NMR (100 MHz, (CD$_3$)$_2$SO): δ (ppm) = 18.2 (ethoxy **CH$_3$**); 7.18, 22.2, 29.9, 32.2, 45.7, 62.6 (tether **CH$_2$**); 57.7 (ethoxy **CH$_2$**); 27.2 & 27.5 (**CH**(CH$_3$)$_2$ *ANILINE*); 22.6, 23.2, 25.3, 26.4 (CH(**CH$_3$**)$_2$ *ANILINE*); 80.9, 82.8, 83.1, 89.5, 90.3 (**CH$_{ARENE}$**); 109.8 (**C$_{ARENE}$**), 129.2, 129.8, 139.6, 153.9, (**CH**pyr); 156.3 (**C**pyr); 124,4, 124.6, 129.0, 140.3, 141.1, 148.1 (**CH** and **C$_{ANILINE}$**); 173.1 (**CH**-*imine*). Elemental Analysis (%): Calc. For C$_{61}$H$_{75}$BClN$_3$O$_5$RuSi (1105.4): C, 66.26; H, 6.84; N, 3.80; Found: C, 66.18; H, 6.64; N, 4.14. MS (ESI, *m/z*): 786.3 [M]$^+$. Melting Point: 110-113 ˚C

Complex **C3.7**: Dark brown solid, yield 35 %. IR: FT-IR, *v*/cm^{-1}: 1704 (s, urethane carbonyl), 1065, 949, 773 (siloxane), 732, 703 (s, B-C). ^{1}H NMR (300 MHz, (CD$_3$)$_2$SO): δ (ppm) = 0.51 (bt, 2H, **CH$_2$**Si(OCH$_2$CH$_3$)$_3$), 0.86 (d, $^3J_{H-H}$ = 6.5 Hz, 3H, CH(**CH$_3$**)$_2$ *ANILINE*), 1.22 (d, 3H, CH(**CH$_3$**)$_2$ *ANILINE*, *overlap with methyl of ethoxy group*), 1.14 (t, $^3J_{H-H}$ = 7.3 Hz, 9H, Si(OCH$_2$**CH$_3$**)$_3$), 1.29 (d, $^3J_{H-H}$ = 6.8 Hz, 3H, CH(**CH$_3$**)$_2$ *ANILINE*), 1.43 (d, $^3J_{H-H}$ = 6.5 Hz, 3H, CH(**CH$_3$**)$_2$ *ANILINE*), 1,44 (m, 2H, CH$_2$**CH$_2$**CH$_2$Si, *masked by CH(CH$_3$)$_2$ groups of aniline*), 1.76 & 1.88 (m, 2H, CH$_2$**CH$_2$**CH$_2$OCONH), 2.44 (t, 2H, **CH$_2$**CH$_2$CH$_2$OCONH, *masked by DMSO signal*), 2.95 (m, 2H, NH**CH$_2$**CH$_2$CH$_2$Si), 3.13 (s, 3H, Pyr**CH$_3$**), 3.72 (bq, 6H, Si(O**CH$_2$**CH$_3$)$_3$), 3.96 (bt, 2H, CH$_2$CH$_2$**CH$_2$**OCONH), 5.10 (s, 2H, Ar$_{ARENE}$), 5.81 (d, $^3J_{H-H}$ = 6.2 Hz, 1H, Ar$_{ARENE}$), 6.03 (t, $^3J_{H-H}$ = 6.5 Hz, 1H, Ar$_{ARENE}$), 6.59 (d, $^3J_{H-H}$ = 5.3 Hz, 1H, Ar$_{ARENE}$), 6.78, 6.92, 7.18 (t, t, m, 20H, B(Ph)$_4$), 7.41-7.51 (m, 3H, Ar$_{ANILINE}$), 7.93 (d, $^3J_{H-H}$ = 9.1 Hz, 1H, Pyr), 8.11 (m, 2H, Pyr), 8.95 (s, 1H, **CH**-*imine*). ^{13}C {^{1}H} NMR (75 MHz, (CD$_3$)$_2$SO): δ (ppm) = 11.3 (propyl **CH$_3$**); 22.6, 67.8 (propyl **CH$_2$**); 18.2 (ethoxy **CH$_3$**); 7.19, 22.6, 29.6, 32.4, 45.7, 62.7 (tether **CH$_2$**); 57.7 (ethoxy **CH$_2$**); 82.0, 84.8, 84.9, 88.0, 88.5 (**CH$_{ARENE}$**); 106.8 (**C$_{ARENE}$**), 128.0, 128.5, 139.7, 154.5, (**CH**pyr); 155.9 (**C**pyr); 167.2 (**CH**-*imine*). Elemental Analysis (%): Calc. For C$_{62}$H$_{77}$BClN$_3$O$_5$RuSi·3.0H$_2$O (1173.5): C, 63.44; H, 7.13; N, 3.58; Found: C, 63.65; H, 6.55; N, 4.20. MS (ESI, *m/z*): 800.3 [M]$^+$. Melting Point: 117-120 ˚C

Complex **C3.8**: Greyish yellow solid, yield 53 %. IR: FT-IR, *v*/cm^{-1}: 1703 (s, urethane carbonyl), 1067, 955, 764 (siloxane), 733, 704 (s, B-C). ^{1}H NMR (300 MHz, (CD$_3$)$_2$CO): δ

Chapter 3: Synthesis and Characterization of Model and Siloxane Functionalized RuCl(arene)(N,N) Complexes with Siloxane Tether via the Arene Ring

---

(ppm) = 0.59 (t, $^3J_{\text{H-H}}$ = 8.4 Hz, 2H, **CH$_2$**Si(OCH$_2$CH$_3$)$_3$), 1.18 (t, $^3J_{\text{H-H}}$ = 7.0 Hz, 9H, Si(OCH$_2$**CH$_3$**)$_3$), 1,59 (m, 2H, CH$_2$**CH$_2$**CH$_2$Si), 1.99 (m, 2H, CH$_2$**CH$_2$**CH$_2$OCONH, *masked by Acetone signal*), 2.73 (t, 2H, **CH$_2$**CH$_2$CH$_2$OCONH, *masked by H$_2$O signal*), 3.09 (m, 2H, NHC**H$_2$**CH$_2$CH$_2$Si), 3.79 (q, $^3J_{\text{H-H}}$ = 6.9 Hz, 6H, Si(OC**H$_2$**CH$_3$)$_3$), 4.08 (t, $^3J_{\text{H-H}}$ = 6.5 Hz, 2H, CH$_2$CH$_2$**CH$_2$**OCONH), 5.89 (t, $^3J_{\text{H-H}}$ = 5.7 Hz, 1H, Ar$_{ARENE}$), 6.03 (d, $^3J_{\text{H-H}}$ = 6.0 Hz, 2H, Ar$_{ARENE}$), 6.30 (dt, $^3J_{\text{H-H}}$ = 6.0 Hz, 2H, Ar$_{ARENE}$), 6.77, 6.92, 7.34 (t, t, m, 20H, B(Ph)$_4$), 7.76 (t, $^3J_{\text{H-H}}$ = 5.6 Hz, 2H, Pyr), 8.27 (t, $^3J_{\text{H-H}}$ = 7.6 Hz, 2H, Pyr), 8.54 (d, $^3J_{\text{H-H}}$ = 7.0 Hz, 2H, Pyr), 9.59 (d, $^3J_{\text{H-H}}$ = 5.6 Hz, 2H, Pyr). ^{13}C {^{1}H} NMR (100 MHz, (CD$_3$)$_2$CO): δ (ppm) = 18.8 (ethoxy **CH$_3$**); 8.44, 24.4, 31.0, 44.3, 63.9 (tether **CH$_2$**, *expected signal at 29.0 ppm masked by Acetone signal*); 58.9 (ethoxy **CH$_2$**); 82.5, 84.5, 91.0 (**CH**$_{ARENE}$); 109.4 (**C**$_{ARENE}$), 128.4, 137.1, 140.9, 156.7, (**CH***pyr*); 156.0 (**C***pyr*); 167.2 (**CH**-*imine*). Elemental Analysis (%): Calc. For C$_{53}$H$_{61}$BClN$_3$O$_5$RuSi·3.0H$_2$O (1049.4): C, 60.65; H, 6.43; N, 4.00; Found: C, 60.17; H, 6.32; N, 4.83. MS (ESI, *m/z*): 676.2 [M]$^+$. Melting Point: Decomposed without melting (107-113 ˚C)

Chapter 3: Synthesis and Characterization of Model and Siloxane Functionalized RuCl(arene)(N,N) Complexes with Siloxane Tether via the Arene Ring

3.5 References

1.   Y. Miyaki, T. Onishi, H. Kurosawa, *Inorg. Chim. Acta*, **2000**, 300, 369.

2.   L.C. Matsinha, S.F. Mapolie, G.S. Smith, *Polyhedron*, **2013**, 53, 56.

3.   J. Soleimannejad, A. Sisson, C. White, *Inorg. Chim. Acta*, **2003**, 352, 121.

4.   C. White, *Organometallics*, **2005**, 24, 2538.

5.   M.A. Furrer, F. Schmitt, M. Wiederkehr, L. Juillerat-Jeanneret, B. Therrien, *Dalton Trans.*, 2**012**, 41, 7201.

6.   W.H. Ang, E. Daldini, L. Juillerat-Jeanneret, P.J. Dyson, *Inorg. Chem.*, **2007**, 46 , 9048.

7.   A.J. Birch, *J. Chem. Soc.*, 1950, 1551.

8.   G.R. Fulmer, A.J.M. Miller, N.H. Sherden, H.E. Gottlieb, A. Nudelman, B.M. Stoltz, J.E. Bercaw, K.I. Goldberg, *Organometallic*s, **2010**, 29, 2176.

Chapter 4: Immobilization of RuCl(arene)(N,N) Complexes on MCM-41 and SBA-15

4.1 Introduction

The two major advantages of heterogeneous catalysts that have resulted in sustained interest in their preparation and application in a wide range of processes are the ease whereby they can be separated from the product mixture and the possibility of recycling the catalyst for further runs. Although homogeneous systems still usually possess higher activities and selectivities when compared to their heterogeneous counterparts, the possibility of the abovementioned recovery and subsequent recycling for further runs may start to compensate for the usual shortcomings of heterogeneous systems. The holy grail of such heterogeneous systems however still remain a catalyst that can be recycled, separated and reused without any significant drop in the activity and selectivity. A bonus would be if the activity and selectivity of the heterogeneous system is even higher than its homogeneous counterpart. To achieve such systems one has to firstly select the appropriate support material. It is imperative to choose a support that does not only retain its heterogeneity but also remains stable under harsh reaction conditions. Mesoporous silicate materials meet all of the above criteria and have the added advantage of ease of synthesis and functionalization. Couple this to the extent to which these materials have been studied and one is left with a material which is almost perfect for use as a support for heterogenized catalysts.

The synthesis of mesoporous silica materials has been widely reported in literature and a simplified reaction scheme for the general synthesis of mesoporous silicate material is shown in Scheme 4.1. The addition of an appropriate silica source (inorganic precursor) to either an acidic or basic solution containing the correct surfactant molecule (template) leads to the formation of a mesoporous material with a hexagonal array of cylindrical pores [1]. Different types of surfactant molecules can be used for the synthesis of the above mentioned supports. For the target materials selected as supports for this project, MCM-41 and SBA-15, cationic (cetyltrimethylammonium bromide) and polymeric (tri-block copolymer) surfactants were respectively used for the synthesis of the silicas [2-4]. The choice of surfactant or template together with the reaction conditions results in the formation of similarly looking mesoporous materials with different surface areas and pore sizes.
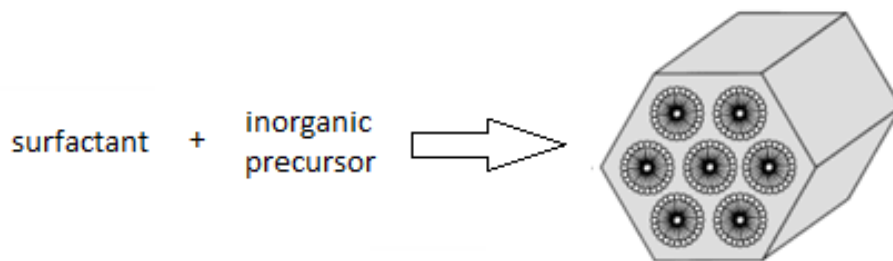
Scheme 4.1 Simplified representation of the synthesis of MCM-41 [10].

MCM-41 and SBA-15 have been extensively studied and employed as supports for the heterogenization of homogeneous catalysts. Mesoporous supports have also found application in fields other than catalysis as seen in a paper by García *et al*. They reported the use of periodic mesoporous silica as a support material for a tris(bipyridine)ruthenium complex which exhibits photovoltaic and electrochemiluminescent properties [5]. A sequential approach allowed for the successful covalent immobilization of their heteroleptic tris(bipyridine)ruthenium complex onto the surface of the mesoporous support while still maintaining the properties of the hexagonal mesoporous silica. Immobilization was achieved by the condensation of the siloxane functionality on the synthesized complex with surface silanol groups on the surface of the silica. They concluded that mesoporous materials could be useful for the preparation of optoelectronic devices.

The versatility of mesoporous materials is further illustrated by work done by Tuel *et al.* where they incorporated heteroelements into the structure of mesoporous materials to afford as an example a Ti-doped mesoporous material [6]. This introduction of titanium post-synthetically results in the formation of materials which are active as oxidation catalysts with aqueous H_2O_2 or anhydrous *tert*-butyl hydrogenperoxide as oxidants.

Wan *et al.* functionalized the surface of SBA-15 by introducing an amine functionalized tether used for immobilization during the synthesis of the support. This results in the formation of NH_2-modified SBA-15 which can coordinate metal precursors to afford immobilized catalysts [7]. The presence of the amine groups as well as the introduction of the $RuCl_2(PPh_3)_3$ complex

into the silica framework could be confirmed by making use of different analytical techniques; such as nitrogen adsorption/desorption isotherms, powder XRD, TEM, solid state ^{29}Si MAS NMR and ^{13}C CP MAS NMR to name but a few. Most of these techniques were also employed to characterize and confirm the successful immobilization of our siloxane functionalized complexes onto the surface of mesoporous MCM-41 and SBA-15. The heterogenized homogeneous catalyst exhibited comparative activity when compared to the homogeneous derivative with the added advantage of it being recoverable for at least four times without any significant drop in the catalyst activity.

With all this in mind we set about to immobilize our synthesized siloxane functionalized complexes previously discussed in Chapter 2 and Chapter 3 onto MCM-41 and SBA-15 support materials.

4.2   Results and discussion

4.2.1   Synthesis and characterization of mesoporous silicas, MCM-41 and SBA-15

Adaptation of synthetic procedures reported by Cai and Zhao allowed us to synthesize both MCM-41 and SBA-15 with relative ease [8,9]. The synthesis of MCM-41 involved the use of cetyltrimethylammonium bromide (CTAB) as surfactant in a basic solution (pH ~ 12). A silica source in the form of tetraethyl orthosilicate (TEOS) was added to the solution after homogeneity was reached.   By changing the surfactant from CTAB to poly(ethyleneglycol)-block-poly(propyleneglycol)-block-poly(ethyleneglycol) (PEG-PPG copolymer) and switching to more acidic conditions SBA-15 could be synthesized.   Both silica types were isolated as white powders after washing with water and drying under vacuum. Calcination at 550 ˚C was carried out to remove the surfactant molecules that originally acted as a template during the synthesis of the silica materials.

4.2.1.1   Characterization of native MCM-41 and SBA-15

MCM-41 and SBA-15 were characterized by small-angle powder X-ray diffraction, infrared spectroscopy, scanning electron microscopy (SEM), transmission electron microscopy (TEM), thermal gravimetric analysis (TGA), solid state NMR (^{29}Si) and nitrogen adsorption/desorption (BET) surface analysis.

4.2.1.1.1   Characterization of MCM-41 and SBA-15 silicas by means of FT-IR spectroscopy (ATR)

Analysis by means of FT-IR spectroscopy confirmed the successful synthesis of the silicate materials, MCM-41 and SBA-15. Characteristic absorption bands for both were obtained and correlate well to reported literature values [10]. Bands at around 3409, 1631, 1053/1055, and 789/798 cm^{-1} are assigned to water -OH stretching, water -OH bend, Si-O stretching and O-Si-O stretching respectively and is shown in Figure 4.1.
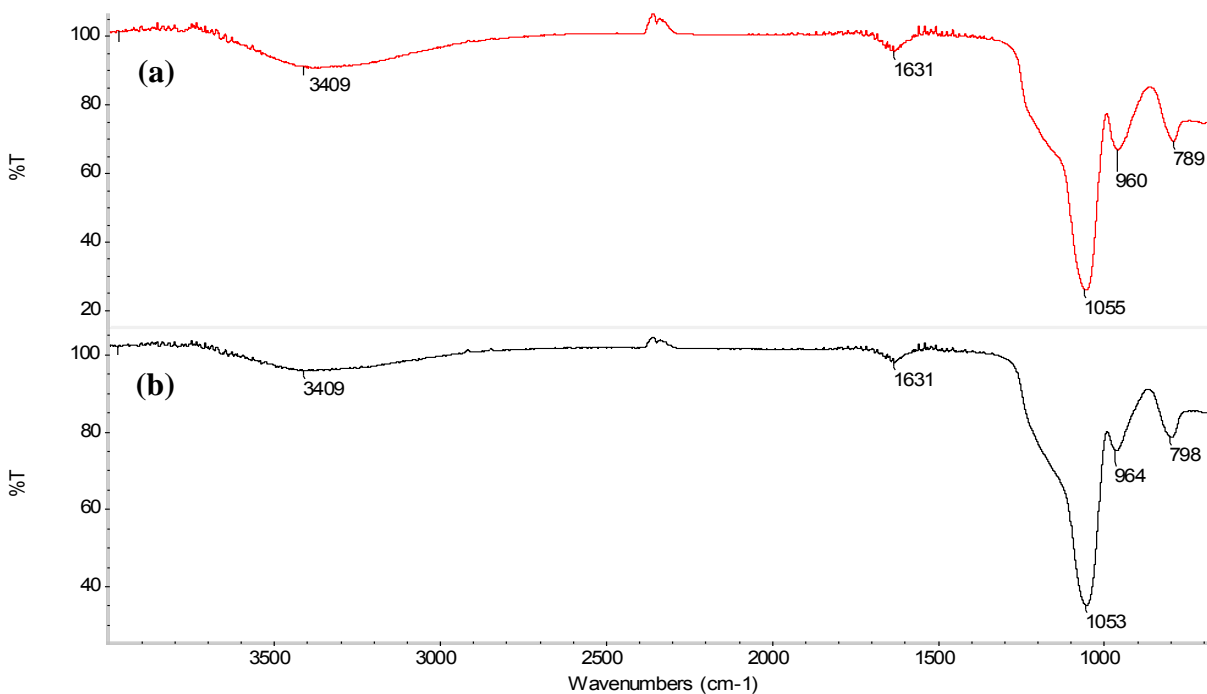
Figure 4.1 FT-IR spectra of native MCM-41 (a) and SBA-15 (b).

Chapter 4: Immobilization of RuCl(arene)(N,N) Complexes on MCM-41 and SBA-15

No significant differences between MCM-41 and SBA-15 can be observed when comparing their respective IR spectra.

4.2.1.1.2 Characterization of MCM-41 and SBA-15 by means of BET (Brunauer Emmett Teller) surface analysis

BET surface analysis was used to determine the surface area and average pore diameter of the synthesized supports. The samples were degassed in the range of 150-230 °C for 18 hours to ensure that the samples were completely dry and solvent free. The relative pressure was increased from 0 to 1 relative pressure (P/Po) and the amount of nitrogen adsorbed was measured. There are different types of nitrogen adsorption isotherms and they are classified by the adsorption profile they exhibit. The types range from I-V and the differences between each of these are shown in Figure 4.2. The type of material and the micropore structure would determine which isotherm profile or type will be observed for a certain material.
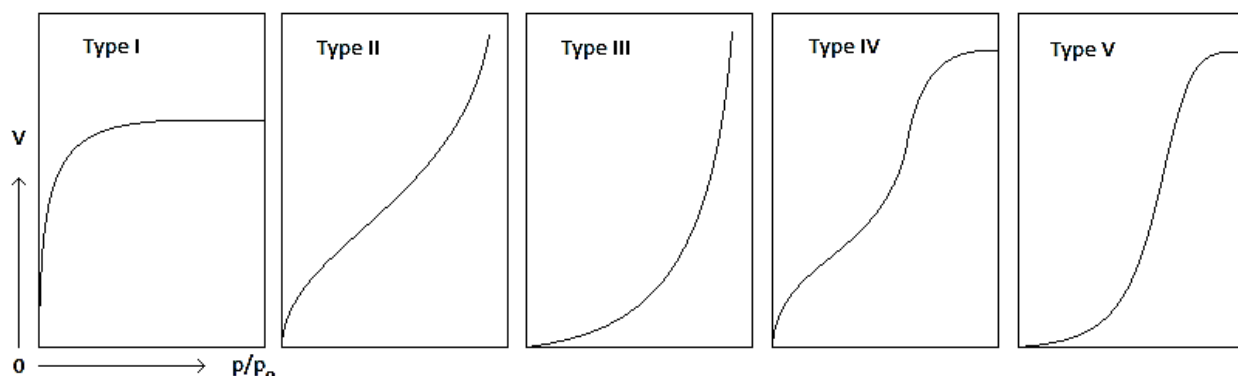
Figure 4.2 Different types of isotherm plots (types I-V).

Two distinctly different looking isotherm plots were obtained for MCM-41 and SBA-15 and are shown in Figure 4.3. Typical type IV isotherms were obtained for both materials with a more pronounced H1 hysteresis loop being observed for SBA-15. This is characteristic for materials with large pores of constant cross-section, be it cylindrical or hexagonal [11]. The slight absence

of a hysteresis loop for the isotherm obtained for MCM-41 is ascribed to the size of the mesopores. It has been reported that the nitrogen hysteresis only appears at temperatures below 70 K or when the pore diameter is greater than 40 Å [12, 13]. In our case all the BET analyses were carried out at 77 K using nitrogen as the adsorption gas. The absence of a hysteresis loop for MCM-41 would then mean that we can expect to have a material with a pore diameter of less than 40 Å. This is indeed what was observed with MCM-41 showing pores with a diameter of around 26 Å compared to the much larger pores of SBA-15 with diameters of 55 Å.

From the higher volume of nitrogen gas adsorbed onto the surface of MCM-41 compared to that of SBA-15 it can be concluded that MCM-41 would have a larger surface area than SBA-15.
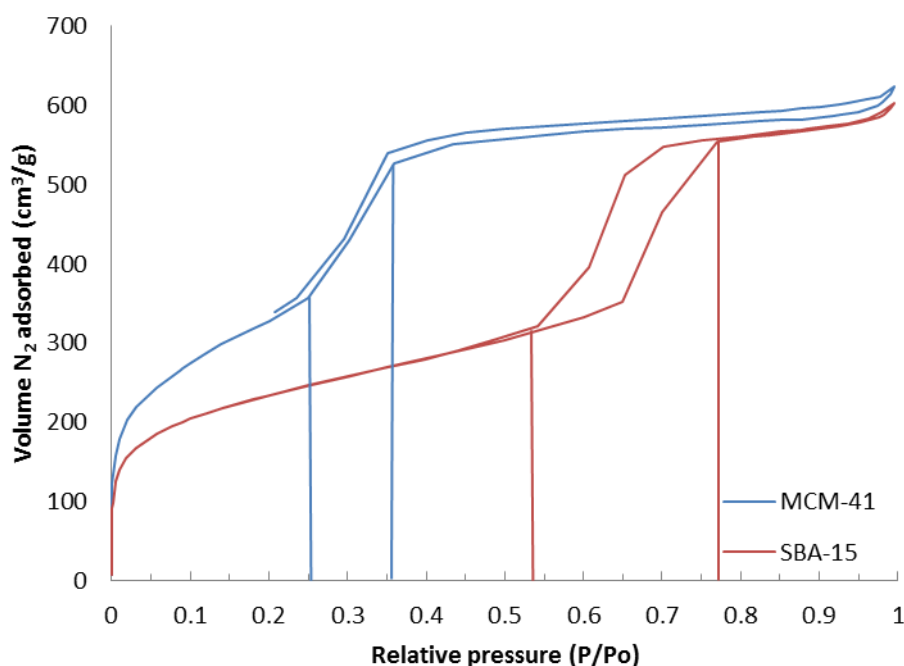
Figure 4.3 Isotherm plots for MCM-41 and SBA-15.

Another observation that can be made from this is that SBA-15 would have thicker silica walls as wall thickness is inversely proportional to surface area [14]. The pore-filling steps of the MCM-41 and SBA-15 occur at P/Po 0.25-0.35 and 0.53-0.77 relative pressures respectively

Chapter 4: Immobilization of RuCl(arene)(N,N) Complexes on MCM-41 and SBA-15

showing that the pores of MCM-41 is filled over a much smaller range than that of SBA-15. From this one can conclude that MCM-41 would have a much narrower pore size distribution than SBA-15. This narrower pore size distribution is confirmed when plotting the desorption pore volume against the pore diameter (Figure 4.4). The pore diameter is calculated by making use of Barret-Joyner-Halenda (BJH) calculations (Eq. 1) and desorption data.

$$t = 3.5400x[-5.0000/\ln(P/P_o)]0.3330 \tag{1}$$

From the obtained plot it is possible to estimate the pore diameters of MCM-41 and SBA-15 as 28 and 57 Å respectively.
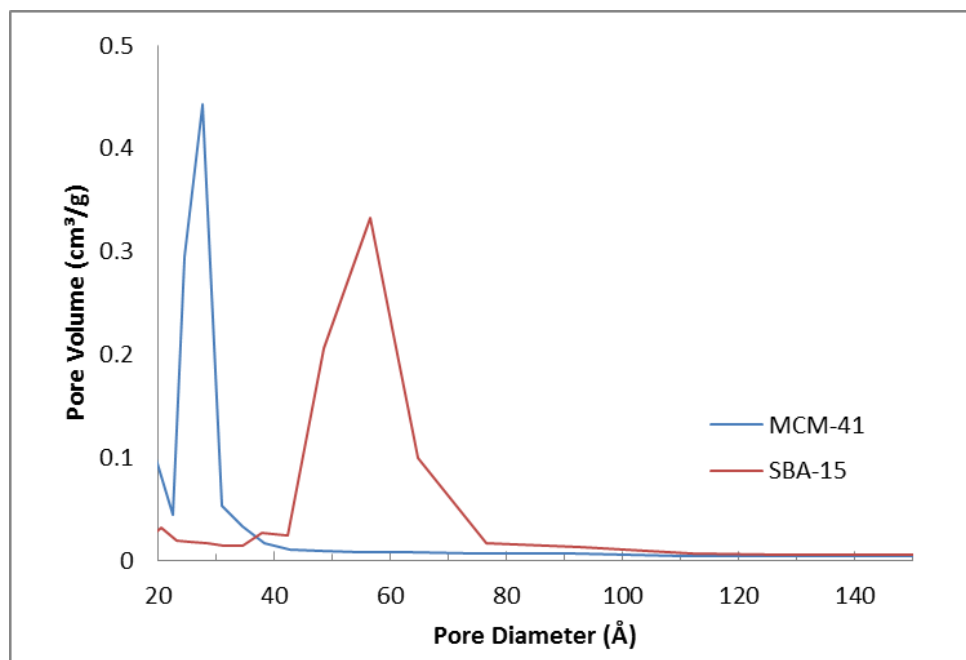
Figure 4.4 Pore size distribution plot of MCM-41 and SBA-15.

In Table 4.1 the surface area, average pore diameter and pore volume data calculated from BET results for MCM-41 and SBA-15 are summarized. MCM-41 shows a much higher surface area than SBA-15 (~300 cm^2/g greater). SBA-15 on the other hand has much larger pores than MCM-41 (43 compared to 31 Å). The difference in the total pore volumes is negligible being 0.93 and 0.91 cm^3/g for MCM-41 and SBA-15 respectively. These results are consistent with results reported in literature [15-17].

Table 4.1   Summary of BET surface area, average pore diameter and total pore volume of MCM-41 and SBA-15.

Material	BET Surface Area (cm^2/g)	Average Pore Diameter (Å)	Total Pore Volume (cm³/g)
MCM-41	1190.76	31.38	0.93
SBA-15	836.43	43.53	0.91

4.2.1.1.3 Characterization of native MCM-41 and SBA-15 by means of powder XRD

For both MCM-41 and SBA-15 three well resolved peaks that can be indexed as (100), (110) and (200) diffractions associated with a 2-D hexagonal symmetry, indicating a well-ordered mesostructure, can be identified (Figure 4.5 and Figure 4.6). These powder X-ray diffraction patterns of the produced MCM-41 and SBA-15 are typical for these types of mesoporous silica materials [18,19]. The diffraction peaks of SBA-15 occur at much lower angles than that of MCM-41 which is characteristic for SBA-15 and illustrates the effect that different reaction conditions and templating agents have on the properties of the resulting material. Intense reflection peaks are observed for both MCM-41 and SBA-15 at around $2\theta = 2.10$ ˚ and 0.82 ˚ respectively corresponding to the (100) reflection planes. Three more peaks are observed for MCM-41 and were assigned to the (110), (200) and (210) reflection planes at $2\theta = 3.72$ ˚, 4.35 ˚ and 5.83 ˚ (although much less pronounced) respectively.
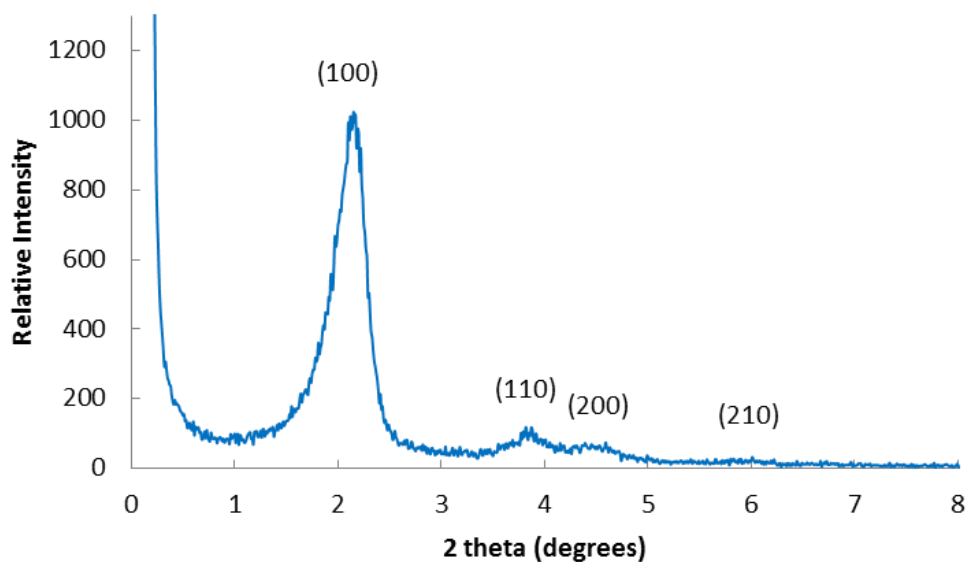
Figure 4.5 Powder XRD plot of MCM-41.
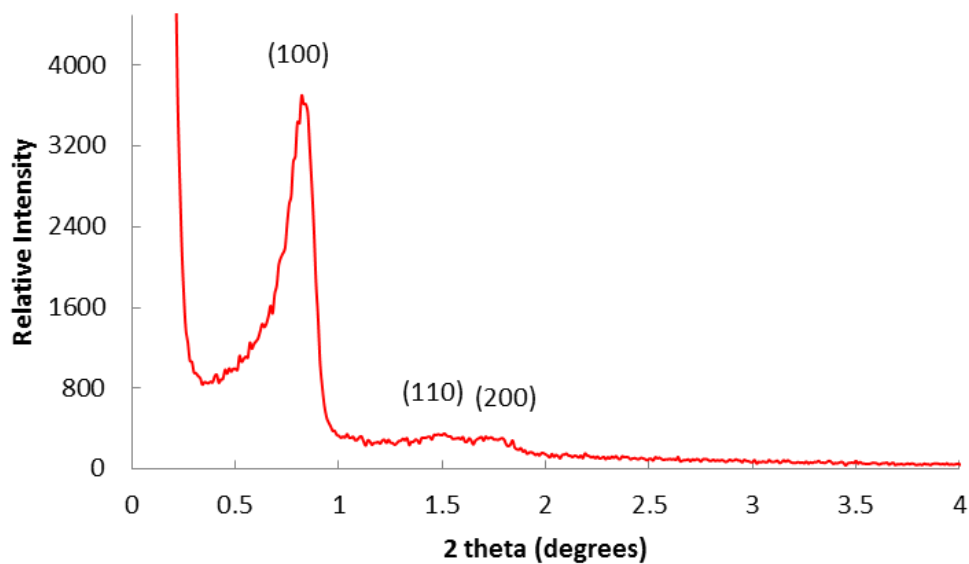
Figure 4.6 Powder XRD plot of SBA-15.

Chapter 4: Immobilization of RuCl(arene)(N,N) Complexes on MCM-41 and SBA-15

The presence of this fourth (210) and sometimes fifth peak (300) indicates that the material is of good quality [20]. For SBA-15 two more peaks at $2\theta = 1.44$ ˚ and 1.68 ˚ are observed and correspond to the (110) and (200) reflection planes respectively. These values are in agreement with reported 2-D hexagonal ordered structures expected for these two mesoporous materials. The angles for the different diffraction peaks of MCM-41 and SBA-15 are summarized in Table 4.2.

Table 4.2 Powder XRD diffractions of MCM-41 and SBA-15.[a]

Material	(100)	(110)	(200)	(210)
MCM-41	2.10 ˚	3.72 ˚	4.35 ˚	5.83 ˚
SBA-15	0.82 ˚	1.44 ˚	1.68 ˚	-

[a] Angles given as degrees 2 theta

By using Bragg's equation (Eq. 2) it is possible to calculate the interplanar spacing for the (100) reflection plane of both MCM-41 and SBA-15. The calculated d spacing for the reflection plane d_{100} was found to be 42.0 Å for MCM-41 and 107.6 Å for SBA-15 ($\lambda = 1.5406$ Å and n for $d_{100} = 1$). From this the unit cell parameter a could be calculated as 48.52 Å and 124.26 Å for MCM-41 and SBA-15 respectively (Eq. 3) [21].

$$2d\sin\theta = n\lambda \tag{2}$$

$$a = 2d/\sqrt{3} \tag{3}$$

Chapter 4: Immobilization of RuCl(arene)(N,N) Complexes on MCM-41 and SBA-15

4.2.1.1.4 Characterization of MCM-41 and SBA-15 by means of transmission electron microscopy (TEM)

The TEM micrographs of MCM-41 and SBA-15 show regular arrays of mesoporous channels packed in a hexagonal arrangement. The presence of the hexagonal fine structure is much more pronounced for SBA-15 than for MCM-41 as can be seen in Figure 4.7 and Figure 4.8 below. This can be ascribed to incomplete crystallization during the aging process when the material was synthesized. Increased aging time will result in a material with higher crystallinity but by no means a different material. Parameters like calcination temperature and time can also influence the exact physical appearance of the formed material.
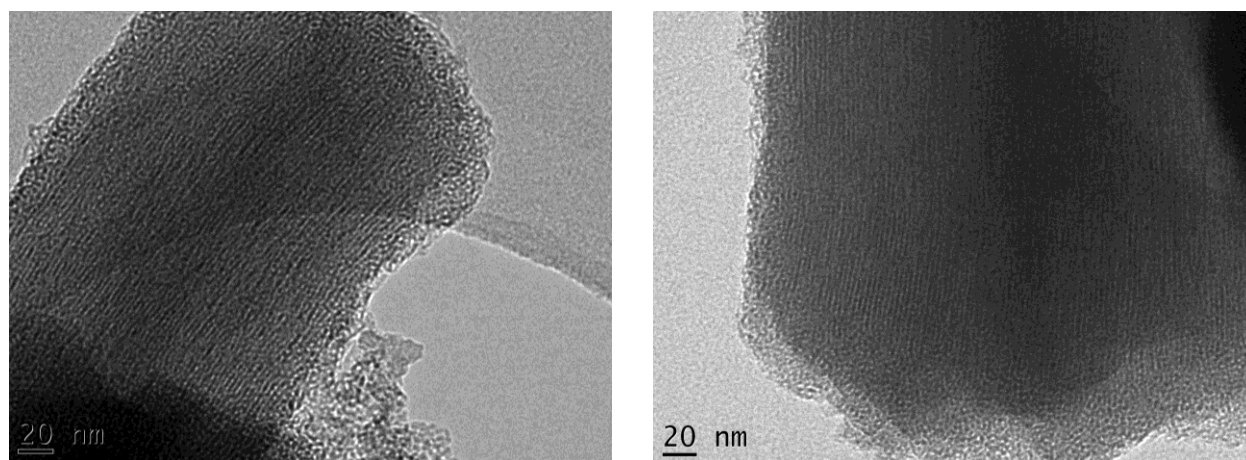
Figure 4.7 Transmission electron micrographs (TEM) of MCM-41.

The repeat distances between the channels can be measured by making use of ImageJ software. The distances were measured as 32.7 ± 1.3 Å for MCM-41 and 84.1 ± 4.4 Å for SBA-15 respectively which compares relatively well to the d_{100} spacing calculated from powder XRD results. The silicate wall thickness of SBA-15 could also be measured from the obtained TEM micrographs. A summary of all parameters is shown in Table 4.3.

Chapter 4: Immobilization of RuCl(arene)(N,N) Complexes on MCM-41 and SBA-15
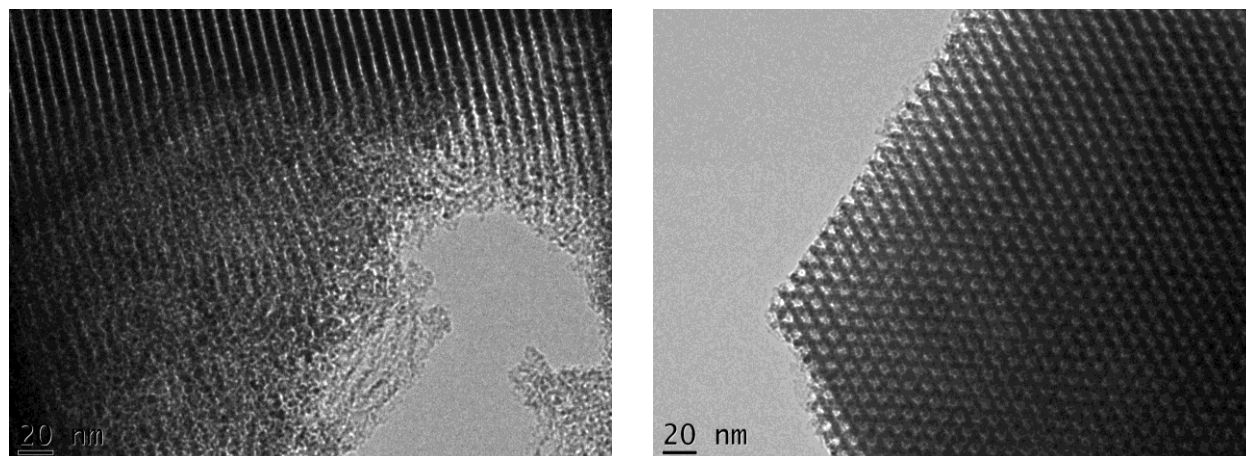
Figure 4.8 Transmission electron micrographs (TEM) of SBA-15.

Table 4.3   Summary of BET surface area, average pore diameter and pore volume of MCM-41 and SBA-15.

Material	d_{100} Spacing (Å)[a]	Unit Cell Parameter a (Å)[a]	Measured Channel Repeat Distance (Å)[b]	BJH Pore Diameter (Å)[c]	Channel Diameter (Å)[b]
MCM-41	42.0	48.5	32.7 ± 1.3	25.89	23.0 ± 3.5
SBA-15	107.6	124.3	84.1 ± 4.4	55.15	59.0 ± 5.5

[a] Calculated from powder XRD angles for the d_{100} plane; [b] Measured from TEM micrographs using ImageJ; [c] Calculated from adsorption branch of isotherm (BET analysis)

The wall thickness for SBA-15 was found to be around 37 Å which compares well with literature values for this type of material [22]. Unfortunately the obtained micrographs of MCM-41 did not allow us to accurately measure the silicate wall thickness. Channel diameters measured from TEM micrographs compare favorably with pore diameters determined using nitrogen adsorption/desorption data.

4.2.1.1.5 Characterization of MCM-41 and SBA-15 by means of thermal gravimetric analysis (TGA)

Both supports were analyzed using TGA to determine the thermal stability of the silicate materials. An initial loss just below 100 °C is observed for both materials and could be attributed to the loss of water absorbed onto the surface of the materials after synthesis. No significant loss is observed between 100 and 600 °C which confirms that these materials have very good thermal stabilities at high temperatures making them suitable for use as catalyst supports (Figure 4.9). The slight drop in the weight of the silicas (around 2-3 % over the temperature range) can be attributed to small amounts of templating agent or unreacted TEOS that might not have been completely removed during the calcination process.
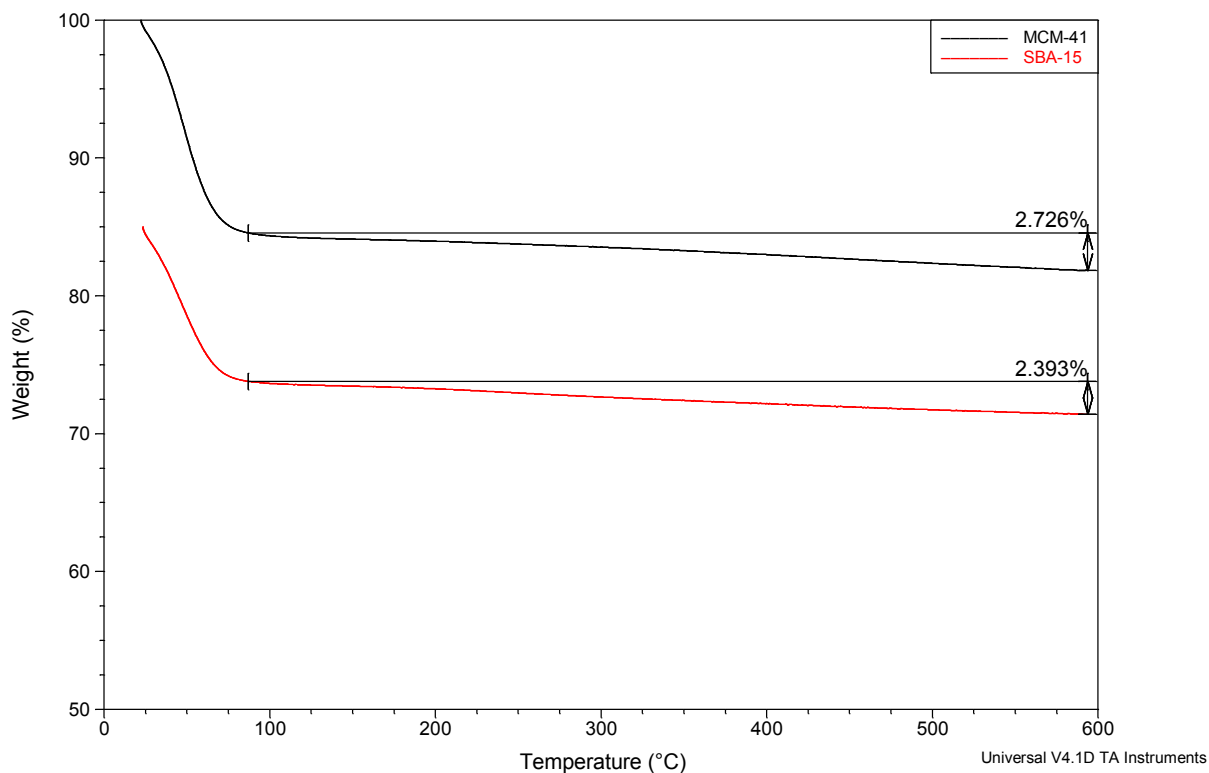
Figure 4.9 TGA analysis of native MCM-41 and SBA-15.

Chapter 4: Immobilization of RuCl(arene)(N,N) Complexes on MCM-41 and SBA-15

4.2.1.1.6 Characterization of MCM-41 and SBA-15 by means of scanning electron microscopy (SEM)

The two silica supports were also characterized by scanning electron microscopy (SEM) to verify the morphology of the materials. Characteristic micrographs were obtained for MCM-41 and SBA-15 with both showing clear hexagonal structures (Figure 4.10 and Figure 4.11). The latter however tends to arrange in chain-like structures compared to MCM-41 which tends to give more discrete particles.
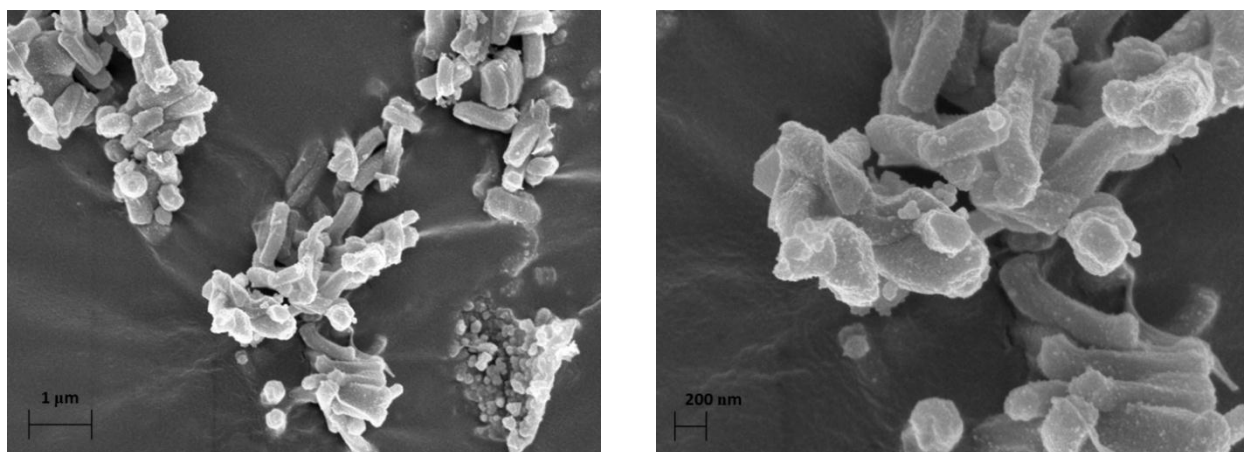
Figure 4.10 Scanning electron micrographs (SEM) of MCM-41.
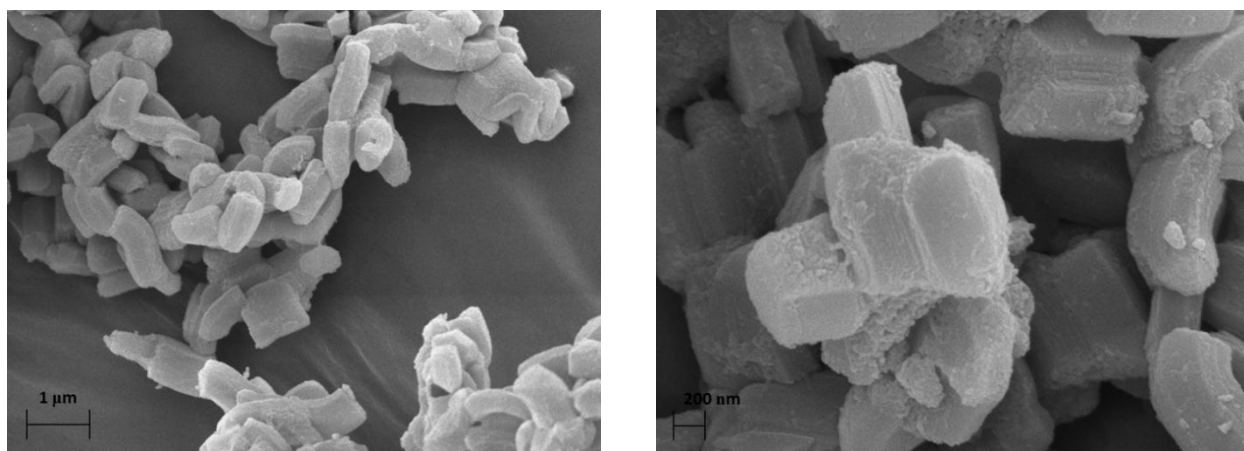
Figure 4.11 Scanning electron micrographs (SEM) of SBA-15.

From the SEM micrographs it is possible to verify the hexagonal morphology of the silicas as well as to get a good indication of the particle sizes of the silicas. Larger particles were obtained for SBA-15 when compared to the much smaller MCM-41 particles. This difference in particle size is a result of different templating agents and pH used for the synthesis of the respective materials. These results are characteristic for hexagonal mesoporous materials and compare favorably with what is reported in the literature [18,19].

Measurement of the particle sizes of MCM-41 and SBA-15 showed that these particles had diameters of around 300 nm as shown in Figure 4.12. For MCM-41 the particle diameter was found to be around 280 nm compared to SBA-15 measuring between 320 and 370 nm.

Energy-dispersive X-ray spectroscopy (EDS) was carried out on MCM-41 and SBA-15 to determine the content of the material. These materials are basically all SiO_2 and one would thus expect an atom ratio of 2:1. From EDS data one can determine the atomic % of an area of the material and it was found that the atomic % of MCM-41 was 67.77 % (Si) and 32.23 % (O) and for SBA-15 67.89 % (Si) and 32.11 % (O) respectively. This is in agreement with the ratio one would expect for mesoporous materials.
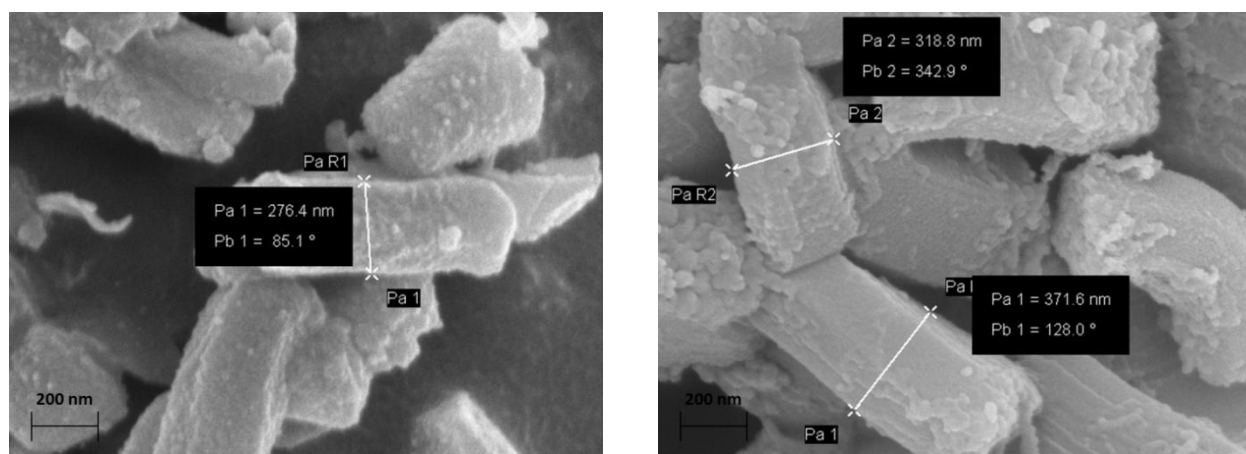
Figure 4.12   Comparison of particle sizes of MCM-41 (left) and SBA-15 (right) measured from SEM.

Chapter 4: Immobilization of RuCl(arene)(N,N) Complexes on MCM-41 and SBA-15

4.2.2 Synthesis and characterization of immobilized ruthenium arene catalysts

A procedure for the preparation of the immobilized Ru(II)(*p*-cymene) catalysts **IC4.1**-**IC4.6** with the siloxane tether attached to the imine nitrogen is shown in Scheme 4.2. In Scheme 4.3 the preparation of immobilized catalysts **IC4.7**-**IC4.12** is shown. Here the tether to the support material is incorporated via the arene ring.
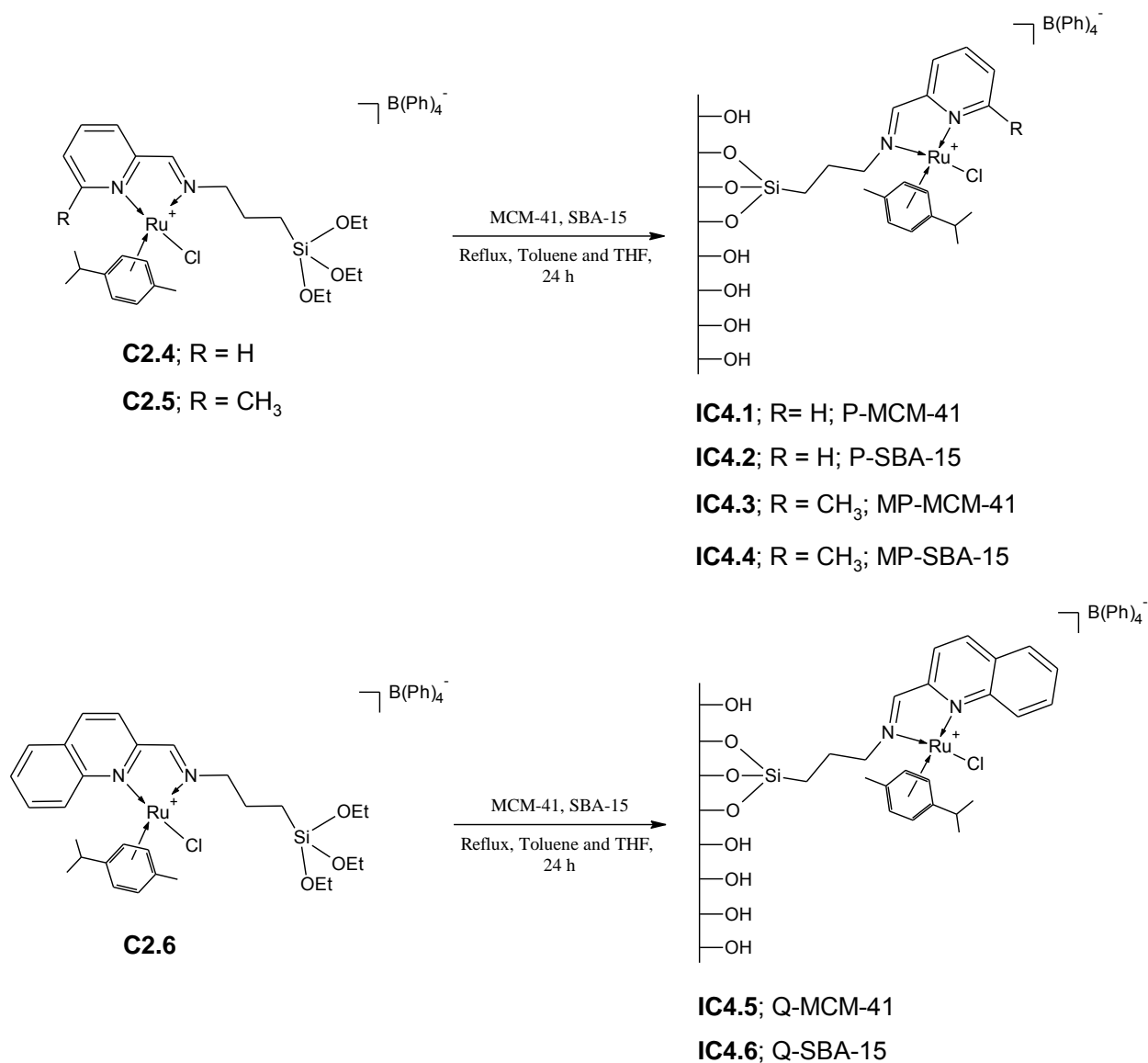
Scheme 4.2 Synthesis of MCM-41 and SBA-15 immobilized catalysts IC4.1-IC4.6 with the tether via the imine nitrogen.

Chapter 4: Immobilization of RuCl(arene)(N,N) Complexes on MCM-41 and SBA-15

C3.5-C3.7

MCM-41, SBA-15
Reflux, Toluene and THF,
24 h

IC4.7; P-P-MCM-41

IC4.8; P-P-SBA-15

IC4.9; P-A-MCM-41

IC4.10; P-A-SBA-15

IC4.11; MP-A-MCM-41

IC4.12; MP-A-SBA-15
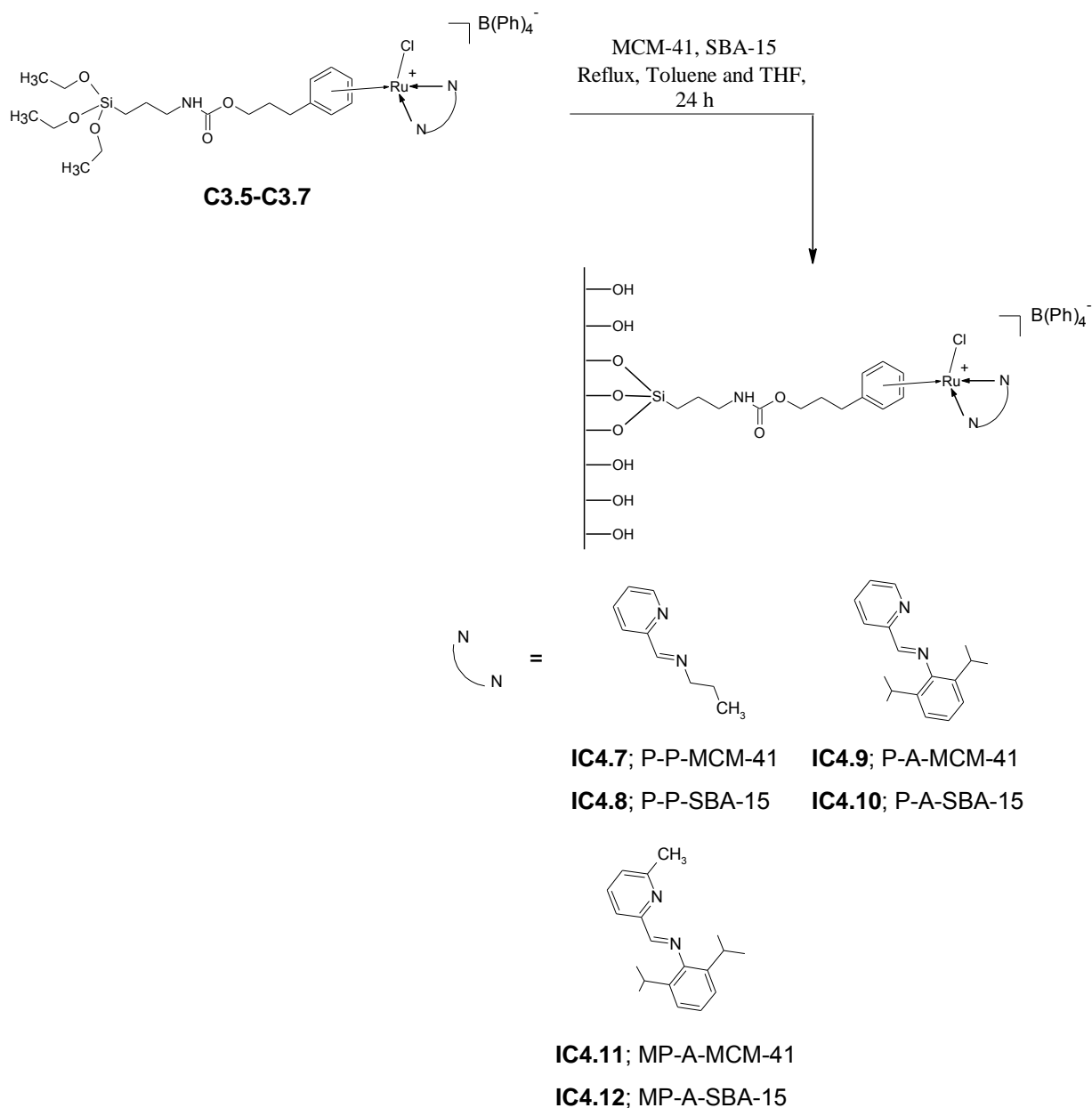
Scheme 4.3 Synthesis of MCM-41 and SBA-15 immobilized catalysts IC4.7-IC4.12 with the tether via the arene ring.

For our study, 10 weight % siloxane functionalized complex relative to the support material was utilized to produce the immobilized catalysts. The immobilization of the siloxane functionalized complexes onto the different silica supports is achieved through the condensation of the surface silanol groups (Si-OH) of the support with the siloxane (Si(OEt)$_3$) group of the functionalized

complex. This condensation reaction results in the formation of the covalently bound immobilized catalyst. The native supports were heated at 150 °C for 24 h and cooled in a vacuum desiccator before immobilization of the functionalized complexes were carried out. Reported methods for the immobilization of complexes onto the surface of silica supports involved refluxing the complex and support material in toluene as solvent. Attempts to immobilize the functionalized complexes making use of this method were unsuccessful due to the low solubility of the functionalized complexes in toluene. It was therefore decided to pre-dissolve the functionalized complexes in a solvent in which it showed good solubility before being added to a slurry of the support material in toluene. THF was found to be a suitable solvent for these complexes and as a result the complexes were dissolved in a small amount of THF before it was added to a stirring slurry of the appropriate support in toluene. The slurry was allowed to reflux under a nitrogen atmosphere for 24 h. The obtained powders were recovered by filtration, washed with THF and dried under vacuum and stored in a glove box until further use. MCM-41 and SBA-15 immobilized catalysts **IC4.1**-**IC4.12** were characterized by small-angle powder X-ray diffraction, infrared spectroscopy, scanning electron microscopy (SEM), transmission electron microscopy (TEM), thermal gravimetric analysis (TGA), solid state NMR (^{13}C and ^{29}Si), inductively coupled plasma optical emission spectroscopy (ICP-OES) and nitrogen adsorption/desorption (BET) surface analysis.

4.2.2.1 Characterization of MCM-41 and SBA-15 immobilized catalysts IC4.1-IC4.12 using low angle powder XRD

In general the obtained diffraction patterns of the immobilized catalysts do not differ significantly when compared to their native supports MCM-41 and SBA-15 and show that the ordered mesoporisity and structural integrity of the support materials were retained during the immobilization of the siloxane functionalized complexes. This shows that the support material was not significantly altered during the immobilization process and that it retained its high degree of crystallinity. Powder XRD plots of the MCM-41 and SBA-15 immobilized catalysts **IC4.1**-**IC4.12** are shown in Figures 4.12 to 4.15. For the immobilized catalysts in which the tether is attached to the imine nitrogen (**IC4.1**-**IC4.6**) only minor differences in the relative intensities of the peaks in the XRD plots of the MCM-41 immobilized catalysts **IC4.1**, **IC4.3** and

IC4.5 are observed. These differences can be ascribed to the change in the degree of ordering of the silicate material brought about by the immobilization process (Figure 4.13). A negligible shift in the 2 theta angle of immobilized catalyst **IC4.1** is observed. No differences in the intensities of the reflections of SBA-15 supported catalysts **IC4.2**, **IC4.4** and **IC4.6** are however observed (Figure 4.14). For the immobilized catalysts where the tethering is via the arene ring (**IC4.7**-**IC4.12**) a general shift in the 2 theta angles of all the catalysts is observed when compared to the native support materials MCM-41 and SBA-15 (Figure 4.15 and Figure 4.16). The intensities and expected reflection peaks however are retained and therefore one can assume that the support material was not affected by the immobilization process. Characterization by means of powder XRD demonstrated that the immobilized catalysts **IC4.1**-**IC4.12** still retained the highly ordered mesoporous arrays of the support materials confirming the retention of the properties of MCM-41 and SBA-15.
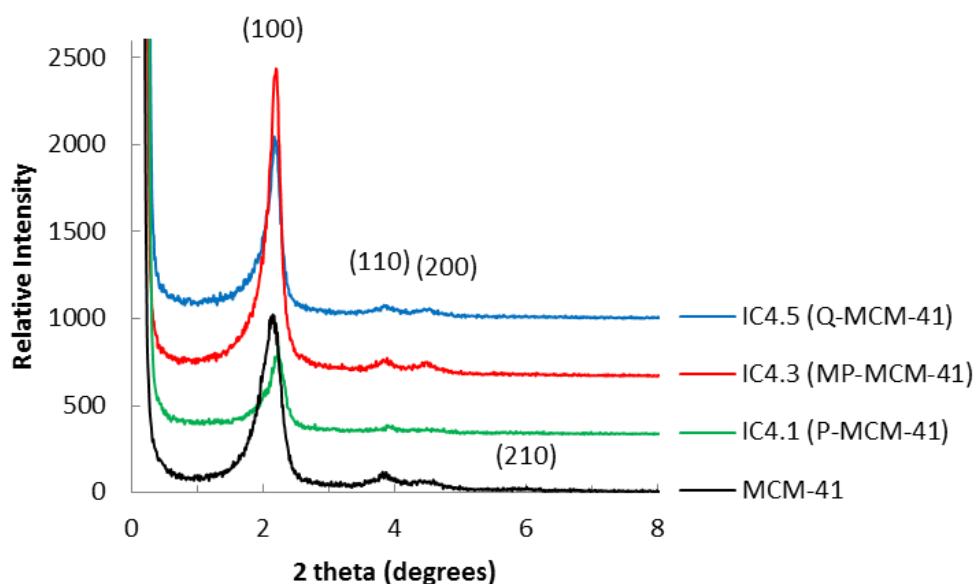
Figure 4.13 Powder XRD plots for MCM-41 immobilized catalysts IC4.1, IC4.3 and IC4.5 (tether via imine nitrogen).

Chapter 4: Immobilization of RuCl(arene)(N,N) Complexes on MCM-41 and SBA-15
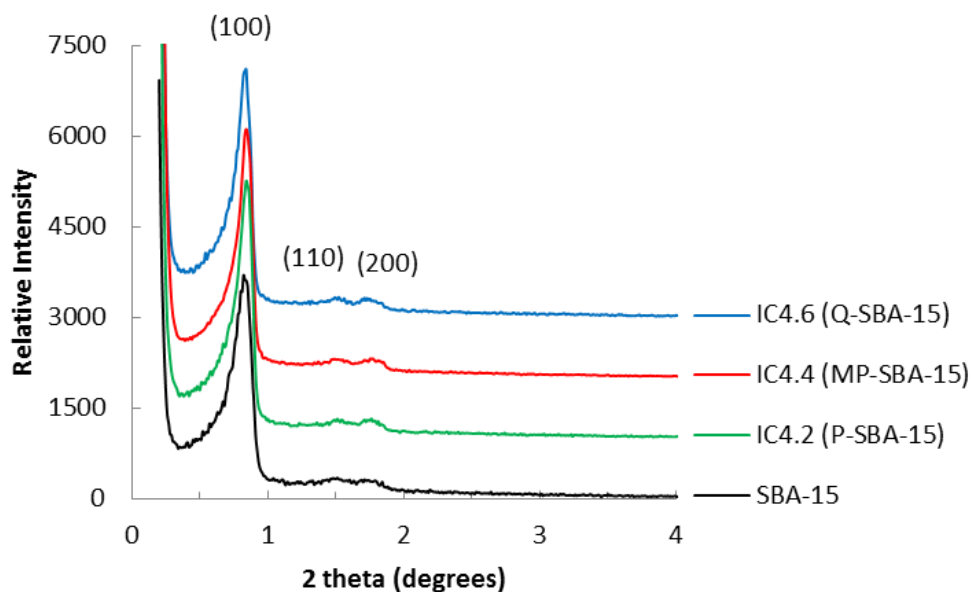
Figure 4.14 Powder XRD plots for SBA-15 immobilized catalysts IC4.2, IC4.4 and IC4.6 (tether via imine nitrogen).
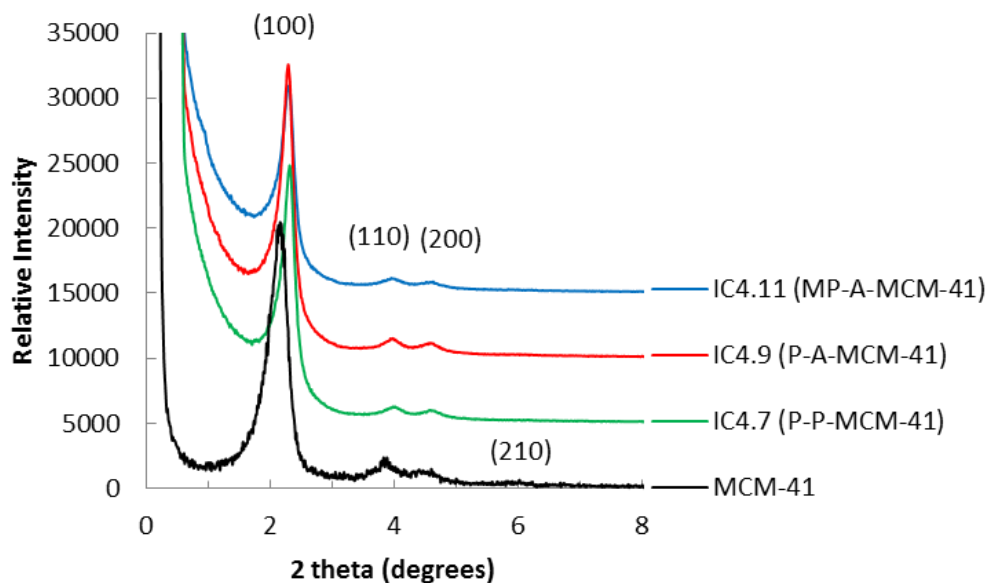
Figure 4.15 Powder XRD plots for MCM-41 immobilized catalysts IC4.7, IC4.9 and IC4.11 (tether via arene ring).
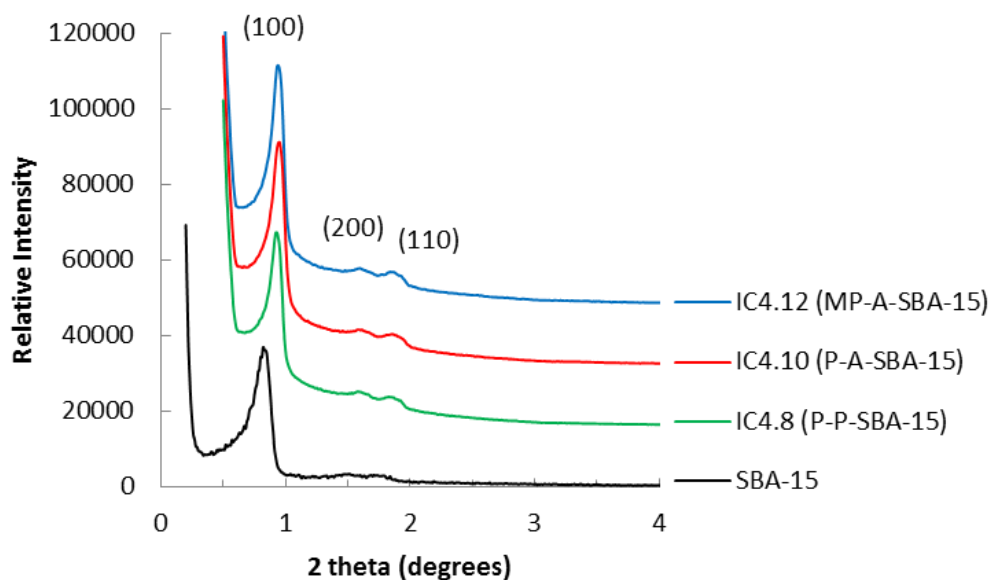
Figure 4.16 Powder XRD plots for SBA-15 immobilized catalysts IC4.8, IC4.10 and IC4.12 (tether via arene ring).

4.2.2.2   Characterization of MCM-41 and SBA-15 immobilized catalysts IC4.1-IC4.12 using nitrogen adsorption/desorption analysis and ICP-OES

Typical type IV isotherms with H1 hysteresis loops were obtained for both MCM-41 and SBA-15 supports as well as the immobilized catalysts **IC4.1**-**IC4.12**; characteristic for mesoporous materials (pore diameters between 2 and 50 nm) with cylindrical channels (Figures 4.17 to 4.20). The H1 hysteresis loops were however much less pronounced for MCM-41 than for SBA-15 (as seen for the native supports). As expected, a decrease in the total volume of nitrogen being absorbed onto the surface of the supported catalysts compared to their native supports MCM-41 and SBA-15 is observed. The decrease in the volume absorbed can be attributed to the successful immobilization of the functionalized complexes which would now occupy space on the surface of the support. In general a larger decrease in the amount of nitrogen absorbed onto the surface of the supported catalysts is observed for the MCM-41 immobilized derivatives.

Figure 4.17 Isotherm plots for MCM-41 immobilized catalysts IC4.1, IC4.3 and IC4.5.
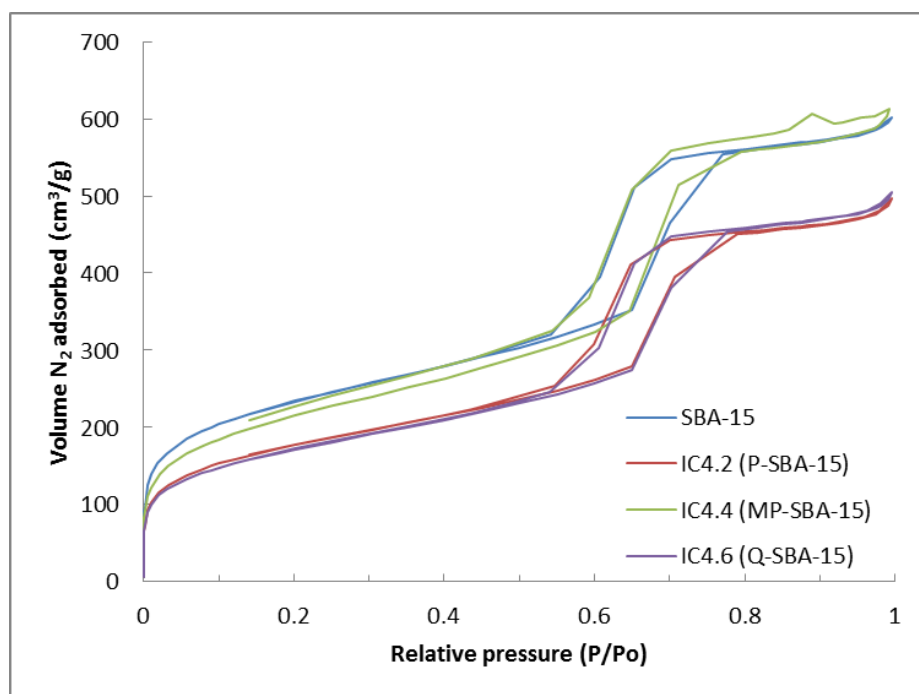
Figure 4.18 Isotherm plots for SBA-15 immobilized catalysts IC4.2, IC4.4 and IC4.6.
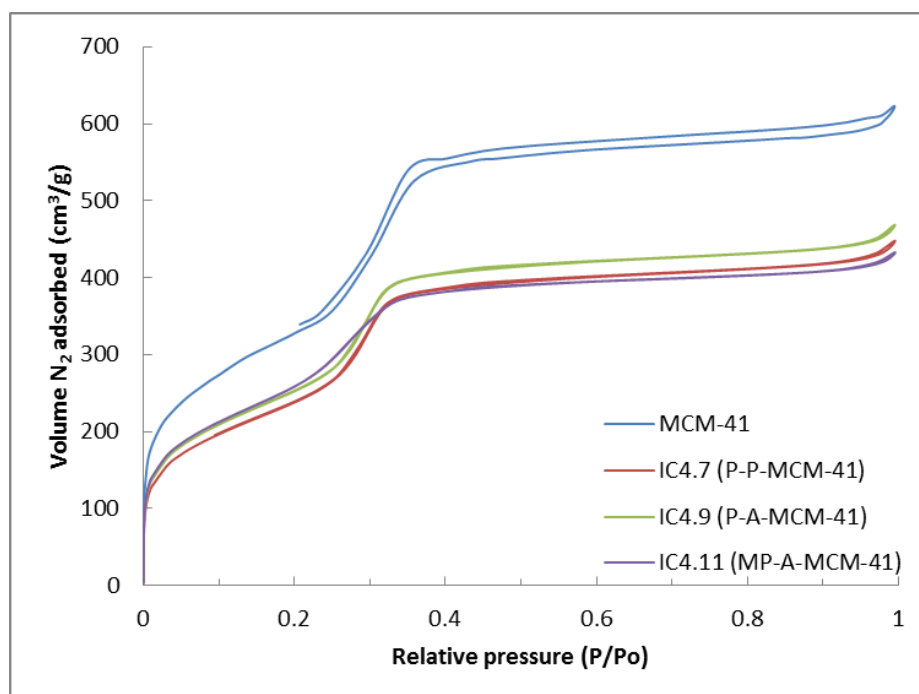
Figure 4.19 Isotherm plots for MCM-41 immobilized catalysts IC4.7, IC4.9 and IC4.11.
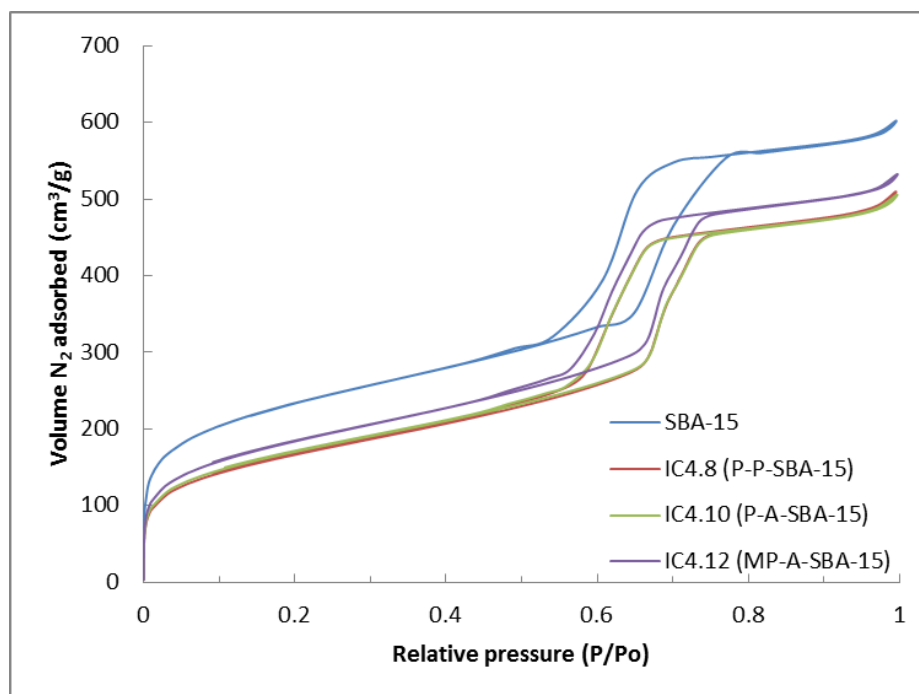
Figure 4.20 Isotherm plots for SBA-15 immobilized catalysts IC4.8, IC4.10 and IC4.12.

Chapter 4: Immobilization of RuCl(arene)(N,N) Complexes on MCM-41 and SBA-15

For the SBA-15 immobilized derivative **IC4.4** however almost the exact same adsorption plot is obtained with no significant change in the volume being absorbed (Figure 4.18). Although no decrease in the amount of nitrogen that was adsorbed onto the surface during this analysis was observed, it will later be shown that a decrease in the total calculated BET surface area was still obtained for this catalyst. Though it is possible to estimate the success of the immobilization process by comparing the adsorption/desorption isotherm plots, a better method would be to compare the calculated BET surface areas. Significant decreases in the obtained BET surface areas of the immobilized catalysts are observed as a result of the anchoring of the functionalized complexes to the surface of the support materials and the results are summarized in Table 4.4. For MCM-41 and SBA-15 immobilized catalysts **IC4.1**-**IC4.6** (tether via the imine nitrogen) derivatives **IC4.5** and **IC4.6** (both quinoline derivatives) for example, showed the largest decrease in surface areas with a decrease in the measured surface area from 1190.76 and 836.43 m^2/g to 894.85 and 614.85 m^2/g respectively. This equates to a change in the total surface area of around 200-300 m^2/g and gives a very good indication of the efficiency of the immobilization process. This compares well with the obtained ICP-OES results which indicated that these two examples did indeed have the highest ruthenium content and therefore best immobilization.

For the derivatives **IC4.7**-**IC4.12**, with the tether attached to the arene ring, the largest changes in the surface areas were seen for immobilized catalyst **IC4.7** and **IC4.8** (pyridine-propyl derivative) with a change from 1190.76 and 836.43 m^2/g to 912.88 and 589.74 m^2/g for the MCM-41 and SBA-15 derivatives respectively. For the immobilized MCM-41 derivatives a general decrease in the average pore diameter and pore volume is observed, as one would expect when the complex is successfully tethered to the surface of the support. This would cause a decrease in the pore diameter and in the pore volume. For the SBA-15 derivatives however an increase in the pore diameters for all immobilized catalyst compared to the native SBA-15 support is observed. A decrease is however observed for the pore volume with the only exception being **IC4.4**. This increase in the pore diameter can probably be ascribed to post synthetic modification of the SBA-15 support during the immobilization process at the elevated temperatures employed. SBA-15 has been found to have lower thermal stability when compared to MCM-41.

Table 4.4 Summary of BET nitrogen adsorption/desorption and ICP-OES results for immobilized catalysts IC4.1-IC4.12.

Material	Ru Loading (% w/w)[a]		Adsorption/Desorption Measurements		
	Theoretical	Actual	BET Surface Area (m^2/g)	Average Pore Diameter (Å)	Total Pore Volume (cm^3/g)
MCM-41	-	-	1190.76	31.38	0.93
IC4.1 (P-MCM-41)	1.02	0.24	1033.72	29.24	0.76
IC4.3 (MP-MCM-41)	1.01	0.38	914.27	29.38	0.67
IC4.5 (Q-MCM-41)	0.97	0.63	894.85	29.40	0.66
IC4.7 (P-P-MCM-41)	0.93	0.75	912.88	29.82	0.68
IC4.9 (P-A-MCM-41)	0.83	0.34	965.22	29.51	0.71
IC4.11 (MP-A-MCM-41)	0.82	0.12	1017.82	25.91	0.66
SBA-15	-	-	836.43	43.53	0.91
IC4.2 (P-SBA-15)	1.02	0.26	636.32	46.71	0.74
IC4.4 (MP-SBA-15)	1.01	0.19	772.46	47.48	0.92

Material	Ru Loading (% w/w)[a]		Adsorption/Desorption Measurements		
	Theoretical	Actual	BET Surface Area (m^2/g)	Average Pore Diameter (Å)	Total Pore Volume (cm^3/g)
IC4.6 (Q-SBA-15)	0.97	0.37	614.85	49.12	0.76
IC4.8 (P-P-SBA-15)	0.93	0.72	589.74	52.63	0.78
IC4.10 (P-A-SBA-15)	0.83	0.49	604.34	50.86	0.77
IC4.12 (MP-A-SBA-15)	0.82	0.62	650.57	49.75	0.81

[a] Analyzed by ICP-OES to determine Ru loading of immobilized catalysts; mg Ru per g of silica

Celar *et al*. showed that treatment of SBA-15 at 100 °C in water for extended periods of time resulted in an increase in the primary mesopore size causing a decrease in the pore diameters from 10.3 to 6.6 nm for their samples. This can explain why an increase in the average pore diameter is only observed for SBA-15 immobilized catalysts and not for their MCM-41 counterparts [23].

SEM-EDS analysis confirmed the presence of ruthenium on the surface of the heterogenized catalysts. EDS however only gives an indication of the amount of ruthenium present on the surface of the catalysts and cannot give an indication of complexes immobilized in the pores of the silica supports.

4.2.2.3   Characterization of MCM-41 and SBA-15 immobilized catalysts IC4.1-IC4.12 using microscopic studies (SEM and TEM)

In Figures 4.21 to 4.23 the SEM micrographs of MCM-41 and SBA-15 immobilized catalysts **IC4.1**-**IC4.12** are compared to that of the native supports MCM-41 and SBA-15. No significant changes in the microstructure of the supported catalysts are observed when they are compared to the native supports. Slightly more fragmentation is observed for the immobilized catalysts which is as a result of sintering caused by stirring during the immobilization process.
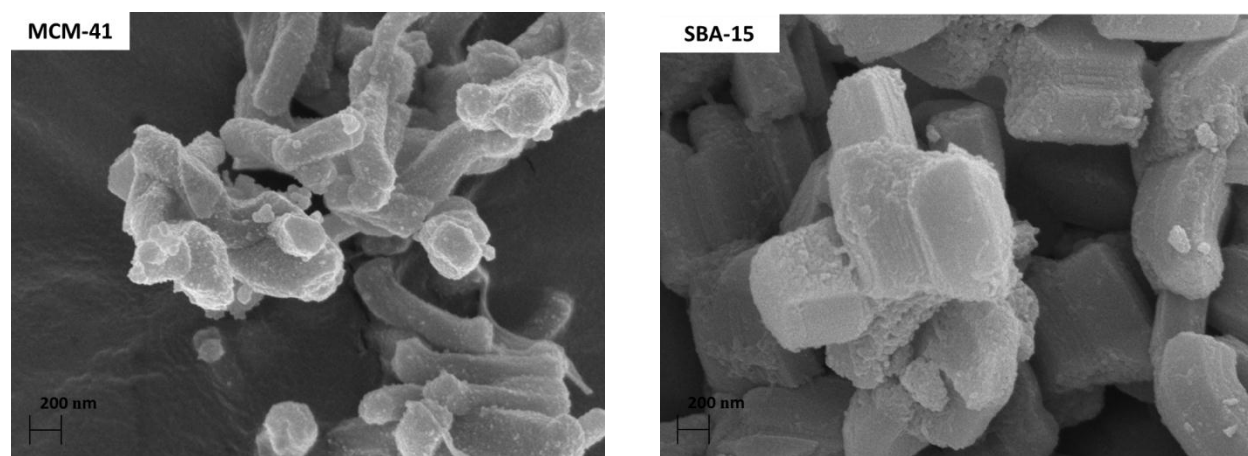
Figure 4.21 SEM micrographs of MCM-41 (left) and SBA-15 (right).
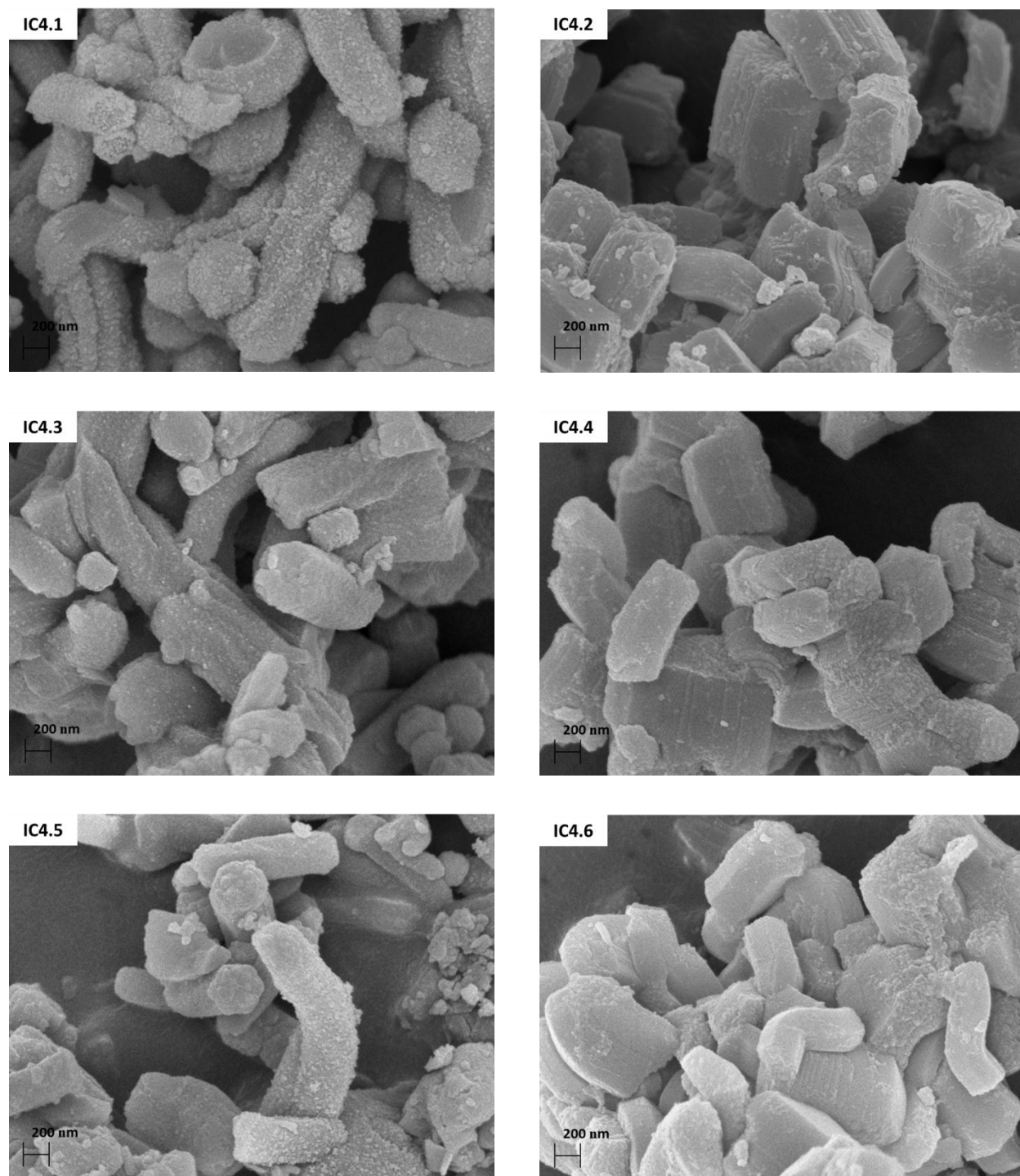
Figure 4.22 SEM micrographs of MCM-41 (left) and SBA-15 (right) immobilized catalysts IC4.1-IC4.6.
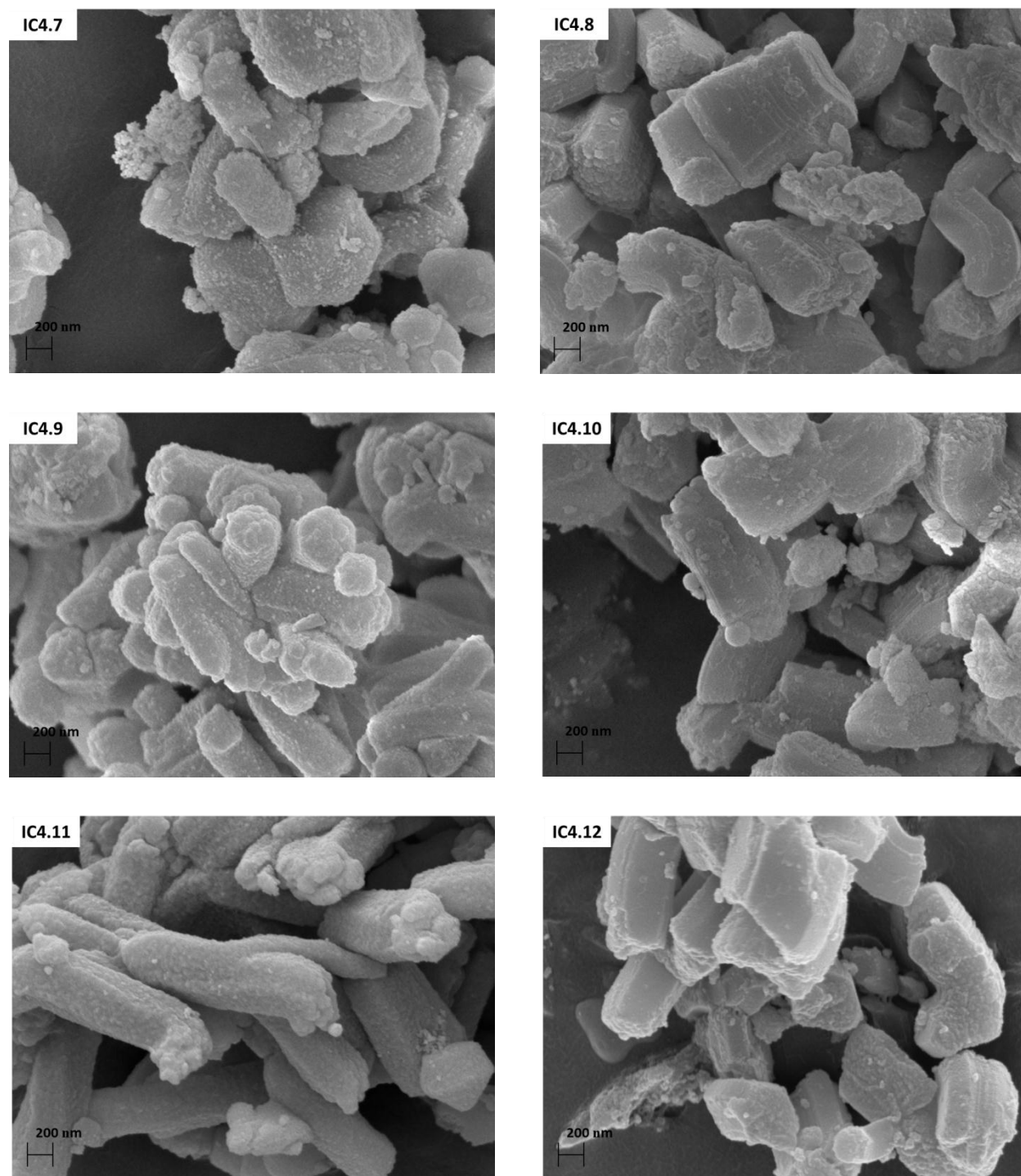
Figure 4.23 SEM micrographs of MCM-41 (left) and SBA-15 (right) immobilized catalysts IC4.7-IC4.12.

More prevalent for the MCM-41 immobilized catalysts is the presence of fine particles on the surface of the support material. All in all the immobilized catalysts maintained their structural integrity when compared to the native silica supports MCM-41 and SBA-15.

TEM micrographs of MCM-41 and SBA-15 immobilized catalysts **IC4.1**-**IC4.12** are shown in Figures 4.24 to 4.26. Although a significant change in the pore diameters of the immobilized catalysts calculated from BET surface analysis was observed, no real difference in the TEM micrographs could be observed when compared to the native supports, MCM-41 and SBA-15.
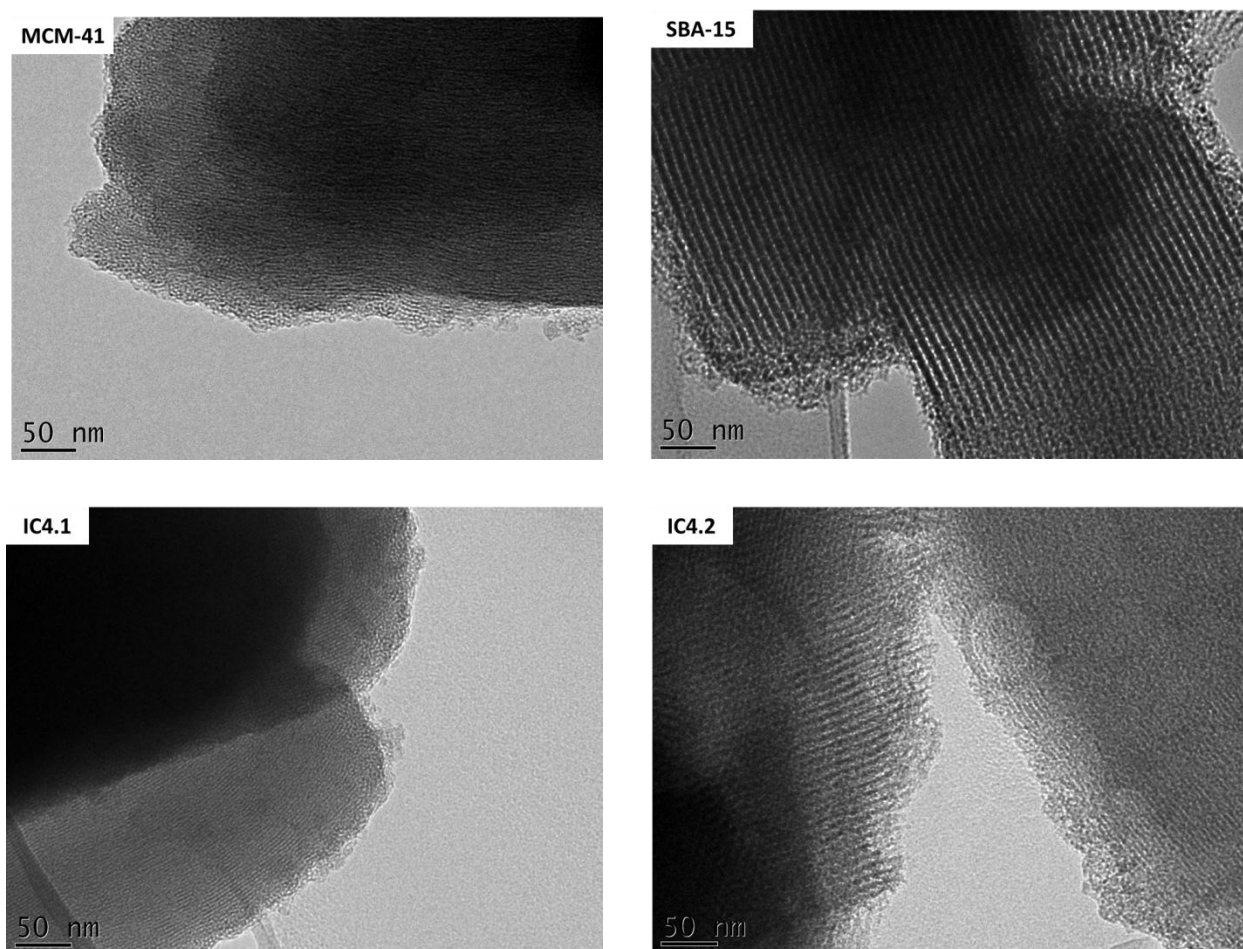
Figure 4.24 TEM micrographs of MCM-41 (left) and SBA-15 (right) immobilized catalysts IC4.1 and IC4.2.
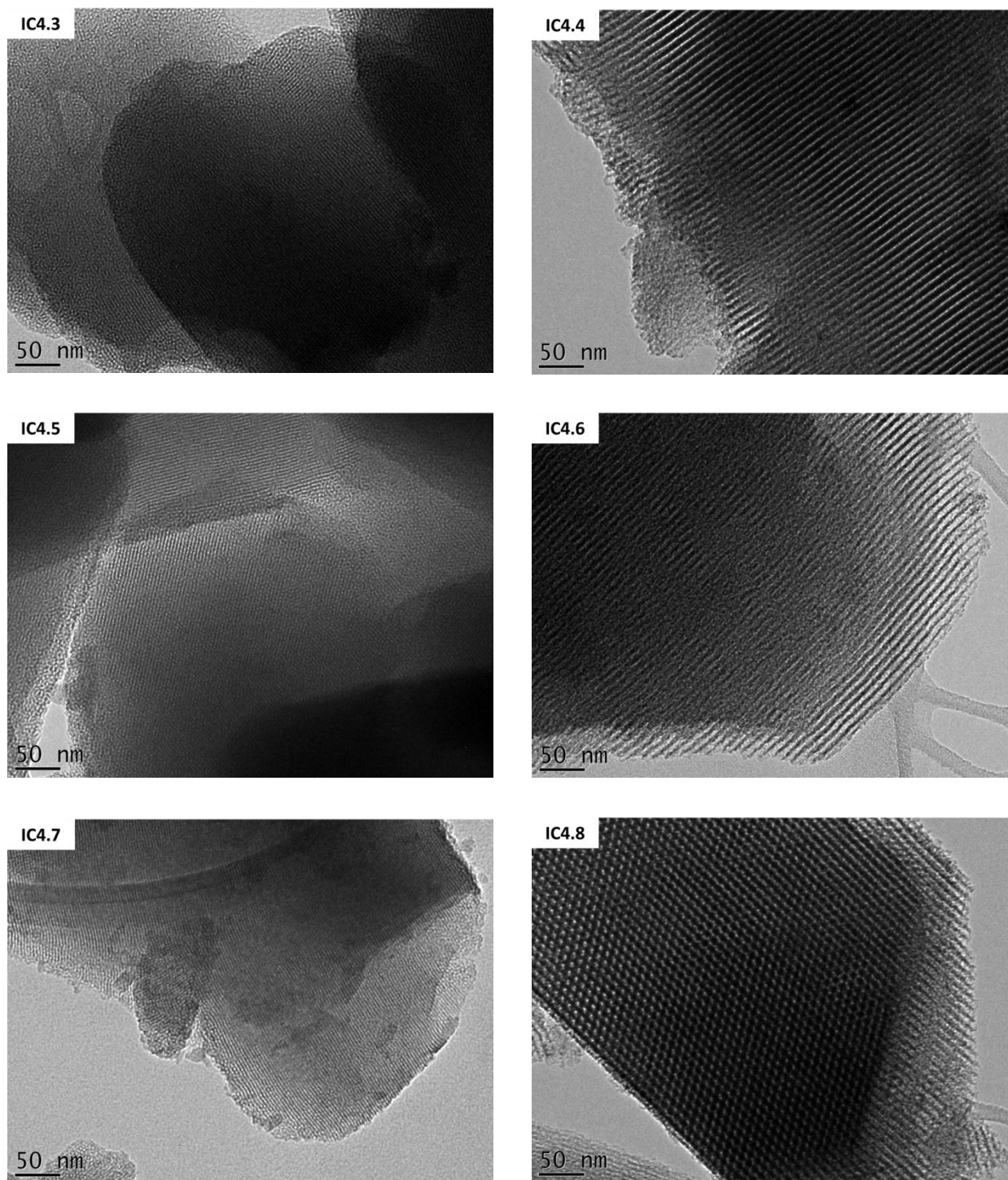
Figure 4.25 TEM micrographs of MCM-41 (left) and SBA-15 (right) immobilized catalysts IC4.3-IC4.8.
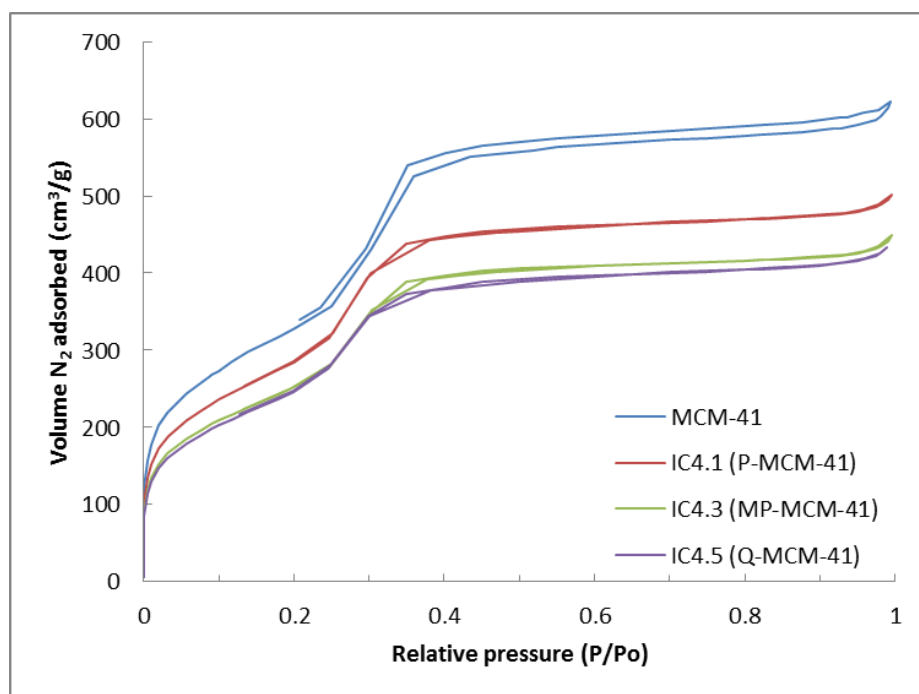
Chapter 4: Immobilization of RuCl(arene)(N,N) Complexes on MCM-41 and SBA-15
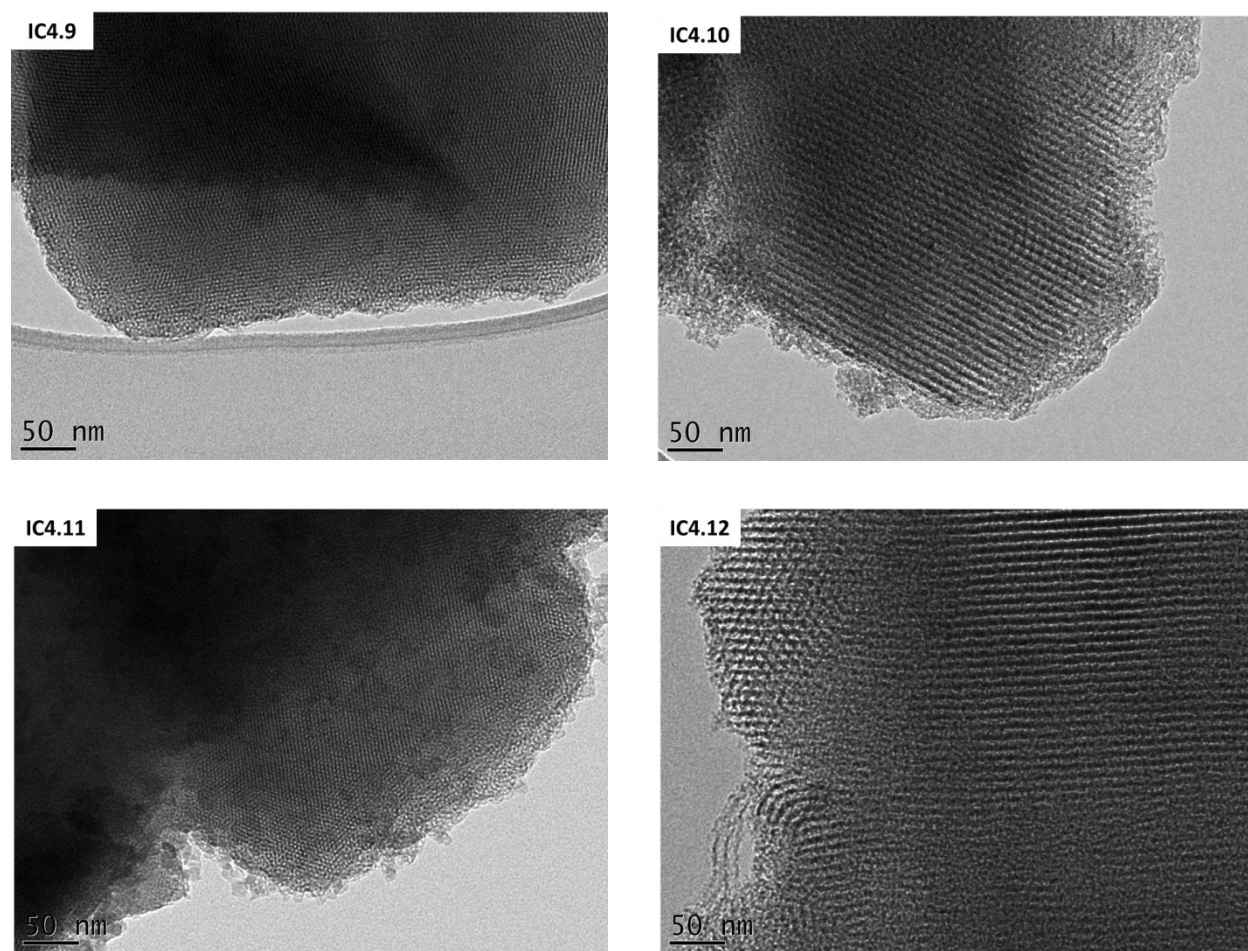
Figure 4.26 TEM micrographs of MCM-41 (left) and SBA-15 (right) immobilized catalysts IC4.9-IC4.12.

4.2.2.4   Characterization of immobilized catalysts IC4.1-IC4.12 using FT-IR spectroscopy

In Figure 4.27 and Figure 4.28 the FT-IR spectra of selected MCM-41 and SBA-15 immobilized catalysts are shown. For the MCM-41 derivatives a definite change in the spectra is observed when comparing the immobilized catalysts to the native MCM-41 support material. The appearance of a shoulder at 1240 cm^{-1} together with the reduction in the intensity of the band at 956 cm^{-1} is observed. A slight decrease in the intensity of the band corresponding to the surface OH-groups can also be observed and corresponds to a decrease in the amount of silanols on the surface as a result of now being bonded to the siloxane of the functionalized complex.
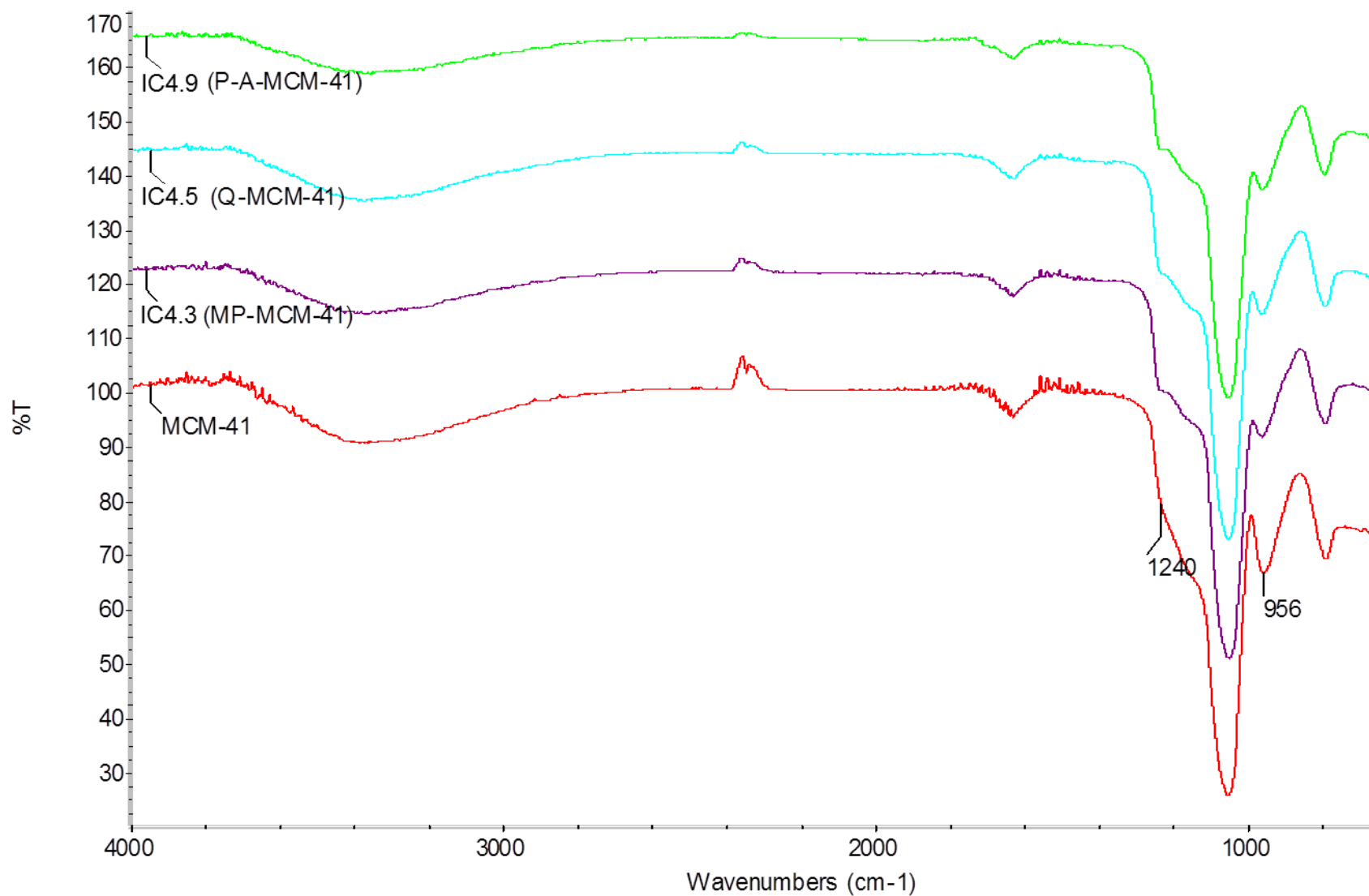
Figure 4.27 FT-IR spectra of MCM-41 immobilized catalysts IC4.3, IC4.5 and IC4.9.
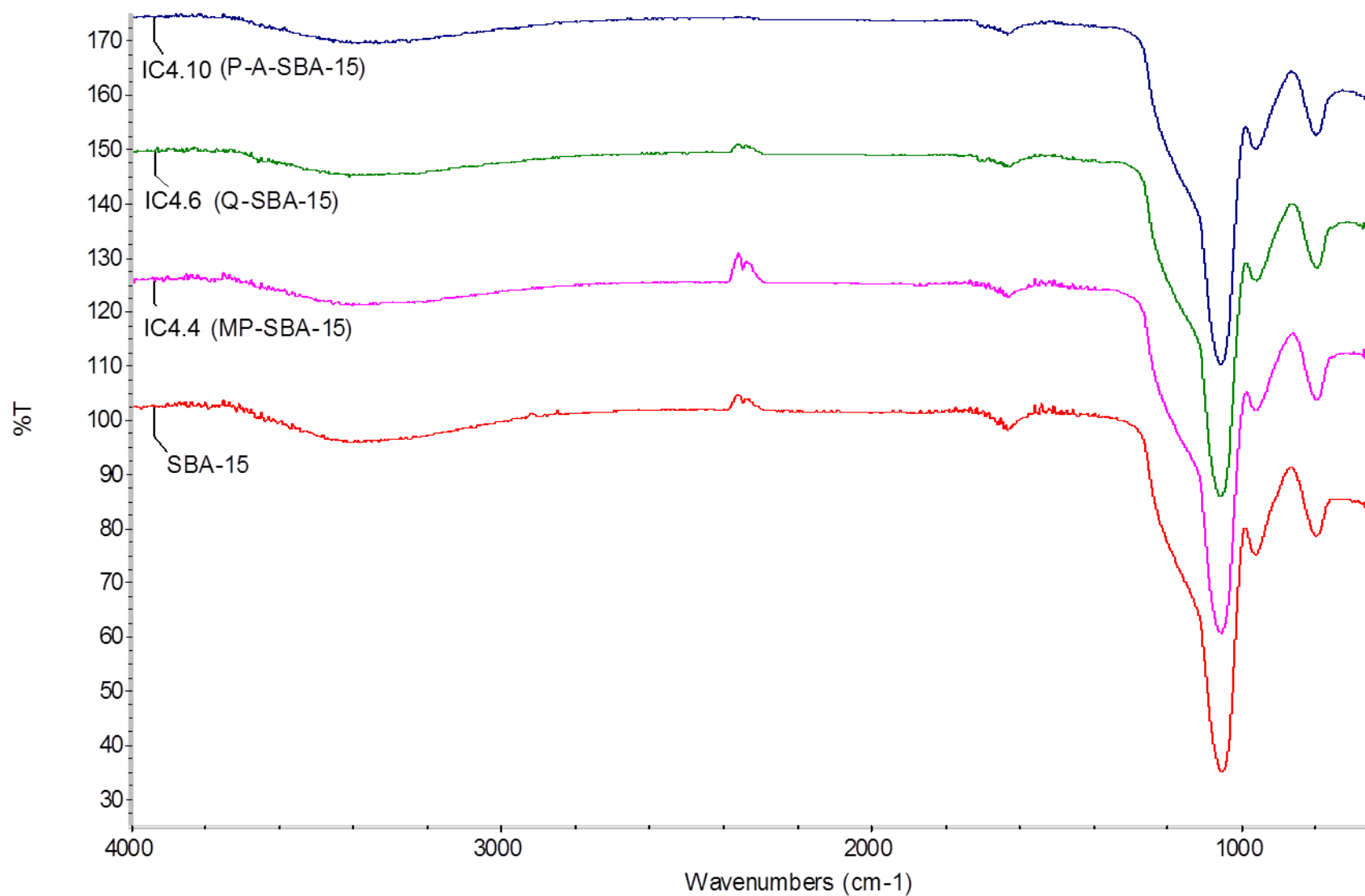
Figure 4.28 FT-IR spectra of SBA-15 immobilized catalysts IC4.4, IC4.6 and IC4.10.

Chapter 4: Immobilization of RuCl(arene)(N,N) Complexes on MCM-41 and SBA-15

For the SBA-15 derivatives however no real difference in the obtained IRs are observed at all. Once again a slight decrease in the band at 3300 cm^{-1} corresponding to the free silanols on the surface of the support can be observed. The reason for the lack of signals corresponding to the immobilized catalyst can be attributed to the low ratio of immobilization (10 weight %) resulting in the spectra being dominated by the intense bands of the silica support.

4.2.2.5   Characterization of MCM-41 and SBA-15 immobilized catalysts IC4.1-IC4.12 using solid-state NMR spectroscopy: ^{13}C and ^{29}Si

Native supports, MCM-41 and SBA-15, as well as selected immobilized catalysts were subjected to characterization by means of solid state ^{29}Si MAS NMR and ^{13}C CP MAS NMR and spectroscopy. In Figures 4.29 and 4.30 the ^{29}Si MAS NMR spectra of MCM-41 and SBA-15 are shown (left) together with their deconvoluted counterparts (right). For both spectra mainly two peaks are observed at around -108 and -97 ppm which can be assigned to the Q^4 [(SiO)$_4$Si] and Q^3 [(SiO)$_3$SiOH] framework silicas sites and silanol sites respectively [9, 24]. The negligible presence of Q^2 sites can just about be observed in the obtained spectra.
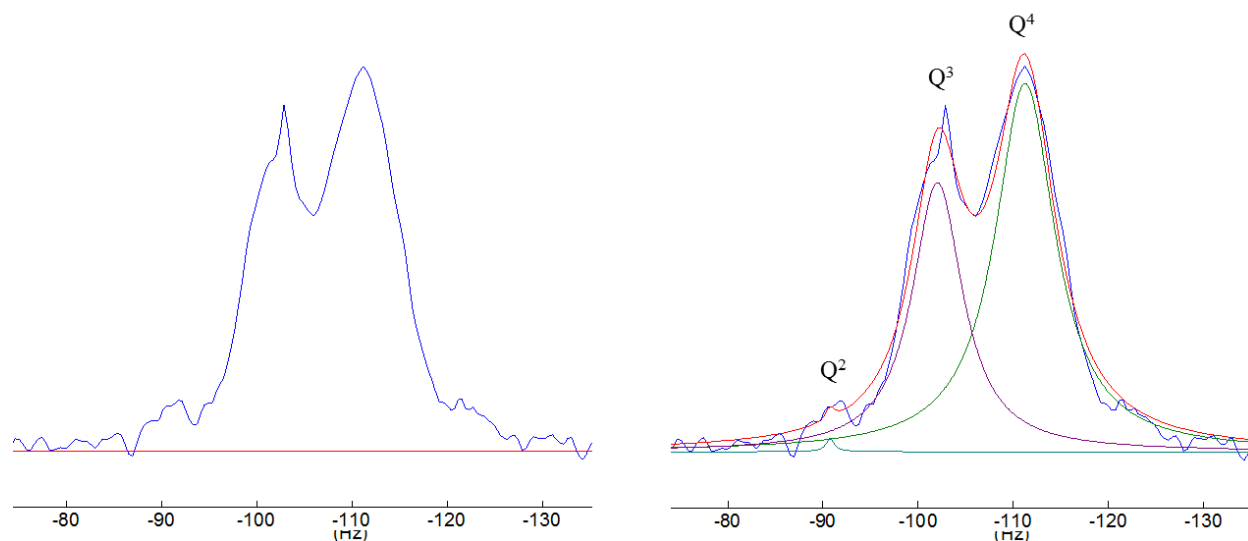
Figure 4.29   Solid-state ^{29}Si single-pulse MAS NMR spectra of MCM-41:   experimental (left) and deconvoluted spectra (right).

Chapter 4: Immobilization of RuCl(arene)(N,N) Complexes on MCM-41 and SBA-15
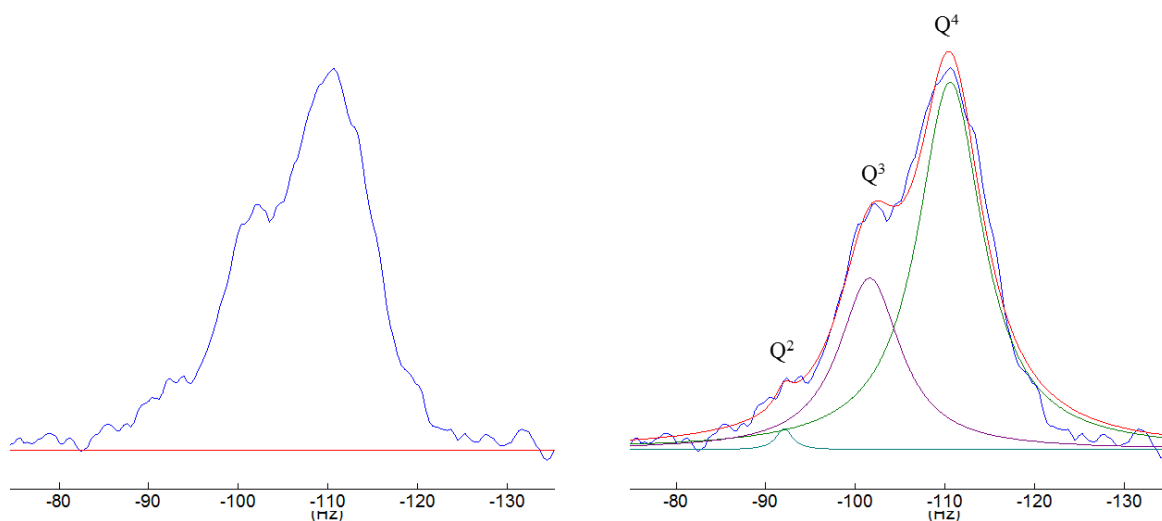
Figure 4.30 Solid-state ^{29}Si single-pulse MAS NMR spectra of SBA-15: experimental (left) and deconvoluted spectra (right).

The dominant peak for both spectra is found to be the Q^4 site. The Q^4 sites percentages compared to those of the Q^3 sites were found to be around 62 % and 38 % for MCM-41 and 69 % and 31 % for SBA-15. This means that MCM-41 has more surface silanols present on the surface when compared to SBA-15.

Selected spectra of immobilized catalysts are shown in Figures 4.31 and 4.32 below. In general a decrease in the amount of Q^3 sites is observed, as would be expected. Immobilization is expected to result in the decrease in the amount of free silanols present on the surface of the support material due to the covalent anchoring of the siloxane functionalized complexes. For three of the four analyzed samples this was observed with the only exception being SBA-15 immobilized catalyst **IC4.8**. The reason for this increase in the amount of surface silanols when compared to the native SBA-15 support material could be as a result of physical changes to the support material during the immobilization process. An increase in the pore diameter was observed throughout for the SBA-15 immobilized catalysts with the largest change being observed for immobilized catalyst **IC4.8**.
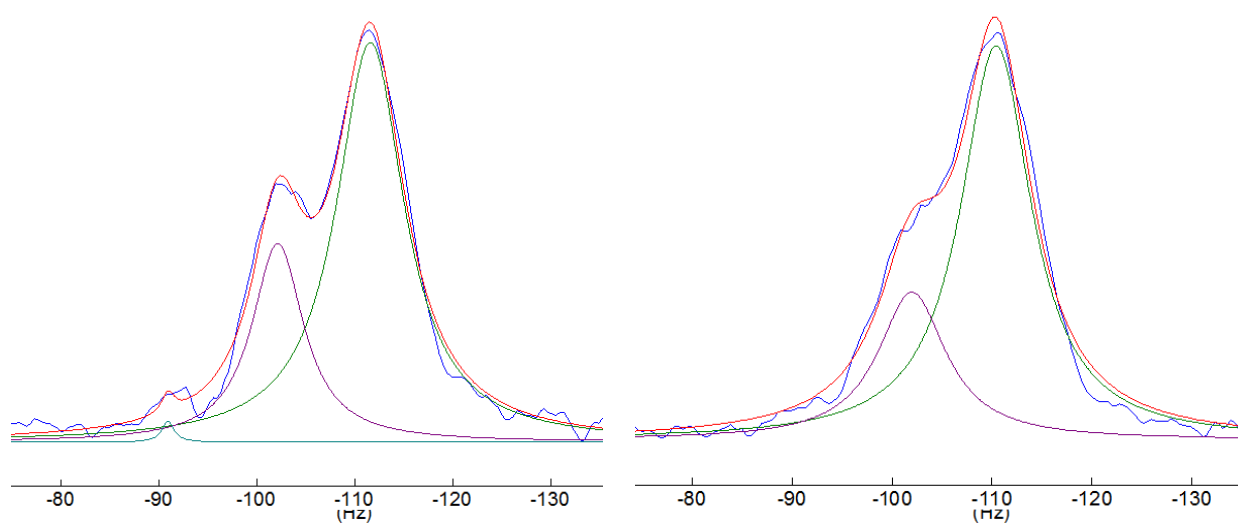
Figure 4.31   Solid-state ^{29}Si single-pulse MAS NMR spectra of MCM-41 and SBA-15 immobilized catalysts IC4.1 (left) and IC4.6 (right).
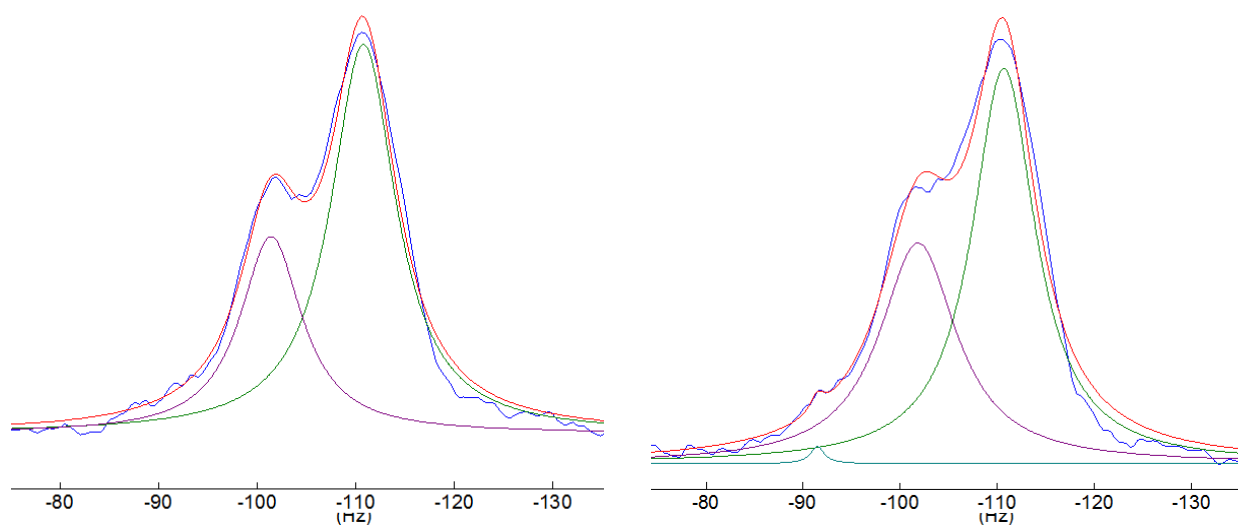
Figure 4.32   Solid-state ^{29}Si single-pulse MAS NMR spectra of MCM-41 and SBA-15 immobilized catalysts IC4.7 (left) and IC4.8 (right).

As mentioned above, this can probably be ascribed to a physical change in the support itself during the immobilization process and can be as a result of the elevated temperatures employed

Chapter 4: Immobilization of RuCl(arene)(N,N) Complexes on MCM-41 and SBA-15

during the preparation and/or mechanical agitation as a result of the stirring process. Some sintering was observed when comparing SEM micrographs of the immobilized catalysts to those of the native supports and this was found to be more prevalent for the SBA-15 immobilized catalysts. A summary of the change in the Q^4 and Q^3 sites in the supported catalysts is shown in Table 4.5 below.

Table 4.5   Summary of the obtained Q^4, Q^3 and Q^2 sites in the native and immobilized MCM-41 and SBA-15 catalysts.

Material	Silica Framework		
	Q^4	Q^3	Q^2
MCM-41	61.72	37.95	0.33
IC4.1 (P-MCM-41)	72.06	27.25	0.69
IC4.7 (P-P-MCM-41)	67.47	32.53	0
SBA-15	68.62	30.38	1
IC4.6 (Q-SBA-15)	73.50	26.50	0
IC4.8 (P-P-SBA-15)	59.29	40.20	0.51

Solid state ^{13}C CP MAS NMR confirmed the presence of the complexes on the surface of the support material. Spectra of MCM-41 and SBA-15 immobilized catalysts **IC4.1**, **IC4.6**, **IC4.7** and **IC4.8** are shown in Figure 4.33. In the solution ^{13}C NMR spectra, the ethyl of the siloxane functionality is observed as very intense resonances at 18 and 58 ppm for all of the functionalized complexes. In the solid state NMR spectra no real intense resonances are observed at 18 and 58 ppm. A weak resonance at around 62 ppm is the closest resonance that can possibly be attributed to the siloxane methylene carbon. For a palladium complex with a similar tether to that of the immobilized catalysts **IC4.1**-**IC4.6**, two distinct resonances could be observed at 20 and 59 ppm corresponding to the methyl and methylene carbons of the siloxane functionality.
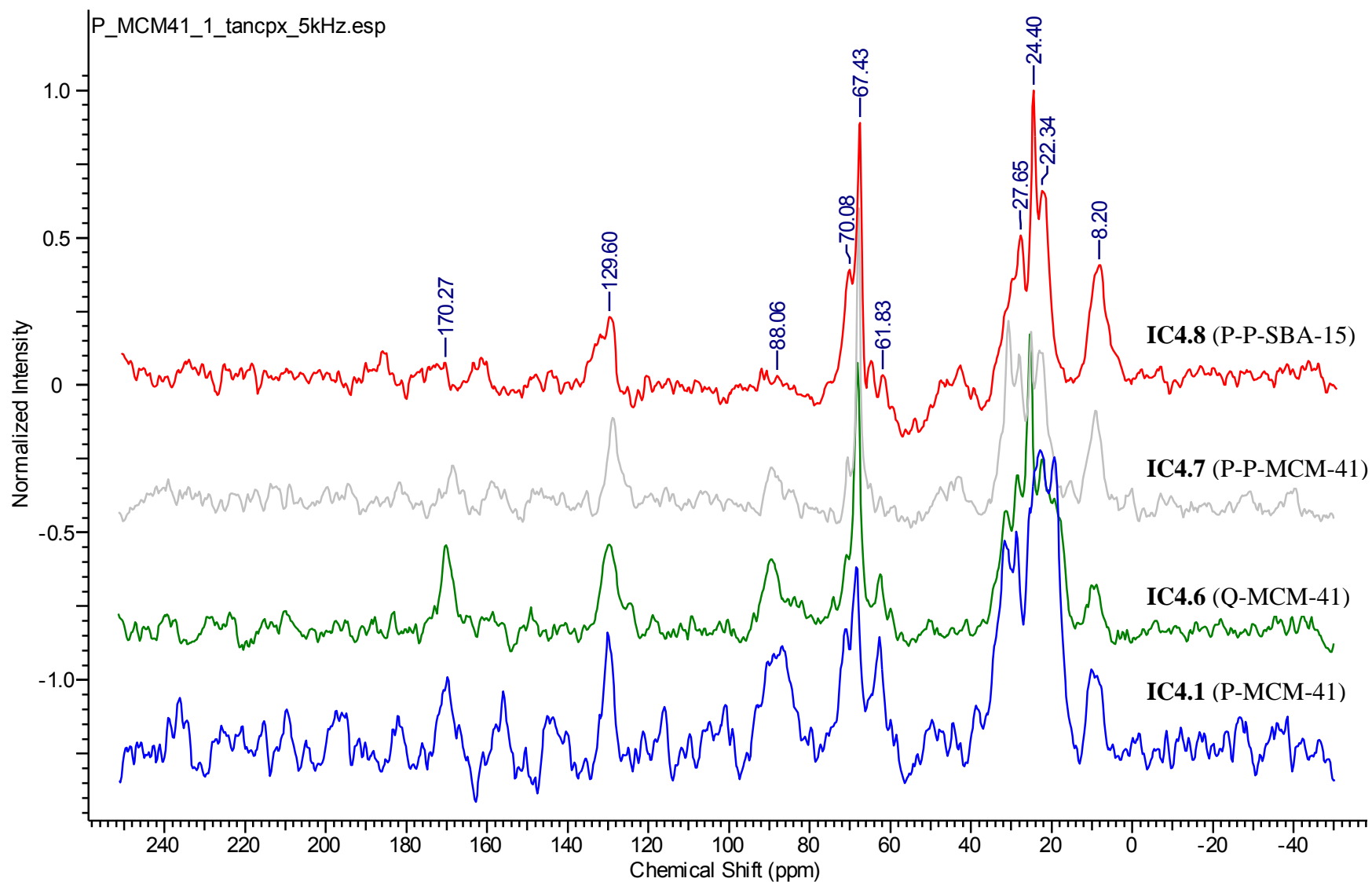
Figure 4.33 Solid state ^{13}C CP MAS-NMR of selected MCM-41 and SBA-15 immobilized catalyst.

The absence of these signals in the spectra of our catalysts confirmed the condensation of the ethoxy functionality of the complexes with the surface silanols resulting in the covalent anchoring of the complexes on the support. Intense resonances are observed in the aliphatic region of the spectra at around 25 and 70 ppm. These can be assigned to the methylene carbons of the propyl tether that connects the complex to the support.

4.2.2.6   Characterization of immobilized catalysts IC4.1-IC4.12 using TGA

TGA plots for immobilized catalysts **IC4.1**-**IC4.12** are summarized in Figures 4.34 to 4.37. An initial weight loss is observed just below 100 °C for all of the immobilized catalysts as well as the native supports. Silica material is known to absorb water very easily and this loss was attributed to the loss absorbed atmospheric moisture.

A gradual weight loss between 100-340 °C is observed for all the immobilized catalysts **IC4.1**-**IC4.12**. A steeper loss is observed at higher temperatures for all of the immobilized catalysts with the exception of the SBA-15 immobilized catalysts **IC4.8**, **IC4.10** and **IC4.12**. For these catalysts a gradual decrease is observed from 100-600 °C. The weight loss over this temperature range is attributed to the decomposition of the organic framework of the immobilized complexes.

For the MCM-41 and SBA-15 immobilized catalysts, **IC4.1**-**IC4.6** with the tether via the imine nitrogen, a consistent weight loss of between 7.7-10.7 weight % is observed. For immobilized catalysts **IC4.7**-**IC4.12** with the tether attached to the arene ring a weight loss of between 7.0-9.4 weight % was observed. After the subtraction of the weight % lost by the native support materials (2-3 weight %) this equates to around 5.0-8.0 weight % loss for the MCM-41 immobilized catalysts compared to a 6.0-7.2 weight % loss for the SBA-15 immobilized catalysts. The target weight % of the complexes should theoretically be around 10 weight % as determined by the immobilization of the functionalized complexes relative to the support materials. It is however expected that the metal oxide would remain on the silica support after thermal decomposition of the complex and could explain the lower than expected weight loss.

Figure 4.34 TGA analysis of MCM-41 immobilized catalysts IC4.1, IC4.3 and IC4.5.
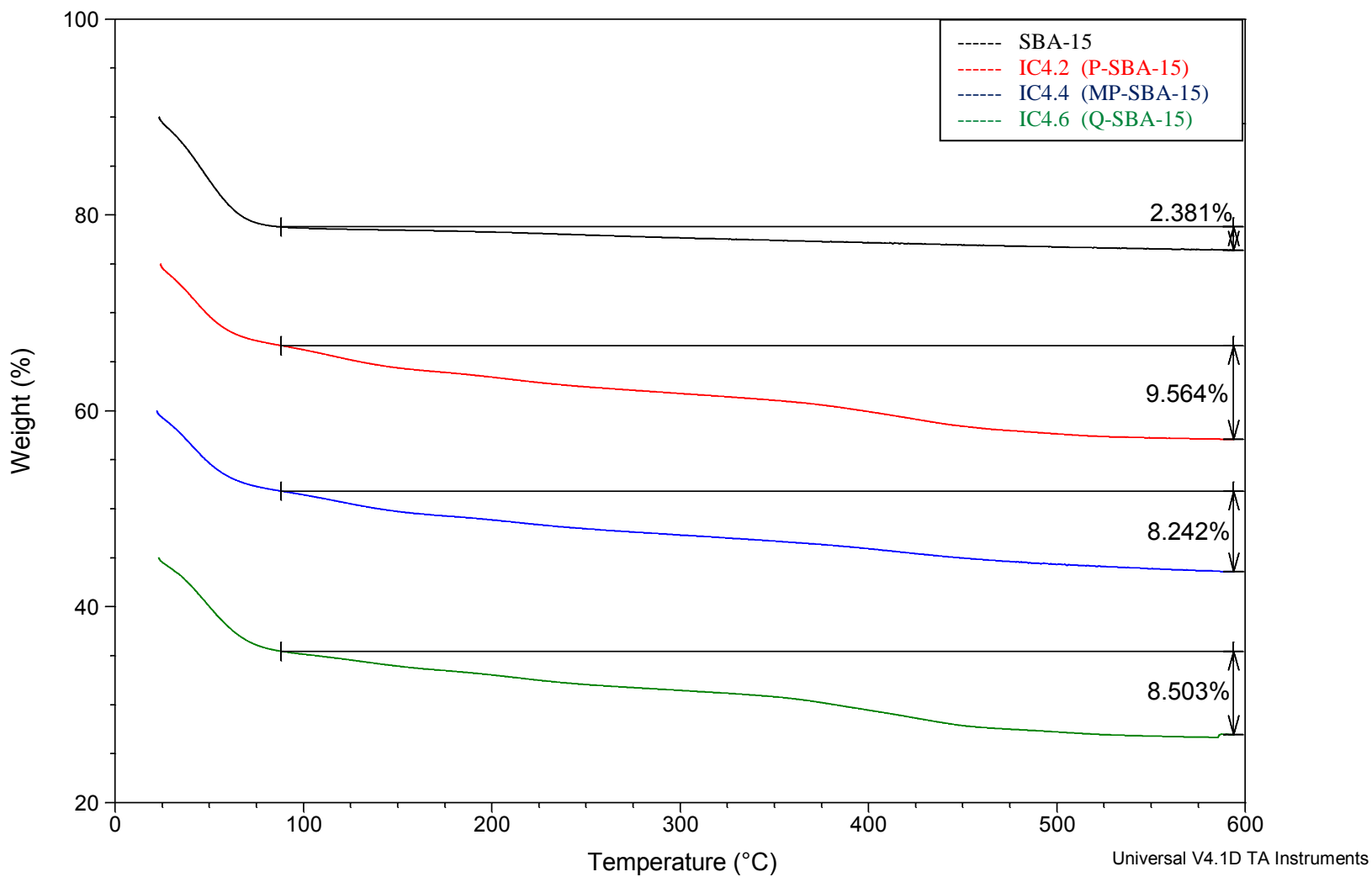
Figure 4.35 TGA analysis of SBA-15 immobilized catalysts IC4.2, IC4.4 and IC4.6.
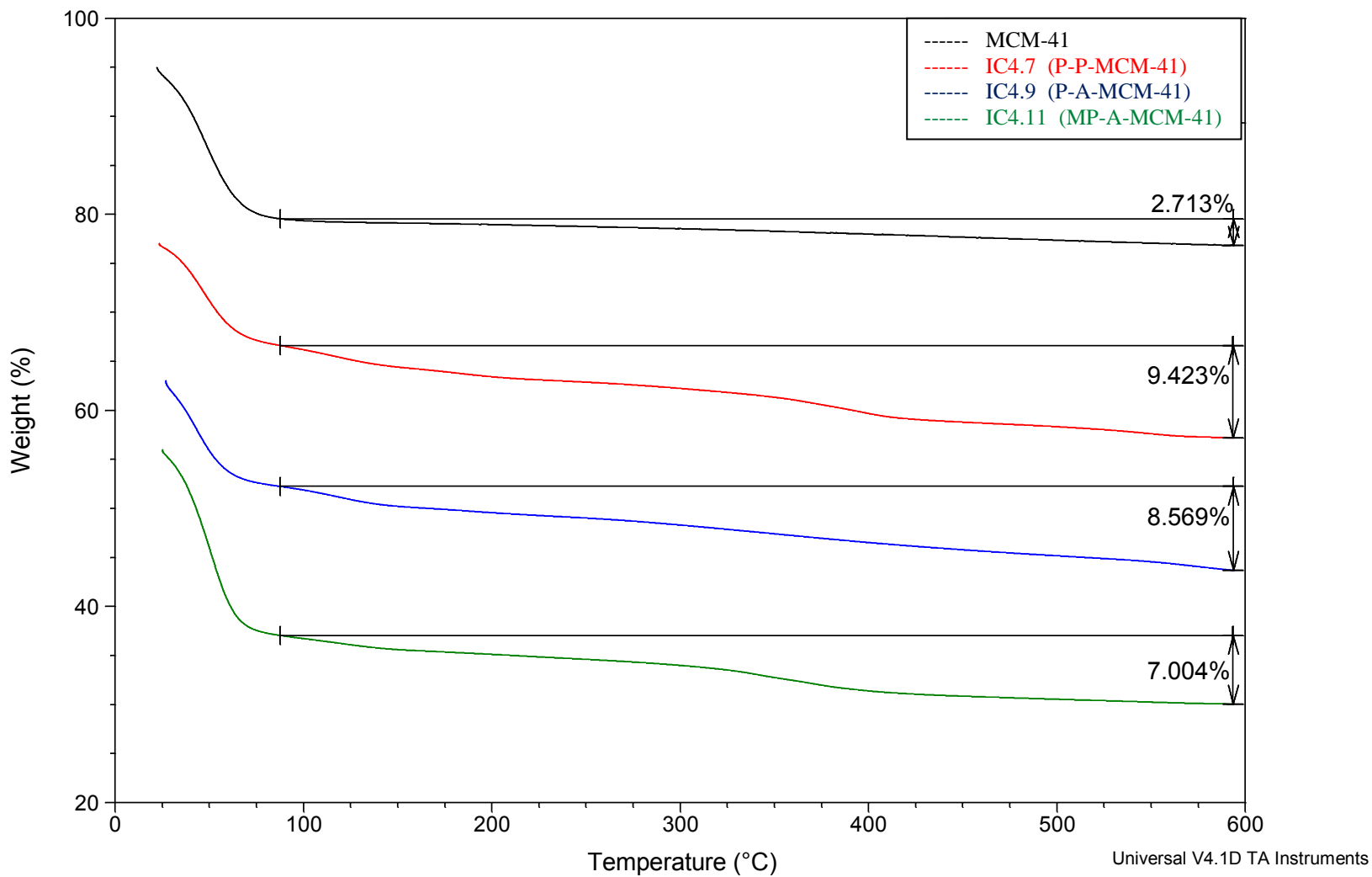
Figure 4.36 TGA analysis of MCM-41 immobilized catalysts IC4.7, IC4.9 and IC4.11.
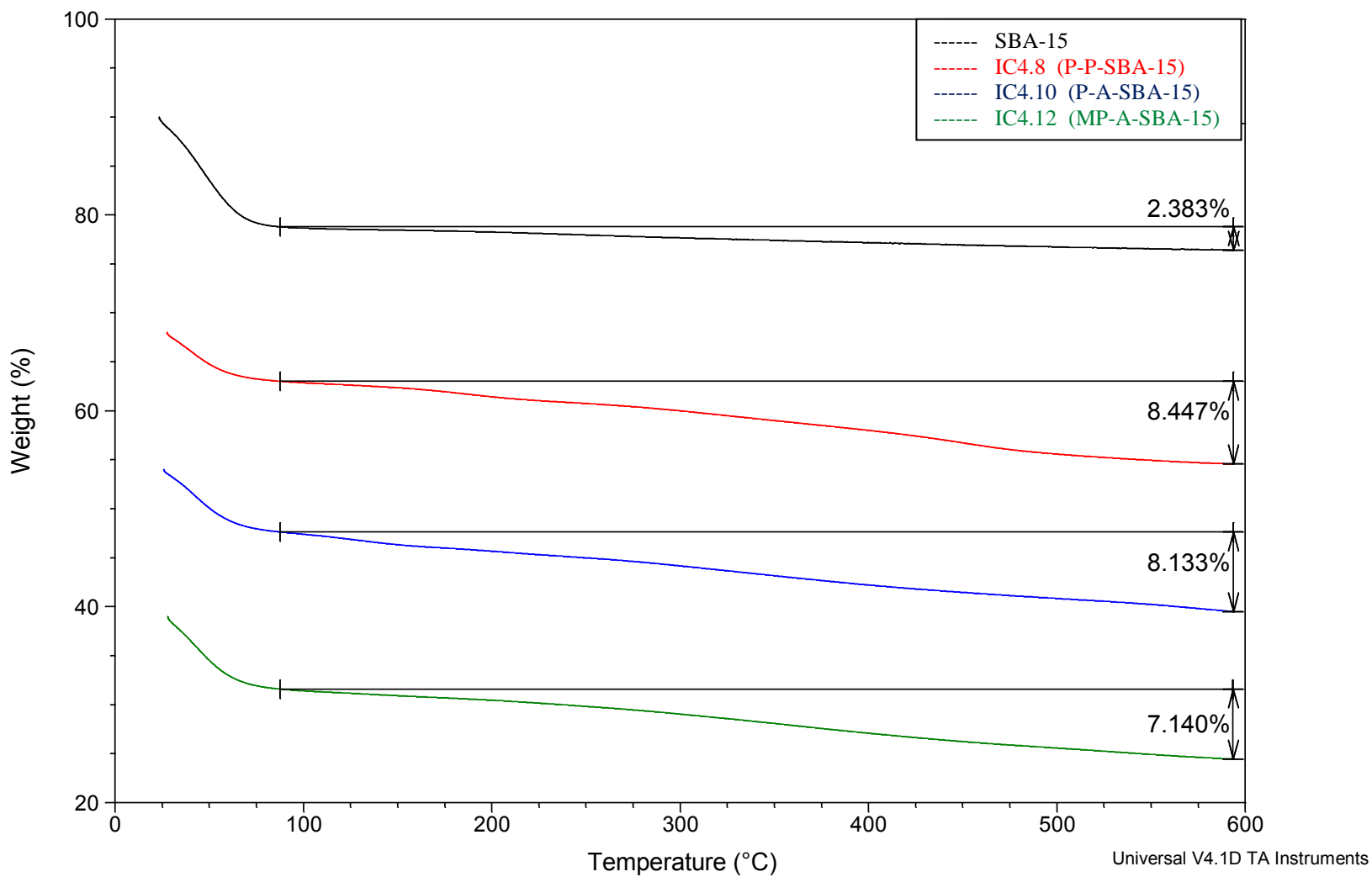
Figure 4.37 TGA analysis of SBA-15 immobilized catalysts IC4.8, IC4.10 and IC4.12.

4.3 Concluding remarks

Six siloxane functionalized complexes were successfully immobilized onto solid mesoporous silicas MCM-41 and SBA-15 to afford twelve immobilized catalysts **IC4.1**-**IC4.12**. These heterogenized catalysts were characterized using a wide range of solid state analytical techniques to not only verify successful immobilization but also to determine the extent of immobilization.

Although solubility issues were encountered during the immobilization of the siloxane functionalized complexes, substitution of toluene as a solvent with a mixture of toluene and THF allowed for the successful and efficient immobilization onto the mesoporous silica supports. The immobilization was confirmed mainly by monitoring the change in surface area (BET analysis) and determining the metal content on the support using ICP. ICP-OES proved a useful technique to quantify the amount of ruthenium present on the support material and allowed for direct correlation between the model and immobilized catalysts during catalysis. Powder XRD confirmed that the structural integrity and high degree crystallinity of the support material was maintained before and after immobilization of the functionalized complexes.

The novel approach used to synthesize immobilized catalysts **IC4.7**-**IC4.12** involved the tethering of the catalysts through the arene ring, instead of it being attached through the imine nitrogen as was the case for immobilized catalysts **IC4.1**-**IC4.6**.

4.4 Experimental section

4.4.1 General remarks and instrumentation

All reactions were carried out under nitrogen making use of standard Schlenk techniques. Highly air-sensitive materials were stored in a nitrogen purged glovebox and all manipulations with these materials were carried out in the glovebox to prevent decomposition or oxidation. The synthetic procedures used for the synthesis of MCM-41 and SBA-15 supports were adapted from work previously reported by Cai and Zhao [8,9].

Fourier transfer infrared (FT-IR) spectra were recorded using an ATR accessory on a Nicolet Avatar 330 FT-IR spectrometer. NMR spectra were recorded on Varian Unity Inova instruments at 300, 400 or 600 MHz for ^{1}H and 75, 100 and 150 MHz for ^{13}C. Powder XRD analysis was done on an X'Pert Pro Multi Purpose Diffractometer with a Reflection Transmission Spinner. Nitrogen adsorption/desorption analysis was done on an ASAP 2010 (Accelarated Surface Area end Porosimetry System) instrument (77 K). The samples were degassed at 273 K overnight before carrying out the measurement. A Zeiss Auriga Field Emission Gun high resolution SEM was operated at 5kV to obtain secondary electron images and 20kV to obtain EDS spectra. The images were collected with an in-lens secondary electron detector, whereas the EDS spectra were collected with an Oxford X Max solid state silicon drift detector. TEM images were obtained using a FEI Tecnai F20 field emission gun high resolution TEM operated at 200kV in bright field mode. The images were collected on a Gatan Ultrascan 2000 CCD camera. Detection of Ru emissions at 240.272 nm was performed using a SPECTRO Arcos ICP-OES spectrometer operating with a RF power set to 1600 W using Burgener T2002 nebulizer and cyclonic spray chamber. The samples were transferred directly from the column to the nebulizer by PEEK tubing with internal diameter of 0.12 mm. The nebulizer flow rate was set at 0.6 mL/min, auxiliary gas flow rate was set to 2 L/min and coolant flow rate to 16 L/min. The ruthenium standard curves were constructed using NIST Standard Reference Material standards (Inorganic Ventures, USA). The samples were prepared by digesting between 35-40 mg of the immobilized catalysts in concentrated nitric acid (1 mL) while being heated. The samples were filtered to remove any remaining solids and made up to a total volume of 25 mL.

4.4.2 Materials

Reagents were purchased from Sigma-Aldrich and Merck and used as received; these include Cetyltrimethylammonium bromide (CTAB), tetraethyl orthosilicate (TEOS) and Poly(ethylene)-*block*-poly(propylene)-*block*-poly(ethylene). Solvents were purchased from Sigma-Aldrich and Kimix Chemicals and were dried by refluxing over the appropriate drying agents. Tetrahydrofurane (THF) and toluene were dried in Pure Solv™ Micro solvent purification systems fitted with activated alumina columns.

4.4.3 Synthesis of solid mesoporous silica supports, MCM-41 and SBA-15

4.4.3.1 Synthesis of MCM-41

Cetyltrimethylammonium bromide (2.402 g) was dissolved in distilled water (120 mL). Once the surfactant was totally dissolved (The mixture was heated slightly (30 ˚C) to obtain a homogeneous solution) an ammonia solution (8 mL, 33 %) and TEOS (10 mL) were added. A white precipitate soon formed and the solution was allowed to stir at room temperature for 1 hour. The white solid was recovered by suction filtration and was washed with distilled water (400 mL). After being dried on the Buchner funnel for 10 minutes, the silica was further dried under vacuum at 70 ˚C for 2 hours. The white solid obtained was calcined at 560 °C (temperature slowly increased). The calcination process was kept running for 5 hours after reaching the required temperature.

Yield: 3.248 g

4.4.3.2 Synthesis of SBA-15

Poly(ethylene)-*block*-poly(propylene)-*block*-poly(ethylene) (8.032 g) was dissolved in a HCl solution (360 mL, 2 M solution) while being stirred at 35 °C. TEOS (18.2 mL) was added to this stirred solution (after everything dissolved) and was stirred at 35 °C for 20 hours. The temperature of the mixture was then increased to 80 °C and the mixture "aged" for a further 24 hours without being stirred. A solid product formed and it was filtered off and washed with

distilled water (1000 mL) and dried at room temperature overnight. The obtained white powder was dried at 70 °C for 2 hours under vacuum followed by calcination at 550 °C for 5 hours.

Yield: 11.455 g

4.4.4   Synthesis of immobilized catalysts IC1-IC12

The initial approach to reflux the functionalized siloxane complexes together with the appropriate silica support for 24 h in toluene was unsuccessful. Solubility of the complexes seemed to be an issue because after the allotted time some dark brown non-silica particles were still observed in the reaction mixture. A new approach was developed which involved the complexes (10 weight %; 0.100 g per 1 g of silica) firstly being dissolved in 2-3 mL THF and the solution then added to a stirring slurry of the appropriate silica in toluene (7-8 mL). Care was taken to ensure that the silica particles were uniformly dispersed in the toluene before adding the complex in THF. This mixture was then carefully refluxed at 110 ˚C for 24 hours to allow for the immobilization of the complexes. After the allotted time the reaction was left to cool to room temperature and the solid filtered off. The obtained off-white solids were repeatedly washed with small amounts of THF to remove any unreacted complex. After allowing the solids to dry at room temperature it was further dried under vacuum at 40 °C and stored in the glovebox until further use.

4.5 References

1.   J. Y. Ying, C. P. Mehnert, M. S. Wong, *Angew. Chem. Int. Ed.*, **1999**, 38, 56.

2.   L. Sierra, J-L. Guth, *Micropor. Mesopor. Mater.*, **1999**, 27, 243.

3.   L. Sierra, B. Lopez, A. Ramírez, *Stud. Surf. Sci. Catal.*, **2001**, 135.

4.   M. Mesa, L. Sierra, B. Lopez, A. Ramirez, J-L. Guth, *Solid State Sci.*, **2003**, 5, 1303.

5.   J. Font, P. de March, F. Busqué, E. Casas, M. Benitez, L. Teruel, H. García, *J. Mater. Chem.*, **2007**, 17, 2336.

6.   A. Tuel, *Micropor. Mesopor. Mater.*, **1999**, 27, 151.

7.   Y. Wan, F. Zhang, Y. Lu, H. Li, *J. Mol. Catal. A: Chem.*, **2007**, 267, 165.

8.   Q. Chai, W.Y. Lin, F. Xiao, W. Pang, B. Zhou, X. Chen, *Micropor. Mesopor. Mater.*, **1999**, 32.

9.   D. Zhao, Q. Huo, J. Feng, F.G. Chmelka, D. Stucky, *J. Am. Chem. Soc.*, **1998**, 120, 6024.

10.   S. Jin, G. Qiu, F. Xiao, Y. Chang, C. Wan, *J. Am. Ceram. Soc.*, **2007**, 90, 957.

11.   A. de Sousa, K.C. de Souza, P.M. da Silva Leite, R.G. de Sousa, E.M.B. de Sousa, *J. Nanomat.*, **2014**, 1.

12.   V.B. Fenelonov, V.N. Romannikov, A.Yu. Derevyankin, *Micropor. Mesopor. Mater.*, 1999, 28, 57.

13.   P.L. Llewellyn, Y. Grillet, F. Schuth, H. Reichert, K.K. Unger, *Micropor. Mesopor. Mater.*, **1994**, 3, 345.

14.   F. di Renzo, D. Desplantiér, A. Galarneau, F. Fajula, *Catal. Today*, **2001**, 66, 75.

15.   E.C. de Oliveira, C.T. Pires, H.O. Pastore, *J. Braz. Chem. Soc.*, **2006**,17, 16.

16.   A. de Sousa, K.C. de Souza, P.M. da Silva Leite, R.G. de Sousa, E.M.B. de Sousa, *J. Nanomat.*, **2014**, 1.

17.   L-X. Xu, C-H. He, M-Q. Zhu, K-J. Wu, Y-L. Lai, *Catal. Lett.*, **2007**, 118, 248.

18.   J.S. Beck, J.C. Vartuli, W.J. Roth, M. Leonowicz, E. Kresge, C.T. Schmitt, K.D.C. Chu, T-W. D. Olson, H.E. Sheppard, W. McCullen,; S.B. Higgins, J.B. Schlenkert, *J. Am. Chem. Soc.*, **1992**, 114, 10834.

19.   H. Zhang, J. Sun, D. Ma, X. Bao, A. Klein-Hoffmann, G. Weinberg, D. Su, R. Schlgl, *J. Am. Chem. Soc.*, **2004**, 126, 7440.

20.   Q. Huo, D.I. Margolese, G.D. Stucky, *Chem. Mater.*, **1996**, 8, 1147.

22.   J.P. Thielemann, F. Girgsdies, R. Schlög, C.H. Beilstein *J. Nanotechnol.*, **2011**, 2, 110.

23.   E.B. Celer, M. Kruk, Y. Zuzek, M. Jaroniec, *J. Mater. Chem.*, **2006**, 16, 2824.

24.   D. Pérez-Quintanilla, I. del Hierro, M. Fajardo, I. Sierra, *J. Hazard. Mater.*, **2006**, 134, 245.

Chapter 5: Oxidative Cleavage of Selected Alkenes

5.1   Introduction

The oxidative cleavage of alkenes is a very important reaction in synthetic organic chemistry and has been widely investigated. By varying the reaction conditions it is possible to form aldehydes or ketones as well as carboxylic acids. This process is usually performed using stoichiometric amounts of ozone which is an expensive oxidant and has several hazards associated with its use [1,2]. From as early as 1953 it has been known that ruthenium compounds can be utilized as an oxidant in the form of ruthenium tetroxide. Since then numerous reports have shown that ruthenium compounds can successfully cleave or oxidize alkenes to form diols, aldehydes or carboxylic acids [3-6].

Sharpless *et al.* described the use of $RuCl_3 \cdot xH_2O$ and $NaIO_4$ with a solvent system consisting of $H_2O/MeCN/CCl_4$ in a ratio 3:2:2. This system was successfully applied in the oxidative cleavage of alkenes as well as the oxidation of alcohols, ethers, and aromatic rings. They underlined the importance of the addition of acetonitrile and CCl_4 to the system, although CCl_4 is not a very environmentally friendly solvent. The importance of these solvents was emphasized when it was observed that in their absence little to no activity could be detected [5]. An explanation for this in the context of our results will be discussed in more detail in the sections to follow.

Wolfe *et al.* reported the cleavage of cyclohexene to adipic acid by reacting cyclohexene in CH_2Cl_2 with an aqueous solution of $RuCl_3 \cdot xH_2O$ and NaOCl as oxidant [7]. In a system similar to that of Sharpless *et al.*, Carlesen *et al.* reported on the conversion of cyclopentene to glutaric acid using a biphasic solvent system of $CCl_4/CH_3CN/H_2O$ with $NaIO_4$ as the oxidant [8].

More recently Shoair *et al.* has shown that $Ru(bipyridine)_2Cl_2 \cdot 2H_2O$ can successfully be employed as a catalyst precursor for the oxidative cleavage of numerous alkenes to their respective acids in high yields. They reported an increased activity when using $IO(OH)_5$ as oxidant compared to previous systems employing $RuCl_3 \cdot xH_2O$ with either NaOCl or $NaIO_4$ as oxidant. They attributed the lower activity when using $NaIO_4$ and NaOCl as oxidants to the formation of poorly soluble $NaIO_3$ and NaCl during the reaction [9]. Other oxidizing agents,

Chapter 5: Oxidative Cleavage of Selected Alkenes

such as hydrogen peroxide and oxygen, have also been applied as oxidants for alkene cleavage reactions but to a much lesser extent.

The commonly proposed active species for these transformations is RuO_4, which in most cases is formed *in situ* during the reaction rather than being prepared beforehand. These cleavage reactions however usually occur at very fast rates and generally result in the formation of carboxylic acids as the major products.

To the best of our knowledge there are no examples of the application of Ru(arene)(N,N) type complexes as catalysts in the oxidative cleavage of alkenes. It was therefore decided to explore this class of compounds as catalyst precursors for this reaction. A range of novel Ru(arene)(N,N) systems, both model and immobilized were synthesized and applied in the oxidative cleavage of alkenes. Work reported by Shoair *et al.* where they found that the incorporation of the nitrogen coordinating bipyridine ligand resulted in a tenfold lower catalyst loading being required, was the main driving force behind this investigation. As stated earlier however, Shoair *et al.* found that their system gave carboxylic acids as the major products and this therefore prompted us to investigate alternative systems that could potentially offer better selectivity towards the formation of aldehydes rather than over-oxidation products. The focus of the investigation was on the effect that the incorporation of different Schiff base ligands would have on the system. In the case of the immobilized systems, the role of the catalyst support was also investigated in detail.

5.2   General procedure for oxidative cleavage of alkenes

With the above mentioned objectives in mind, some test reactions were carried out to ascertain how our range of catalyst precursors would perform in the oxidative cleavage of a model alkene, viz. 1-octene. The reaction conditions for the test reactions were adapted from work reported by Shoair *et al.* [9]. For a typical reaction the following conditions were employed: 23 ˚C, 0.01 mmol catalyst and a biphasic solvent system of CH_3CN, CCl_4 and H_2O (5 mL, 5 mL and 10 mL respectively). Periodic acid, $IO(OH)_5$ (10 mmol), was used as oxidant (Scheme 5.1). The substrate amount was taken as 2 mmol. Possible products for the oxidative cleavage of 1-octene

Chapter 5: Oxidative Cleavage of Selected Alkenes

are heptaldehyde and heptanoic acid. Some unwanted side reactions are however also possible which can lead to the formation of the 1,2-epoxyoctane and 1,2-octanediol [9].
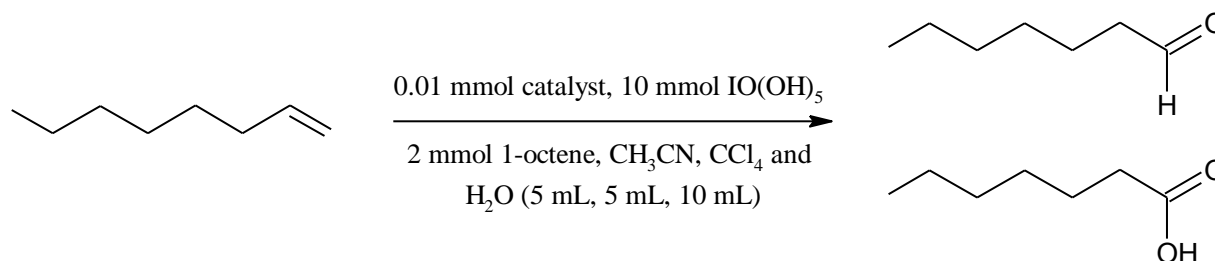
Scheme 5.1 A general procedure for the oxidative cleavage of 1-octene.

5.2.1 Model complexes C2.1-C2.3 and C3.1-C3.4 and immobilized catalysts IC4.1-IC4.12 employed as catalyst precursors for the oxidative cleavage of alkenes

Model complexes **C2.1-C2.3** and **C3.1**-**C3.4**, as well as their immobilized counterparts **IC4.1-IC4.12**, were evaluated as catalyst precursors for the oxidative cleavage of 1-octene and styrene (**C2.1**-**C2.3** and **IC4.1**-**IC4.6**). The exact metal loading of the immobilized systems were determined by ICP-OES allowing for direct comparison between the model and immobilized systems at similar metal concentrations. A summary of all the systems mentioned above is shown in Figure 5.1 and Figure 5.2.

5.2.2 Evaluation of base-line reaction conditions

1-Octene was chosen as a model substrate to optimize the reaction conditions and the results are summarized in Table 5.1. It was found that the ratio of 1:1:2 (CCl_4:CH_3CN:H_2O) was indeed the optimum ratio of solvent mixture and therefore this ratio was kept constant throughout this investigation. For the first run, Entry 1, $Ru(bipy)_2Cl_2$ was used as catalyst precursor to try and reproduce the results reported by Shoair *et al.* [9]. $Ru(bipy)_2Cl_2$ was synthesized using a procedure published by Sullivan *et al.*, which was the same reference cited by Shoair *et al.*, to access this material [10]. They reported a conversion of 1-octene to heptanoic acid of around 70 % after a mere 2 hours. However in our hands under the same reaction conditions a

Chapter 5: Oxidative Cleavage of Selected Alkenes

conversion of only 14 % could be achieved after 3 hours and this increases to around 36 % after 6 hours (Entry 2). Complete conversion of the 1-octene was only obtained after allowing the reaction to proceed for around 24 hours. This was thus far lower than the conversions reported by Shoair *et al.* A fresh batch of $Ru(bipy)_2Cl_2$ was synthesized and the catalytic reaction was repeated however no improvement in the conversion could be observed. Upon further investigation of the literature it was learnt that impurities in the solvent CCl_4 could potentially decrease the lifetime of the formed active species (RuO_4). Thus a new freshly distilled and thoroughly dried batch of CCl_4 was obtained and employed in the abovementioned catalytic reaction.

C2.1; R_1 = H

C2.2; R_1 = CH_3

C2.3; Quinoline
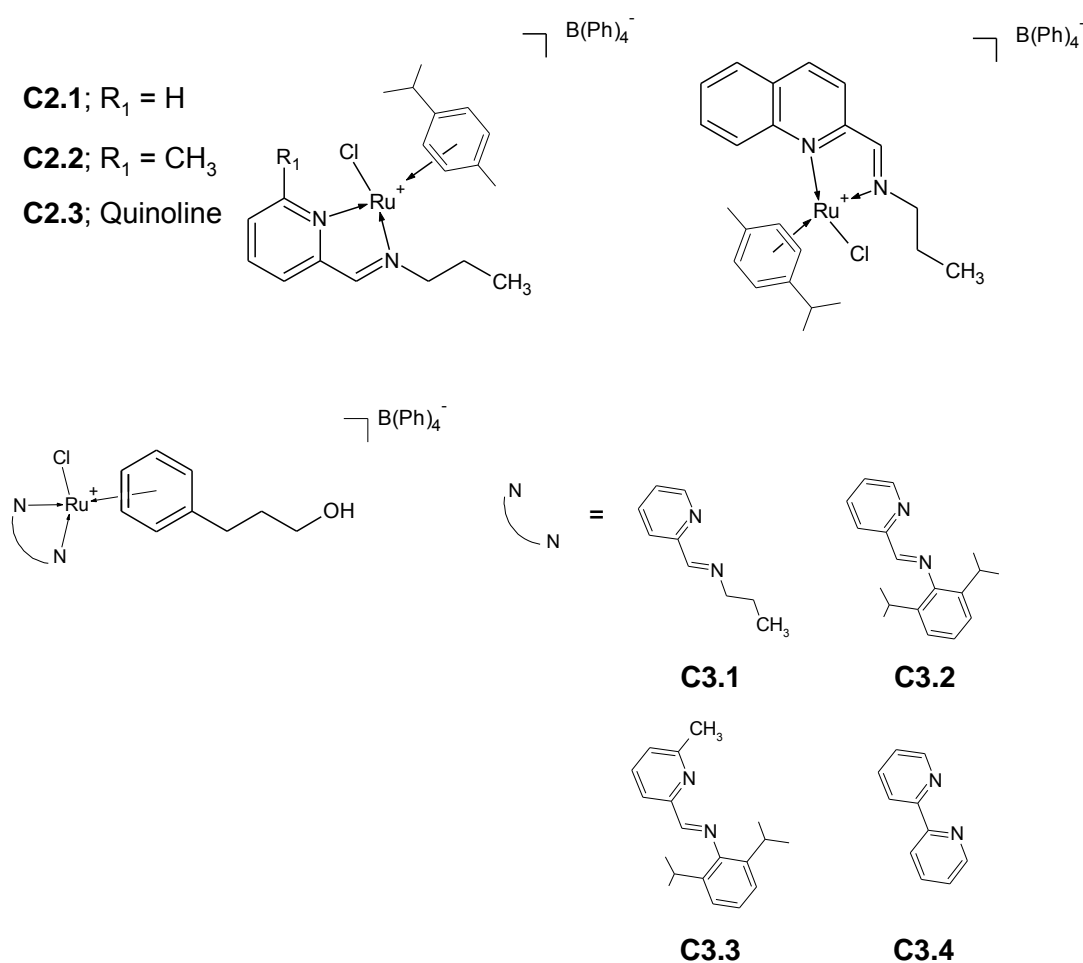
Figure 5.1 Model complexes C2.1-C2.3 and C3.1-C3.4 employed as catalyst precursors for the oxidative cleavage of alkenes.

Chapter 5: Oxidative Cleavage of Selected Alkenes
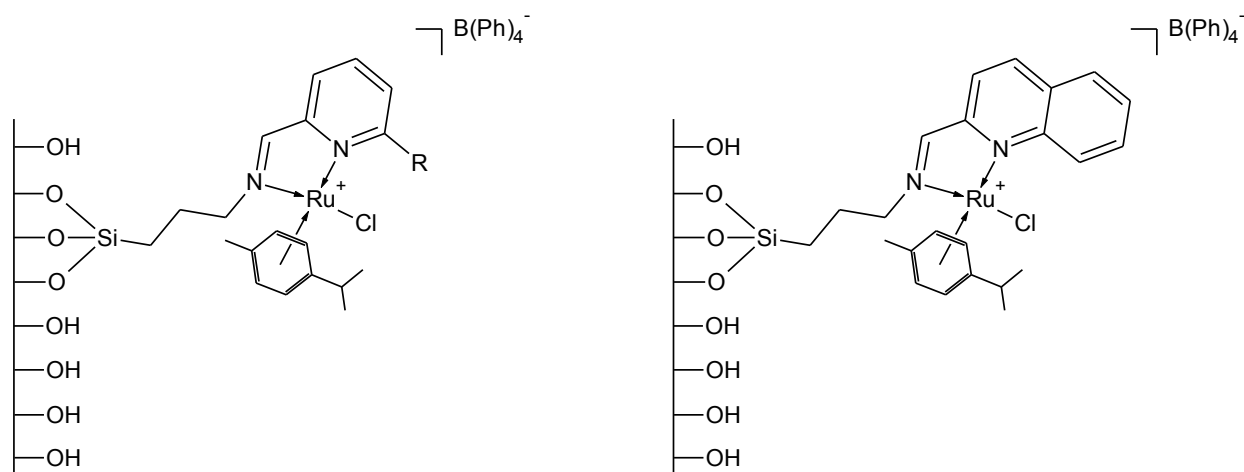
IC4.1; R= H; P-MCM-41

IC4.2; R = H; P-SBA-15

IC4.3; R = CH$_3$; MP-MCM-41

IC4.4; R = CH$_3$; MP-SBA-15

IC4.5; Q-MCM-41

IC4.6; Q-SBA-15
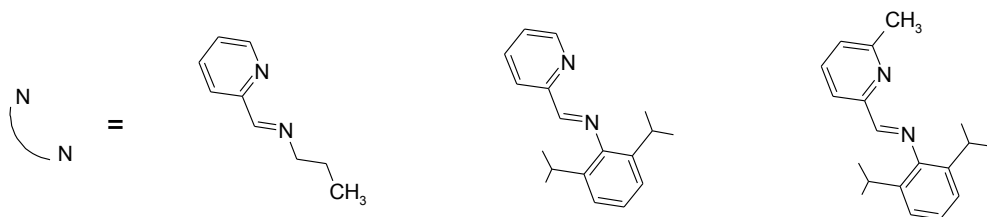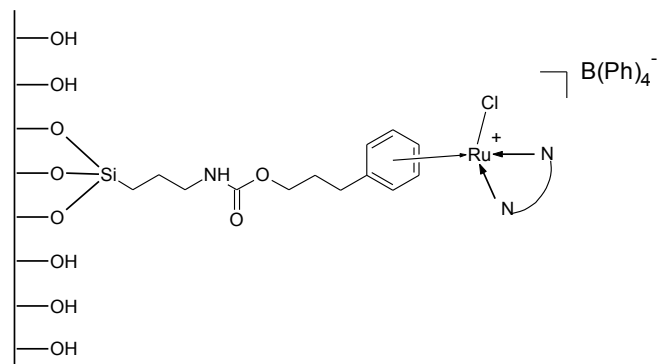
IC4.7; P-P-MCM-41   **IC4.9**; P-A-MCM-41   **IC4.11**; MP-A-MCM-41

IC4.8; P-P-SBA-15   **IC4.10**; P-A-SBA-15   **IC4.12**; MP-A-SBA-15

Figure 5.2 MCM-41 and SBA-15 immobilized catalysts IC4.1-IC4.12 employed as catalyst precursors for the oxidative cleavage of alkenes.

Chapter 5: Oxidative Cleavage of Selected Alkenes

However no significant change in the activity was observed. The effect of the stirring rate did also not influence the activity (slow vs. rapid stirring). No difference in conversion was observed when flushing the round bottomed flask with nitrogen, before adding substrate and oxidant, or carrying out the reaction under nitrogen. A further reaction was carried out under an atmosphere of oxygen (1 bar) with the other reaction conditions kept constant. After 3 hours the exact same conversion of 1-octene was achieved when compared to a reaction in the absence of oxygen. Thus in summary we could not reproduce the results reported by Shoair *et al*.

Table 5.1 Base-line reactions for the oxidative cleavage of 1-octene.[a]

Entry	Complex	Substrate: 1-Octene (mmol)	Oxidant: $IO(OH)_5$ (mmol)	Time (h)	Conversion (%)[c]
1	$Ru(bipy)_2Cl_2$	2	10	3	14
2		2	10	6	36[b]
3	C2.2	2	10	3	28
4		2	10	6	73
5		2	10	12	100
6		2	5	12	63
7		4	10	12	99
8	C2.1	2	10	12	94
9		4	10	12	99

[a] Reaction conditions: 23 °C, 0.01 mmol catalyst, CH_3CN, CCl_4 and H_2O (5 mL, 5 mL and 10 mL respectively); [b] After 15 and 24 hours, conversions of 80 % and 100 % could respectively be achieved; [c] Conversion calculated by monitoring the consumption of 1-octene by GC

Chapter 5: Oxidative Cleavage of Selected Alkenes

It was decided to continue with the investigation using complex **C2.2** (methyl-pyridine derivative). For model complex **C2.2**, a significant increase (Entry 3) in the conversion from 14 % to 28 % was observed after 3 hours when compared to Ru(bipy)$_2$Cl$_2$ (Entry 1). Complete conversion of 1-octene could be achieved after 12 hours compared to the 24 hours required for Ru(bipy)$_2$Cl$_2$ (Entry 5). Decreasing the oxidant amount (Entry 6) to 5 mmol from 10 mmol resulted in a decrease in the conversion from 100 % to 63 % after 12 hours. Almost complete conversion could also be obtained after 12 hours when doubling the substrate amount from 2 mmol to 4 mmol (Entry 7).

For complex **C2.1**, similar conversions, when compared to complex **C2.2**, were obtained after 12 hours when using 2 mmol and 4 mmol of 1-octene respectively (Entry 8 and 9). The reaction times required to achieve complete conversion of 1-octene using model complexes **C2.1** and **C2.2** were significantly longer than that reported by Shoair *et al.* using Ru(bipy)$_2$Cl$_2$ as catalyst. However compared to the results obtained using Ru(bipy)$_2$Cl$_2$ (in our hands), complexes **C2.1** and **C2.2** performed significantly better with complete conversion being obtained after a mere 12 hours, compared to Ru(bipy)$_2$Cl$_2$ which only achieved complete conversion after 24 hours.

In Table 5.2 the product distribution of some of the reactions reported in Table 5.1 is shown. At lower conversions, using complex **C2.2** as catalysts precursor (Entries 3 and 4), heptaldehyde is formed as the only product. As the conversion nears 100 % (Entry 5), selectivity towards heptaldehyde is 19 % compared to 100 % at lower conversions (Entry 4).

At this stage all results point to the initial formation of aldehyde followed by the oxidation of the formed aldehyde to the carboxylic acid through further oxidation. This will be discussed in more detail later in the chapter.

Table 5.2 Product distribution for the oxidative cleavage products of 1-octene using complex C2.1 and C2.2.[a]

Entry	Complex	Substrate (mmol)	Time (h)	1-Octene Conversion (%)	Selectivity (%)			
					Heptaldehyde	Heptanoic Acid	Epoxyoctane	Unidentified
1	**Ru(bipy)$_2$Cl$_2$**	2	6	36	100	0	0	-
2		2	15	80	80	7	13	-
3	**C2.2**	2	3	28	100	0	0	-
4		2	6	73	100	0	0	-
5		2	12	100	19	79	0	2
7		4	12	99	66	25	2	7
8	**C2.1**	2	12	94	87	13	0	-
9		4	12	99	86	12	2	-

[a] Reaction conditions: 23 ˚C, 0.01 mmol catalyst, 10 mmol IO(OH)$_5$, CH$_3$CN, CCl$_4$ and H$_2$O (5 mL, 5 mL and 10 mL respectively)

Chapter 5: Oxidative Cleavage of Selected Alkenes

5.2.2.1   The role of acetonitrile and carbon tetrachloride (CCl_4) during the reaction

At this stage it was decided to investigate the influence of the addition of acetonitrile and CCl_4 to the reaction mixture. It was previously reported that the addition of acetonitrile increases the activity of the catalyst but no real explanation was given as to why [11]. The influence of acetonitrile on the reaction was probed by carrying out a similar reaction in the absence of acetonitrile (Reaction conditions: 23 ˚C, 10 mmol $IO(OH)_5$, 2 mmol 1-octene, CCl_4 and H_2O (5 mL and 10 mL respectively), 9 hours.). A conversion of only 8 % could be achieved after 9 hours, compared to a conversion of more than 80 % when acetonitrile was present under the same reaction conditions.

Sharpless *et al.* suggested that this decreased activity was caused by the formation of insoluble carboxylate complexes. These carboxylate complexes form as a result of the complexation between the low-valent ruthenium species and the carboxylic acids being formed as part of the reaction. They confirmed this by synthesizing a μ_3-oxo-triruthenium carboxylate complex, $[(Ru_3O(OAc)_6(H_2O)_3^+{}^-OAc]$, and testing it as a catalyst precursor for the oxidative cleavage of 1-octene in the $CCl_4/H_2O/IO_4^-$ system. They found that this complex was inactive for the cleavage reaction. However upon the addition of acetonitrile to this inactive system, the oxidative cleavage to the carboxylic acid was observed. The presence of the acetonitrile caused the disruption of the formation of these complexes resulting in an active Ru species being returned to the catalytic cycle [5]. It has been shown that nitriles (especially acetonitrile) have the unique ability to resist oxidation while maintaining good ligating ability towards low-valent transition metals. It is thought that the low-valent ruthenium species (III/II) are stabilized by the acetonitrile during the catalytic cycle which in turn results in an increased activity [5,12].

CCl_4 has been found to be a very good solvent for the volatile RuO_4 species and thus prevent its evaporation. The solubility of RuO_2 however is what makes this process catalytic. RuO_2 is soluble in solvents like CCl_4 and CH_3CN and can be rapidly re-oxidized to RuO_4 making use of an appropriate oxidant. This is one of the main reasons why the addition of CCl_4 is so important for this type of reaction [13].

Chapter 5: Oxidative Cleavage of Selected Alkenes

5.2.3 Using model complexes C2.1-C2.3 and immobilized catalysts IC1-IC6 (siloxane tether attached to the imine nitrogen) as catalyst precursors

Timed reactions were carried out to monitor the conversion of 1-octene while also monitoring the formation of the aldehyde and carboxylic acid. The reaction conditions chosen were as follows for both the model and immobilized systems: 23 °C, 0.01 mmol catalyst, 10 mmol $IO(OH)_5$, 2 mmol 1-octene and a biphasic solvent system of CH_3CN, CCl_4 and H_2O (5 mL, 5 mL and 10 mL respectively).

The first plot represents the conversion of 1-octene using $Ru(bipy)_2Cl_2$ as catalyst precursor (Figure 5.3). As can be seen a certain amount of heptaldehyde is formed initially and reaches a maximum at around 15 hours after which it steadily decreases with a concomitant increase in the formation of heptanoic acid. A maximum of just below 60 % (15 h) of heptaldehyde is formed before it gets converted to heptanoic acid which reaches a yield of 100 % after 24 hours.

An initially unknown product was formed during the reaction but was later identified as 1,2-epoxyoctane. The formation of 1,2-epoxyoctane during this reaction was initially thought to be unusual, however upon further research it was realized that it could potentially be formed when using bipyridine as ligand and that this is consistent with what was reported by Shoair *et al.* [9]. From a literature search it was found that tuning the reaction conditions resulted in the formation of epoxides instead of the cleavage products. As stated in the introduction of this chapter, sometimes side reactions can occur concurrently with the cleavage reactions which result in the epoxide formation. Balavoine *et al.* found that by adding bipyridine as a ligand to $RuCl_3 \cdot xH_2O$ and $NaIO_4$ as oxidant in a solvent system of CH_2Cl_2/H_2O, it was possible to form epoxides of compounds that included terminal double bonds [14]. It was suggested that ligands that possess good electron donating abilities might be able to influence the formation of epoxides over the alkene cleavage reaction in the system. Bailey *et al.* later showed that a ruthenium(II) species can successfully catalyze the epoxidation reaction under the abovementioned conditions. $[RuO_2(bipy)\{IO_3(OH)_3\}]\cdot1.5H_2O$ was synthesized and found to be an even more active epoxidation catalyst when compared to the system reported by Balavoine *et al.* [15]. This explains why epoxide formation is observed for the $Ru(bipy)_2Cl_2$ system as shown in Figure 5.3. It is possible that under these reaction conditions $[RuO_2(bipy)-\{IO_3(OH)_3\}]\cdot1.5H_2O$ is formed in small amounts and that this accounts for the formation of 1,2-epoxyoctane. The hydrolysis of

1,2-epoxyoctane to 1,2-octanediol followed by the conversion to heptaldehyde and heptanoic acid can occur concurrently. The reason why no 1,2-octanediol is observed could be ascribed to the rapid rate at which the 1,2-octanediol is converted to heptaldehyde under these reaction conditions.
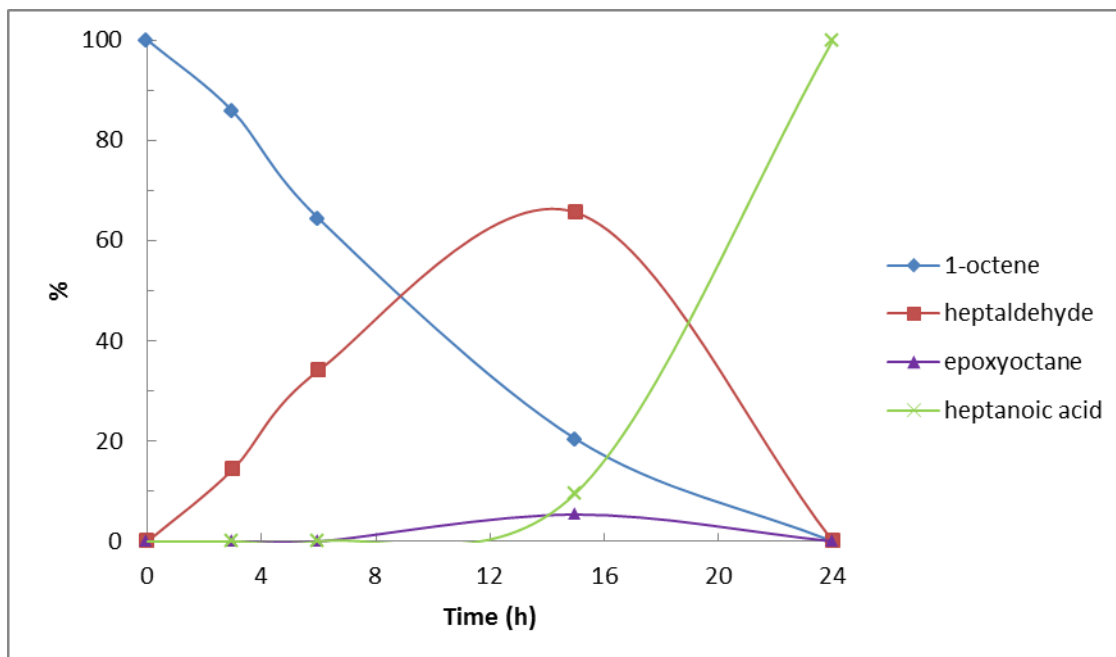
Figure 5.3 Conversion of 1-octene together with the formation of oxidation products using Ru(bipy)₂Cl₂ as catalyst.

When switching to complex **C2.2** as catalyst precursor, a dramatic increase in the rate of the reaction is observed (Figure 5.4). At 6 hours 73 % heptaldehyde is present with almost no heptanoic acid being observed. Allowing the reaction to continue for 24 hours resulted in the complete conversion of the heptaldehyde to heptanoic acid. No 1,2-epoxyoctane was however observed when using complex **C2.2** as the catalysts precursor.

It is immediately apparent that the choice of ligand has a dramatic effect on the rate, as well as the product distribution of the cleavage reaction. As mentioned above, using bipyridine as a

ligand resulted in the formation of a small amount of epoxide compared to our system employing a pyridine Schiff base diimine ligand (**C2.2**), where no epoxide formation is observed.
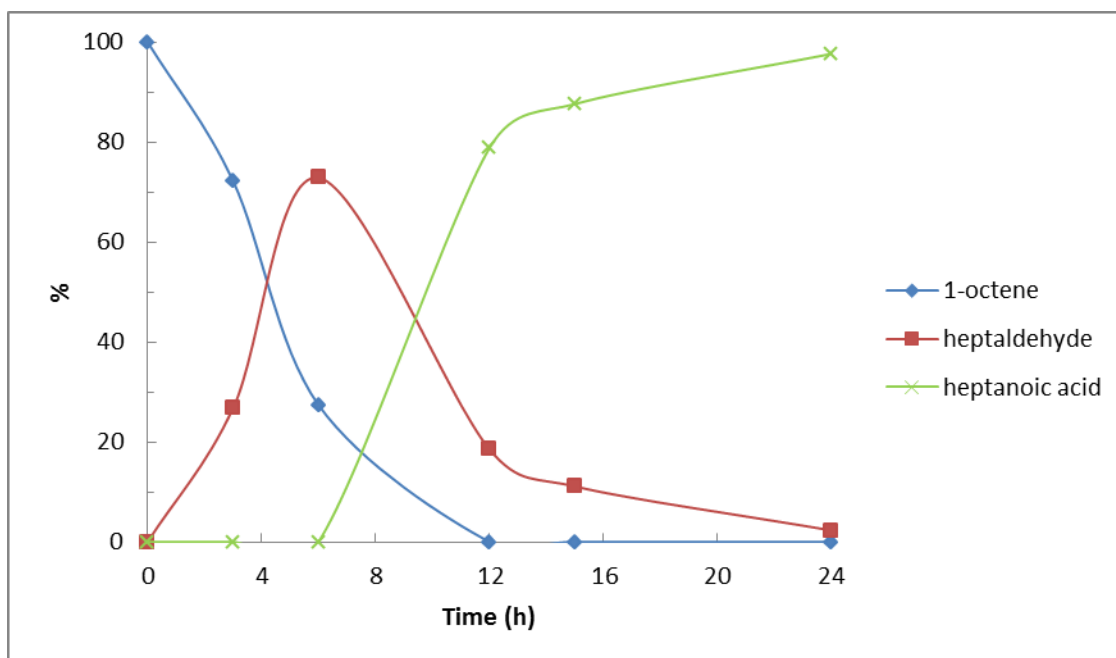
Figure 5.4 Conversion of 1-octene using complex C2.2 as catalyst precursor.

A summary of the conversions and product formation for complexes **C2.1**-**C2.3** is shown in Figure 5.5. After 3 hours, complex **C2.2** showed the lowest conversion (28 %) when compared to complexes **C2.1** and **C2.3** with the latter two showing similar conversions of around 60 %. After 6 hours however all three complexes show similar conversion with **C2.3** showing marginally higher conversion compared to the other two. At this stage (6 hours) heptaldehyde is observed as the only product with the exception being a small amount of heptanoic acid being observed for the reaction using complex **C2.3**.   For the quinoline derivative **C2.3**, almost complete conversion to heptanoic acid is observed after 12 hours. At the same time significantly lower selectivity towards heptanoic acid is observed for the pyridine and methyl-pyridine derivatives, **C2.1** and **C2.2**.

Chapter 5: Oxidative Cleavage of Selected Alkenes
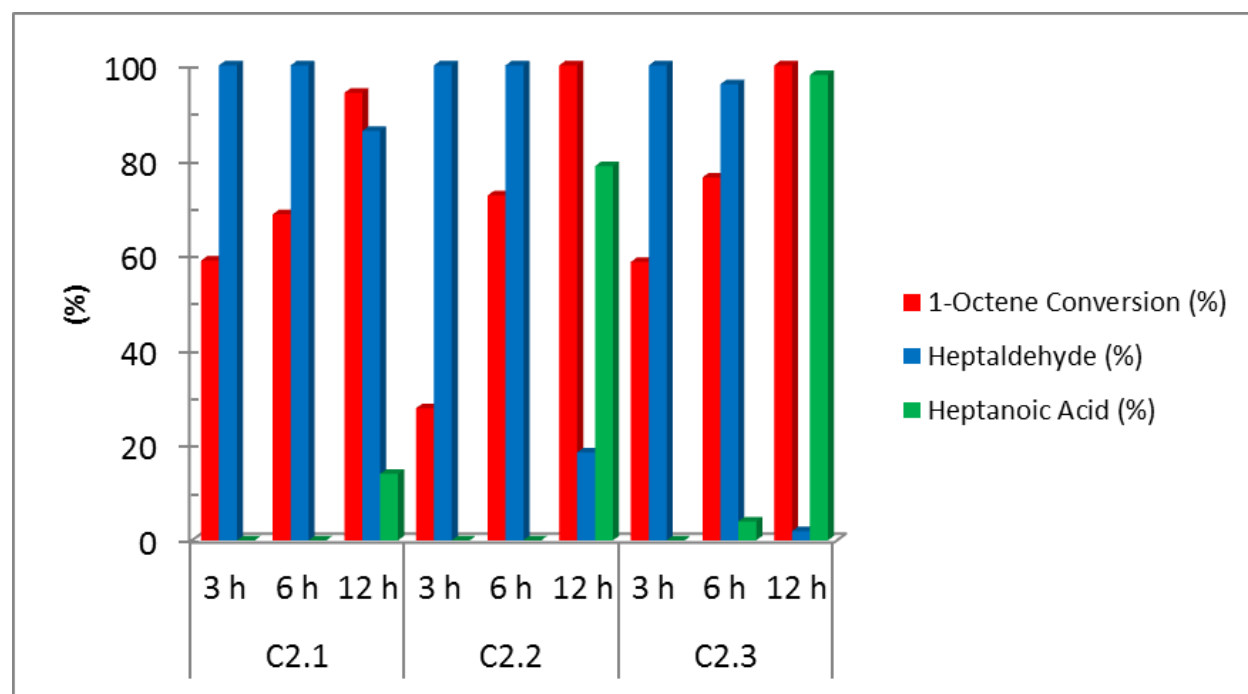
Figure 5.5 Conversion of 1-octene using model complexes C2.1-C2.3 as catalyst precursors with their respective product distributions over time (0.01 mmol catalyst).

To try and get a handle on what would affect the coordination ability of these ligands, the Lewis basicity of different pyridine and quinoline ligands were investigated. It was found that pyridine has a relative basicity (pK_b) of 8.8, with quinoline and methyl-pyridine having values of 9.1 and 8.0 respectively. The lower basicity of quinoline relative to pyridine means that the quinoline ligand would be more weakly coordinated to the ruthenium metal center when compared to the pyridine ligand. This weaker coordination ability would result in easier dissociation from the metal center and could possibly explain why the quinoline derivative (**C2.3**) performed better during the oxidative cleavage of 1-octene when compared to its pyridine derivative **C2.1**. The higher relative basicity of the methyl-pyridine ligand however would result in a stronger coordination to the metal center. This could explain why after 3 hours the methyl-pyridine derivative (**C2.2**) performed worse than the other derivatives. If you take into account that the ruthenium complex is only the catalysts precursor for the formation of the proposed RuO_4 species, the weakest coordinated ligand would dissociate faster and facilitate the formation of active species. This could possibly result in a higher initial activity (as is observed in

Chapter 5: Oxidative Cleavage of Selected Alkenes

Figure 5.5 after 3 hours). It is however difficult to speculate on the effect of the ligand once the active species have been formed. As discussed earlier in the chapter, Balavoine *et al.* found that by adding bipyridine as ligand to a system of $RuCl_3 \cdot xH_2O$ and $NaIO_4$, they were able to tune the activity of the system so they could form epoxides instead of cleavage products [14].

It is however known that bulky substituents in the α-position of a pyridine ring would reduce the coordinating ability of the pyridine ligand [19]. Larger, more bulky ligands could possibly facilitate dissociation from the metal center resulting in an increase in the rate of formation of the RuO_4 species, believed to be the active species. This could explain why the two more bulky methyl-pyridine and quinoline derivatives, **C2.2** and **C2.3**, show a higher activity after prolonged reaction times, when compared to model complex **C2.1** (pyridine). The exact mechanism by which the catalyst precursor is transformed into the RuO_4 species is however not known at this stage.

Griffith *et al.* reported the oxidative cleavage of numerous alkenes to their respective carboxylic acids employing exactly the same reaction conditions used for model complexes **C2.1**-**C2.3**. The reported system used $RuCl_3 \cdot xH_2O$ (0.01 mmol) as their catalysts precursor and yields of heptanoic acid of 70 % could be achieved for the oxidative cleavage of 1-octene after 2 hours [11]. Note that the major product is the carboxylic acid and not, as in our case, the aldehyde. Although this system performs better than our model system at short reaction times, more control in the formation of products is possible using our system with only longer reaction times resulting in the formation of the carboxylic acid.

With the optimized reaction conditions in hand it was decided to evaluate the MCM-41 and SBA-15 heterogenized counterparts of complex **C2.2** for the oxidative cleavage of 1-octene. MCM-41 immobilized catalyst **IC4.3** (heterogenized system of complex **C2.2**) was employed as catalyst precursor under the exact reaction conditions employed for the homogeneous counterparts above and the results are shown in Figure 5.6. A dramatic increase in the rate of the reaction was observed with almost complete conversion being observed after around 3 hours when compared to the 12 hours for complex **C2.2**. At 3 hours a maximum yield of heptaldehyde of almost 90 % is observed with very little carboxylic acid being seen (<10 %). After 3 hours the presence of the aldehyde decreases systematically coinciding with the formation of heptanoic acid. For the SBA-15 immobilized catalyst **IC4.4**, a similar trend was observed and this is

shown in Figure 5.7. Although a lower yield of heptaldehyde is observed when compared to the MCM-41 immobilized catalyst **IC4.3**, at around 3 hours still only aldehyde is formed (67 % yield) with less than 3 % carboxylic acid being present. Allowing the reaction to continue resulted in the formation of the corresponding carboxylic acid in nearly quantitative yields after 12 hours.
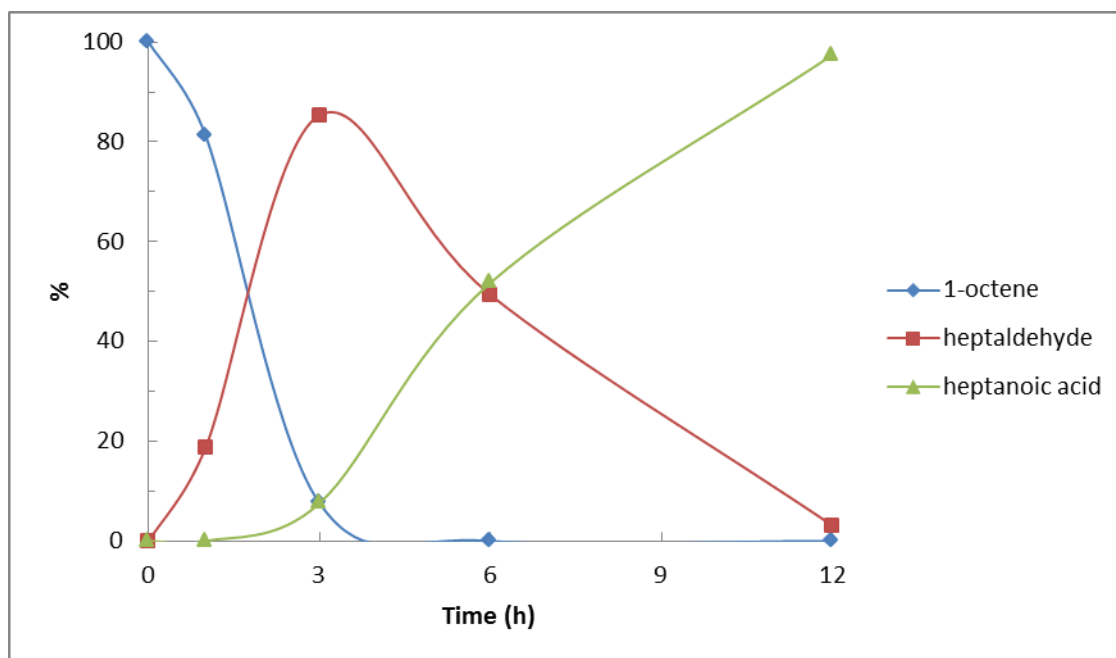
Figure 5.6   Conversion of 1-octene using MCM-41 immobilized catalyst IC4.3 as catalyst precursor.

Although it was initially thought that loadings were kept at 0.01 mmol ruthenium throughout, it was discovered that the loadings used for the immobilized systems were in fact 0.001 mmol (0.05 mol %) and not 0.01 mmol (0.5 mol %), as was used for the model systems. This was a significant discovery and the error crept in during the conversion of the obtained loadings (ICP-OES results) to the amounts of immobilized catalyst needed for catalysis. This puts the obtained activities of the immobilized systems in perspective with a dramatic increase in activity seen coupled with a 10 fold decrease in ruthenium loading.

Chapter 5: Oxidative Cleavage of Selected Alkenes
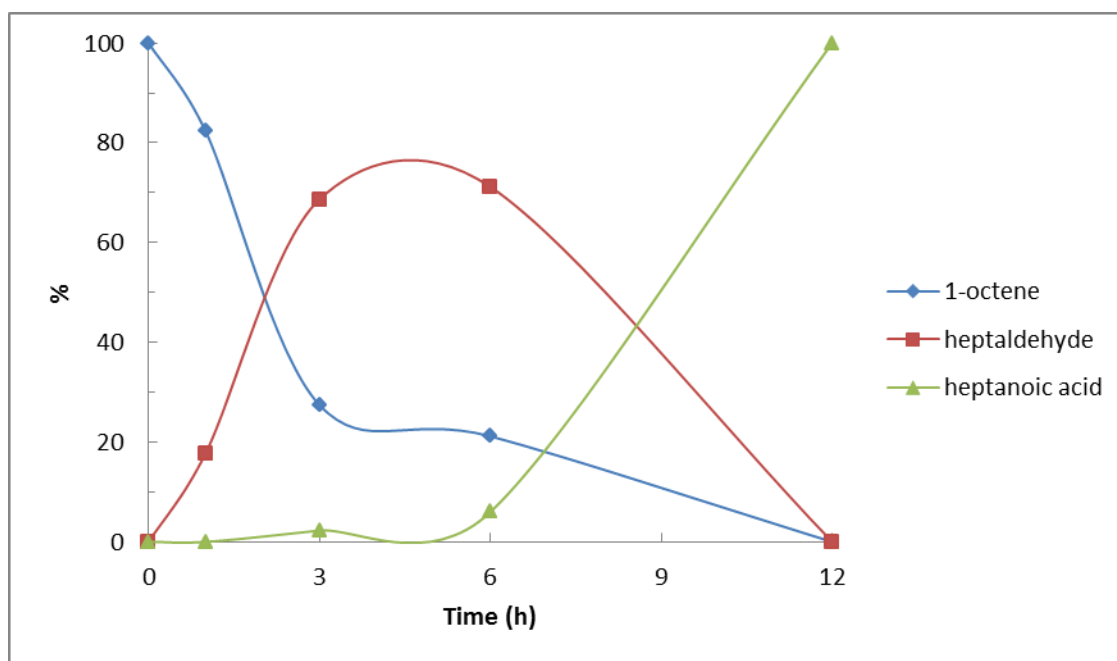
Figure 5.7   Conversion of 1-octene using SBA-15 immobilized catalyst IC4.4 as catalyst precursor.

Reactions with model complexes **C2.1**-**C2.3** as the catalyst precursors were subsequently repeated at this lower ruthenium loading of 0.001 mmol (0.05 mol %) and compared to their immobilized counterparts **IC4.1**-**IC4.6**, as well as the reactions previously carried out using 0.01 mmol (0.5 mol %) complex. A summary comparing the different ruthenium loadings are shown in Table 5.3. Significantly lower conversions after 3 hours were observed when carrying out the reactions using 0.001 mmol of complex instead of the previously used 0.01 mmol. This does however make the results obtained for the immobilized catalysts all that more surprising and leads one to believe that the support itself has to play a major role during the course of the reaction.

Table 5.3 Comparison of different ruthenium loadings for the oxidative cleavage of 1-octene using model complexes C2.1-C2.3.[a]

Complex	Catalyst Amount (mmol)	1-Octene Conversion (%)	Selectivity (%)	
			Heptaldehyde	Heptanoic acid
C2.1	0.01	59	100	0
	0.001	5	100	0
C2.2	0.01	28	100	0
	0.001	17	100	0
C2.3	0.01	59	100	0
	0.001	10	100	0

[a] Reaction conditions: 23 ˚C, 10 mmol $IO(OH)_5$, 2 mmol 1-octene, CH_3CN, CCl_4 and H_2O (5 mL, 5 mL and 10 mL respectively), 3 hours.

A summary for the product distribution of MCM-41 and SBA15 immobilized catalysts **IC4.1-IC4.6** is shown in Figure 5.8. After 3 hours immobilized catalysts **IC4.1**, **IC4.2** (pyridine derivatives) and **IC4.5** (quinoline derivative) were found to have the lowest conversions of 1-octene under these reaction conditions with 23 %, 42 % and 35 % conversion being obtained respectively. As was observed with the model systems, no heptanoic acid formation is observed at these low conversions with only heptaldehyde being formed. With the exception of the immobilized catalyst **IC4.4**, complete conversion of 1-octene was observed for immobilized catalysts **IC4.1**-**IC4.3**, **IC4.5** and **IC4.6** after 6 hours.
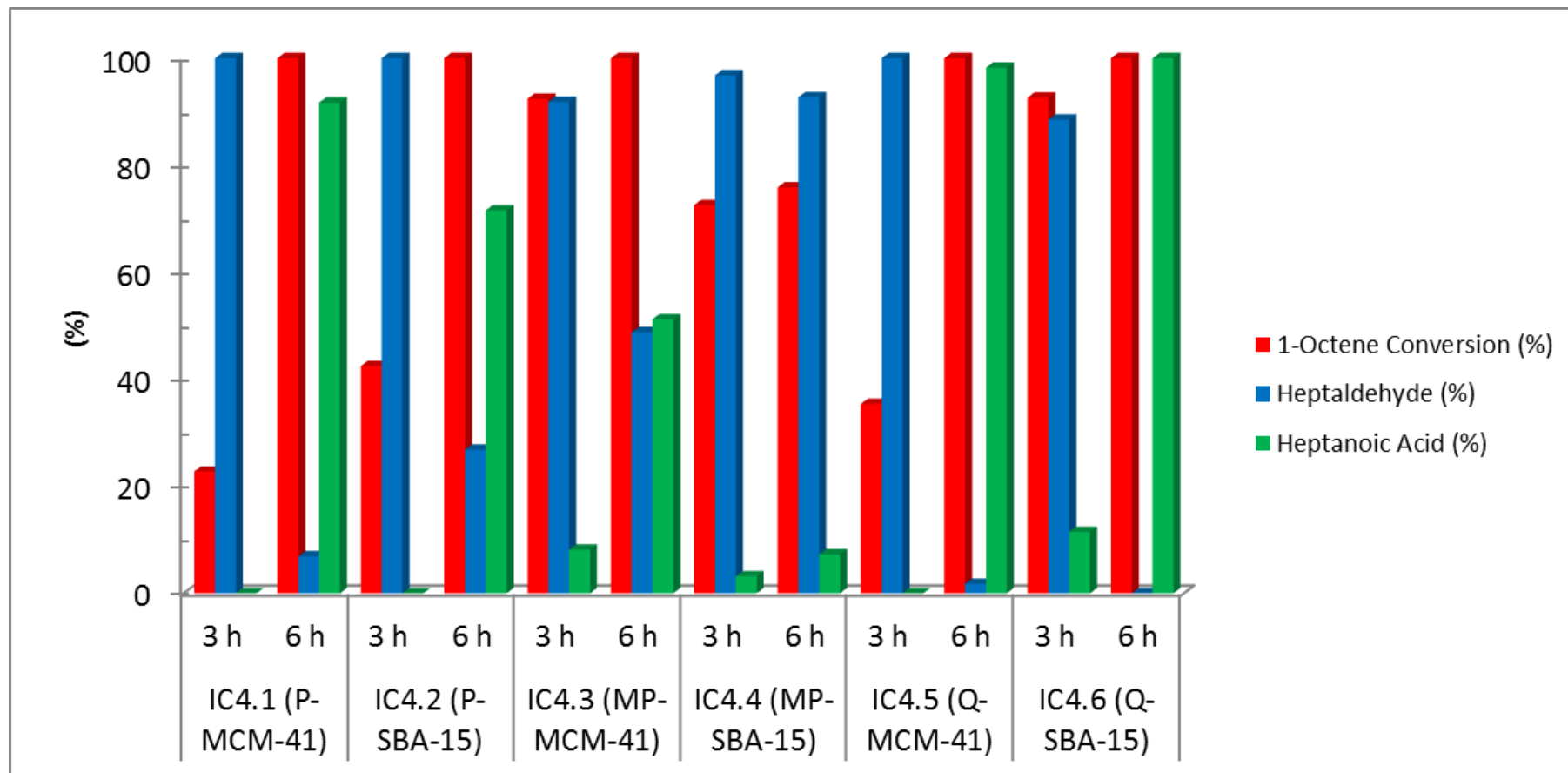
Figure 5.8 Conversion of 1-octene using MCM-41 and SBA-15 immobilized catalysts IC4.1-IC4.6 as catalyst precursors with their respective product distributions over time (0.001 mmol ruthenium).

Chapter 5: Oxidative Cleavage of Selected Alkenes

In comparison to the analogous model systems, this is a significant increase in the activity of the catalysts given that complete conversion of 1-octene was only observed after around 12 hours for the model catalysts **C2.1**-**C2.3**. After 6 hours the majority of the products being observed is heptanoic acid with almost complete conversion to the carboxylic acid being observed for immobilized catalysts **IC4.5** and **IC4.6**. This compares well to the model systems in that the highest activity being observed was for the quinoline derivatives in both the model and immobilized systems. Complete conversion of the formed aldehyde to heptanoic acid is achieved at longer reaction times and confirms that the mechanism would involve the initial formation of aldehyde followed by the oxidation of the said aldehyde to its corresponding carboxylic acid. This was confirmed by the reaction of heptaldehyde under the same reaction conditions used for cleavage reactions, with complete conversion to heptanoic acid being achieved in less than 3 hours (using model complex **C2.2**).

A comparison of the activity of the immobilized catalysts prepared with other ruthenium catalysts reported in the literature revealed just how active these immobilized systems actually are. The system reported here achieved favorable results for the cleavage of 1-octene using a relatively low ruthenium loading of 0.05 mol %. Examples of systems using $RuCl_3 \cdot xH_2O$ as catalyst precursors were reported by Griffith and Yang *et al.* [11, 17]. They reported the use of 6 mol % and 3.5 mol % ruthenium loadings respectively for the cleavage of various alkenes to their corresponding carboxylic acids. The original system reported by Sharpless *et al.* required the use of 2.2 mol % ruthenium catalyst to achieve the cleavage of 1-decene after 2 hours [5].

The introduction of a nitrogen donating ligand however has been shown to result in a decrease in the metal loading required to catalyze the reaction. Shoair *et al.* reported a $Ru(bipy)_2Cl_2$ system which required 0.5 mol % ruthenium loading to achieve the cleavage of 1-octene and other alkenes to their respective carboxylic acids [9]. Kogan *et al.* showed that a $[Ru(dmp)_2(H_2O)_2](PF_6)_2$ system could cleave numerous alkenes to their respective aldehydes with a loading of 1 mol % ruthenium [19]. These systems all are however examples of homogenous systems. Very few examples are reported in the literature where heterogeneous ruthenium catalysts are employed for the oxidative cleavage of alkenes. One of these systems, reported by *Kumar et al.*, showed that ruthenium on carbon could be used as a catalyst for the cleavage of numerous alkenes under similar conditions employed in the above mentioned

examples [20]. Loadings as low as 1 mol % Ru/C were sufficient to effectively cleave the reported alkenes to their respective aldehydes while it was possible to recycle the catalyst for up to 5 runs.

Both model and immobilized systems were also employed as catalyst precursors in the oxidative cleavage of styrene and the results are shown in Figure 5.9 (model complexes **C2.1**-**C2.3**) and Figure 5.10 (immobilized catalysts **IC4.1**-**IC4.6**). The reaction conditions were kept the same as were used for the oxidative cleavage of 1-octene with the only exception being the use of a ruthenium loading of 0.001 mmol for the immobilized systems. For the model systems complete conversion could be achieved after around 1 hour with benzaldehyde being formed as the only product (except for **C2.2**). After prolonged reaction times the formation of benzoic acid is observed with around 60 % being observed after 12 hours for all three derivatives (**C2.1**-**C2.3**). The oxidation of the benzaldehyde to benzoic acid however occurs at a much slower rate than was observed for the oxidation of heptaldehyde to form heptanoic acid (during the oxidative cleavage of 1-octene).
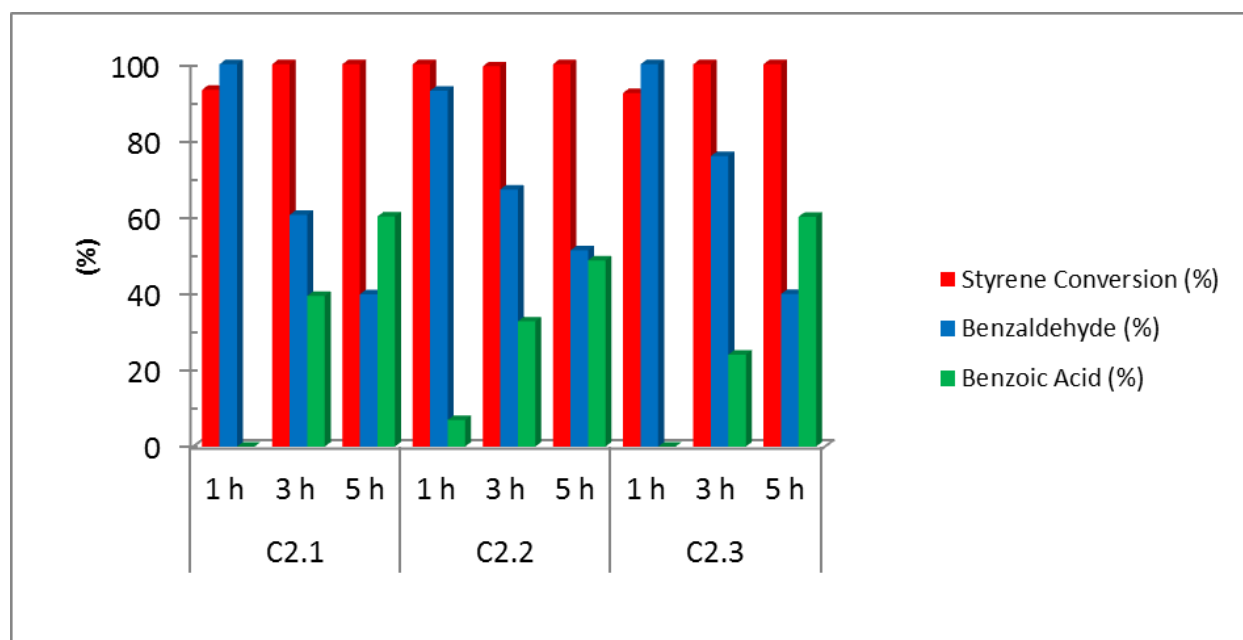
Figure 5.9   Oxidative cleavage of styrene using model complexes C2.1-C2.3 as catalyst precursors (0.01 mmol catalyst).

Chapter 5: Oxidative Cleavage of Selected Alkenes

Figure 5.10   Oxidative cleavage of styrene using MCM-41 and SBA-15 immobilized catalysts IC4.1-IC4.6 as catalyst precursors (0.001 mmol ruthenium).

Chapter 5: Oxidative Cleavage of Selected Alkenes

For the immobilized systems, complete conversion (as was the case for the model systems) could be achieved after only 1 hour, with the exception of immobilized catalyst **IC4.1**. After 3 hours, mainly benzaldehyde is observed for all of the reactions using the immobilized catalysts, with 15 % to 22 % benzoic acid observed throughout. Although the selectivity towards benzoic acid after 3 hours is lower than the model systems, it is important to remember that these reactions (for the immobilized catalysts) were carried out using a much lower catalysts amount (0.001 mmol ruthenium) than what was used for the model systems (0.01 mmol).

5.2.4 Using model complexes C3.1-C3.4 and immobilized catalysts IC4.7-IC4.12 (siloxane tether via the arene ring)

For immobilized catalysts **IC4.7**-**IC4.12** with the siloxane tether via the arene ring significantly lower activity towards the oxidative cleavage of 1-octene was observed when being compared to **IC4.1**-**IC4.6**. The model systems **C3.1**-**C3.4** were evaluated at both 0.01 and 0.001 mmol catalyst precursor amount and the results are shown in Figure 5.11. All the other reaction conditions were kept the same as previously mentioned: 23 ˚C, 10 mmol $IO(OH)_5$, 2 mmol 1-octene and a biphasic solvent system of CH_3CN, CCl_4 and H_2O (5 mL, 5 mL and 10 mL respectively).

All the reactions were initially carried out using 0.01 mmol ruthenium for 3 hours. The highest conversions were obtained for the complexes possessing the more bulky ligands (**C3.2**-**C3.4**). For the pyridine propylimine derivative, **C3.1**, a conversion of only 30 % could be achieved after 3 hours. A dramatic increase in the conversion is achieved by the substitution of the propyl substituent with a bulky 2,6-diisopropylphenyl substituent at the imine nitrogen with a conversion of just below 60 % being obtained (**C3.2**). The introduction of a methyl group on the pyridine ring resulted in a drop in the conversion to 50 %, which is still higher than the 30 % obtained using the pyridine propylimine derivative, **C3.1**. For the bipyridine derivative **C3.4** a conversion of 1-octene of around 35 % was achieved. It seems that the more bulky ligands resulted in enhanced activity towards the cleavage of 1-octene under these reaction conditions. The larger ligands could possibly facilitate the formation of the RuO_4 species by being more readily dissociated during RuO_4 formation.

Chapter 5: Oxidative Cleavage of Selected Alkenes

A dramatic decrease in the conversion is observed when using 0.001 mmol complex instead of the abovementioned 0.01 mmol. After 3 hours, at this lower ruthenium amount, no significant conversion could be achieved using these homogeneous catalysts. To achieve any significant conversion, the reaction was allowed to continue for 6 hours and even after this time a conversion of only around 10 % could be achieved using these model catalysts.
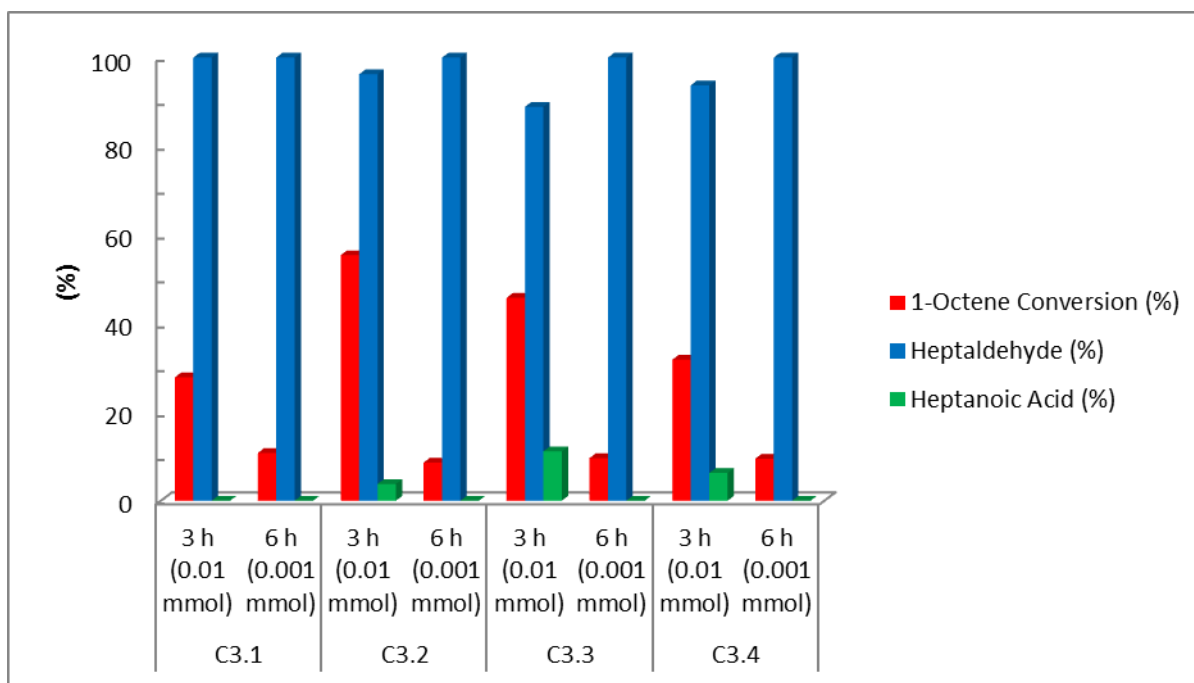
Figure 5.11   Oxidative cleavage of 1-octene using model complexes C3.1-C3.4 as catalyst precursors.

At the same loading of 0.001 mmol ruthenium much higher conversions could be achieved using the immobilized systems **IC4.7**-**IC4.12** with the results shown in Figure 5.12. A maximum conversion of around 40 % is achieved after 6 hours. Although this is much lower when compared to immobilized catalysts **IC4.1**-**IC4.6**, it is still significantly higher than the model systems **C3.1**-**C3.4** where little to no activity (10 % maximum) was achieved after 6 hours at a similar catalyst amount of 0.001 mmol.

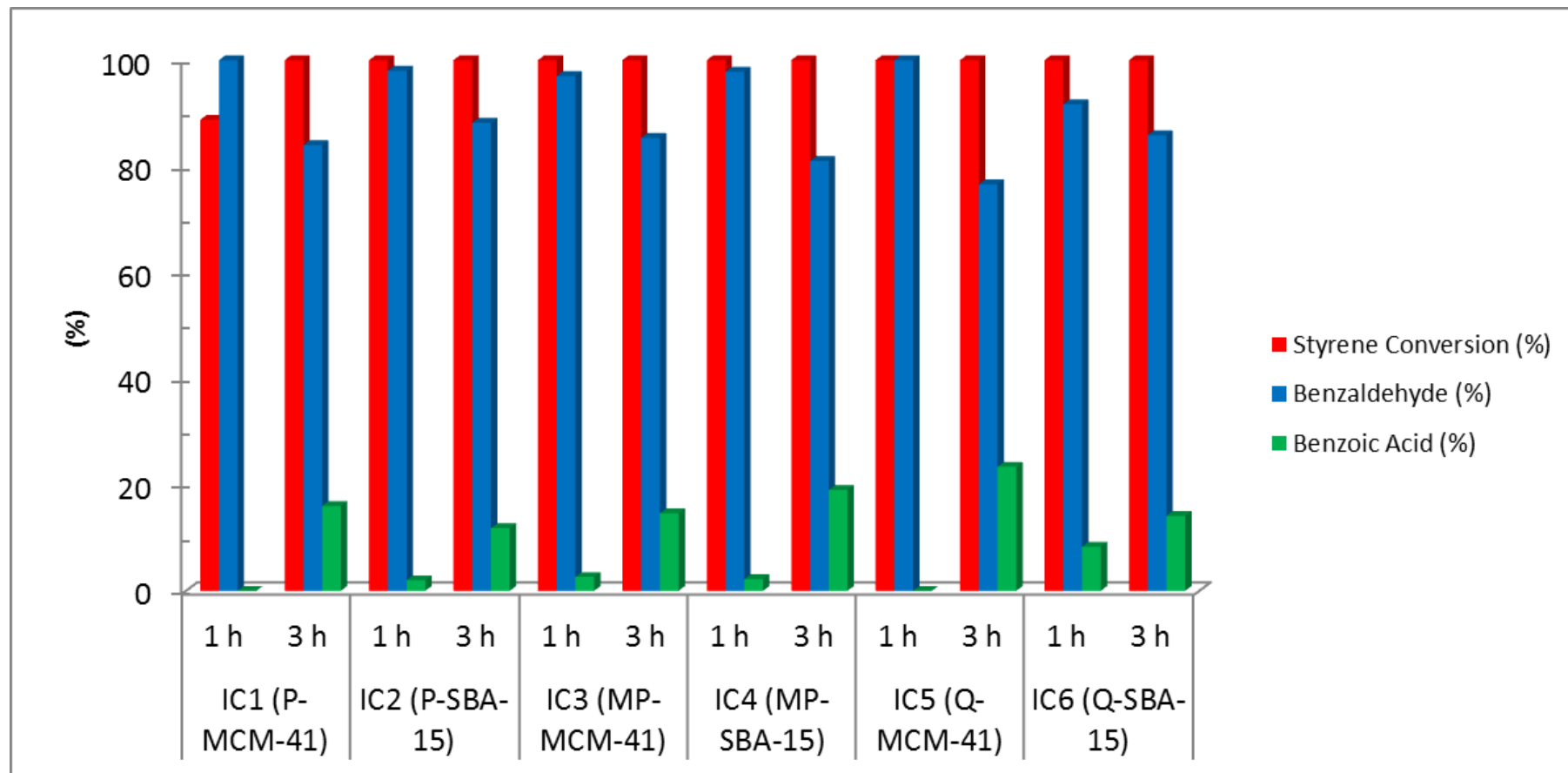**Chapter 5: Oxidative Cleavage of Selected Alkenes**
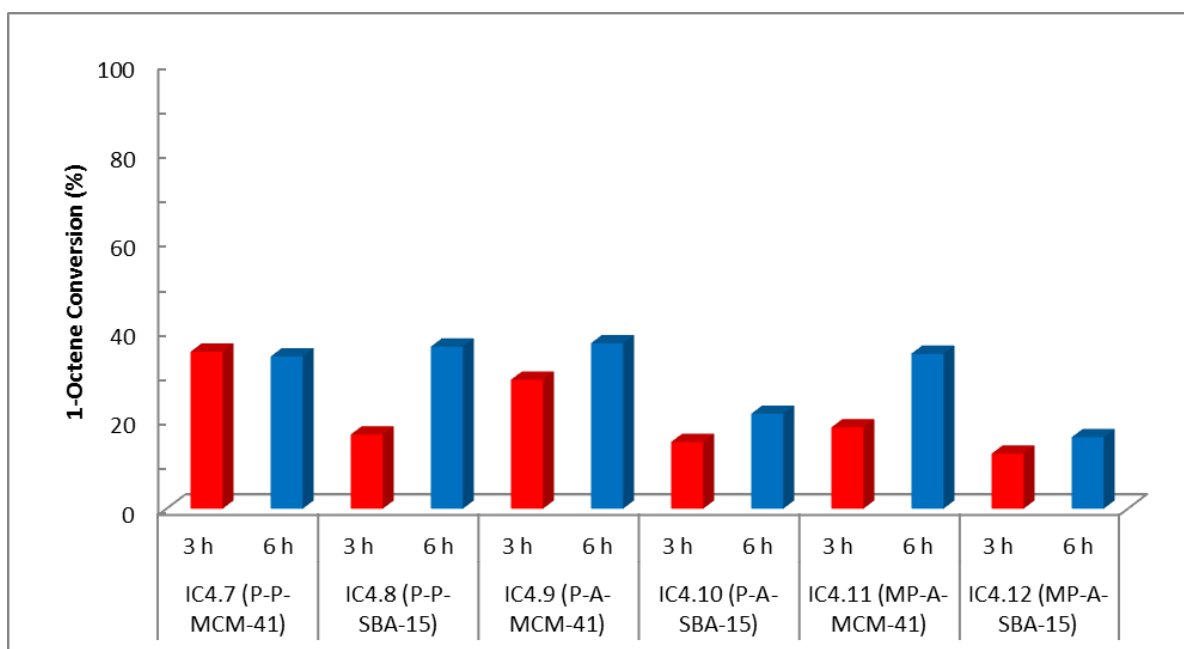
Figure 5.12   Oxidative cleavage of 1-octene using MCM-41 and SBA-15 immobilized catalysts IC4.7-IC4.12 as catalyst precursors (0.001 mmol ruthenium).

The decreased activity observed for the immobilized catalysts **IC4.7**-**IC4.12** compared to immobilized catalysts **IC4.1**-**IC4.6**, can be ascribed to the lower stability of the former catalysts in solution. After a typical run using the systems with the siloxane tether attached to the imine nitrogen, a yellow reaction solution was observed. This is in contrast to the systems with the siloxane via the arene ring where a black coating of ruthenium is observed on the side of the round bottomed flask, which points to the formation of Ru(0) during the reaction. This could explain why no significant increase in the conversion of 1-octene is observed even at extended times, because the amount of ruthenium present in solution is dramatically reduced resulting in lower activity. The stability of the model complexes under these reaction conditions were probed using UV-Vis spectroscopy. The model complex **C3.1** (model derivative of **IC4.7** and **IC4.8**) was found to decompose after an hour in the presence of the oxidant. This is in comparison to model complex **C2.2** (model derivative of **IC4.3** and **IC4.4**) where, even after 24 hours, the complex was still detected to be intact using UV-Vis spectroscopy. A more detailed study is shown and discussed in section 5.2.6 to follow.

Chapter 5: Oxidative Cleavage of Selected Alkenes

5.2.5 Role of the support material MCM-41 and SBA-15 during the oxidative cleavage reaction

The effect of the support material was investigated to see whether the support itself or simply the immobilization process was responsible for the observed difference in the activity of the catalysts. Experiments were carried out under the same reaction conditions used for the cleavage reactions mentioned above (0.01 mmol catalyst). When model complex **C2.2** was used as catalyst precursor for the oxidative cleavage of 1-octene, 30 % conversion was observed after 3 hours. In Figure 5.13 the effect of adding pure MCM-41 and SBA-15 (previously dried native support material) to the reaction mixture in a 1:10 weight ratio of complex:silica on activity, is shown. After 3 hours a significant increase in the conversion is observed for the reaction containing added silica. A conversion just shy of 60 % was obtained for the **C2.2**/MCM-41 system while an increase in the conversion to just over 30 % was observed for the **C2.2**/SBA-15 system. This however is still lower than the activities obtained when purely immobilized catalysts were used. Using various ratios of complex **C2.2**:silica viz. 1:5, 1:10 and 1:20, a significant change in the conversions after 3 hours were observed with the ratio of 1:10 (by weight) giving the highest activity (Figure 5.14).
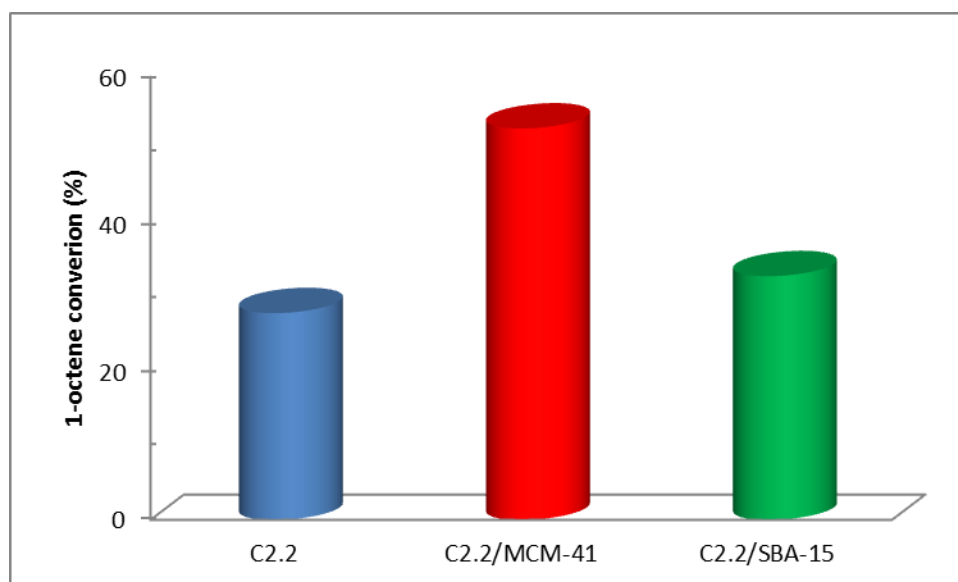
Figure 5.13 Influence of the addition of silica (MCM-41 and SBA-15) on the activity of complex C2.2 (1:10 complex:silica ratio for both MCM-41 and SBA-15 systems).

Chapter 5: Oxidative Cleavage of Selected Alkenes
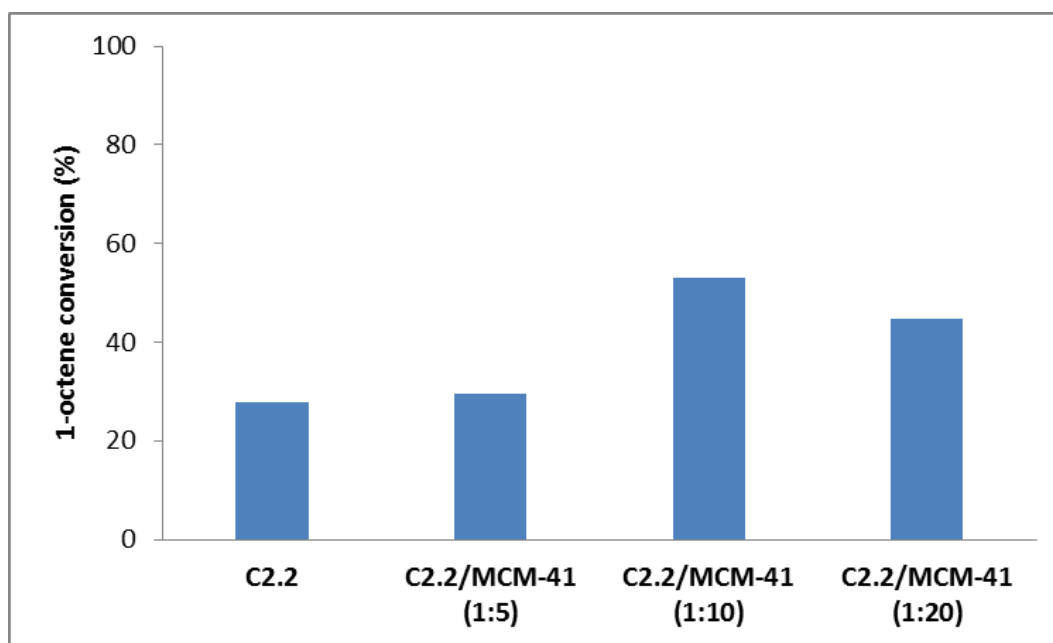
Figure 5.14 Effect of different ratios of complex C2.2:MCM-41.

When no complex or oxidant was added and only silica used no conversion was observed. It was thought that the surface silanols could possibly be enhancing the reaction by stabilizing formed intermediates.

It was thought that the surface silanols of the silica support could possibly be stabilizing the formed RuO_4 species seeing that it is very susceptible to decomposition. This could possibly increase the catalyst lifetime which in turn would result in an increase in the activity of a said catalyst. To verify the possible interaction of the surface silanols with the formed active species it was decided to "cap" the support with an appropriate capping agent which would remove any silanol functionalities on the support material. The deactivation of the silanols was achieved by the reaction of the dried native supports with excess hexamethyl disilazane following literature procedures used to render the surface of the silica material more non-polar. Characterization, using infrared spectroscopy, confirmed successful capping with no –OH band being present in the obtained IR spectrum [18]. The results of this reaction with the capped silicas are shown in Figure 5.15. Although no significant decrease in the conversion is observed when comparing the

capped SBA-15 to native SBA-15, a dramatic decrease in the conversion was however observed for the capped MCM-41 system.
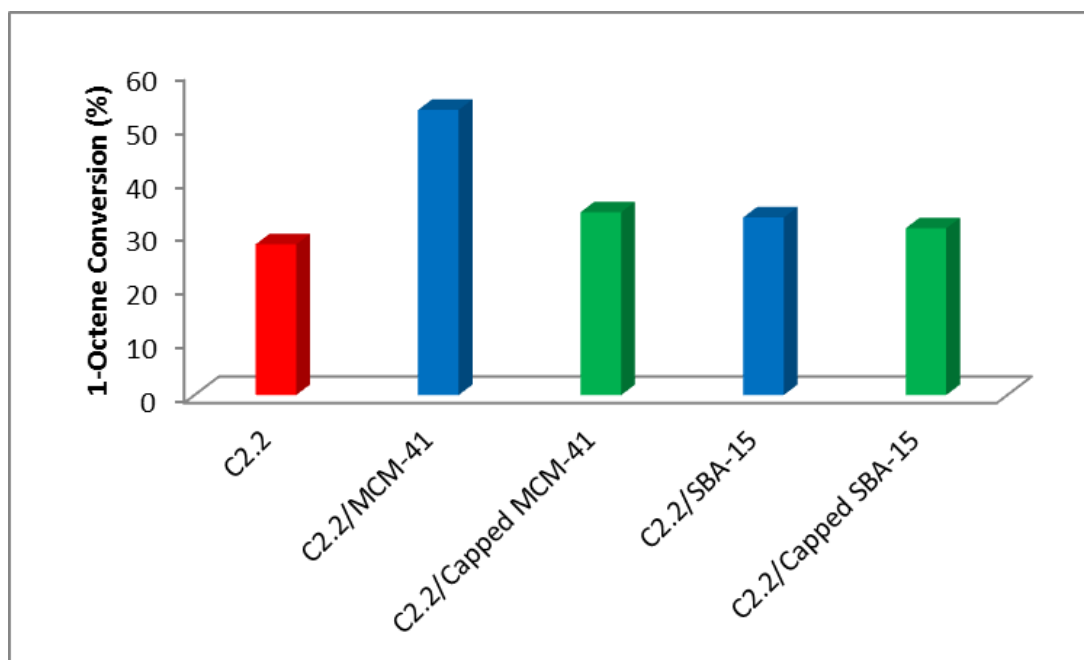
Figure 5.15   Oxidative cleavage of 1-octene with complex C2.2 in the presence of capped MCM-41 and SBA-15.

A decrease in conversion from 54 % to 34 % is observed which would suggest that the silanols on the support surface does in fact play a positive role during the reaction. Although addition of native MCM-41 and SBA-15 caused an increase in the conversion of 1-octene, this was not as dramatic when compared to those obtained when using the immobilized systems. This would suggest that not only the support but also the immobilization process itself contributing greatly towards the observed increase in activity. It is known that immobilization helps to disperse the catalyst over a large area on the support surface which could facilitate the formation of the active species (RuO_4) with the free surface silanols on the support helping to stabilize this species during the course of the reaction. This would also explain why such a dramatic difference

between the addition of MCM-41 and SBA-15 on the conversion is observed with the latter having a much smaller surface area and thus less free surface silanols.

5.2.6   Confirming the possible active species during the cleavage reaction: RuO_4

Shoair *et al.* proposed that the reaction is mediated by the *in situ* formed RuO_4 species. The presence of the RuO_4 species was confirmed by monitoring the reaction using UV-Vis spectroscopy, in the absence of substrate. Characteristic peaks for this species, with associated fine structure, were observed between 370 and 420 nm [9]. Similarly we performed a reaction under the reaction conditions used for the base-line reactions with the only difference being the absence of any substrate. Attempts to reproduce this reaction using $Ru(bipy)_2Cl_2$ were however unsuccessful and after prolonged reaction times only the spectrum of the complex could be observed. Although RuO_4 could potentially be formed, unfortunately the complex absorption peaks were observed in the same region where the RuO_4 peaks are expected to be observed. This therefore made it difficult to unambiguously confirm the formation of RuO_4 using $Ru(bipy)_2Cl_2$ as precursor. RuO_4 was generated by reacting $RuCl_3 \cdot xH_2O$ under the above mentioned reaction conditions for 1 hour with the obtained UV-Vis spectrum shown in Figure 5.16.
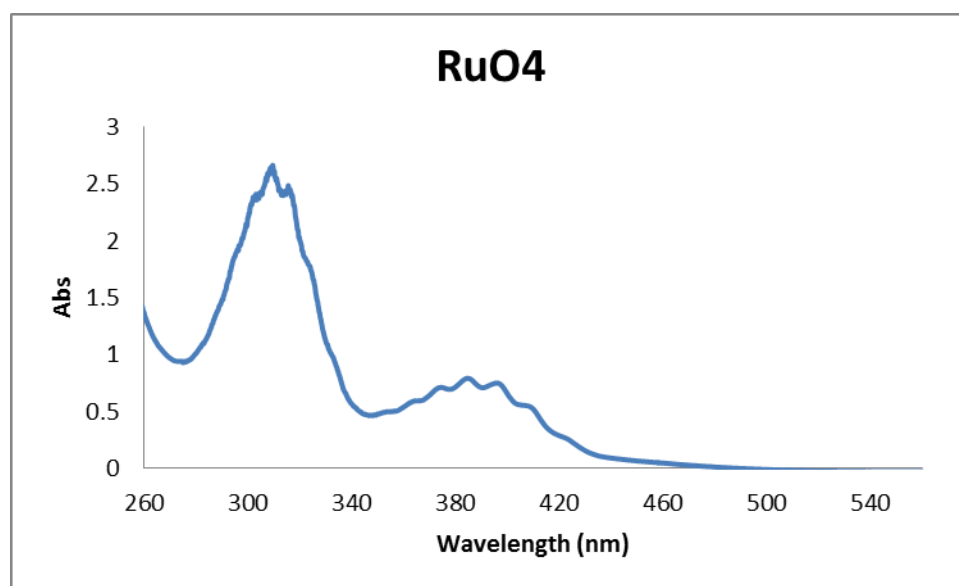
Figure 5.16 Formation of RuO_4 using $RuCl_3 \cdot xH_2O$ as precursor.

Chapter 5: Oxidative Cleavage of Selected Alkenes

The presence of the peak between 370 and 420 nm as was reported by Shoair *et al.* could be confirmed. Another peak was also observed at 310 nm which was consistent with other examples reported in literature [21,22]. Seeing that our results showed that the model complexes were more active for the oxidative cleavage of 1-octene than $Ru(bipy)_2Cl_2$ (in our hands), it was decided to carry out this exact reaction using model complex **C2.2** instead. Shoair *et al.* did not state for how long the reaction was allowed to stir before sampling commenced. It was therefore decided to do the reaction for different lengths of time. Reactions were carried out for reaction times between 1-24 hours with the obtained UV-Vis spectra shown in Figure 5.17. At shorter reaction times (1, 3, 6 and 10 hours), only the untransformed complex **C2.2** can be observed. However at similar times for the oxidative cleavage of 1-octene, conversion of the substrate was already observed (almost 90 % after 10 hours). Although RuO_4 is not observed at these times, its signal is possibly obscured by the presence of unreacted model complex which show absorption peaks in similar regions of the UV-Vis spectrum. After allowing the reaction to continue for prolonged reaction times (15, 20 and 24 hours), the characteristic fine structure of the RuO_4 absorption peaks can be observed.
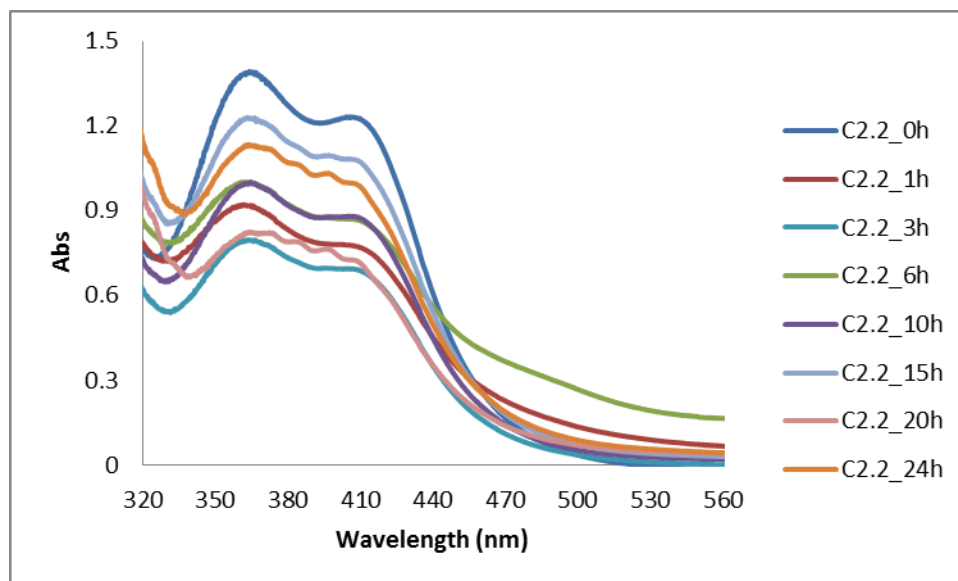
Figure 5.17 UV-Vis spectra of the organic layer (50 % dilution) of reaction mixtures using complex C2.2 as catalyst precursor (1-24 hours).

Chapter 5: Oxidative Cleavage of Selected Alkenes

The presence of the model complex **C2.2** is also still detected in the UV-Vis spectrum. At these longer reaction times more RuO_4 is present in the reaction mixture which makes it possible to observe the RuO_4 species. The above mentioned UV-Vis experiment showed that very small amounts of RuO_4 are needed to efficiently cleave 1-octene. It was shown however that at the lowered ruthenium loadings employed for the immobilized catalysts (0.001 mmol) that the model systems showed very low activity. This possibly means that the formation of the RuO_4 species from the catalyst precursor is the rate limiting step for this cleavage reaction.

Previous results have shown that conversions obtained for the cleavage of 1-octene using model complexes **C3.1**-**C3.4** could not compare to that of model complexes **C2.1**-**C2.3**. To understand why the former showed lower activity, the same UV-Vis experiment in the absence of 1-octene was carried out. The obtained spectra are shown in Figure 5.18. After 1 and 3 hours, the presence of complex **C3.1** cannot be detected anymore. This confirmed a previous observation that the complexes with the tether via the arene ring were found to decompose during the cleavage reaction. For model complex **C2.2**, no significant change in the obtained UV-Vis spectrum, even after 24 hours, was observed.
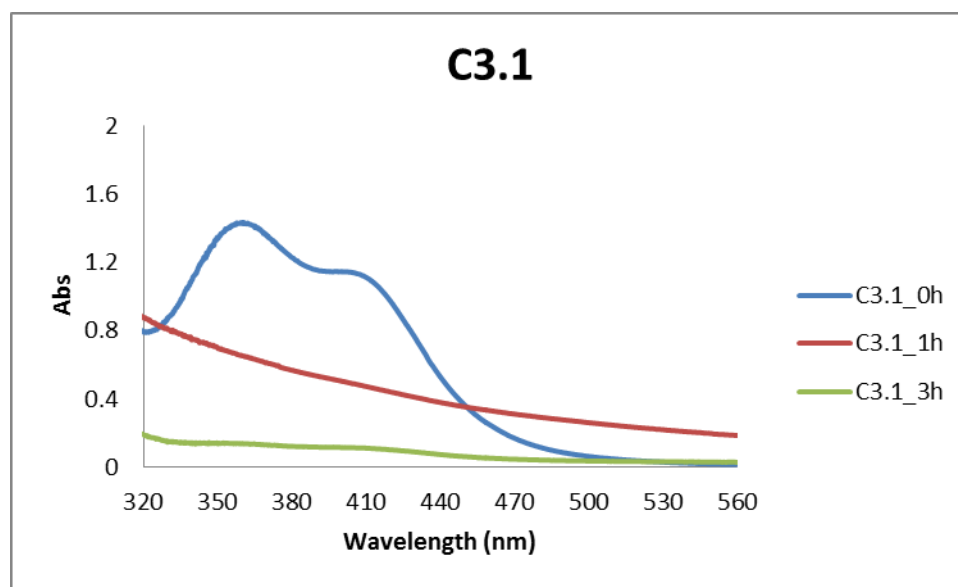
Figure 5.18 UV-Vis spectra of the organic layer (50 % dilution) of reactions using complex C3.1 as catalyst precursor (1 and 3 hours).

Chapter 5: Oxidative Cleavage of Selected Alkenes

This showed that under these reaction conditions complex **C3.1** was much more unstable than complex **C2.2**. The presence of the RuO_4 species could not be observed using complex **C3.1**, but is believed to be present in very small amounts, given that appreciable 1-octene conversion was observed using this complex.

To probe why the immobilized catalysts showed such a dramatic increase in the conversion of 1-octene compared to their homogeneous counterparts, the same reactions were carried out using the immobilized analogues of the above mentioned model complexes **C2.2** and **C3.1**. The obtained UV-Vis spectra of solutions of catalysts **IC4.3** (tether attached to the imine nitrogen) and **IC 4.7** (tether via the arene ring) are shown in Figure 5.19 and Figure 5.20. For immobilized catalysts **IC4.3** and **IC4.7** the presence of RuO_4 is observed after carrying out the reaction for only 1 hour. It seems after longer reaction times the amount of RuO_4 increases, with the peak at 310 nm also becoming better resolved. It was previously shown that the immobilized catalysts could not be recovered and reused after a typical cleavage reaction.
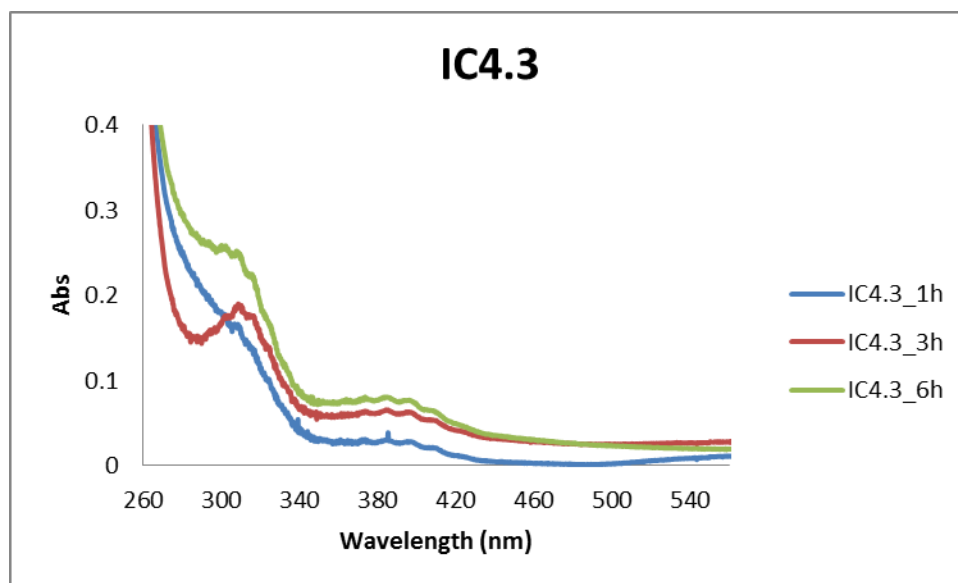
Figure 5.19   UV-Vis spectra of the organic layer (50 % dilution) of reactions using immobilized catalyst IC4.3 (tether attached to the imine nitrogen) as catalyst precursor (1, 3 and 6 hours).

Chapter 5: Oxidative Cleavage of Selected Alkenes
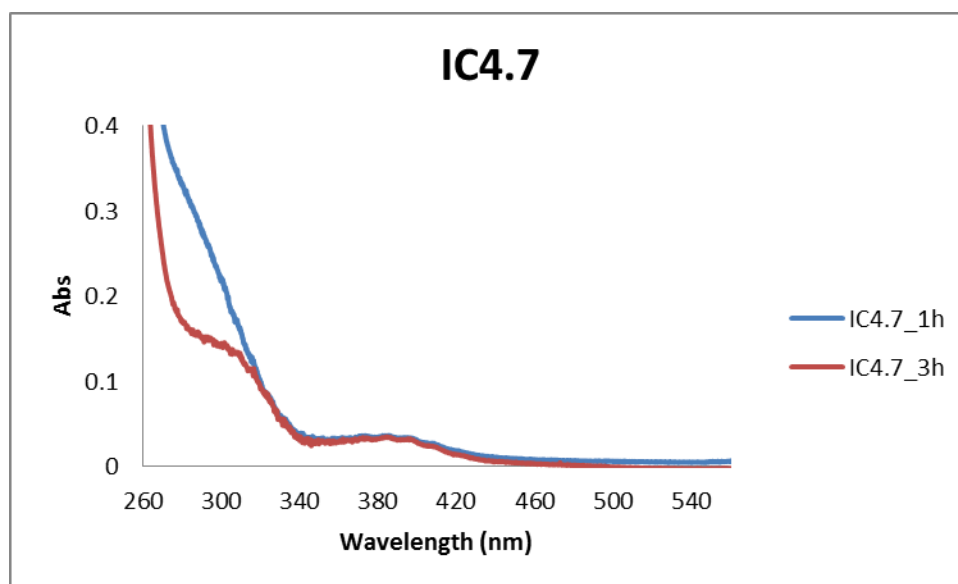
Figure 5.20   UV-Vis spectra of the organic layer (50 % dilution) of reactions using immobilized catalyst IC4.7 (tether via the arene ring) as catalyst precursor (1 and 3 hours).

It was concluded that all of the heterogenized complex present in the immobilized system was converted to soluble RuO_4 during the first catalytic run. This remains in solution when the supported catalyst is filtered off after run 1 and therefore no residual catalyst precursor was left to be converted to the active species during the second run. This also confirms that most of the immobilized catalyst is converted to RuO4 which would explain the enhancement in the activity compared to the model systems.

Experiments carried out previously involved the addition of native MCM-41 and SBA-15 to solutions of the model complex **C2.2**. This resulted in an increase in the conversion in the oxidative cleavage reactions of 1-octene. This increase was the largest when MCM-41 was added in a 1:10 ratio of complex:silica. It was therefore decided to investigate the role of the addition of silica to the model complex **C2.2** further by following the formation of the RuO_4 species in the absence of substrate using UV-Vis spectroscopy. The reactions were carried out employing the same reaction times mentioned earlier for a similar UV-Vis experiment using model complex **C2.2** on its own. The ratio of added MCM-41 was chosen as 1:10 because it was previously shown to be the optimum addition ratio and it also mimicked the immobilization ratio

Chapter 5: Oxidative Cleavage of Selected Alkenes

of 1:10 as well. A comparison of the obtained UV-Vis spectra is shown in Figure 5.21 and Figure 5.22. For the experiments where only complex **C2.2** was used, the RuO_4 species could only be detected after the reaction was allowed to progress for 15 hours. For the systems where native MCM-41 was added, RuO_4 could be detected in the reaction mixture from around 6 hours with the fine structure of the RuO_4 signal species observed at 385 nm. This enhanced rate of the formation of the RuO_4 species when MCM-41 is added to the reaction mixture verified previous results where an increase in the conversion of 1-octene from around 30 % to 58 % was achieved in the presence of the silica material.
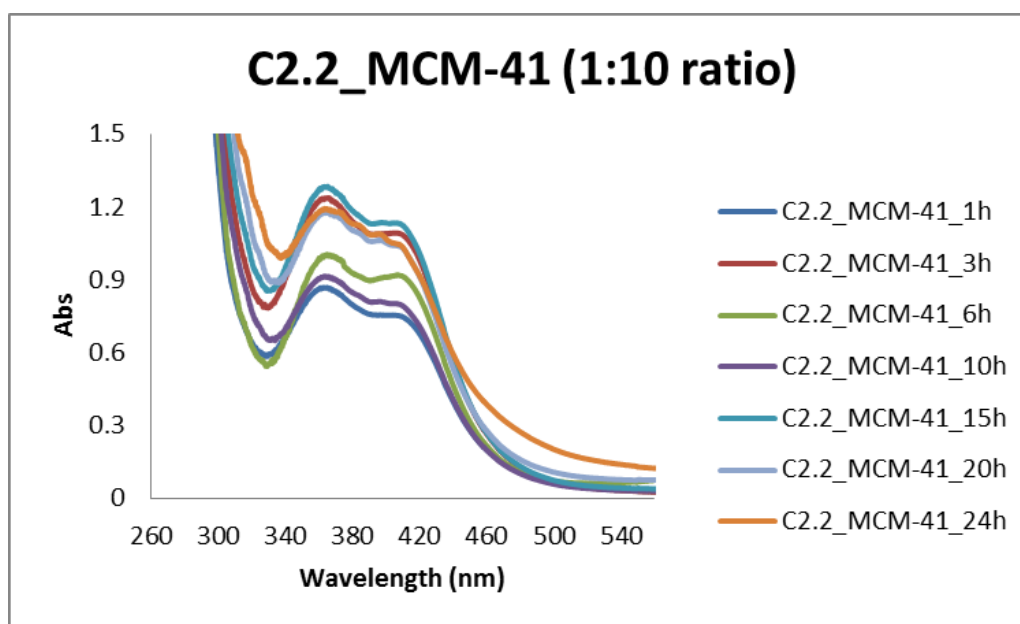
Figure 5.21 UV-Vis spectra of the organic layer (50 % dilution) of reactions using a 1:10 ratio of model complex C2.2:MCM-41 as catalyst precursor (1-24 hours).

From these results it clear that the support material does not only act as a carrier for the complex but also has an effect on the rate at which the active species is formed. Although the exact mechanism by which the RuO_4 species is formed from the catalyst precursor is not known, it is possible to speculate on the effect of the support material. Given that the support material's (MCM-41 and SBA-15) surface is covered with silanol groups, it is possible that the oxidant,

IO(OH)$_5$, as well as the complex is adsorbed onto the surface of the support. This could potentially bring the oxidant and complex into close proximity allowing for more efficient interaction between the complex and the oxidant.
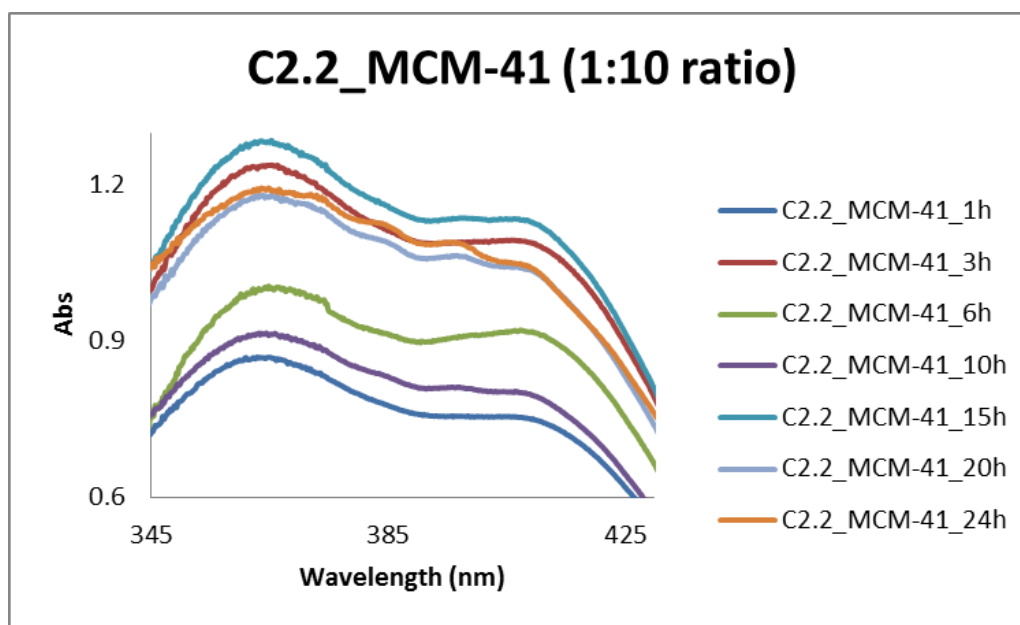
Figure 5.22 UV-Vis spectra (focusing on peaks between 345 and 430 nm) of reactions using a 1:10 ratio of model complex C2.2:MCM-41 as catalyst precursor (1-24 hours).

5.2.7 Possible mechanism for the oxidative cleavage of alkenes

Most reports suggest that the carboxylic acid is formed as either the major or only product. Shoair *et al.* proposed that in the oxidative cleavage of cyclohexene with Ru(bipy)$_2$Cl$_2$ that initially the epoxide is formed followed by the formation of the carboxylic acid (adipic acid) [18]. Their proposed mechanism did not involve the formation of aldehyde whatsoever (Scheme 5.2) and thus it's unlikely that our reactions follow a similar mechanism. Although the mechanism in Scheme 5.2 is shown for a cyclic alkene, it is expected that the epoxidation mechanism would be the same for linear alkenes as well.

Chapter 5: Oxidative Cleavage of Selected Alkenes

$$Cis\text{-}[Ru(bipy)_2Cl_2] + 3IO(OH)_5 \rightarrow RuO_4 + 3HIO_3 + 2bipy + 2HCl + 5H_2O \qquad (1)$$

$$2\ Cyclohexene + RuO_4 \rightarrow 2\ Cyclohexene\ epoxide + RuO_2 \qquad (2)$$

$$RuO_2 + 2IO(OH)_5 \rightarrow RuO_4 + 2HIO_3 + 4H_2O \qquad (3)$$

$$2\ Cyclohexene\ epoxide + RuO_4 \rightarrow 2\ Adipic\ acid + RuO_2 \qquad (4)$$
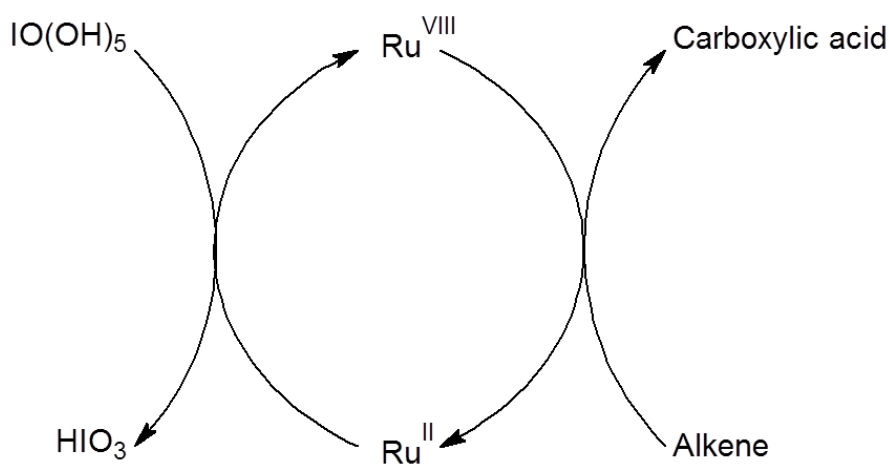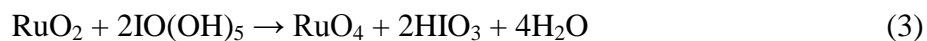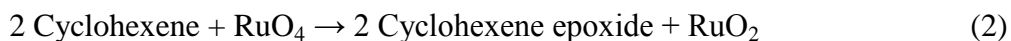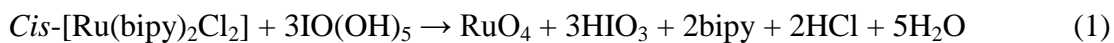
Scheme 5.2 Proposed reaction scheme for the formation of adipic acid from cyclohexene [18].

A more likely mechanism for the oxidative cleavage reaction using our systems is shown in Scheme 5.3. The mechanism using RuO_4 as active species does not involve the formation of epoxy or diol intermediates, as is shown in mechanism (**a**) in Scheme 5.3. After coordination of the RuO_4 species to the alkene, a ruthenium (IV) diester is formed via a 3+2 pericyclic reaction. The stability and lifetime of this formed diester is important as it was shown that upon rearrangement this diester yields aldehydes. Hydrolysis of this diester would result in the formation of diols; mechanism **b** [13]. Excess oxidant would result in the further oxidation of the formed aldehyde to its respective carboxylic acid.

Chapter 5: Oxidative Cleavage of Selected Alkenes
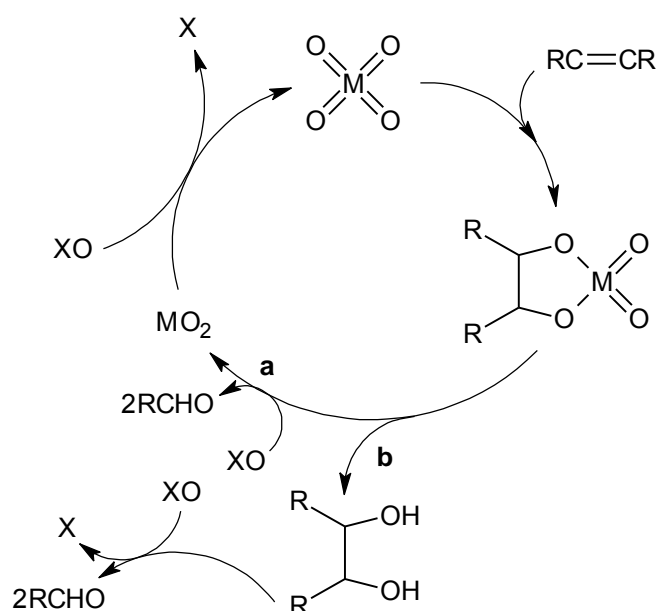
Scheme 5.3   General catalytic cycle for the oxidative cleavage of alkenes involving metal (M) tetroxides [13].

This formation of the ruthenium diester was also proposed by Yang *et al.* and a simplified mechanism for the rearrangement is shown in Scheme 5.4 [17]. It was shown that the amount of epoxide formed during side reactions did not decrease when more aldehyde started to form over time. They concluded that a Ru(VI) diester was probably forming and after rearrangement allowed for the formation of the corresponding aldehyde. In our experiments it was confirmed that the oxidation of the aldehyde by the catalyst was responsible for the formation of the carboxylic acid and only started when a certain amount of aldehyde had already formed.

The ability of the catalyst to promote the oxidation of heptaldehyde to heptanoic acid was confirmed independently by reacting a certain amount of aldehyde under the exact reaction conditions used for the oxidative cleavage reactions. This can possibly lend credence to fact that the pathway shown in Scheme 5.4 is most likely for our transformations whereby aldehydes are formed instead of epoxides.

Chapter 5: Oxidative Cleavage of Selected Alkenes

ruthenium (VI) diester
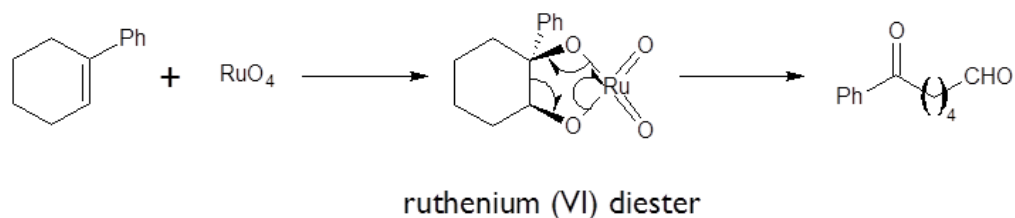
Scheme 5.4   Proposed mechanism for the formation of aldehyde during the oxidative cleavage of alkenes [17].

By combing these two catalytic cycles, the proposed catalytic cycle for our system is shown in Scheme 5.5.
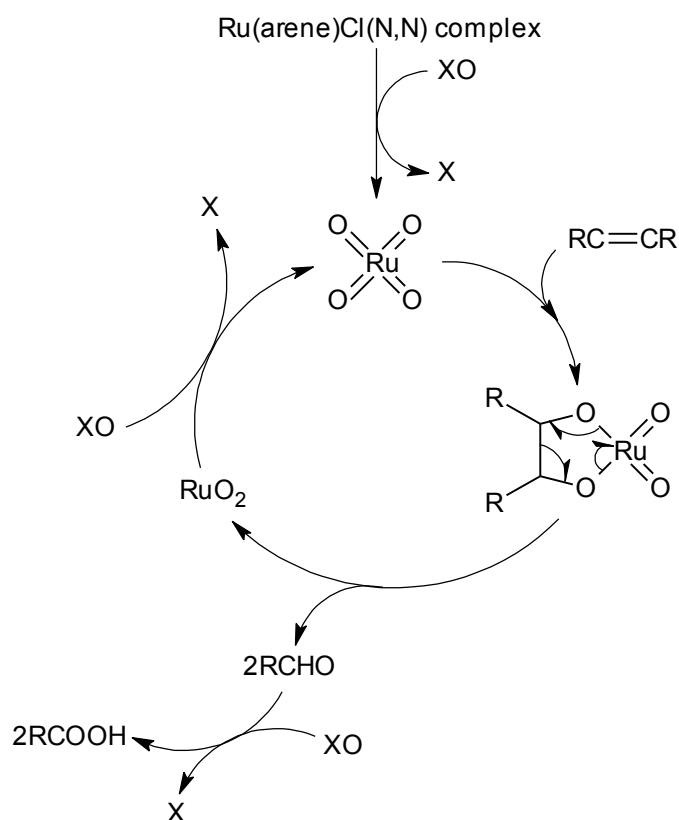
Scheme 5.5   The proposed mechanism for the formation of aldehyde and carboxylic acid during the oxidative cleavage of alkenes using a Ru(arene)Cl(N,N) complex as catalyst precursor.

Chapter 5: Oxidative Cleavage of Selected Alkenes

It was shown earlier that the oxidative cleavage of 1-octene is mediated by the *in situ* formed RuO$_4$ species. The first step of the cycle would most likely involve the dissociation of the ligands bound to the ruthenium metal followed by its oxidation to RuO$_4$. Although it is not clear at this stage how this occurs, UV-Vis experiments suggest that the formation of the tetroxide species could potentially be the rate limiting step for the reaction. The coordination of the alkene to the tetroxide species possibly results in the formation of a Ru(VI) diester which, upon rearrangement, liberates the aldehyde.   The formed RuO$_2$ is re-oxidized to RuO$_4$ and can continue for another cycle. The formed aldehyde, as was observed from the catalytic studies, can be further oxidized by the RuO$_4$ to form the corresponding carboxylic acid.

5.3   Concluding remarks

Model and immobilized systems **C2.1**-**C2.3** and **IC4.1**-**IC4.6** allowed us to selectively and in high yields form either heptaldehyde or heptanoic acid in the oxidative cleavage of 1-octene by varying the reaction times. At shorter reaction times (3-5 hours) mostly heptaldehyde was formed. Increased reaction times resulted in the formation of heptanoic acid via the oxidation of the formed aldehyde over time. It was possible to completely convert the formed heptaldehyde to heptanoic acid in less than 6 hours using immobilized catalysts **IC4.1**-**IC4.6**.

Styrene could be converted to benzaldehyde in near quantitative yields in 1 hour. Although the immobilized catalysts **IC4.7**-**IC4.12** did not fare as well as **IC4.1**-**IC4.6**, a still significant increase in the activity was observed when compared to its model counterparts **C3.1**-**C3.3**.

What makes the results for the immobilized catalysts even more impressive is the low catalyst amount that is needed to carry out the cleavage of 1-octene. If you take into account that 2 mmol 1-octene can be almost completely converted to either heptaldehyde or heptanoic acid (depending on the reaction time) using only 0.001 mmol ruthenium compared to the 0.01 mmol complex needed to give even comparable conversions.

UV-Vis spectroscopy proved to be a valuable tool to probe the formation of the proposed active species, RuO$_4$. It was shown that the propanol arene complex **C3.1** was unstable under the catalytic conditions and after 1 hour was no longer present in the solution. This is in comparison

to the *p*-cymene derivative **C2.2** which could still be observed in solution even after 24 hours. The formation of the proposed active species was observed for both immobilized catalysts **IC4.3** and **IC4.7** after 1 hour showing that the support indeed plays a valuable role during the reaction.

It was shown that the immobilization together with the nature of support material was responsible for the increase in activity when comparing the immobilized systems to their model counterparts. By capping the native silicas with HMDS a decrease in the conversion, although more pronounced for the MCM-41 system than for SBA-15 system, was observed. This led us to believe that the surface silanols are indeed interacting with the complex and/or the oxidant by potentially stabilizing it during the course of the reaction.

5.4   Experimental section

5.4.1   General remarks and instrumentation

All reactions were carried out in 100 mL round bottomed flasks sealed with silicone stoppers. CCl_4, CH_3CN and diethylether were obtained from Sigma Aldrich and dried over appropriate drying agents before use (CCl_4 was pre-distilled to rid solvent of any impurities). $IO(OH)_5$ was obtained from Sigma Aldrich and used without any further purification. Samples were analyzed by a Varian 3900 GC fitted with a polar Cyclosil-B column (30 m, 0.250 mm diam. and 0.25 μm film) using helium as carrier gas.

5.4.2   Typical procedure for the oxidative cleavage of alkenes: 1-octene

To model complex **C2.2** (7.5 mg, 0.0099 mmol) dissolved in a mixture of CCl_4 (5 mL) and CH_3CN (5 mL) was added 1-octene (0.313 mL, 1.994 mmol). Oxidant, $IO(OH)_5$ (2.280 g, 10.00 mmol) was dissolved in distilled water (10 mL) and added to the stirring yellow mixture in a 100 mL round bottomed flask which was sealed with a silicone stopper. This biphasic reaction mixture was allowed to stir for the required time at 23 °C after which the contents of the round bottomed flask was transferred to a separating funnel. The mixture was extracted with 3x10 mL dried diethylether and the organic layer allowed to dry over $MgSO_4$ before being sampled.

After the mixture was sampled (1 mL), *p*-xylene (0.100 mL) was added as the internal standard to be able to quantify the product formation. Conversions were determined by GC.

Chapter 5: Oxidative Cleavage of Selected Alkenes

5.5   References

1. B.C. Ranu, S. Bhadra, L. Adak, *Tetrahedron Lett.*, **2008**, 49, 2588.

2. T.K.M. Shing, B.M. Trost, I. Fleming, In Comprehensive Organic Synthesis, Pergamon Press: Oxford, **1991**; Vol. 7, 703.

3. C. Djerassi, R.R. Engle, *J. Am. Chem. Soc.*, **1963**, 75, 3838.

4. A. Behr, N. Tenhumberg, A. Wintzer, *RSC Adv.*, **2013**, 3, 172.

5. H.J. Carlsen, T. Katsuki, V.S. Martin, K.B. Sharpless, *J. Org. Chem.*, **1981**, 46, 3937.

6. K. Kaneda, S. Haruna, T. Imanaka, K. Kawamoto. *J. Chem. Soc. Chem. Commun.*, 1990, 1467.

7. S. Wolfe, S.K. Hasan, J.R. Campbell, *J. Chem. Soc. Chem. Commun.*, **1970**, 1420.

8. B. Huang, M. Khrapov, K.C. Hansen, J.P. Idoux, *Synth. Commun.*, **1995**, 25, 2709.

9. A.G.F. Shoair, R.H. Mohamed, *Synth. Commun.*, **2006**, 36, 59.

10. B.P. Sullivan, D.J. Salmon, T.J. Meyer, *Inorg. Chem.*, **1978**, 17, 3334.

11. W.P. Griffith, E. Kwong, *Synth. Commun.*, 2003, 33, 2945.

12. J. Dehand, J. Rosé, *J. Chem. Res.*, **1979**, 155

13. P. Spannring, P.C.A. Bruijnincx, B.M. Weckhuysen, R.J.M. Klein Gebbink, *RSC Adv.*, **2013**, 3, 6606.

14. G. Balavoine: C. Eskenazi, F. Meunier, H. Riviere, *Tetrahedron Lett.*, **1984**, 25, 3187.

15. A.J. Bailey, W.P. Griffith, A.J.P. White, D.J. Williams, *J. Chem. Soc. Chem. Commun.*, **1994**, 1833.

16. S. Cenini, F. Ragaini, Catalytic reductive carbonylation of organic nitro compounds, Springer Science & Business Media, **1996**, 19, 29.

17.   F. Goethals, E. Levrau, E. De Canck, M.R. Baklanov, C. Detavernier, I. Van Driessche, P. Van Der Voort, *Materials*, **2013**, *6*, 570.

18.   D. Yang, C. Zhang, *J. Org. Chem.*, **2001**, 66*, 4814.

19.   V. Kogan, M.M. Quintal, R. Neumann, *Org. Lett.*, **2005**, 7, 5039.

20.   V.A. Kumar, V. Prakash Reddy, R. Sridhar, B. Srinivas, K. Rama Rao, *Synlett.*, **2009**, 5, 739.

21.   M.Y. Suh, C.H. Lee, K.S. Choi, B.C. Song, Y.J. Park, W.H. Kim. Bull. *Korean Chem. Soc.*, **2002**, 23, 1819.

22.   G.L. Donald, M. van den Engh. *Can. J. Chem.*, **1972**, 50, 3129.

Chapter 6: Transfer Hydrogenation of Selected Ketones

6.1 Introduction

The reduction of aldehydes and ketones to afford corresponding primary and secondary alcohols through transfer hydrogenation has extensively been studied over the past decade [1-6]. Compared to normal reduction reactions which necessitate the use of high hydrogen pressure or dangerous reducing agents, transfer hydrogenation reactions require milder reaction conditions and offer a more environmentally friendly and selective alternative [7]. Ruthenium catalysts have shown favorable reactivity and selectivity towards the reduction of polar bonds and have even been found to exceed the performance of traditional hydrogenation catalysts based on rhodium and iridium [8-12].

Cadierno *et al.* described ruthenium(II) complexes containing hemilabile iminophosphorane-phosphine ligands which were found to be very active catalysts for the transfer hydrogenation of cyclohexanone using *i*-PrOH as hydrogen source (Scheme 6.1) [13]. They investigated the influence of the arene ring on the activity of the catalyst by varying the arene from benzene and *p*-cymene to 1,3,5-trimethylbenzene and hexamethylbenzene. Yields for cyclohexanol were found to be 22-99 % for complexes **24a-f**.

complex	arene
24a	C_6H_6
24b	$1\text{-}^{i}Pr\text{-}4\text{-}C_6H_4Me$
24c	$1,3,5\text{-}C_6H_3Me_3$
24d	$1,2,3,4\text{-}C_4H_2Me_4$
24e	$1,2,4,5\text{-}C_6H_2Me_2$
24f	C_6Me_6

24a-f
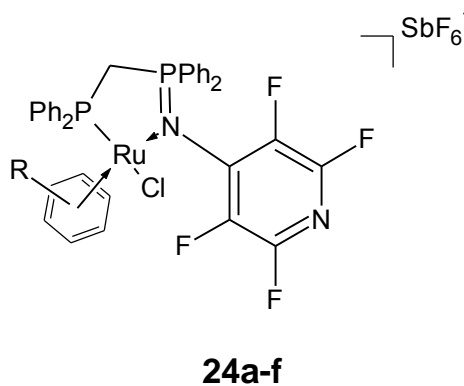
Scheme 6.1 (η^6-arene)-Ruthenium(II) complexes containing the iminophospharane-phosphine ligand, $Ph_2PCH_2P(=N\text{-}p\text{-}C_5F_4N)Ph_2$ [13].

Chapter 6: Transfer Hydrogenation of Selected Ketones

The proposed mechanism for the reaction is shown in Scheme 6.2 below. This is the generally accepted mechanism for transfer hydrogenation facilitated by a ruthenium hydride species which is formed from the hydrogen source, in this case *i*-PrOH. It has been shown that the catalytic activity remained unaffected by the presence of free arene (250 fold excess) or free iminophospharane-phosphine ligand. It was concluded that the active species could not arise as a result of the dissociation of these ligands from the catalytic precursors and therefore supported the proposed catalytic cycle [13].
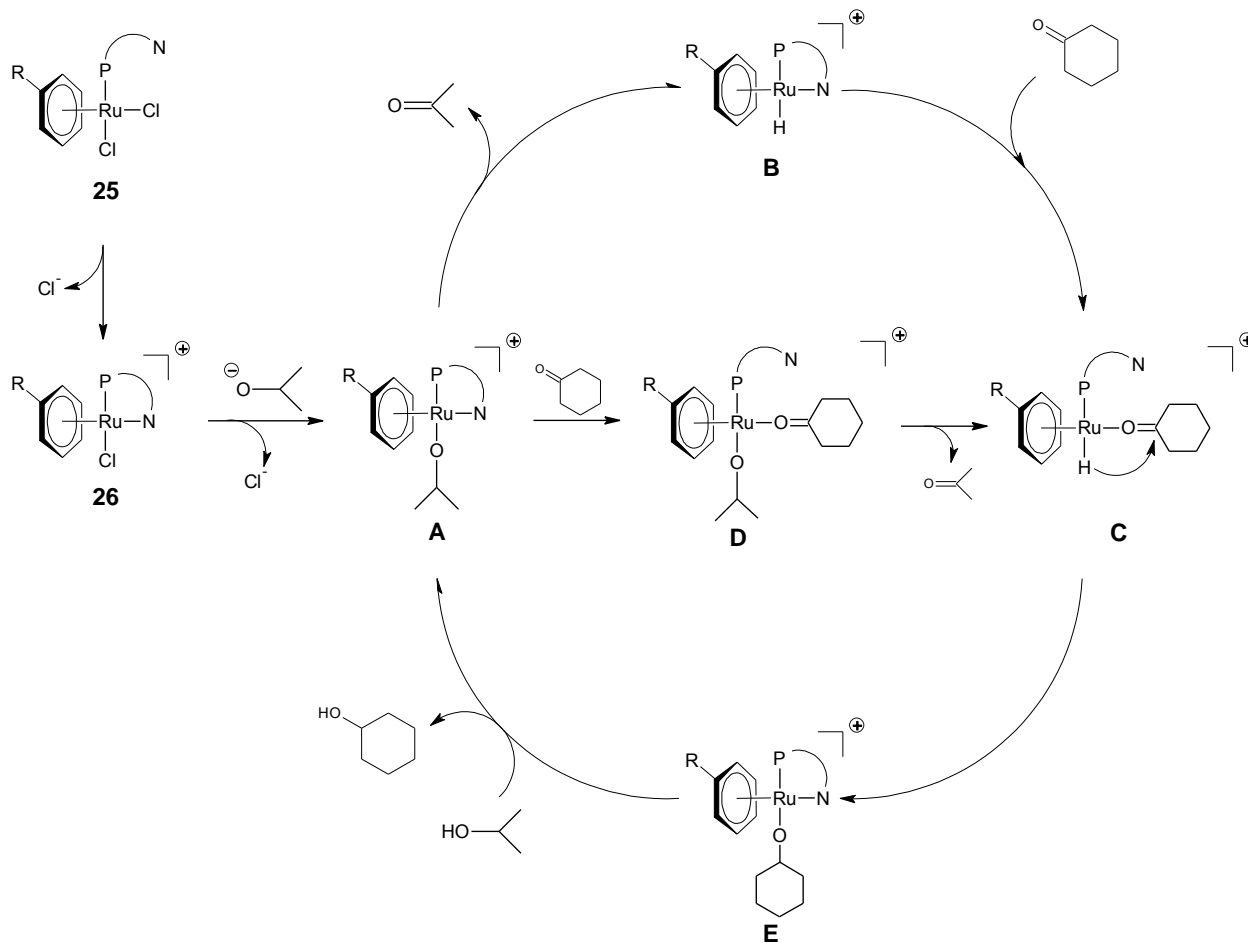
Scheme 6.2   Cadierno *et al.*'s proposed catalytic cycle for the transfer hydrogenation of cyclohexanone [13].

Chapter 6: Transfer Hydrogenation of Selected Ketones

Standfest-Hauser *et al.* carried out a similar investigation on half-sandwich Ru(II) aminophosphine complexes and showed that the mechanism can occur through the dissociation of the Ru-N bond affording an open coordination site. It has previously been shown that β-elimination could involve ring slippage as shown in Scheme 6.3 [14]. It was proposed that either Ru-N bond cleavage or η^5 to η^3 ring slippage can take place to allow the formation of species **E**.
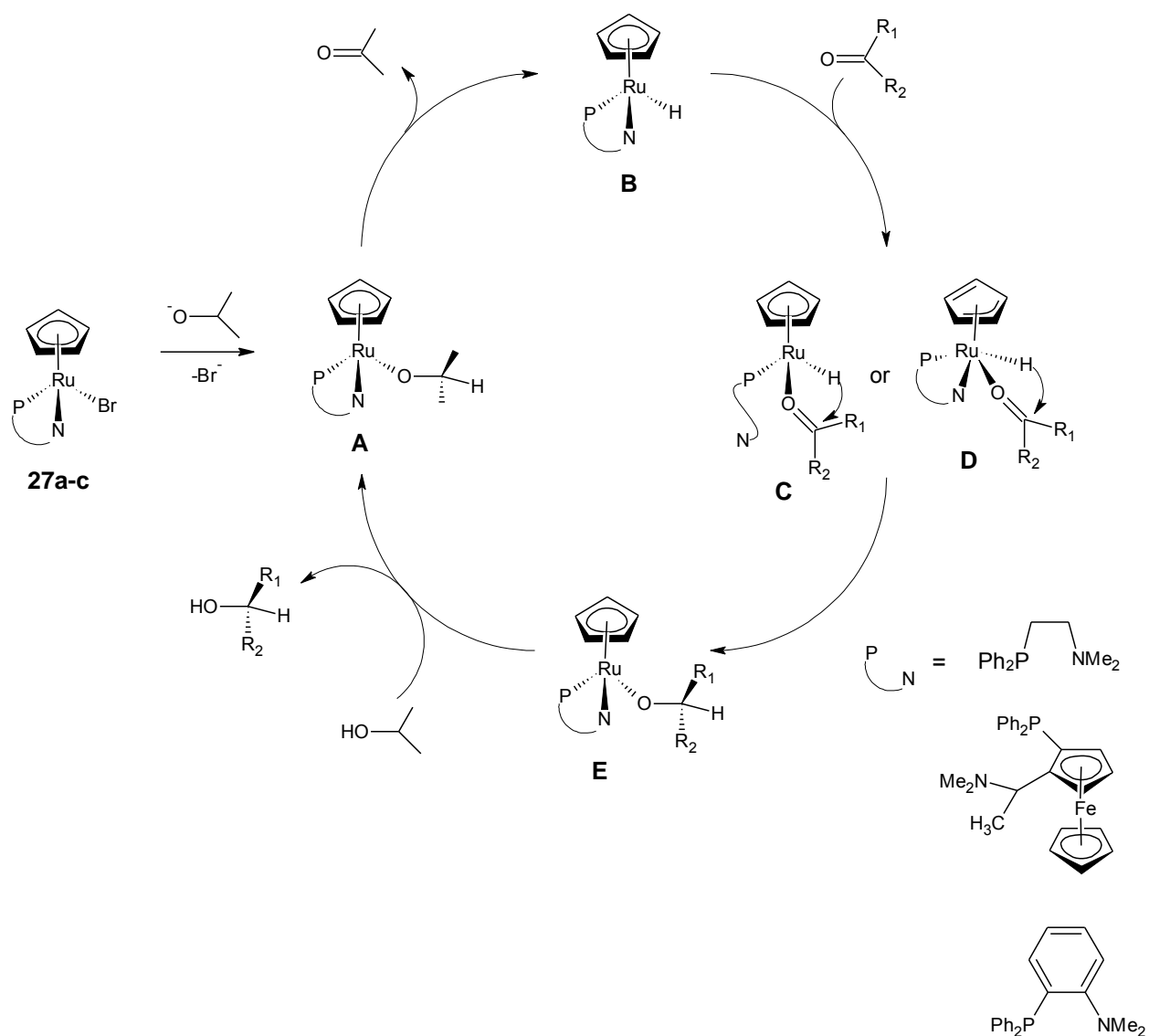
Scheme 6.3   A reasonable mechanism for the transfer hydrogenation of ketones as proposed by Standfest-Hauser *et al.* [15].

It was concluded that for this system the most likely scenario would be the Ru-N bond cleavage since these diastereopure systems were not enantioselective in the hydrogenation of any of their chosen substrates excluding the formation of intermediate **D** through ring slippage [15].

6.2   General procedure for transfer hydrogenation of ketones

A typical reaction involved charging of a reaction tube with the appropriate amount of catalyst dissolved in *i*-PrOH (hydrogen source) followed by the addition of base and substrate. It was imperative that the tubes be flushed with nitrogen to remove oxygen to reduce the possibility of oxidation during the reaction.   The base-line reaction conditions were adopted from work reported by Zhao *et al.* and a general reaction for the transfer hydrogenation of acetophenone is shown is Scheme 6.4 [16].
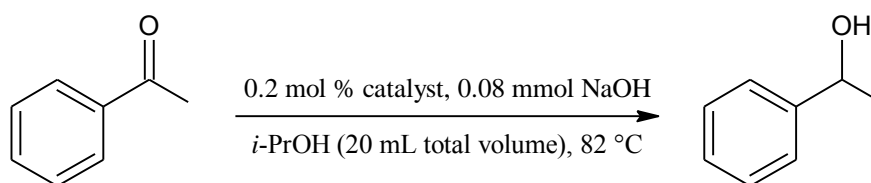
Scheme 6.4 A general procedure for the transfer hydrogenation of acetophenone (2 mmol).

6.2.1 Model complexes (C1I-C3I, C1-C3) and immobilized catalysts (IC1-IC6) employed in transfer hydrogenation reactions

Model complexes **C1I-C3I** (hexafluorophosphate derivatives) and **C1-C3** (tetraphenylborate derivatives) as well as their immobilized counterparts **IC1-IC6** were tested as catalyst precursors for the transfer hydrogenation of acetophenone. The exact metal loading of immobilized systems was previously determined by ICP-OES allowing direct comparison between the model and immobilized systems at the same metal concentration. A summary of all the systems employed are shown in Figure 6.1.

C2.1I; R$_1$ = H, X$^-$ = PF$_6^-$
C2.2I; R$_1$ = CH$_3$, X$^-$ = PF$_6^-$
C2.3I; Quinoline, X$^-$ = PF$_6^-$
C2.1; R$_1$ = H, X$^-$ = B(Ph)$_4^-$
C2.2; R$_1$ = CH$_3$, X$^-$ = B(Ph)$_4^-$
C2.3; Quinoline, X$^-$ = B(Ph)$_4^-$

IC4.1; P-MCM-41
IC4.2; P-SBA-15
IC4.3; MP-MCM-41
IC4.4; MP-SBA-15
IC4.5; Q-MCM-41
IC4.6; Q-SBA-15
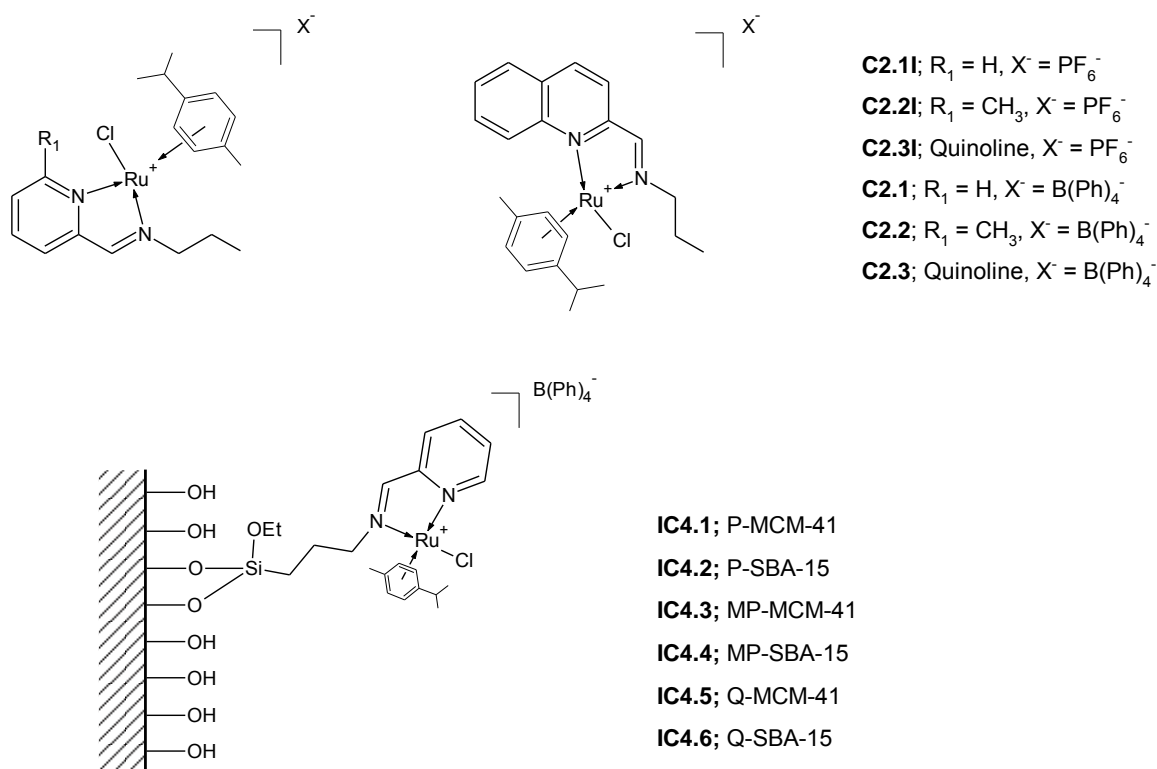
Figure 6.1 Model complexes and immobilized catalysts employed as catalysts for transfer hydrogenation of ketones.

6.2.2 Evaluation of standard reaction conditions

Using the reaction condition reported by Zhao and his group the optimization of our system was attempted [16]. A typical reaction involved the addition of the appropriate catalyst (0.2 mol %) to a reaction vessel flushed with nitrogen. This was followed by the addition of dry 2-propanol (9 mL) and NaOH (0.08 mmol; 0.8 mL of 0.1 M solution) to the reaction tubes. The reaction tubes were sealed with a screw on top with a silicone septum and allowed to warm to the required temperature (82 °C). After the reaction temperature stabilized acetophenone (0.233 mL, 2.0 mmol) was added via syringe through the silicone septum and the nitrogen feed closed off on the tube cap. After the allotted time the tubes were submersed in an ice bath to allow them to cool to room temperature and sampled.   Conversion was calculated by monitoring 1-phenylethanol formation.

Chapter 6: Transfer Hydrogenation of Selected Ketones

The three model complexes **C2.1**-**C2.3** were employed as catalysts under the reaction conditions reported by Zhao *et al*. with the only modification being the use of 10 mL 2-propanol instead of the reported 20 mL. The effect of solvent volume on the amount of product that formed was investigated and it was observed that changing the reaction volume in the range 5-20 mL did not result in any significant change in the yield of 1-phenylethanol which resulted in the selection of 10 mL total volume for all further reactions. Under these reaction conditions it was found that the model methyl-pyridine derivative **C2.2** showed the highest activity in the transfer hydrogenation of acetophenone when compared to the other model derivatives **C2.1** and **C2.3** (Entries 1-3, Table 6.1). All further optimization reactions were thus carried out with complex **C2.2**. By changing the base from NaOH to KOH, Entry 4, an increase in the conversion from 49 % to 65 % was observed and by increasing the reaction time from 3 h to 6 h the conversion could be further increased to a very respectable 93 %. This increased activity when carrying out the reaction in KOH as base could possibly be ascribed to the increased solubility shown by KOH in 2-propanol when compared to NaOH.

To investigate the effect of temperature on the activity of the catalyst, the temperature was lowered to 50 and 25 ˚C respectively (Entry 5) which resulted in a dramatic decrease in the activity of the catalyst with almost no conversion to 1-phenylethanol being observed at these lower temperatures.

It has been reported that this catalytic transformation can occur without the addition of any base, but it was found that without the presence of base (Entry 7) very little activity was observed, even after allowing the reaction to continue for 24 h. It was also very important to evaluate the activity of the [RuCl$_2$(*p*-cymene)]$_2$ precursor (Ru-dimer) to verify that the coordination of the diimine ligand to form the complex indeed had a positive effect on the activity of the catalyst. It was observed that the Ru-dimer had a much lower activity with a conversion of only 17 % after 6 h being obtained (Entry 8). In the absence of catalyst, no conversion of acetophenone was observed (Entry 6).

No real difference in the activity of the catalyst was observed when substituting KOH for *t*-BuOK (Figure 6.2). KOH was thus chosen as base for all further reactions.

Table 6.1 Summary of optimization reactions for the transfer hydrogenation of acetophenone to 1-phenhylethanol with model complexes C2.1-C2.3 (tetraphenylborate derivatives).

Entry	Catalyst	Catalyst Loading (mol %)	Base (mmol)	Substrate (mmol)	Reaction Volume (mL)	Temp. (°C)	Time (h)	Conversion (%)
1	**C2.1** (Pyridine)	0.2	0.08 (NaOH)	2.0	10	82	3	15
2	**C2.2** (Methyl-pyridine)	0.2	0.08 (NaOH)	2.0	10	82	3	49
3	**C2.3** (Quinoline)	0.2	0.08 (NaOH)	2.0	10	82	3	20
4	**C2.2**	0.2	0.08 (KOH)	2.0	10	82	3	65
							6	93
5	**C2.2**	0.2	0.08 (KOH)	2.0	10	25	3	1.8
						50	6	2.7
6	-	-	0.08 (KOH)	2.0	10	82	3	0
7	**C2.2**	0.2	-	2.0	10	82	3	1.5
							24	1.8
8	[RuCl$_2$(p-cymene)]$_2$	0.2	0.08 (KOH)	2.0	10	82	6	17

Chapter 6: Transfer Hydrogenation of Selected Ketones
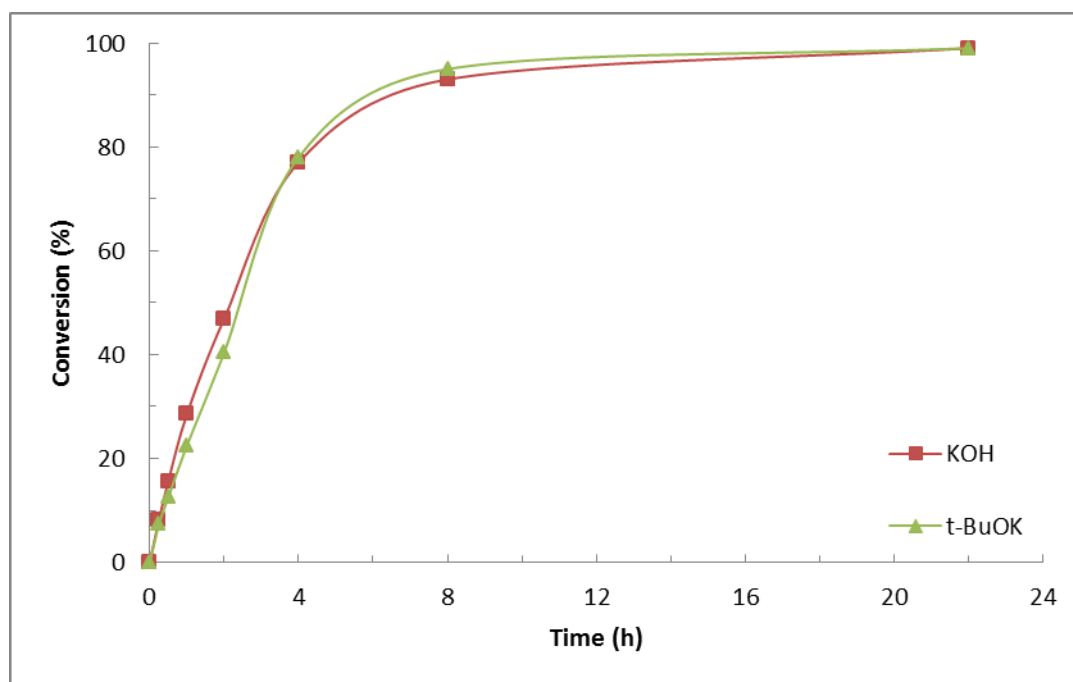
Figure 6.2 Effect of a different base on the activity of model complex C2.2.

6.2.3 Effect of the catalyst:substrate:base (C:S:B) ratio on acetophenone conversion using model complex C2.2

The effect of different reaction parameters such as catalyst loading and the nature of base and substrate amount were investigated and the results are summarized in Figure 6.3. The reaction conditions that were chosen for this investigation were: *i*-PrOH (10 mL total solvent volume), 82 ˚C, 6 h, model complex **C2.2** and acetophenone. Varying the catalyst loading from 0.1-0.3 mol % did not have any significant effect on the amount of product obtained but it was seen that 0.2 mol % was indeed the optimum metal loading under these reaction conditions. By keeping the metal loading at 0.2 mol % the substrate amount was varied from 1.2-2.6 mmol with no real difference in the conversion between 1.2 mmol and 2.0 mmol of substrate being observed. The substrate amount of 2.0 mmol was chosen and the base amount (KOH) varied between 0.04 mmol and 0.16 mmol. An amount of 0.08 mmol KOH, as reported by Zhao *et al.*, was found to be the optimum amount for this reaction. The optimum catalyst:substrate:base (**C:S:B**) ratio was found to be 1:300:20 but because there was no real difference in the activity when using 1.2 or 2.0 mmol substrate, the chosen ratio was 1:500:20 for further reactions.
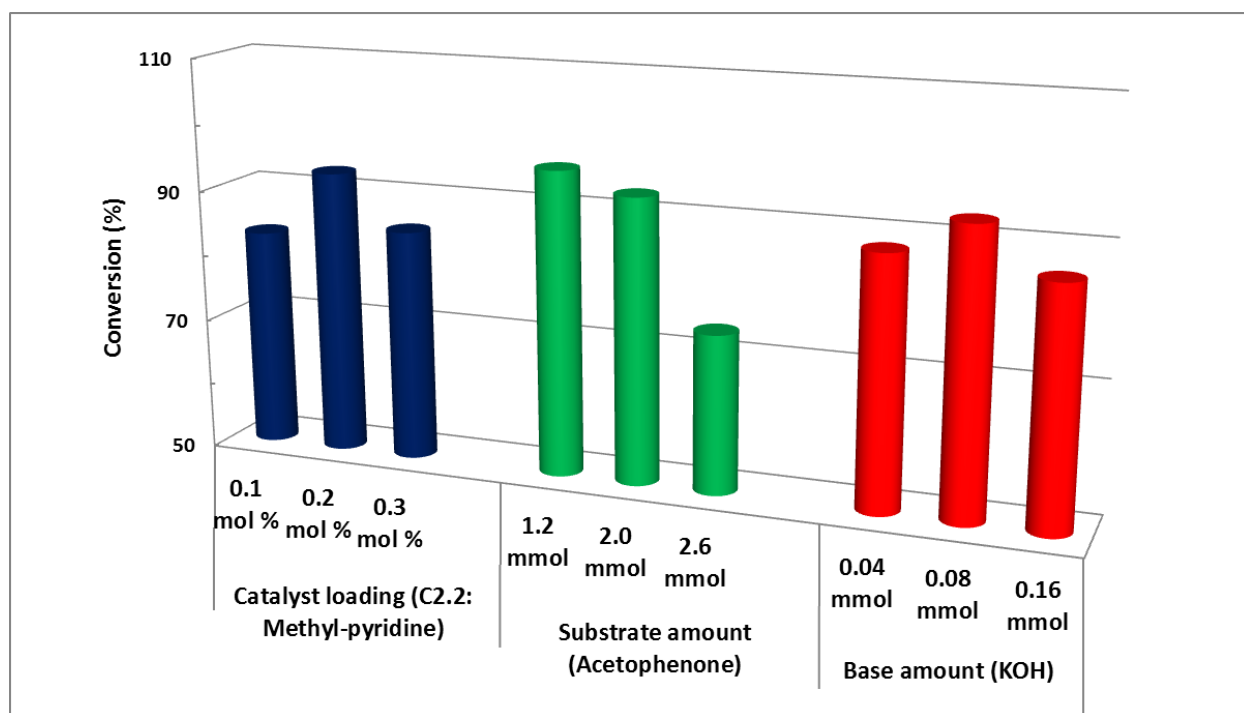
Figure 6.3 Summary of acetophenone conversion by varying catalyst:substrate:base ratios.

6.2.4 Timed reactions over 6 h: model complexes C2.1-C2.3 (C:S:B ratio of 1:500:20)

Model complex **C2.2** showed a higher overall activity after 3 hours when compared to the other two derivatives **C2.1** and **C2.3** using NaOH as base. However a different trend was observed when the base is changed to KOH as shown in Figure 6.4. After 3 hours the methyl-pyridine complex **C2.2** showed the lowest conversion of acetophenone to 1-phenylethanol when compared with the pyridine and quinoline derivatives **C2.1** and **C2.3** (64 % compared to 80 and 78 % respectively). After this time however the conversion for complex **C2.2** was still increasing reaching more than 90 % after 6 hours with activity for complexes **C2.1** and **C2.3** leveling off without any significant increase in activity being observed after 6 hours. After prolonged reaction times (24 h) the reaction catalyzed by complex **C2.2** went to completion with complexes **C2.1** and **C2.3** reaching a peak at around 80 %. The only explanation for this observation is that complex **C2.2** must be more stable under these reaction conditions. For complexes **C2.1** and **C2.3** no increase in the amount of 1-phenylethanol is observed after 3 hours

Chapter 6: Transfer Hydrogenation of Selected Ketones

which leads one to suspect that these complexes decompose and could thus not catalyze the reaction any further.
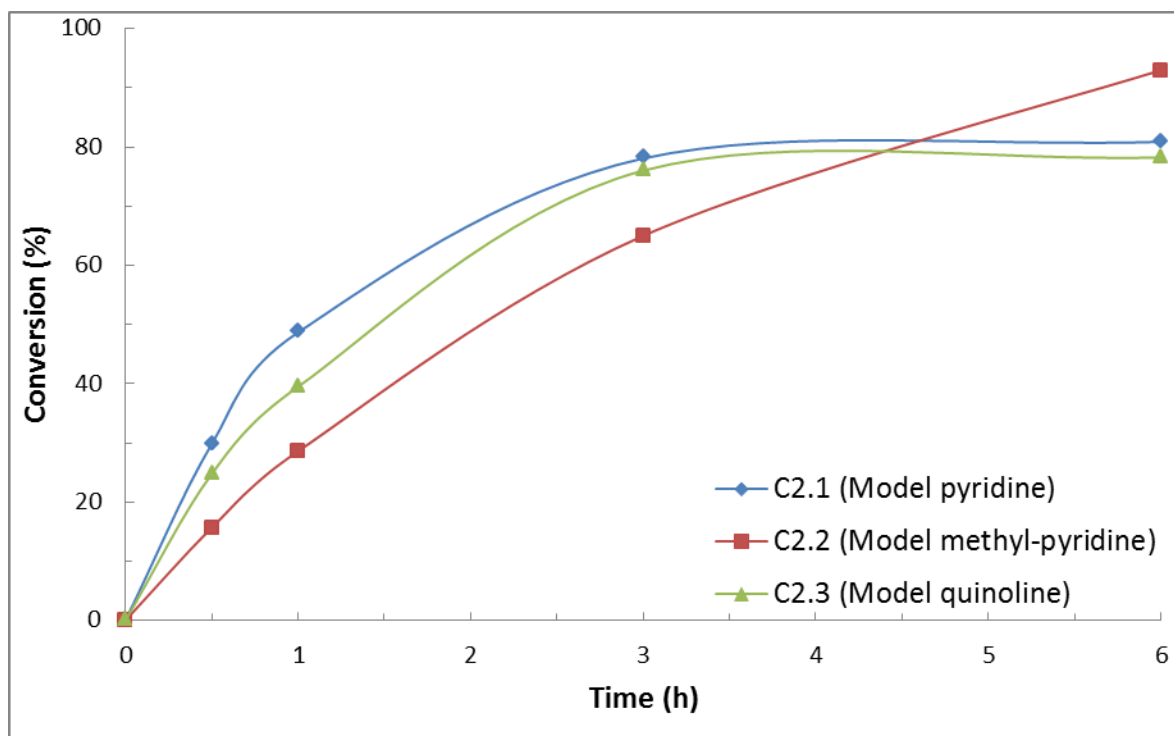
Figure 6.4 Activity of model derivatives C2.1-C2.3 over time using KOH as base (0.08mmol) and acetophenone as substrate (2 mmol).

6.2.5 Effect of a different counter-ion on the activity of the model complexes C2.1-C2.3

The hexafluorophosphate derivatives (**C2.1I**-**C2.3I**) were initially the target molecules but after unsuccessful synthesis of their siloxane functionalized derivatives it was decided to change to the larger, more stable tetraphenylborate derivative. The activity of these complexes was compared to that of model complexes **C2.1-C2.3** (tetraphenylborate derivatives) and the results are shown in Figure 6.5. These reactions were carried out under the same reaction conditions as stated earlier: 82 °C over 6 hours using 2 mmol substrate with a **C:S:B** ratio of 1:500:20.

It can be clearly seen that the hexafluorophosphate derivatives show a decreased activity towards the transfer hydrogenation of acetophenone when compared to their tetraphenylborate derivatives. The most dramatic decrease was seen for the quinoline derivative with a drop in conversion from 80 % for complex **C2.3** to around 20 % for the hexafluorophosphate complex **C2.3I**. This decrease in conversion for reactions using hexafluorophosphate complexes as catalysts can possibly be ascribed to the decreased solubility of these derivatives in *i*-PrOH compared to their tetraphenylborate counterparts.
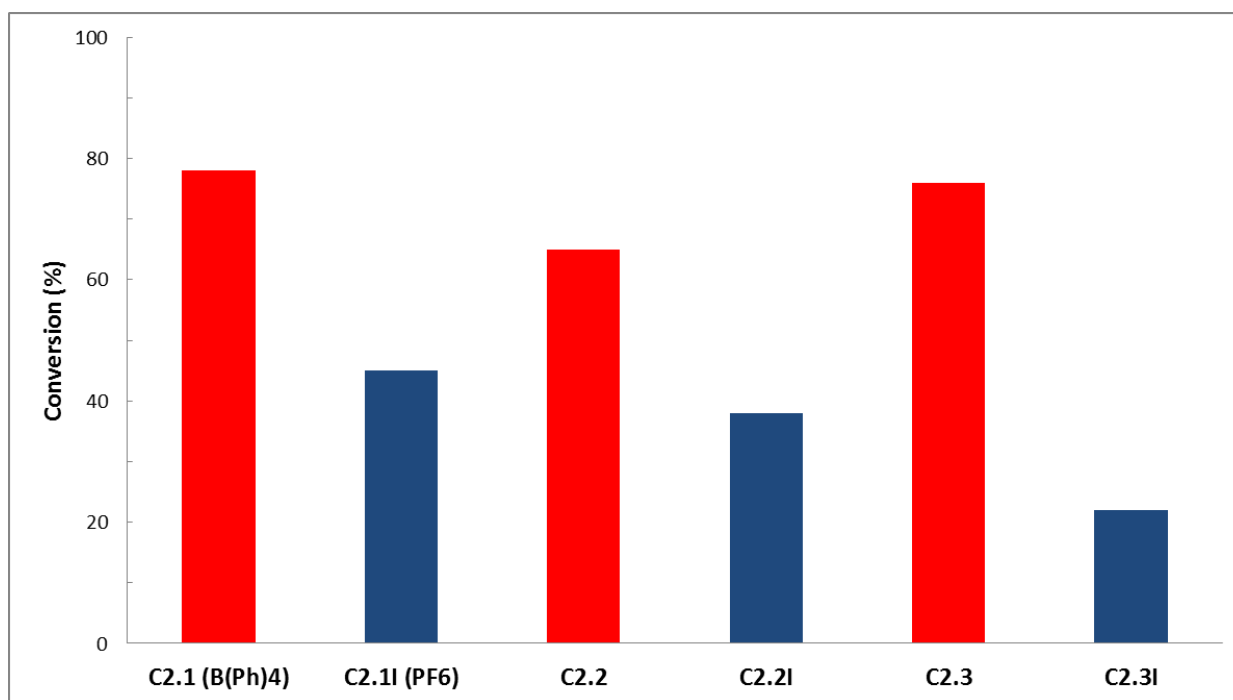
Figure 6.5 The effect of different counter-ions on the conversion of acetophenone.

Another factor to take into account could be the relative stability of these complexes (hexafluorophosphate vs. tetraphenylborate). The synthesis of the siloxane functionalized Ru(*p*-cymene)(N,N) complexes with hexafluorophosphate as counter-ion was not successful (discussed in Chapter 2). Substitution with tetraphenylborate as counter-ion however allowed for the isolation of very stable solids in high yields (functionalized complexes **C2.4**-**C2.6**). This

increased stability that is instilled when tetraphenylborate is used as counter-ion could explain why there is such a dramatic difference in the activity of these model complexes.

6.2.6 Activity of model complexes C2.1-C2.3 towards the transfer hydrogenation of other ketones

The activity of the model complexes **C2.1-C2.3** towards the transfer hydrogenation of other ketones were investigated and are shown in Table 6.2. Fairly good conversions over the 6 h period were observed for all the derivatives with the methyl-pyridine derivative **C2.2** in general showing the highest catalytic activity.
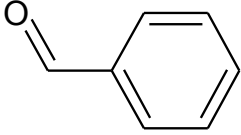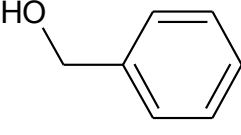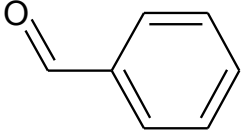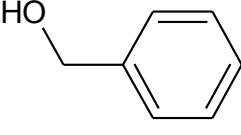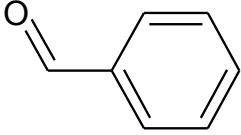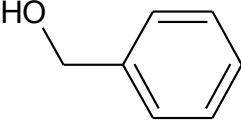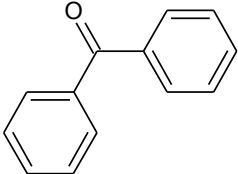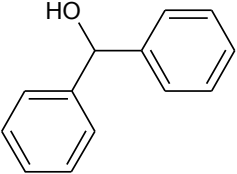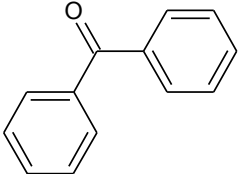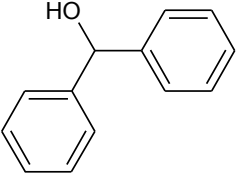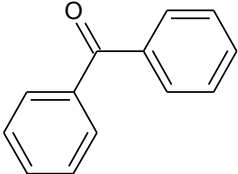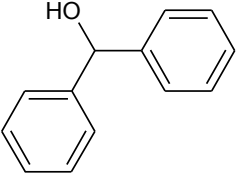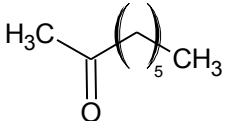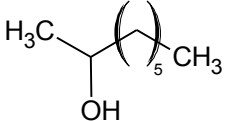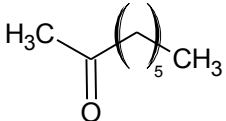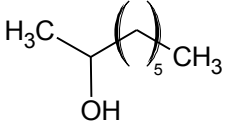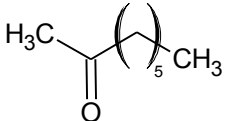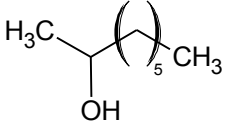
Increased steric bulk around the ketone (Entries 4-6, benzophenone) did not have any significant influence on the activity of the catalysts with similar conversions being observed as was observed when acetophenone was used as the substrate. A slight drop in activity was observed for the transfer hydrogenation of 2-octanone though with conversions of 70-76 % being observed (Entries 7-9).   Throughout the highest conversion were observed for the methyl-pyridine derivative **C2.2**.

6.2.7 Influence of addition sequence of base and substrate on the activity of catalyst C2.2 towards the transfer hydrogenation of acetophenone

The effect of the sequence of addition of the substrate and base was investigated and is shown in Figure 6.6. Three different sequences are examined where either both the base and acetophenone (substrate) were added at 25 ˚C and heated to 82 ˚C (sequence 1) or both KOH and acetophenone was added at 82 ˚C (sequence 2). For sequence 3, KOH was added at 25 ˚C followed by the substrate at 82 ˚C. All reactions was stopped after 3 hours and employed a **C:S:B** ratio of 1:500:20 (0.004:2.0:0.08 mmol).

Table 6.2 Transfer hydrogenation of different ketones catalyzed by model complexes C2.1-C2.3[a]

Entry	Catalyst	Substrate (ketone)	Product (alcohol)	Conversion (%)
1	**C2.1** (pyridine)			81
2	**C2.2** (methyl-pyridine)			93
3	**C2.3** (quinoline)			78
4	**C2.1**			85
5	**C2.2**			88
6	**C2.3**			83
7	**C2.1**			76
8	**C2.2**			76
9	**C2.3**			70

[a] Conditions: reactions were carried out at 82 ˚C over 6 hours using 2 mmol substrate. **C:S:B** ratio of 1:500:20 used for all reactions

Sequence 1: When both the substrate and base was added at 25 ˚C (keep in mind the time was started when both the substrate and base was introduced and heating started) the initial rate of the reaction was very slow. This is as expected especially when compared to reactions that previously showed conversions of only 2 % and 3 % at 25 ˚C and 50 ˚C respectively. A steep increase in the conversion is observed between 30 min and 1 h when the reaction temperature reached around 80 ˚C with the conversion increasing from 11 % to 55 % respectively. From there it steadily increased to reach complete conversion after only 3 hours. This addition

Chapter 6: Transfer Hydrogenation of Selected Ketones

sequence emphasized the importance of the reaction temperature to achieve maximum conversion of acetophenone.

Sequence 2: For this addition sequence both the substrate and base were added at 82 °C and stirred for the required length of time. A dramatic difference in the activity was observed when comparing to the addition sequence 1 with the conversion reaching 83 % after 30 min compared to the meager 11 % obtained for sequence 1 after the same time. After 3 hours a conversion of nearly 100 % could be observed.

Sequence 3: Until now all reactions were carried out by following the method reported by Zhao and co-workers.[32] This sequence involves the addition of the base at 25 °C after the addition of the catalyst and proton source (*i*-PrOH). At 82 °C the substrate is introduced and the reaction continued for the allotted time. The initial activity (at time less than 1 h) is higher when compared to addition sequence 1. At time 1 h the conversions for the various sequences are as follows: sequence 1 - 55 %, sequence 2 - 89 % and sequence 3 - 60 %. Although the conversion after 3 hours is still increasing, it is still significantly lower when compared to the other two sequences at the same time.

Sun *et al.* showed that the order of addition of substrate and base played a significant role in the activity of their rhodium catalyst [17]. An increased activity towards the transfer hydrogenation of acetophenone was observed when the base was introduced after the addition of the substrate to the reaction mixture (acetophenone and rhodium complex stirred in *i*-PrOH for 30 min before the addition of sodium isopropoxide). These reactions were carried out at room temperature and the addition sequence was shown not to have any effect on the ee (enantiomeric excess) of the formed products. They proposed that the activity of the catalyst would decrease even more the longer the catalyst was in contact with the base in the absence of substrate.

Chapter 6: Transfer Hydrogenation of Selected Ketones
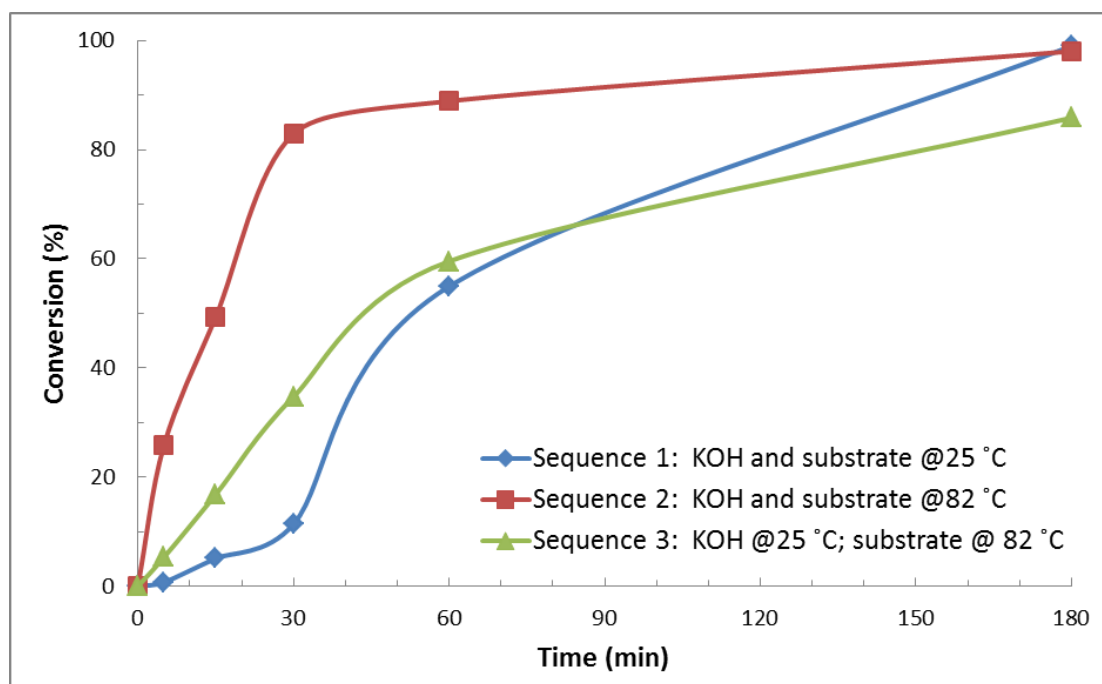
Figure 6.6 The effect of the order of addition of substrate and base on the activity of the catalyst C2.2.

To confirm this statement an experiment was set up to investigate the effect of the "contact time" between the catalyst and base (KOH in our case) in the absence of substrate (acetophenone) with the result shown in Figure 6.7. Four different reactions were set up with contact times of 0, 30, 60 and 120 min before the substrate was added to the reaction mixture and then allowed to stir for a further 60 min. A **C:S:B** ratio of 1:500:20 was chosen for this study with complex **C2.2** as catalyst. The reactions were carried out at 82 ˚C under nitrogen atmosphere in a total solvent volume of 10 mL.

At time 0 min, with base and substrate being added together at 82 ˚C, a very good conversion of almost 80 % was obtained under these reaction conditions. When allowing the catalyst to be stirred in the presence of base and absence of substrate for 30 minutes, a dramatic decrease in the conversion of acetophenone to 1-phenylethanol from almost 80 % to around 42 % was observed.

Chapter 6: Transfer Hydrogenation of Selected Ketones
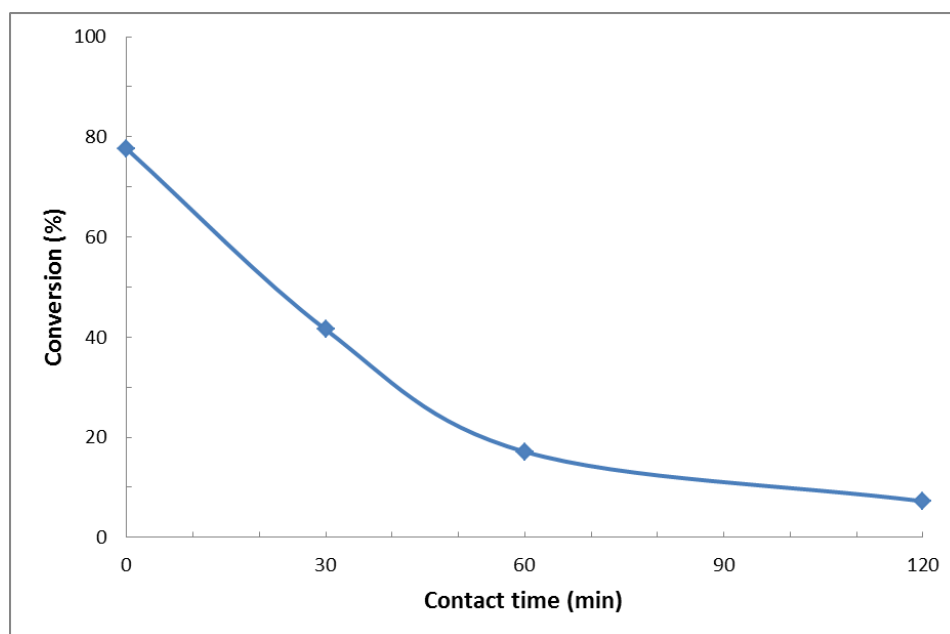
Figure 6.7 Effect of contact time between catalyst C2.2 and KOH before the addition of acetophenone (conversion calculated 1 hour after addition of substrate).

An even greater decrease in the activity of the catalyst was observed when the contact time was increased to 1 and 2 hours with conversions of 18 and 10 % being obtained respectively. Both Sun and Gladiali *et al*. reported an increase in the conversion when adding the base after the substrate is introduced. A decreased activity was observed when adding the base before the substrate and was attributed to other competitive side reactions taking place when following this sequence of addition. These included the dimerization of their $[Rh(N,N)_2]^+Cl^-$ catalyst precursor (forming $[Rh(N,N)_2]_2^{2+}$) and the transfer of the outersphere chloride to the inner coordination sphere to afford the neutral pentacoordinate complex $[Rh(N,N)_2Cl]$. This dimer and neutral complex are inactive as catalysts and limit the amount of the active rhodium species available for catalysis.

An alternative and possibly more probable explanation proposed by these authors was the potential coordination of the isopropoxide (base in excess) to the rhodium center after the formation of the proposed active rhodium-hydride species. This would result in a decreased ability of the acetophenone to coordinate to the catalyst. Although our catalyst is a ruthenium

Chapter 6: Transfer Hydrogenation of Selected Ketones

system and the reaction is performed at a higher temperature, this could possibly explain why such a significant difference between sequence 1 and sequence 3 is observed. It is possible that a stable, unreactive base-coordinated form of the ruthenium catalyst is generated when the catalyst is in the presence of base but in the absence of any substrate. This then blocks the possible active site for coordination of the acetophenone and decreases the amount of active catalyst available for the catalytic cycle in return decreasing the conversion.

6.2.8 Activity of immobilized catalysts IC4.1-IC4.6 in the transfer hydrogenation of acetophenone

Immobilized catalysts **IC4.1-IC4.6** were employed as catalysts for the transfer hydrogenation of acetophenone (Figure 6.8). Reaction conditions for these reactions were as follows: **C:S:B** ratio of 1:500:20, 82 ˚C, 24 h.
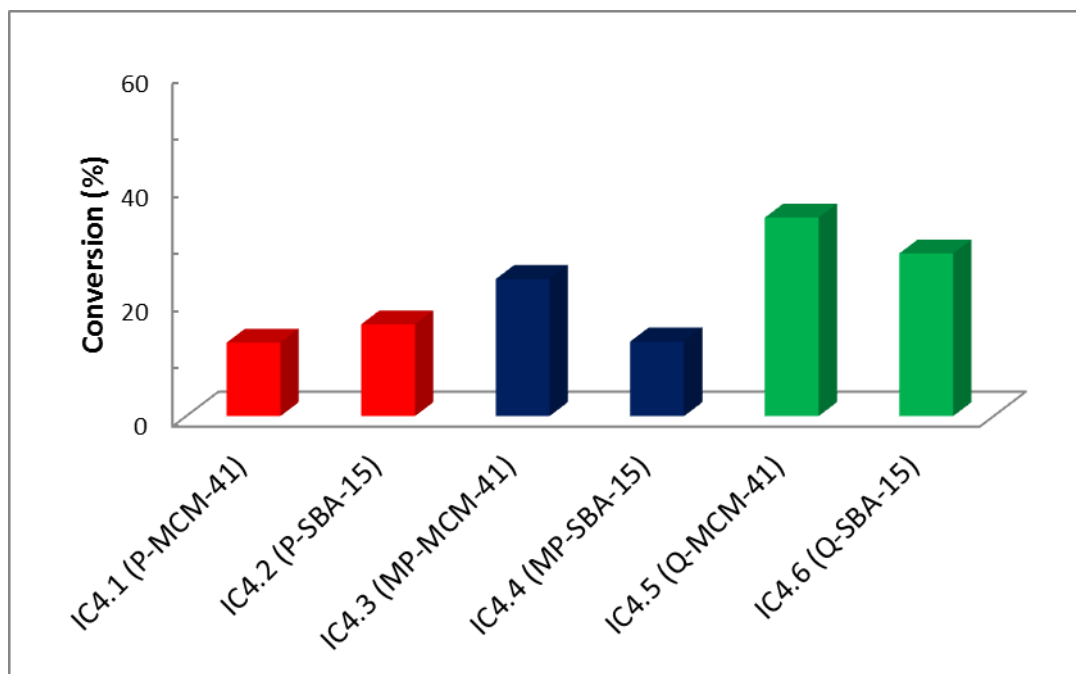
Figure 6.8   Activity of immobilized catalysts IC4.1-IC4.6 towards the transfer hydrogenation of acetophenone.

Chapter 6: Transfer Hydrogenation of Selected Ketones

Initially very low conversions were obtained after the 24 h period for the immobilized catalysts **IC4.1-IC4.6** when compared to their model derivatives **C2.1-C2.3** which over this period would have reached complete conversion. The highest conversion was observed for immobilized catalysts **IC4.3** and **IC4.6** with conversion of 35 % and 28 % respectively. The methyl-pyridine derivative supported on MCM-41 and SBA-15 (**IC4.2 and IC4.5**), which were found to be the most active of the three model systems, could only achieve conversions of 24 % and 13 % respectively. These lower than expected conversions were ascribed to possible mass transfer problems associated with the use of heterogeneous systems. To try and understand why the immobilized systems showed such decreased activity when compared to the model systems, the recyclability of these systems was attempted. The catalyst from the first run was separated from the reaction mixture by filtration and washed with small amounts of *i*-PrOH to remove any substrate or product left over from the previous run. Upon recycling of these catalysts however a general increase in the activity was observed when compared to run 1 (except for **IC4.3**) and this is shown in Figure 6.9.

Conversions of acetophenone to 1-phenylethanol upwards of 50 % could be achieved for runs 2 and 3. The dramatic increase in the activity of run 2 compared to run 1 can possibly be explained by taking a closer look at a possible mechanism of this reaction. If one assumes the reaction follows the classical ruthenium hydride (Ru-H) mechanism one can deduce that after the first run a certain amount of Ru-H species is already present in the catalyst. This would mean that the catalyst precursor would not have to first be transformed into the Ru-H intermediate, which is proposed to be an active species in the mechanism. This would decrease the so called induction period resulting in an increased conversion. A general decrease in the conversion was observed after run 3 with very little activity being observed when the catalyst was tested for a 4th recycling run. This very low conversion for run 4 was possibly due the catalyst being totally deactivated after the 4th run under these reaction conditions.

Visual leaching of the catalyst was observed after run 2 and 3 with the reaction mixture (being relatively clear after run 1) turning a darkish brown color as can be seen in Figure 6.10.
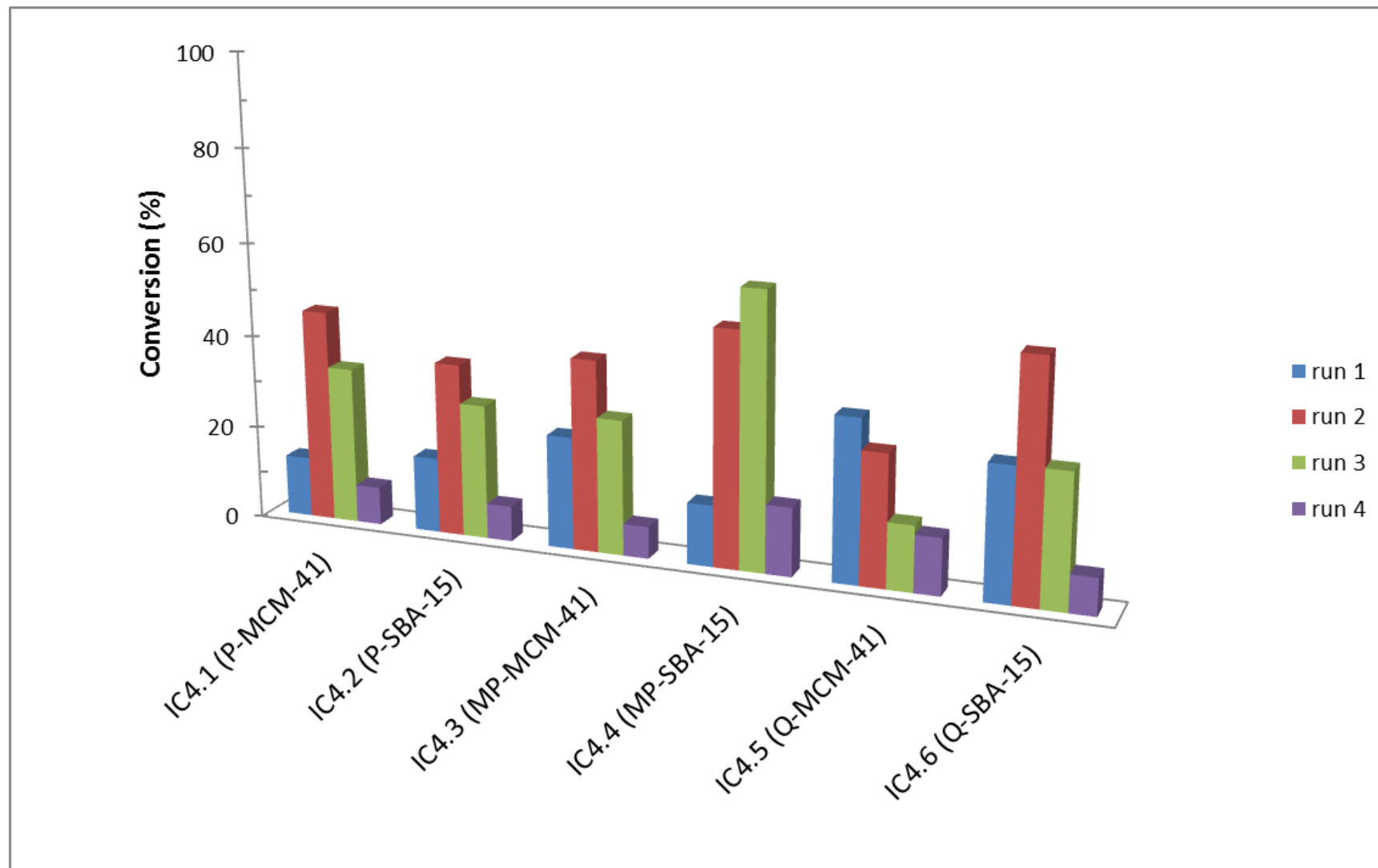
Figure 6.9 Recyclability of immobilized systems IC4.1-IC4.6 (4 runs)
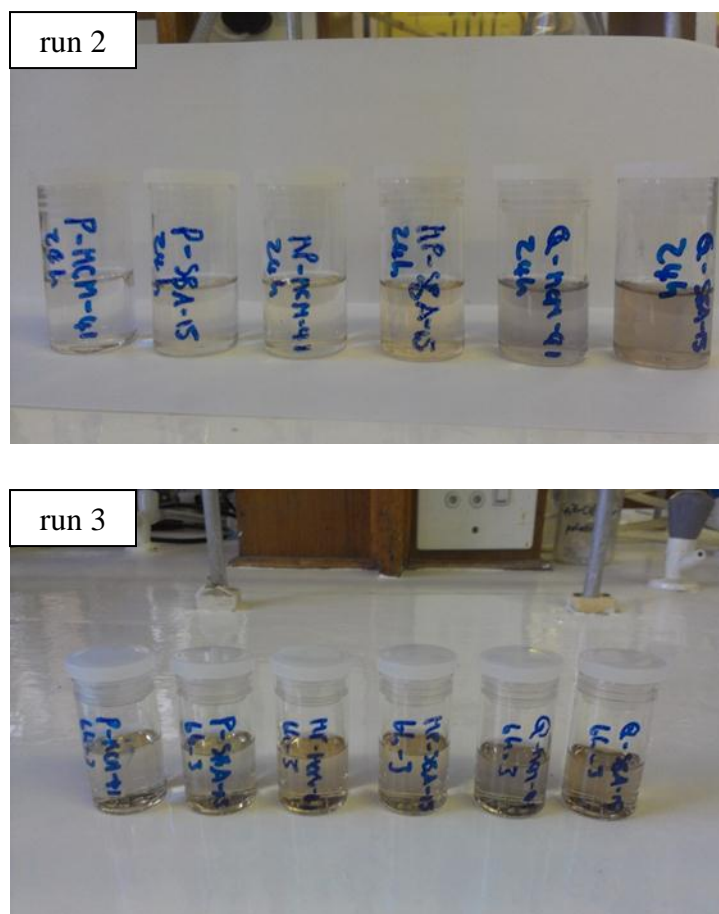
Figure 6.10 Leaching of immobilized catalysts IC4.1-IC4.6 after 2 and 3 runs respectively.

6.2.9 Possible mechanism

If the reaction follows the conventional mechanism as previously discussed then a ruthenium hydride species must be formed. By combining the two previously discussed mechanisms a proposed mechanism for the transfer hydrogenation of acetophenone with complex **C2.1** is shown in Scheme 6.5. Based on literature evidence it can be assumed that Cl⁻ dissociation takes place and is usually favored in polar solvents such as *i*-PrOH. The generally accepted active species during the reaction is the isopropoxide complex **A** which can be readily formed when the alkoxide anion attacks the metal center.

Chapter 6: Transfer Hydrogenation of Selected Ketones
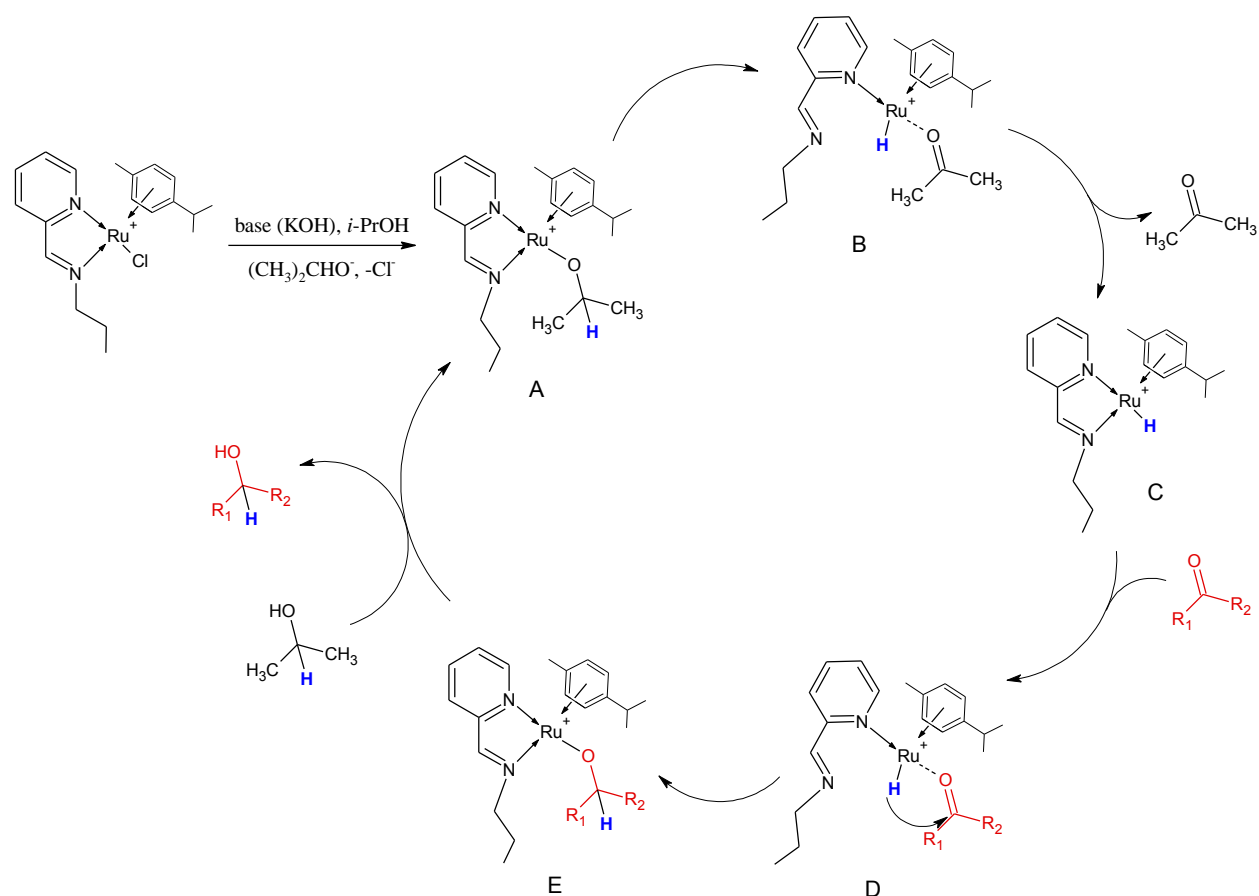
Scheme 6.5   Proposed mechanism for the transfer hydrogenation of acetophenone using model complex C2.1.

β-Elimination from **A** through intermediate **B** forms the expected hydride complex **C** while at the same time liberating acetone. If this part of the mechanism is believed to be correct, acetone should form even in the absence of substrate. The formation and detection of acetone could possibly point towards the formation of a ruthenium-hydride species. Evidence for the formation of acetone was confirmed by carrying out an experiment in the absence of any substrate under the reaction conditions mentioned earlier for the model systems. This confirmed that this part of the pathway could be plausible and that the mechanism possibly involves the formation of the Ru-H species **C**. Acetophenone is now able to coordinate to the Ru-H complex **C** through possible Ru-N bond cleavage to afford the open site forming intermediate **D**. Hydride transfer

from the ruthenium to the carbonyl group occurs to yield **E** which regenerates complex **A** by alkoxide exchange at the same time liberating the alcohol.

To confirm the step of the mechanism where acetone is liberated, a reaction was carried out in the absence of the substrate. If the formation of the Ru-H complex **C** does in fact occur then acetone must be formed, even in the absence of substrate. This reaction was carried out under the exact reaction conditions used earlier and the formation of acetone was observed when analyzing the reaction mixture with GC. Directly after the addition of base the reaction mixture changed color from light yellow to a dark purple. Acetone formation was confirmed by injecting a standard mixture of *i*-PrOH and acetone as reference. Although this is not conclusive proof that the mechanism involves the formation of the Ru-H species **C**, this does however support this statement and can be the only explanation for the formation of the acetone during the reaction. Attempts to verify the formation of the Ru-H species using ^{1}H NMR spectroscopy were unsuccessful and no definitive proof for the formation of the hydride could be seen.

6.3   Concluding remarks

Model complexes **C2.1I**-**C2.3I** and **C2.1**-**C2.3** were found to be active as catalyst precursors for the transfer hydrogenation of acetophenone to form the corresponding alcohol, 1-phenylalcohol, in high yields. The methyl-pyridine derivative **C2.2** was found to be the most active of the model complexes and a yield towards 1-phenylalcohol of more than 90 % could be achieved over a 6 hour period with its model pyridine (**C2.1**) and quinoline (**C2.3**) derivatives seemed to reach a maximum after 3 hours with yields of just below 80 %. A significant decrease in the activity of the model catalyst precursors were observed when exchanging the counter-ion for hexafluorophosphate. The general decrease was attributed to the lowered solubility of these complexes in *i*-PrOH under these reaction conditions.

Heterogenization of the complexes on silica supports MCM-41 and SBA-15 did not result in an increase in the activity of the respective catalysts. This was an unexpected result as one would have expected that the immobilization would stabilize the catalyst and could potentially result in an increase in the activity. Even after 24 hours only a yield of 60 % for **IC4.4** (methyl-pyridine

derivative) could be achieved. At the same stage almost complete conversion was observed for model complex **C2.2**. Mass transfer problems (decreased ease of access of the substrate to the active sites) could probably have caused this lowered activity. Despite the lower activity of these systems it was possible to recycle these catalysts at least three times before activity became negligible due to extensive catalyst leaching. The highest activity was in general observed after the 1st recycling with yields towards 1-phenylethanol reaching 38-58 %.

Although it was thought that these catalysts could possibly instill some sort of enantiomeric control in the formation of the alcohols, throughout an enantiomeric excess of 50 % was observed. This trend was also seen for the immobilized catalysts, which were thought could possibly increase the selectivity towards either form because of the pores of the support material.

Chapter 6: Transfer Hydrogenation of Selected Ketones

6.4   Experimental section

6.4.1   General remarks and instrumentation

All reactions were carried out under nitrogen using a Radleys carousel parallel reactor equipped with a gas distribution system. All transformations were carried out under a nitrogen atmosphere allowing for the reaction vessels to be flushed for a few minutes before adding any catalysts. Samples were analyzed by a Varian 3900 GC fitted with a polar Cyclosil-B column (30 m, 0.250 mm diam. and 0.25 μm film) using helium as carrier gas.

6.4.2   Materials

Acetophenone, benzophenone and 2-octanone were obtained from Sigma Aldrich and used without any further purification. NaOH, KOH and *t*-BuOK were obtained from Sigma Aldrich and used as is. *i*-PrOH was dried over molecular sieves overnight before use.

6.4.3   Typical procedure for transfer hydrogenation

Ruthenium catalyst precursor (0.004 mmol, 0.2 mol %) was dissolved in *i*-PrOH (9 mL) under an atmosphere of nitrogen at 25 °C. The appropriate base (KOH; 0.08 mmol; 0.8 mL of 0.1 M solution) was added by pipette and the vessel was sealed. The temperature was increased to 82 °C while being stirred continuously. At this stage the nitrogen feed to the vessels was closed off. After the mixture reached the required temperature, the substrate (2 mmol) was added by syringe through the silicone stopper. The reaction was allowed to continue for the allotted time after which the vessel was removed from the carousel reactor and cooled in an ice bath.

After the mixture was sampled (1 mL), *p*-xylene (0.100 mL) was added as the internal standard to be able to quantify the product formation. Conversions were determined by GC by following the amount of 1-phenylethanol that forms and calculating the acetophenone conversion.

6.5 References

1.   A.M. Hayes, D.J. Morris, G.J. Clarkson, M. Wills, *J. Am. Chem. Soc.*, **2005**, 127, 7318.

2.   O. Dayan, B. Çetinkaya, *J. Mol. Catal. A: Chem.*, **2007**, 271, 134.

3.   M.C. Carrión, F. Sepúlveda, F.A. Jalón, B.R. Manzano, *Organometallics*, **2009**, 28, 3822.

4.   A.N. Ajjou, J-L. Pinet, *J. Mol. Catal. A: Chem.*, **2004**, 214, 203.

5.   P. Pelagatti, M. Carcelli, F. Calbiani, C. Cassi, L. Elviri, C. Pelizzi, U. Rizzotti, D. Rogolino, *Organometallics* **2005**, *24,* 5836.

6.   S. Gladiali, E. Alberico, *Chem. Soc. Rev.*, **2006**, 35, 226.

7.   P. Crochet, M.A. Fernández-Zumel, C. Beauquis, J. Gimeno, *Inorg. Chim. Acta*, **2003**, 356, 114.

8.   R. Noyori, H. Takaya, *Acc. Chem. Res.*, **1990**, 23, 345.

9.   B.R. James, *Catal. Today*, **1997**, 37, 209.

10   F. Fache, E. Schulz, M.L. Tommasino, M. Lemaire, *Chem. Rev.*, **2000**, 100, 2159.

11   R. Noyori, *Angew. Chem. Int. Ed. Engl.*, **2002**, 41, 2008.

12.   H-U. Blaser, C. Malan, B. Pugin, F. Spindler, H. Steiner, M. Studer, *Adv. Synth. Catal.*, **2003**, 345, 103.

13.   V. Cadierno, P. Crochet, J. García-Álvarez, S.E. García-Garrido, J. Gimeno, *J. Organomet. Chem.*, **2002**, 663, 32.

14.   M. Yamakawa, H. Ito, R. Noyori, *J. Am. Chem. Soc.*, **2000**, 122, 1466.

15.   C. Standfest-Hauser, C. Slugovc, K. Mereiter, R. Schmid, K. Kirchner, L. Xiao, W. Weissensteiner, *J. Chem. Soc*., *Dalton Trans*., **2001**, 2989.

16.   M. Zhao, Z. Yu, S. Yan and Y. Li, *Tetrahedron Lett.*, **2009**, 50, 4624.

17.   X. Sun, G. Manos, J. Blacker, J. Martin, A. Gavriilidis, *Org. Process Res. Dev.*, **2004**, 8, 909.

18.   S. Gladiali, L. Pinnaa, G. Delogub, S. De Martinc, G. Zassinovichc, G. Mestronic, *Tetrahedron: Asymmetry*, **1990**, 1, 635.

Chapter 7:   Concluding Remarks and Future Prospects

7.1 Concluding remarks

Two distinctly different routes towards the heterogenization of Ru(arene)Cl(N,N) complexes on mesoporous silica supports were investigated in this thesis. The first route followed a more widely used approach which involved the functionalization of the diimine ligand with the appropriate siloxane functionality. A second, novel immobilization approach was developed during this project. This approach involved the introduction of a propanol functionality on the arene ligand of the complex allowing for further functionalization to incorporate the siloxane tether. The condensation of the siloxane functionalized complexes with the surface silanols of the support materials allowed for the preparation of MCM-41 and SBA-15 immobilized Ru(arene)Cl(N,N) catalysts.

The preparation of the siloxane functionalized complexes **C2.4**-**C2.6** and **C3.5**-**C3.8** each presented with their own difficulties. It was important to verify and monitor the presence of the siloxane functionality throughout to ensure it does not undergo reduction or is hydrolyzed during any step of the synthetic procedure. This could potentially have led to problems in subsequent reactions. For the synthesis of the model and siloxane functionalized complexes **C2.1**-**C2.6** from ligands **L2.1**-**L2.6**, hexafluorophosphate was initially chosen as the counter-ion to allow for the isolation of the cationic complexes. This was however only really successful for the synthesis for model complexes **C2.1**-**C2.3** which in this case were designated as complexes **C2.1I**-**C2.3I** (hexafluorophosphate derivatives). The hexafluorophosphate counter-ion was however not large enough to efficiently stabilize the formed functionalized complexes (**C2.4**-**C2.6**) and therefore it was opted to use the tetraphenylborate counter-ion instead. This allowed for the isolation of the functionalized complexes as stable orange to brown solids and in moderate yields and by exchanging the solvent to DCM allowed an even further increase in the yield. It was important to achieve decent yields of the functionalized complexes to produce sufficient amounts of immobilized catalysts.

Unfortunately attempts to reduce the imine functionality of functionalized ligands **L2.4**-**L2.6** in an effort to prepare corresponding secondary amine ligands were not entirely successful, as

during the process the siloxane functionality was also reduced. An attempt to avoid this problem by synthesizing a binuclear system from bis(3,3'-aminopropyl)amine, where the siloxane functionality could be introduced at a later stage therefore avoiding reduction, was unfortunately also unsuccessful and resulted in the formation of an unsymmetrical cyclic bis(pyridylimino-3-propyl)-amine compound.

Novel siloxane tethered complexes with the siloxane tether being via the arene ring instead of connected to the imine nitrogen were envisaged. Initial efforts were focused on the synthesis of a urethane linked siloxane functionalized Ru-dimer, which could potentially be cleaved with a range of diimine ligands. This approach unfortunately resulted in the loss of the ethoxy silane functionality due to intermolecular condensation of the siloxane moieties resulting in the formation of a polymer-like siloxane material. Firstly synthesizing alcohol functionalized complexes and then linking them with the siloxane tether proved to be a more promising route. This approach proved to be successful and a range of alcohol functionalized Ru(arene)(N,N) complexes were synthesized where the alcohol functionality was introduced on the arene ligand of the complex. Linkage of these complexes with an appropriate siloxane tether (3-(triethoxysilyl)propyl isocyanate) allowed us to synthesize novel urethane linked siloxane functionalized complexes **C3.5**-**C3.8**. Full characterization of these complexes provided proof of successful linkage without any loss of the structural integrity of the initial complexes. The presence of the siloxane functionality was monitored throughout.

Mesoporous silicas MCM-41 and SBA-15 were synthesized from literature procedures and proved to be very stable inorganic support materials for the siloxane functionalized complexes. The siloxane functionalized complexes were successfully immobilized to afford immobilized catalysts, **IC4.1**-**IC4.12**. The novel approach used to synthesize immobilized catalysts **IC4.7**-**IC4.12** involved the tethering of the catalysts through the arene ring, instead of it being attached through the imine nitrogen as was the case for immobilized catalysts **IC4.1**-**IC4.6**. Initial solubility issues resulted in incomplete immobilization. It was found that by using a mixture of THF and toluene instead of only toluene, successful and efficient immobilization onto the mesoporous silica supports could be achieved. A wide range of solid state analytical techniques allowed for the full characterization of the immobilized catalysts. The immobilization was confirmed mainly by monitoring the change in surface area (BET analysis) and determining the

Chapter 7: Concluding Remarks and Future Prospects

metal content on the support using ICP. ICP-OES allowed for direct comparison of the model and immobilized systems during catalysis ensuring that the ruthenium loadings were kept constant. Scanning and transmission electron microscopy (SEM and TEM) confirmed the morphology of the support material remained unchanged during the immobilization process. Powder XRD confirmed that the structural integrity and high degree crystallinity of the support material was maintained before and after immobilization of the functionalized complexes.

Both the model and immobilized systems with the tether attached to the imine nitrogen, **C2.1**-**C2.3** and **IC4.1**-**IC4.6**, allowed us to selectively and in high yields form either heptaldehyde or heptanoic acid during the oxidative cleavage of 1-octene. This was achieved by varying the reaction times. At shorter reaction times (3-5 hours) mostly heptaldehyde was formed. By increasing the reaction times it was possible to convert the formed aldehyde to its corresponding carboxylic acid in quantitative yields. Styrene could also be converted to benzaldehyde in near quantitative yields in 1 hour. Although the immobilized catalysts **IC4.7**-**IC4.12** did not fare as well as **IC4.1**-**IC4.6**, a still significant increase in the activity was observed when compared to its model counterparts **C3.1**-**C3.3**. A lower ruthenium loading (0.05 mol % for the immobilized systems) could achieve dramatically increased conversions when compared to the model systems at the same times.

UV-Vis experiments were carried out to probe the formation of the proposed active species, RuO_4, during a typical cleavage reaction. Reactions in the absence of substrate were carried out to monitor the conversion of the complexes to the active species, under similar reaction conditions used for the cleavage reactions. The decreased activity of the model and immobilized catalysts with the tether via the arene was probed. It was shown that the propanol functionalized arene complex **C3.1** was unstable under the reaction conditions employed for the catalytic runs and after 1 hour could no longer be detected. This is in stark contrast to the *p*-cymene derivative **C2.2**, which could still be detected in the reaction solution even after 24 hours. This corroborated the difference in the conversions that were observed for the two systems. After 1 hour the presence of the RuO_4 species was observed for both immobilized catalysts **IC4.3** and **IC4.7**. The immobilization process, as well as the support itself, was found to play a crucial role during the oxidative cleavage reactions. It was proposed that the oxidant can adsorb onto the surface of the support coming into close proximity with the complex leading to a higher rate of

Chapter 7: Concluding Remarks and Future Prospects

formation for RuO_4 resulting in a faster rate of reaction. By capping the native silicas with HMDS a decrease in the conversion, although more pronounced for the MCM-41 system than for SBA-15 system, was observed. This led us to believe that the surface silanols are indeed interacting with the complex and/or the oxidant by potentially stabilizing it during the course of the reaction.

Model complexes, **C2.1I**-**C2.3I** and **C2.1**-**C2.3**, were found to be active as catalyst precursors for the transfer hydrogenation of acetophenone to form the corresponding alcohol, 1-phenylalcohol, in high yields. A significant decrease in the activity of the model catalyst precursors was observed when exchanging the counter-ion for hexafluorophosphate and this was ascribed to the lower solubility of these complexes in the reaction medium. Unfortunately a decrease in the activity was observed when carrying out the reaction using immobilized catalysts **IC4.1**-**IC4.6**. This was an unexpected result as one would have expected that the immobilization would stabilize the catalyst and could potentially result in an increase in the activity. Even after 24 hours only a yield of 60 % for **IC4.4** (methyl-pyridine derivative) could be achieved. At the same stage almost complete conversion was observed for model complex **C2.2**. This decreased activity was attributed to mass transfer problems caused by the difficulty of the substrate to get access to the active sites inside the pores of the support material. Although the activities of the immobilized systems were lowered when compared to their model counterparts, recovery of the immobilized systems could be achieved. The immobilized systems could be recovered and reused for a total of 3 runs before the catalysts became inactive.

Although initial focus was to develop heterogenized catalytic systems with the emphasis on recovery and reusability, the influence of the support material on the activity and stability of the catalyst during the oxidative cleavage of 1-octene became the focus point. The support was found to have a positive effect on the activity of the catalyst precursor and seems to stabilize the formed active species in solution. The newly developed urethane linked arene tether, although it was not recyclable and more unstable under the employed reaction conditions, could possibly find application for a different catalytic process.

7.2   Future prospects

During this project a few questions arose which could unfortunately, due to time constraints, not be addressed in full.

Some interesting results were obtained during the oxidative cleavage of alkenes. Although the cleavage of 1-octene was found to occur at a much slower rate than was reported in literature, more control could be achieved using our systems in terms of selectivity to either heptaldehyde or heptanoic acid, depending on the reaction time. It would be interesting to expand the scope of substrates to internal and cyclic alkenes to see what effect that would have on the activity and the selectivity of the catalyst precursors.

It was found that an increase in the size of the ligand resulted in an increase in the rate at which 1-octene was cleaved to form heptaldehyde. It would be interesting to further increase the steric bulk around the metal center to ascertain to what extent this influences the activity of the catalyst precursor.

A more in depth study needs to be undertaken to determine how the ligands influence the formation of the active RuO_4 species during the oxidative cleavage reaction. It needs to be understood what determines the rate at which this species is formed in solution (starting from the complex). Lastly it needs to be established exactly how the support material stabilizes and helps forms the active species during the oxidative cleavage reactions.

Although it was thought that these catalysts could possibly instill some sort of enantiomeric control in the formation of the alcohols during the transfer hydrogenation reactions, throughout an enantiomeric excess of 50 % was observed. The modification of the ligands around the metal center is proposed to prepare systems which could be more selective towards one or the other isomer.